ROCKETDYNE
A DIVISION OF NORTH AMERICAN ROCKWELL CORPORATION
6633 CANOGA AVENUE CANOGA PARK CALIFORNIA 91304

R-7780-1

EFFECTS OF HIGH-PRESSURE HYDROGEN ON METALS AT AMBIENT TEMPERATURE

Final Report

(7 March 1967 through 28 February 1969)

Contract NAS8-19
Schedule Article VIII
and DRL 010, Section
II, Line Item 42

PREPARED BY
R. J. Walter
W. T. Chandler
Rocketdyne Research Division
Canoga Park, California

APPROVED BY

P. D. Castenholz
J-2 Program Manager

NO OF PAGES 200 & xviii

REVISIONS

DATE 28 February 1969

DATE	REV BY	PAGES AFFECTED	REMARKS

328

337

UNCLASSIFIED

Security Classification

DOCUMENT CONTROL DATA - R & D

(Security classification of title, body of abstract and indexing annotation must be entered when the overall report is classified)

1. ORIGINATING ACTIVITY (Corporate author)

Rocketdyne, a Division of North American Rockwell Corporation, 6633 Canoga Avenue, Canoga Park, California 91304

2a. REPORT SECURITY CLASSIFICATION

UNCLASSIFIED

2b. GROUP

3. REPORT TITLE

Effects of High-Pressure Hydrogen on Metals in Ambient Temperatures

4. DESCRIPTIVE NOTES (Type of report and inclusive dates)

Final Report (7 March 1967 through 28 February 1969)

5. AUTHOR(S) (First name, middle initial, last name)

Robert J. Walters; W. T. Chandler

6. REPORT DATE

28 February 1969

7a. TOTAL NO. OF PAGES

7b. NO. OF REFS

19

8a. CONTRACT OR GRANT NO.

NAS8-19

b. PROJECT NO.

c.

d.

9a. ORIGINATOR'S REPORT NUMBER(S)

R-7780-1, -2, -3

9b. OTHER REPORT NO(S) (Any other numbers that may be assigned this report)

None

10. DISTRIBUTION STATEMENT

11. SUPPLEMENTARY NOTES

12. SPONSORING MILITARY ACTIVITY

13. ABSTRACT

Thirty-five alloys were investigated for their susceptibility to high-pressure hydrogen-environment embrittlement at ambient temperature; subsequently they were ranked according to their reduction of notch strength in 10,000-psi hydrogen. The ranking in order of decreasing embrittlement was as follows: (1) high-strength steels and nickel-base alloys; (2) moderate- and low-strength iron-base alloys, pure nickel, and titanium alloys; (3) nonstable AISI type 300 stainless steels, beryllium-copper, and commercially pure titanium and (4) aluminum alloys, pure copper, and the stable AISI type 300 stainless steels. The degree of hydrogen-environment embrittlement was found to increase with increasing hydrogen pressure and to be a complex function of notch severity, passing through a maximum at an intermediate K_t. Low cycle fatigue properties of low alloy steels were reduced considerably by 1000- and 10,000-psi hydrogen environments. The degree of embrittlement decreased with an increasing yield strength/ultimate strength ratio, providing other variables were constant. Results of metallographic studies of specimens fractured in high-pressure hydrogen are presented and conclusions are drawn concerning the mechanism of hydrogen-environment embrittlement.

i-a

DD FORM 1473

UNCLASSIFIED

Security Classification

KEY WORDS	LINK A ROLE	LINK A WT	LINK B ROLE	LINK B WT	LINK C ROLE	LINK C WT
Hydrogen-Environment Embrittlement						
High-Pressure Hydrogen						
Hydrogen-Environment Effects						
Hydrogen Embrittlement						
Mechanical Properties						
Fracture Toughness						
Surface Effects						
Metals						
Steels						
Nickel Alloys						
Titanium Alloys						
Copper Alloys						
Aluminum Alloys						

FOREWORD

This report covers the work performed under National Aeronautics and Space Administration Contract NAS8-19, Task 7, during the period 7 March 1967 to 28 February 1969. The report was prepared by R. J. Walter and W. T. Chandler with the assistance of R. P. Jewett, all of Materials Research, Research Division, Rocketdyne, a Division of North American Rockwell Corporation.

The project was conducted under the cognizance of Messrs. W. B. McPherson and C. E. Cataldo, Metallic Materials Branch, Propulsion and Vehicle Engineering, George C. Marshall Space Flight Center.

Acknowledgment is gratefully given to the following Rocketdyne personnel for their contribution in this investigation:

G. V. Sneesby H. G. Hayes	In charge of setting up the equipment for testing in high-pressure gaseous environments and conducting the tests performed with this equipment
H. H. Guth G. E. Dyer	Testing with high-pressure equipment
D. H. Robie J. Testa J. A. Amy	Electron metallography

ABSTRACT

Thirty-five alloys were investigated for their susceptibility to high-pressure hydrogen-environment embrittlement at ambient temperature; subsequently they were ranked according to their reduction of notch strength in 10,000-psi hydrogen. The ranking in order of decreasing embrittlement was as follows: (1) high-strength steels and nickel-base alloys; (2) moderate- and low-strength iron-base alloys, pure nickel, and titanium alloys; (3) nonstable AISI type 300 stainless steels, beryllium-copper, and commercially pure titanium and (4) aluminum alloys, pure copper, and the stable AISI type 300 stainless steels. The degree of hydrogen-environment embrittlement was found to increase with increasing hydrogen pressure and to be a complex function of notch severity, passing through a maximum at an intermediate K_t. Low cycle fatigue properties of low alloy steels were reduced considerably by 1000- and 10,000-psi hydrogen environments.

The degree of embrittlement decreased with an increasing yield strength/ultimate strength ratio, providing other variables were constant. Results of metallographic studies of specimens fractured in high-pressure hydrogen are presented and conclusions are drawn concerning the mechanism of hydrogen-environment embrittlement.

Preceding page blank

CONTENTS

Preceding page blank

ILLUSTRATIONS

Preceding page blank

TABLES

INTRODUCTION

Over the years, failures of bourdon tubes, compressor parts, small storage vessels, etc., have been attributed to the effect of high-pressure hydrogen. However, relatively recent failures of large, welded hydrogen storage vessels at and below design pressures of 5000 and 6000 psi served to focus attention within NASA, and elsewhere, on the embrittlement of metals by high-pressure hydrogen at ambient temperatures.

An extensive literature (over 1500 papers) has been compiled on the embrittlement of steels and a few other metals by relatively large concentrations of hydrogen introduced by electrolytic charging or quenching after high-temperature exposure to high-pressure hydrogen. This literature has limited pertinency to the effect of a high-pressure hydrogen environment on the mechanical properties of metals.

Investigations into the effects of high-pressure hydrogen on the properties of metals at ambient temperatures were not initiated until the early 1950's. These first programs consisted of exposing specimens to high-pressure hydrogen and then removing and testing them to failure in air or an inert environment. Results from such tests are of limited usefulness. Thus, it was not until after 1960 that results were published for programs in which specimens were tested to failure in high-pressure hydrogen. These latter programs (about seven in number) have yielded the most valuable information on the effects of high-pressure hydrogen at ambient temperatures. The effects of high-pressure hydrogen on metals at elevated temperatures is a separate problem and will not be discussed in this report.

Failures of the large, high-pressure hydrogen storage vessels being used on NASA programs led to the establishment of a NASA working group on storage of hydrogen at high pressure. The working group immediately concluded (Ref. 1) that the most urgent need was for data that could be put to use on the storage vessel problem.

As a result of the failures of the high-pressure hydrogen storage vessels, and somewhat prior to the establishment of the NASA working group, a program was initiated at Rocketdyne (Ref. 2 and 3) to study the effect of high-pressure hydrogen on three pressure vessel steels: ASTM A-302-56 Gr.B modified with nickel, ASTM A-517-64 Gr.F^{b}(T-1), and ASTM A-212-61T Gr.B-FB. Notched and unnotched specimens of weld and parent metal were tensile tested in hydrogen at pressures from 3000 to 10,000 psi at room temperatures. Before testing to failure, the specimens were held under stress in the environment for 1, 10, or 100 days. The strength and ductility of notched specimens and the ductility, but not the strength, of unnotched specimens were considerably reduced by the high-pressure hydrogen environments. Extensive surface cracking occurred in the necked-down region of the unnotched specimens. The ASTM A-212 specimens were significantly less embrittled by 3000- and 5000-psi hydrogen than by 7500- and 10,000-psi hydrogen, but the other two metals were embrittled to about the same degree over the range of pressures studied. No appreciable effect on the degree of embrittlement could be attributed to a variation in the hold time.

In their final report (Ref. 1), the NASA working group concluded that "the unsatisfactory understanding of GH_2-metal interactions posed a serious threat to many of the important NASA future missions. In many ways, these potential problems could be more extensive and serious than the GH_2 storage-vessel emergency." The working group gave the following examples: (1) liquid-fueled rocket engines (e.g., the J-2 engine) are using hydrogen, and will likely continue using hydrogen and at higher pressures and higher temperatures; (2) hydrogen is the leading (perhaps sole) feasible fuel for hypersonic aircraft, so the entire spectrum of alloys used for turbojets and ramjets and combinations or variations thereof must be unaffected by gaseous hydrogen; (3) the nuclear rocket will use hydrogen as the propellant, therefore gaseous hydrogen at various temperatures and pressures must be compatible with the many alloys of the propellant system.

In addition, the working group recommended that studies such as conducted at Rocketdyne "should be continued and expanded to include more realistic

and sophisticated types of tests." They further recommended that "More general and broader engineering type studies should be made to assess the roles of other variables of engineering importance (e.g., cyclic stress, alloy composition, hydrogen purity, surface conditions, protective coatings, temperature, pressure, strength level of alloys, crack sizes, etc.)."

This program was performed to identify possible problem areas when using metals and alloys in hydrogen environments, particularly high-pressure hydrogen environments, at ambient temperatures. In addition, the program was initiated to develop a more comprehensive understanding of the characteristics and, to some extent, the mechanism of high-pressure hydrogen-environment embrittlement. This study involved the investigation of a much broader range of alloys and effects than in the previous work.

The program was divided into the following phases (all investigations were conducted at room temperatures):

I: Influence of Time of Exposure to High-Pressure Hydrogen on Degree of Embrittlement of Metals

II: Effect of a 10,000-psi Hydrogen Environment on the Tensile Properties of a Variety of Alloys

III: Effect of Long-Time Exposure of Stressed Specimens to High-Pressure Hydrogen on the Degree of Embrittlement

IV: Influence of Hydrogen Pressure on the Degree of Embrittlement

V: Influence of Notch Severity on Hydrogen-Environment Embrittlement

VI: Influence of Hydrogen Environment on Low Cycle Fatigue Properties of Alloys

VII: Relation Between the Mechanical Properties of Steels (in Air) and Susceptibility to Hydrogen-Environment Embrittlement

VIII: Protection From Hydrogen-Environment Embrittlement

IX: Effect of Surface Abrasion in Hydrogen on Hydrogen-Environment Embrittlement

X: Posttest Metallographic Analysis (Specimens from Phase I through IX)

In the following, each phase is reported as an independent investigation. In addition, overall General Discussion, Summary, and Conclusions sections are included with the aim of correlating the results from the individual phases. Phase V included a task on "The Influence of Hydrogen Environments on Fracture Toughness." The experimental work on this task extended past the time that would have allowed it to be included in this report, thus, that task is reported in a supplement to this document.

During this program, most hydrogen tests were performed in triplicate for each material and test condition, and most helium or air tests were performed in duplicate. To reduce the bulk of this report, only the averages of duplicate or triplicate tests are usually presented. However, the tables of individual specimen data are contained in the Appendix under separate cover as R-7780-2. References to these Appendix tables are made at appropriate places in this report. Also for easier reading, the complete ASTM alloy designations are abbreviated in the text, while the full designations appear in the tables.

SUMMARY

As noted in the Introduction, this program was divided into 10 separate phases, each with its own distinct purpose. However, in many cases results from one phase served to add supporting information to another. In the following paragraphs, each phase will be summarized, not necessarily in numbered order, and the supporting results from other phases will, in each case, be covered. A more complete summary of each phase is contained in the body of the report under the specific phase numbers.

The hydrogen-environment embrittlement investigated in this program is that which occurs at ambient temperatures, and all tests were performed at room temperatures.

EFFECT OF 10,000-PSI HYDROGEN ENVIRONMENT ON THE TENSILE PROPERTIES OF A VARIETY OF ALLOYS (PHASE II)

Throughout the various phases of this program, the susceptibility to high-pressure hydrogen-environment embrittlement was determined for 35 iron, nickel, titanium, aluminum, and copper-base alloys. Tensile tests on unnotched and notched specimens of the alloys were performed in 10,000-psi hydrogen and, for comparison, in 10,000-psi helium and 1-atmosphere pressure air. In all, 25 alloys were investigated in Phase II. These tensile tests were performed as soon as the desired test environment was established; i.e., without holding the specimen in the environment prior to tensile testing. From the results of these tests, the alloys were classified into the following hydrogen-environment embrittlement categories (refer to Tables 12 through 15, Phase II for a listing of the alloys in each category in the order of decreasing embrittlement):

1. Extreme embrittlement: High-strength steels and high-strength nickel-base alloys are in this category. Embrittlement is characterized by a large decrease of notch strength and ductility and some decrease of unnotched strength in 10,000-psi hydrogen.

Reduction of ductility was between 84 and 92 percent for all 3 measures of ductility (elongation and reduction of area of the unnotched specimens and reduction of area of the notched specimen).

2. Severe embrittlement: The majority of the metals tested are in this category, including ductile, lower-strength steels, Armco Iron, pure nickel, and the titanium-base alloys. Embrittlement is characterized by a considerable reduction of notch strength and ductility, but no reduction of unnotched strength. The measure of ductility most affected by the high-pressure hydrogen environment was the reduction of area of the notched specimens.

3. Slight embrittlement: The nonstable AISI type 300 series stainless steels (AISI types 304L and 305), beryllium-copper and commercially pure titanium are in this category. Embrittlement is characterized by a small decrease of notch strength and small or negligible decrease of unnotched ductility. AISI type 304L and commercially pure titanium also had a moderate (48 and 27 percent) reduction of notch ductility.

4. Negligible embrittlement: The aluminum alloys, stable austenitic stainless steels, A-286 (a precipitation-hardened austenitic stainless steel), and OFHC copper are in this category.

INFLUENCE OF TIME OF EXPOSURE TO HIGH-PRESSURE HYDROGEN ON DEGREE OF EMBRITTLEMENT OF METALS (PHASE I)

The basic test procedure for tensile testing in high-pressure hydrogen (for example, the Phase II tests above) was established in a preliminary series of tests. These tests were performed on ASTM A-302, AISI type 310 stainless-steel, and Ti-6Al-4V specimens to determine the effect of time of exposure of unstressed specimens to 10,000-psi hydrogen on the degree of hydrogen-environment embrittlement. Embrittlement was found to be greatest with zero hold time, and hydrogen-environment

embrittlement of Ti-6Al-4V increased if the test vessels in which the specimens were held for tensile testing in high-pressure hydrogen were evacuated prior to normal pressurization-depressurization purging. Thus, the basic test procedure established to determine the effects of gaseous hydrogen environments on metals included evacuation prior to pressurization-depressurization purging of the test vessels and the performance of the tensile test immediately upon establishment of the test environment.

EFFECT OF LONG TIME EXPOSURE OF STRESSED SPECIMENS TO HIGH-PRESSURE HYDROGEN ON THE DEGREE OF EMBRITTLEMENT (PHASE III)

The effect on the degree of hydrogen-environment embrittlement of holding stressed specimens in 10,000-psi hydrogen for periods up to 100 days was determined for AISI 1020, ASTM A-515, HY-80, H-11 tool steel, and Ti-6Al-4V. Both the unnotched and notched specimens of AISI 1020 were prestrained before testing to investigate the effect of strain aging during the hold period. Hold stresses were below and above the yield strengths for unnotched specimens, and were 80 and 90 percent of the zero hold time notch strength in 10,000-psi hydrogen for the notched specimens.

Results showed that the degree of hydrogen-environment embrittlement was essentially independent of hold time or stress for both notched and unnotched low alloy steel specimens. Reduction of notch strength of the AISI 1020 specimens, however, decreased with increasing hold duration. This decrease of embrittlement was attributed to strain aging, which increased the yield strength/ultimate strength ratio. The effect of strain aging on hydrogen-environment embrittlement will be discussed again later in this summary.

Test results of notched Ti-6Al-4V specimens indicated the hydrogen-environment embrittlement decreased with an increased exposure time to hydrogen by the specimens, which were unloaded (except for gas pressure).

In attempting to hold notched Ti-6Al-4V specimens under load in hydrogen, all specimens failed prematurely, a few on loading to the hold stress but most shortly after hold stress was established. The decrease in hydrogen-environment embrittlement of unloaded Ti-6Al-4V specimens with increasing time of exposure to high-pressure hydrogen is not well understood. Possible factors proposed were: (1) the increase in hydrogen-environment embrittlement because of prior evacuation of the test vessels may be eliminated or reduced on holding in hydrogen; or (2) strain aging of Ti-6Al-4V may have occurred during the hold period, which, as will be discussed below, tends to decrease the degree of embrittlement.

INFLUENCE OF HYDROGEN PRESSURE ON DEGREE OF EMBRITTLEMENT (PHASE IV)

The influence of hydrogen pressure on the degree of embrittlement was determined on unnotched and notched specimens of AISI type 310 stainless steel and ASTM A-302. Hydrogen test pressures were 1 atmosphere, and 100, 1000, and 10,000 psig. The notched AISI type 310 stainless-steel specimens were slightly embrittled by the 10,000-psi hydrogen environment, but not by hydrogen at lower pressures. Hydrogen environment embrittlement of ASTM A-302 decreased with decreasing hydrogen pressure, and reduction of notch strength and unnotched properties were negligible at hydrogen pressures equal to and less than 100 psig. However, notch ductility was considerably reduced even at 1 atmosphere of hydrogen pressure, and surface cracking was observable on unnotched specimens tested in the same environment.

Tests were conducted on Inconel 718 at 1000- and 10,000-psi hydrogen pressures. In 10,000-psi hydrogen, the unnotched specimens had nearly zero ductility, and the notched strength was reduced 51 to 55 percent as compared to that in 10,000-psi helium. In 1000-psi hydrogen, the ductility of notched specimens was reduced to a much smaller degree than in 10,000-psi hydrogen, but the notch strength was still reduced by 35 to 40 percent as compared to that in 1000-psi helium.

A series of tests were conducted in Phase II in a hydrogen-contaminated 10,000-psi helium environment. Hydrogen content was 44 ppm or 0.44 psi partial pressure. Specimens from metals in the slight, severe, and extreme embrittlement categories were tested, and a measurable reduction of notch strength was observed on specimens from each class. Thus, embrittlement by gaseous-hydrogen environments will occur at hydrogen pressures of less than 1 atmosphere, even for materials placed in the slight embrittlement category.

The large volume of tensile data obtained in ambient air and in 10,000-psi helium on a wide variety of alloys gave, in spite of considerable scatter, a good indication of the effect of pressure on the mechanical properties of metals. Yield and ultimate strengths of unnotched specimens and the strength of notched specimens were reduced approximately 10,000 psi when tested in a 10,000-psi helium environment. This strength reduction was caused by the 10,000-psi shear component on the specimens from the hydrostatic pressure. It was also observed that the weaker metals, e.g., OFHC copper, commercially pure titanium, aluminum alloys, and AISI type 300 series stainless steels, had significantly higher elongation and slightly higher reduction of area in 10,000-psi helium than in ambient-pressure air.

INFLUENCE OF NOTCH SEVERITY ON HYDROGEN-ENVIRONMENT EMBRITTLEMENT (PHASE V)

The influence of notch severity on the degree of hydrogen-environment embrittlement in 10,000-psi hydrogen was measured on ASTM A-302, ASTM A-517, and AISI type 310 stainless-steel specimens with notch geometries ranging from $K_t = 1$ (unnotched) to $K_t \simeq 8.4$. In addition, the results for precracked specimens of ASTM A-302 and ASTM A-517 tested in Phase VI were used in the analysis. Embrittlement of the AISI type 310 stainless-steel specimens was restricted to $K_t \simeq 8.4$. No embrittlement was observed at lower K_t factors, and the strength of precracked specimens appeared to be about the same in 10,000-psi helium as in 10,000-psi hydrogen.

Hydrogen-environment embrittlement of ASTM A-302 and ASTM A-517 increased linearly with low values of K_t, passed through a maximum at $K_t \simeq 9$ for ASTM A-302 and 6 for ASTM A-517, and then decreased. The precracked specimens of both steels were less embrittled by hydrogen than were specimens with $K_t \simeq 6$ or 8.4.

Phase V also included a task entitled "Influence of Hydrogen Environments on Fracture Toughness." However, experimental work on that task was extended past the time permitting it to be included in this report. Thus, the work is reported in a supplement to this document.

INFLUENCE OF HYDROGEN ENVIRONMENT ON LOW CYCLE FATIGUE PROPERTIES OF METALS (PHASE VI)

Low cycle tension-tension fatigue tests were conducted on unnotched specimens, as well as notched and fatigue precracked specimens of ASTM A-302 and ASTM A-517, and notched and fatigue precracked specimens of AISI type 310 stainless steel. The tests were conducted in 10,000-psi helium and 1000-psi and 10,000-psi hydrogen, to determine the 1000 cycle fatigue life in these environments.

Low cycle fatigue strengths in the various environments of unnotched specimens of ASTM A-302 and ASTM A-517 and of notched and precracked AISI type 310 stainless-steel specimens were about the same as their tensile strengths in an identical environment. Low cycle fatigue properties of the precracked ASTM A-302 and ASTM A-517 specimens were quite similar to each other in all environments, but were lower in hydrogen and helium than in air. For both materials, the 1000 cycle fatigue strength in 10,000-psi hydrogen was about 1/3 that in 10,000-psi helium, and for the 10,000-psi hydrogen tests, there appeared to be a low cycle fatigue limit that occurred between 1000 and 2000 cycles. Fatigue strengths of precracked ASTM A-302 and ASTM A-517 specimens in 1000-psi hydrogen were about midway between those strengths in 10,000-psi hydrogen and 10,000-psi helium.

Crack propagation during the fatigue tests was monitored by electrical resistivity measurements. These measurements indicated that initiation of crack growth occurred in a fewer number of cycles in hydrogen than in inert environments. There were fewer total crack steps before failure in hydrogen, and the distance the crack traveled per crack step was greater in 1000- and 10,000-psi hydrogen than in inert environments. The relationship between stress amplitude and logarithm of crack growth per cycle was linear for the 10,000-psi hydrogen and 10,000-psi helium environments. Curves in 1000-psi hydrogen deviated from linearity to slower rates of crack growth with increasing crack depth, and it is suggested that the rate of crack propagation was dependent upon the rate at which hydrogen reached the crack tip in 1000-psi hydrogen.

PROTECTION FROM HYDROGEN ENVIRONMENT EMBRITTLEMENT (PHASE VIII)

Investigations into the protection of metals from hydrogen-environment embrittlement through the use of inhibitors in the hydrogen or surface protective coatings on the metal were originally planned for this program. However, because of unexpected findings, it was deemed necessary to follow up with additional work in other phases and the effort planned for Phase VIII was diverted to them. Before work on Phase VIII was stopped, equipment was procured for the addition of closely controlled amounts of impurity gases (inhibitors) to high-pressure hydrogen.

SUMMARY OF RELATIONSHIP BETWEEN PHASES VII, IX, AND X

These last three phases to be summarized were all involved with understanding the embrittlement phenomenon rather than determining the

conditions under which embrittlement occurred and will be covered together. In an earlier program, extensive surface cracking was observed in specimens tested in high-pressure hydrogen. It was suggested that this surface cracking occurred only after the protective self-oxide was ruptured, allowing the hydrogen environment to contact the metal surface. Initiation of surface cracking would therefore depend upon achieving the critical degree of deformation needed to rupture the self-oxide. The higher the stress at which this critical deformation occurred, the less would be the strength loss due to the hydrogen environment. It was further suggested that embrittlement would be a function of the yield strength/ultimate strength ratio of the material.

To test this hypothesis, chemically similar materials (AISI 1042 and AISI 4140) were heat treated (quenched and tempered) to achieve approximately 110 ksi ultimate strengths. After heat treatment, there was approximately 15 and 28 to 35 ksi difference between the yield and ultimate strengths of the AISI 4140 and AISI 1042 specimens, respectively.

Notched specimens of these materials were tested in 10,000-psi hydrogen and helium environments. The results indicated that the degree of hydrogen-environment embrittlement (percent reduction of notch strength) increased with a decreasing yield strength/ultimate strength ratio.

The most definitive experiments conducted in this program on the effect of yield strength/ultimate strength ratio on hydrogen-environment embrittlement were performed on the prestrained AISI 1020 specimens in Phase III. Because of strain aging, holding under stress increased the yield strength; but the ultimate strength in most cases remained essentially constant. After a 100-day exposure, the yield and ultimate strengths were almost the same (i.e., the yield strength/ultimate strength ratio had increased to nearly 1.0 during the hold period). The reduction of strength of the AISI 1020 notched specimens was about 14, 4, and 1 percent after 0, 1, and 100 days of exposure to 10,000-psi hydrogen under tensile stresses of 80 and 90 percent of their strength in that medium.

Other variables such as chemistry and microstructure remained constant for the AISI 1020 specimens, and the only material change was caused by formation of interstitial atmospheres around dislocations, which increased the yield strength. Thus, the decrease of embrittlement during the hold period was evidently associated with an increase in the yield strength/ultimate strength ratio. However, when all of the alloys tested in this program were considered, there was essentially no correlation between the yield strength/ultimate strength ratio and hydrogen-environment embrittlement. The only relationship observed between hydrogen-environment embrittlement and mechanical properties was that embrittlement tended to increase with increasing yield and ultimate strength level for the transition metal-base alloys, which were the most embrittled. The results, therefore, indicate that embrittlement is a function of the yield strength/ultimate strength ratio, providing that other variables such as chemistry, microstructure, and ultimate strength remain constant.

The hypothesis that initiation of surface cracking depends upon achieving a clean surface for gaseous hydrogen contact can be tested most directly by abrading the metal in the hydrogen environment. In Phase IX, unnotched ASTM A-517 specimens were abraded in 10,000-psi hydrogen and then either examined immediately or tested to failure. Specimens abraded prior to tensile testing in hydrogen contained many more surface cracks than specimens tensile tested in hydrogen but without prior abrasion. The degree of hydrogen-environment embrittlement was not as strongly influenced by abrasion as was crack initiation.

A considerable amount of basic information regarding embrittlement was obtained from visual, optical microscopy, and electron microscopy examination of the surface cracks and fractures in specimens tested in this program. The most obvious effect of testing in high-pressure hydrogen was the presence of surface cracks in the necked-down region of the unnotched specimens. These cracks extend circumferentially around the specimen and were deeper and more numerous near the fracture. There

was a relationship between the degree of surface cracking and embrittlement, and the embrittlement categories presented at the beginning of this section could be used to classify surface crack formation and propagation.

Metals in category 4, negligible embrittlement, did not form surface cracks in high-pressure hydrogen, but those metals in category 3, slight embrittlement, tended in the same environment, to form numerous cracks that could be observed only with the aid of low-power (10X) magnification. These cracks were shallow and very blunt, and were not sufficiently deep to initiate fracture as indicated by the fact that there were well-formed shear lips completely around the fractures. Fracture, therefore, initiated within the specimens in hydrogen as well as in air and helium environments.

In high-pressure hydrogen, metals in category 2, severe embrittlement, formed many surface cracks that were easily observed without the aid of magnification. Some of the cracks were fairly deep, and metallographic examination showed that the cracks blunted and were terminated by branching. These surface cracks were fracture initiation sites, and it was obvious from inspection of the fracture that the crack origins were at the surface. There were no shear lips formed on the severely embrittled specimens tested in high-pressure hydrogen, indicating that fracture initiated at the surface rather than inside the specimens.

Metals in category 1, extreme embrittlement, were likely to contain only one surface crack when tested in hydrogen, and this crack initiated catastrophic failure. Shear lip formation on some of the specimens was complete except at the region of the surface crack. Thus, fracture in hydrogen initiated from the crack and propagated inward; final failure, at the side opposite the origin of the surface crack, occurred by ductile shear.

There were two characteristics of the surface cracks formed in hydrogen for metals in all embrittlement categories. These are: (1) crack initiation was a function of degree of plastic deformation, and (2) the type of cracks were independent of hydrogen pressure. It was observed that surface cracks were generally restricted to the necked-down region and that the cracks were most numerous and deepest close to the fracture. Those metals tested at various hydrogen pressures (ASTM A-302, a category 2 metal, and Inconel 718, a category 1 metal) had the same type of surface cracking at all hydrogen pressures. The degree of plastic deformation required for their formation, however, decreased with increasing hydrogen pressure.

Posttest examination of the notched specimens was informative for ascertaining fracture origin and fracture characteristics in the various environments. The part of the fracture affected by the hydrogen environment appeared visually as a partial or complete ring around the fracture periphery. This ring was analogous to the surface cracks that initiated fracture in the unnotched specimens. Electron fractography examination showed that this outer ring of the fracture was brittle, while the remainder of the fracture was ductile. On the other hand, the outer region of iron-, nickel-, and titanium-base alloys was ductile when notched specimens were tested in air or helium environments.

Electron fractography examination showed that the fractures of all notched specimens embrittled by the gaseous hydrogen environment had the following features:

1. Surface cracking was observed on the machined surface at the machined surface/fracture surface interface of most specimens examined.

2. The machined surface/fracture surface interface was brittle at the region of fracture initiation.

3. Initial crack propagation was brittle. The brittle regions were transgranular on steels and titanium-base alloys, and intergranular on the nickel-base alloys and welded low alloy steel specimens containing a notch in the weld metal (Ref. 2). Secondary cracking was usually present in the brittle region. This secondary cracking probably corresponds to the branching of the surface cracks observed in unnotched specimens.

4. The inner region and fracture periphery across from the origin was ductile and appeared the same as the notched fractures in helium or air.

With respect to the examination of titanium and Ti-6Al-4V tested in hydrogen, there was no indication of any of the features characteristic of internal hydrogen embrittlement, i.e., intergranular attack and hydride phase formation. On the contrary, the fractures of these specimens appeared very much like the fractures of low alloy steel specimens tested in hydrogen. The experimental results from several of the phases in this program served to clarify certain aspects of the hydrogen-environment embrittlement mechanism, a discussion of which is contained in the General Discussion section.

GENERAL DISCUSSION

In this section, the results of all the various phases in this program are considered collectively to identify the general characteristics of hydrogen-environment embrittlement and clarify its mechanism.

In all cases in which a metal was found to be subject to hydrogen-environment embrittlement, fractures initiated at the surface of the metal in the hydrogen environment; however, in air or helium environments, the fractures originated within the specimen. This was shown by electron fractographic examination of machined surface fracture surface interfaces. These interfaces were brittle on specimens fractured in hydrogen and in hydrogen-contaminated helium, but were ductile on specimens tested in air and pure helium environments. It was also evident from visual examination of the fractures of specimens tested in high-pressure hydrogen that the surface cracks which initiated fracture had their origin at the metal surfaces. The lack of a sheer lip at the fracture origin of the specimens tested in hydrogen was also indicative of fracture nucleation at the surface.

There is evidence that fracture in hydrogen environments is preceded by rupture of the surface oxide. It was shown that abrading initiates surface cracking in 10,000-psi hydrogen. Rupture of the surface oxide can also occur during tensile deformation and the first indication of surface cracking in hydrogen occurs only after yielding. Decreasing the yield strength/ultimate strength ratio increases embrittlement, providing other variables such as chemistry and microstructure remain constant.

In most instances, catastrophic fracture in hydrogen did not proceed immediately after crack nucleation, and the degree of embrittlement was generally determined by the material's ability to blunt the cracks that initiated on the surface after a critical degree of deformation. Two of the slightly embrittled materials were observed to contain numerous

cracks when tested in hydrogen; but the cracks were so shallow and blunt that they did not initiate failure. On the other hand, often there was only one surface crack observed in extremely embrittled specimens, and it propagated to failure.

Even in notched specimens, fracture did not necessarily proceed immediately after crack initiation. It was observed that crack propagation of notched specimens of ASTM A-517 (a severely embrittled material) proceeded stepwise in hydrogen as the stress was increased; but in air, fracture proceeded instantly to failure after the first sign of crack nucleation. Studies of the relationship between critical strain and crack initiation, the effect of stress intensity on the time spread between crack initiation and failure, and the variation of these parameters with degree of embrittlement are still needed to obtain a coherent picture of embrittlement.

It was shown that a poor correlation existed between the relative susceptibility of metals to hydrogen-environment embrittlement and internal-hydrogen embrittlement. The poorest correlation is for nickel and the high-strength nickel-base alloys (Inconel 718 and Rene 41). Commercially pure nickel is severely embrittled and the nickel alloys are extremely embrittled by high-pressure hydrogen, but they are not embrittled by internal hydrogen introduced by electrolytic charging.

Titanium and titanium-base alloys are embrittled by both exposure to gaseous hydrogen and from internal hydrogen. Posttest examination however indicates that the mechanisms of embrittlement are different. Internal-hydrogen embrittlement of titanium (e.g., commercially pure titanium) and $\alpha - \beta$ titanium alloys (e.g., Ti-6Al-4V) results from hydride formation at grain boundaries. Surface cracks and fractures in commercially pure titanium and Ti-6Al-4V specimens tested in 10,000-psi hydrogen do not contain these features.

There was no indication of a hydride phase associated with any of the fractures, and the fractures were transgranular. In fact, the fractures formed in titanium and Ti-6Al-4V in 10,000-psi hydrogen are very similar in appearance to the fractures formed in the low alloy steels in 10,000-psi hydrogen.

There are three features of hydrogen-environment embrittlement that suggest the embrittlement mechanism involves adsorbed rather than absorbed hydrogen:

1. Embrittlement occurs very rapidly. There is very little time between the beginning of crack propagation, which generally occurs at approximately the time that the maximum load is reached (i.e., at the beginning of necking), and final failure.
2. Embrittlement appears to be independent of the duration of exposure to hydrogen. Specimens held in 10,000-psi hydrogen at a stress midway between their yield and ultimate strengths for 100 days duration were no more embrittled than specimens tested immediately after the environment was established. Held stresses were in some cases close to the ultimate strength. A more definitive experiment, however, would be to hold for sustained periods at a stress level above that required for crack initiation.
3. There are indications that the main effect of hydrogen pressure on embrittlement is through its effect on the rate of movement of hydrogen down the crack to the crack tip to keep up with the propagating crack. It has been observed for Inconel 718 that the fractures in hydrogen-contaminated helium (~1 atmosphere hydrogen pressure) have the same appearance as the fractures produced in 10,000-psi hydrogen, although the degree of embrittlement was considerably different.

The results of fatigue tests indicated that crack propagation in 1000-psi hydrogen was dependent upon the rate at which hydrogen movement to

the crack tip could keep up with the propagation of the crack. Crack propagation in 10,000-psi hydrogen, however, was evidently not limited by the rate of hydrogen movement down the crack. This would suggest that embrittlement is essentially independent of gas pressure at sufficiently slow strain rates, provided contamination of the crack surface by impurities does not occur. A mechanism based on adsorbed hydrogen would better explain hydrogen pressure independence than a mechanism based on absorbed hydrogen. Certainly there is a need for establishing the relationship between embrittlement and strain rate.

GENERAL CONCLUSIONS

Metals studied in this program can be classified into the following categories with regard to their susceptibility to embrittlement in 10,000-psi hydrogen:

1. Extreme embrittlement (i.e., large reduction of notched and unnotched strength and ductility): High-strength steels and nickel-base alloys
2. Severe embrittlement (i.e., considerable reduction of notched strength and unnotched ductility): Ductile, lower-strength steels, Armco Iron, pure nickel, and titanium-base alloys
3. Slight embrittlement (i.e., small reduction of notched strength): Nonstable AISI type 300 series stainless steels, beryllium-copper, and pure titanium
4. Negligible embrittlement: Aluminum alloys, stable austenitic stainless steels, and copper

Following are conclusions concerning the influence of several variables on the degree of hydrogen-environment embrittlement:

1. The degree of hydrogen-environment embrittlement of low alloy steels is independent of time or stress of holding in hydrogen.
2. The degree of hydrogen-environment embrittlement is more severe at higher hydrogen pressures but can still be considerable at lower pressures with effects extending down to 1-atmosphere pressure.
3. The degree of hydrogen-environment embrittlement in low alloy steels is a maximum for notches of intermediate stress concentration factor ($K_t \simeq 6$ to 9) and decreases for sharper and duller notches.

4. The 1000-cycle fatigue strengths of low alloy steels are considerably reduced in high-pressure hydrogen from that in high-pressure helium.

5. The degree of hydrogen-environment embrittlement of low alloy steels increases as the yield strength/ultimate strength ratio decreases, provided other variables such as composition, microstructure, and ultimate strength are essentially constant.

Following are conclusions concerning the fracture characteristics and mechanism of hydrogen-environment embrittlement:

1. Abrasion promotes surface cracking during subsequent tensile deformation in high-pressure hydrogen.

2. The fracture characteristics, as observed by electron fractography, are basically the same for iron-, nickel-, and titanium-base alloys fractured in high-pressure hydrogen.

3. Fracture initiation in a hydrogen-environment embrittled metal occurs in hydrogen at the surface after a critical amount of plastic deformation has taken place.

4. The degree of hydrogen-environment embrittlement of a metal is more a function of the ability of the metal to blunt cracks in hydrogen than of the susceptibility of the metal to form surface cracks.

5. The rate of crack propagation in hydrogen at pressures less than 1000 psi is a function of the rate of movement of the hydrogen down the propagating crack to the crack tip.

6. Hydrogen-environment embrittlement is probably associated with adsorbed rather than absorbed hydrogen.

PHASE I: INFLUENCE OF TIME OF EXPOSURE TO HIGH-PRESSURE HYDROGEN ON DEGREE OF EMBRITTLEMENT OF METALS

INTRODUCTION

A number of the phases in this program involved the tensile testing of specimens in high-pressure hydrogen to screen alloys for susceptibility to hydrogen-environment embrittlement or to determine the influence of various parameters on hydrogen-environment embrittlement. Prior to initiating these test segments, Phase I was conducted to aid in establishing the tensile test procedure to be used. Specifically, tests were performed to determine the effect of exposure time of unloaded (except that due to gas pressure) specimens to 10,000-psi hydrogen on the degree of embrittlement by that environment. Exposure times of up to 24 hours were investigated. Three alloys (ASTM A-302, AISI type 310 stainless steel, and Ti-6Al-4V) were selected for testing in Phase I because these materials have different responses to high-pressure hydrogen environments and thus are generally representative of the wide variety of alloys to be tested later.

Initially, the goal of Phase I was to establish the minimum time of exposure to the high-pressure hydrogen environment that would give the maximum embrittlement and would thus be incorporated in the test procedure used in subsequent phases. As will be discussed, it was found necessary to extend Phase I to include an investigation into the effect of evacuation of test vessels prior to pressurizing with hydrogen on the degree of hydrogen-environment embrittlement.

EXPERIMENTAL PROCEDURES

Materials

Alloys tested in this phase were ASTM A-302, AISI type 310 stainless steel, and Ti-6Al-4V. The chemical compositions, heat treatments, and

mechanical properties of the test materials are presented in Tables 1, 2, and 3, respectively. Alloy Ti-6Al-4V was tested in both the annealed and solution-treated and aged (STA) conditions.

Specimens of ASTM A-302 were prepared from the remainder of the 5-1/8-inch-thick plates used in the previous program (Ref. 2). The tensile specimens tested in the previous program were prepared from only the surface layers of those plates. Although the large plates were highly laminated, it was possible to prepare sufficient tensile specimens for this phase from the surface of the remainder of those plates. To ensure uniform properties, the material cut from the large plates was reheat treated, as given in Table 2. Specimens were prepared with the longitudinal axis oriented parallel to the plate rolling direction.

Tensile Specimen Design

Tensile specimens were basically of the same dimensions as the specimens used previously (Ref. 2). The cylindrical test specimens were 9 inches long and 0.306 inch in diameter, and were threaded for 1 inch on each end. The surfaces were machined to a 16-rms finish. Unnotched specimens contained 1.25-inch-long, 0.250-inch-diameter reduced sections. Notch specimens contained a 60-degree V notch placed midway along the specimen. The specimen diameter at the bottom of the notch was 0.150 ±0.001 inch.

A root radius of 0.00095 ±0.0001 was used to obtain a stress concentration factor (K_t) of approximately 8.4. The stress concentration factor was calculated according to Peterson (Ref. 4).

The reduced section of the unnotched AISI type 310 stainless steel tensile specimens was 0.150-inch diameter instead of the 0.250-inch diameter of the other specimens. This change was necessary because loads sufficient to fracture a 0.250-inch-diameter reduced section of this material would also plastically reduce the larger 0.306-inch-diameter section and cause leakage at the sliding seal.

TABLE 1

CHEMICAL COMPOSITIONS OF PHASE I MATERIALS

Material	C	Mn	P	S	Si	Ni	Cr	Cu	Al	Ti	Mo	Fe	Sn	V	Other
ASTM A-302-56 Gr.B Modified with Nickel (5-1/2-inch plate)	0.25	1.31	0.016	0.021	0.27	0.63						Bal.			B, 0.003
AISI Type 310 Stainless Steel (3/8-inch rod)	0.05	1.34	0.013	0.014	0.64	20.39	24.83	0.11			0.14	Bal.	0.010		Pb, 0.001
Ti-6Al-4V Annealed (3/8-inch rod)	0.024								6.0	Bal.		0.15		4.1	N_2, 0.0241 H_2, 0.0081 O_2, 0.191
Ti-6Al-4V STA (3/8-inch rod)	0.023								6.4	Bal.		0.15		4.2	N_2, 0.014 H_2, 0.008 O_2, 0.14

TABLE 2

HEAT TREATMENT OF PHASE I MATERIALS

Material	Heat Treatment by Supplier (As-Received Condition)	Hardness	Heat Treatment by Rocketdyne
ASTM A-302-56 Gr.B, Modified With Nickel	Not furnished		Annealed 1650 F 1 hour; water quenched; Tempered 1270 F 1 hour; air cooled
AISI Type 310 Stainless Steel	Not furnished; annealed	R_b 79	None
Ti-6Al-4V Annealed	Not furnished; annealed	R_c 35	None
Ti-6Al-4V-STA	Solution treated 1750 F 1 hour, water quenched; aged 4 hours at 1000 F	R_c 40	None

TABLE 3

MECHANICAL PROPERTIES OF PHASE I MATERIALS
(SUPPLIER CERTIFICATION)

Material	Tensile Strength, ksi	Yield Strength, ksi	Reduction of Area, percent	Elongation, percent	Hardness
ASTM A-302-56 Gr.B, Modified With Nickel (5-1/2-inch plate)	114.0[a]	98.0	68.0	21.0	
AISI Type 310 Stainless Steel (3/8-inch rod)	86.0	34.0	60.6	45.7	R_b 79
Ti-6Al-4V Annealed (3/8-inch rod)	159.0	140.0	50.0	18.0	R_c 35
Ti-6Al-4V STA (1/2-inch rod)	173.0	163.0	47.0	17.0	R_c 40

[a] Properties determined at Rocketdyne prior to heat treatment

A number of notched ($K_t \simeq 8.4$) tensile specimens were received from machining with the notch radius out of tolerance. These notches were then reground to obtain the desired notch radius but, in so doing, the root diameter was somewhat reduced, thus lowering the notch concentration factor. The long time delay required to have the specimens fabricated made it necessary to test most of the specimens with the smaller root diameter. The notch concentration factor for each specimen is included with the test data in the Appendix so that effects resulting from deviations in the notch concentration can be observed.

Apparatus

The apparatus used to perform tensile tests on specimens in high-pressure gaseous environments for Phase I and other phases consisted of high-pressure, high-purity gas (hydrogen or helium) supply systems and tensile testing devices. Basic equipment used for the tensile tests was developed during the previous program and was described in detail in Ref. 2. A number of modifications were made to the equipment for this program to increase the accuracy of the tensile test data, to improve gas purity, and to increase the number of tensile test devices and the load capacity of some of them. These modifications were made during the earlier part of the program. Many of the modifications were occasioned by requirements for the other phases. However, for simplicity, the apparatus used for tensile testing as it is now constituted, with all modifications, will be described here.

High-Pressure Gas Supply Equipment. High-pressure hydrogen and helium supply systems consisted, in order, of a purification system, a compressor, high-pressure gas storage receivers, and the pressure regulators, gages, valves, and lines required for each test system. The purification system, compressor, and receivers were common to all the test systems for all of the phases in this program.

High-purity bottled hydrogen with less than 5 ppm total impurities was used. The hydrogen was further purified by means of an Engelhard De Oxo

unit, which converts the oxygen in the hydrogen to water vapor, followed by BaO desiccant to remove the water vapor. Final purification was achieved in the previous program with Linde 5A molecular sieve maintained at boiling nitrogen temperatures. Early in this program, the molecular sieve was replaced by a combination of activated charcoal and activated alumina which was maintained at boiling nitrogen temperatures. This replacement was recommended by Chemical Analysis personnel in the Research Division at Rocketdyne on the basis of extensive experience with hydrogen analyses. Helium was passed through the same system for purification.

After purification, the hydrogen or helium was pressurized to the desired pressure, 15,000 psi for 10,000-psi tests, in the storage vessels. For the previous program and the early part of this program, the gases were pressurized with a Haskell Model AG 152 air-operated, non-lubricated piston compressor. It was found in the previous program (Ref. 2) that this compressor was a serious source of contamination, especially in long-time tests requiring a number of pressurizations by the compressor. Compressor contamination was minimized by enclosing it in a box containing a flowing argon purge. However, because of the necessity for maintaining the highest hydrogen purity, it was decided to replace the piston compressor with a diaphragm compressor. In theory, at least, there should be no contact in a diaphragm compressor between the gas being pressurized and air or other contaminants. Therefore, a Pressure Products Industry Type 3033 triple diaphragm compressor with leak detector and alarm system was installed. The leak detector senses any leak in one of the diaphragms and shuts down the compressor before the other diaphragms rupture, thus preventing contamination. Purity of the hydrogen after pressurization with the diaphragm compressor was analyzed to be <0.5 ppm oxygen, 2.6 ppm nitrogen, <5 ppm total hydrocarbons, <0.5 ppm CO and CO_2, and <0.5 ppm H_2O. The impurity content in hydrogen in the storage vessels did not increase during long-duration tests as it had with the piston compressor in the previous program. The Phase I tensile tests, and a few of the short-time tensile tests under other phases, were performed before the diaphragm compressor was installed.

After pressurization, the hydrogen or helium passed into two separate tensile test systems, each with its own storage vessel. These two systems as they were used in this program are shown schematically in Fig. 1 and 2 . Because of the large number of tensile tests required for the various phases of this program, the capacity of the first system was increased from 10 tensile test stations available for the previous program to the 12 stations shown in Fig. 1 . The control console of the second system was completely reworked to provide for better pressure regulation and for considerably less maintenance for a leak-free system. The hand-loaded pressure regulator used previously on the second system was replaced with a Fisher Governor regulator which activates an Annin Domotor valve as on the first system. Thus, as used in this program, the two systems were identical.

Tensile Test Devices. As noted above, the tensile testing apparatus consisted of two systems, each having 12 individual tensile test stations. The individual test devices are described below.

Each end of a tensile specimen extended through sliding seals at the ends of a small AISI type 316 stainless steel pressure vessel, as shown schematically in Fig. 3 . Design of the sliding seals was somewhat modified from that used in the previous program to eliminate metal-to-metal contact.

Each specimen and test vessel was held in a test frame containing a spring, as shown in Fig. 4 . A ball-and-socket joint was used at each end of the specimen for proper alignment in the test frame. A tensile load was applied to the specimen by compressing the spring with a hydraulic ram loading device (Fig. 5). This loading device was moved from station to station to perform the tests and is shown in place for a test in Fig. 6 .

As shown in Fig. 5 , a Baldwin Emery Motion Pacer Indicator is mounted on the hydraulic power console so that the rate of movement of the ram can

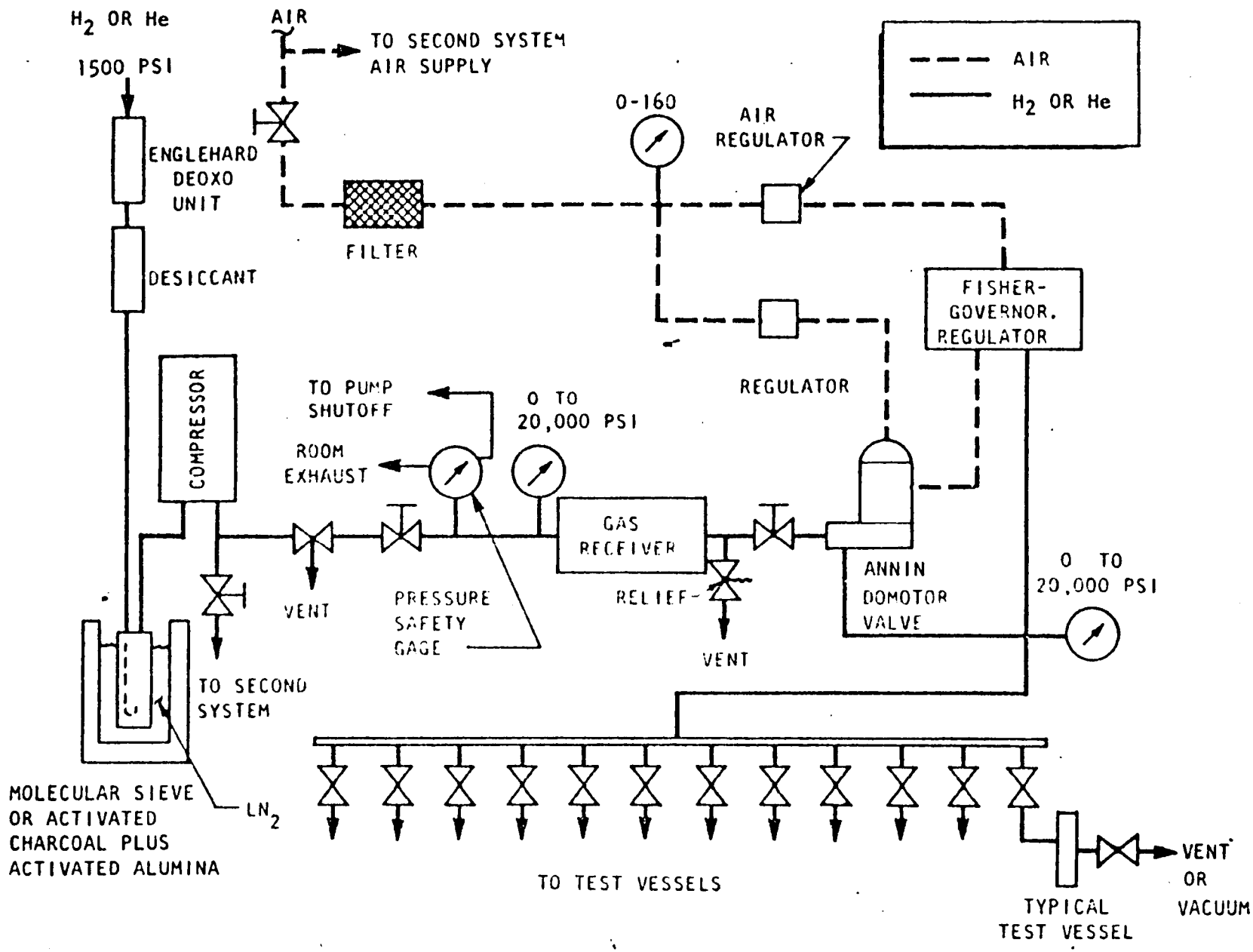

Figure 1. First High-Pressure Gaseous Supply System Schematic

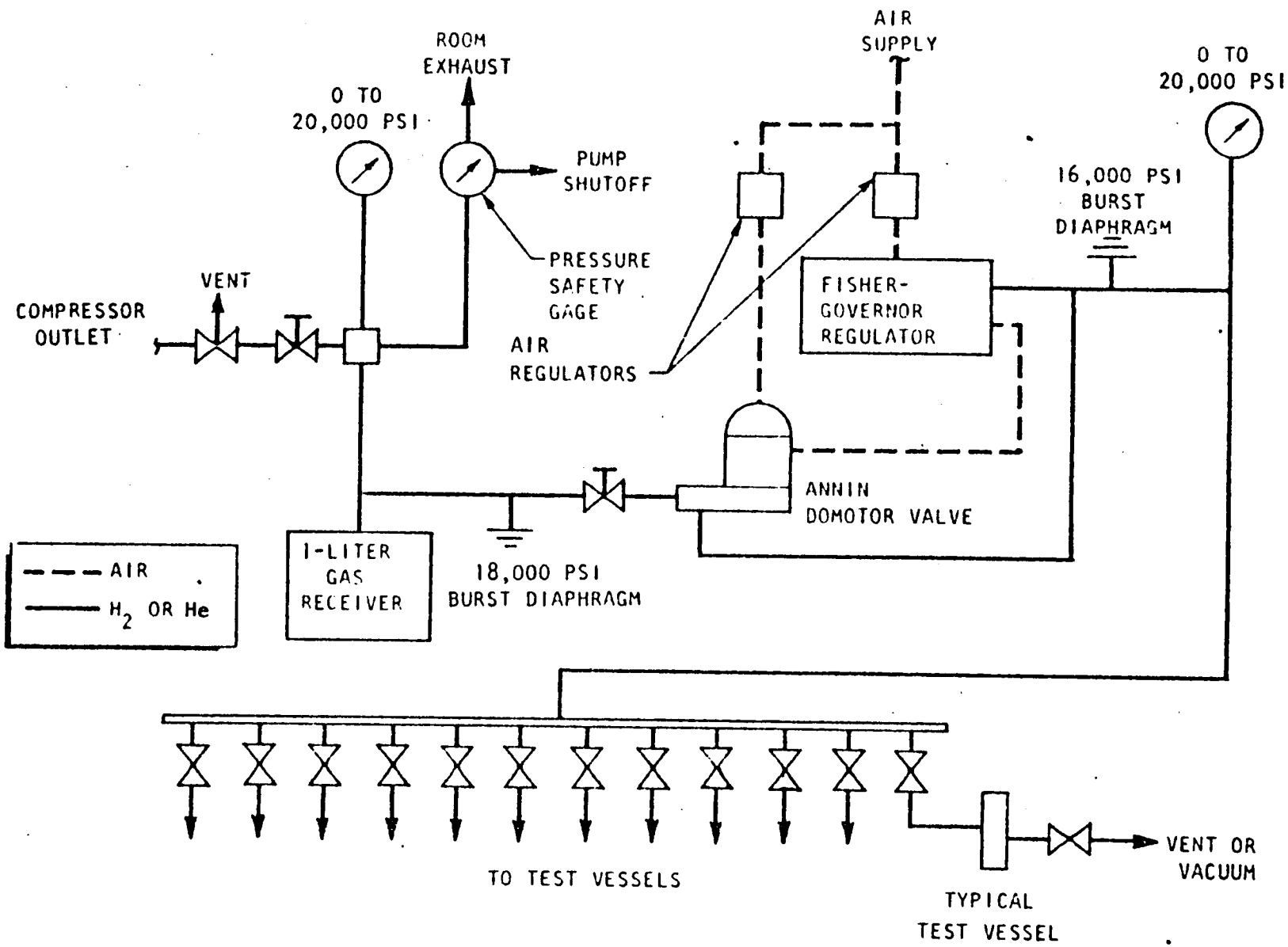

Figure 2. Second High-Pressure Gaseous Supply System Schematic

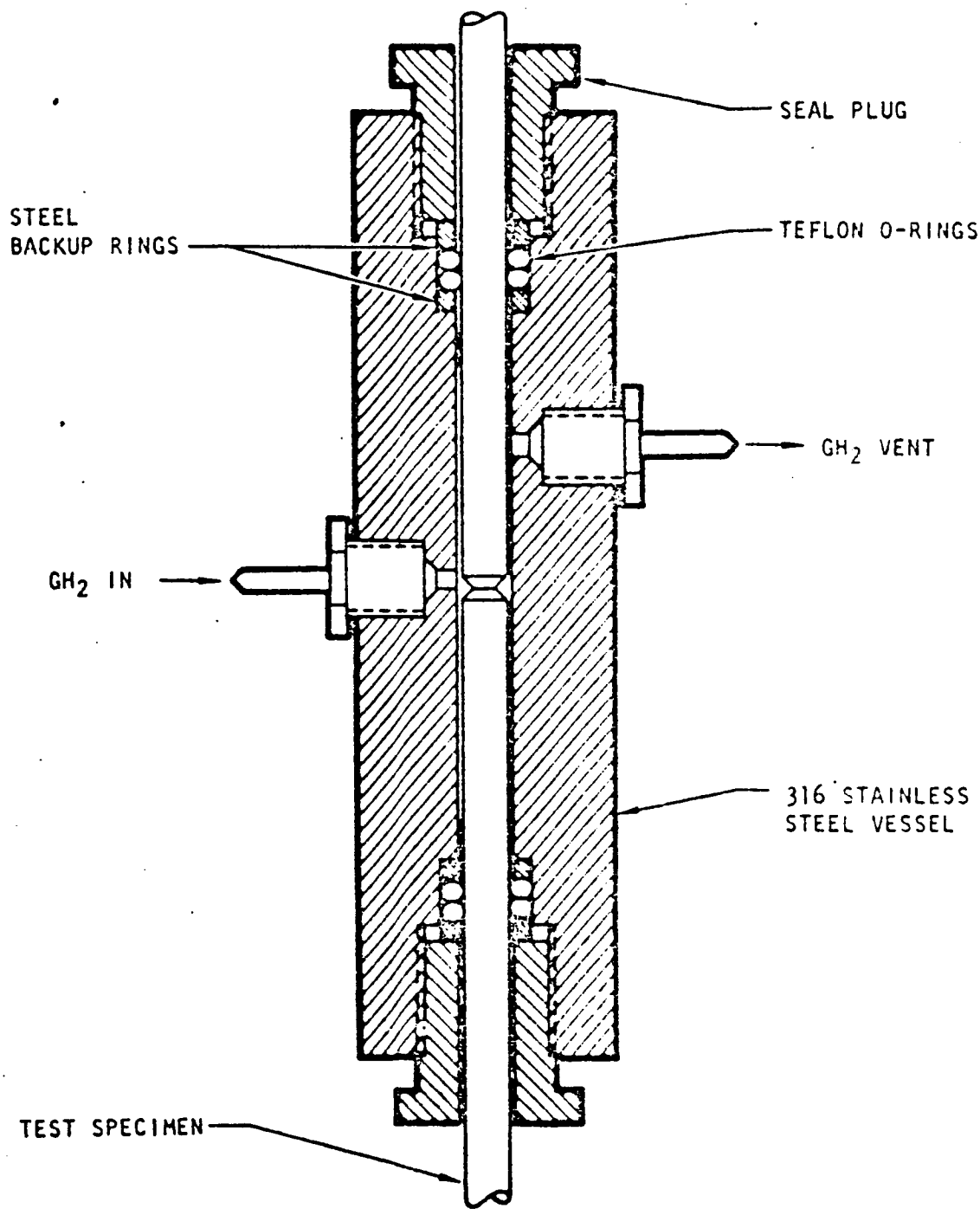

Figure 3. Test Vessel With Specimen (Full Scale)

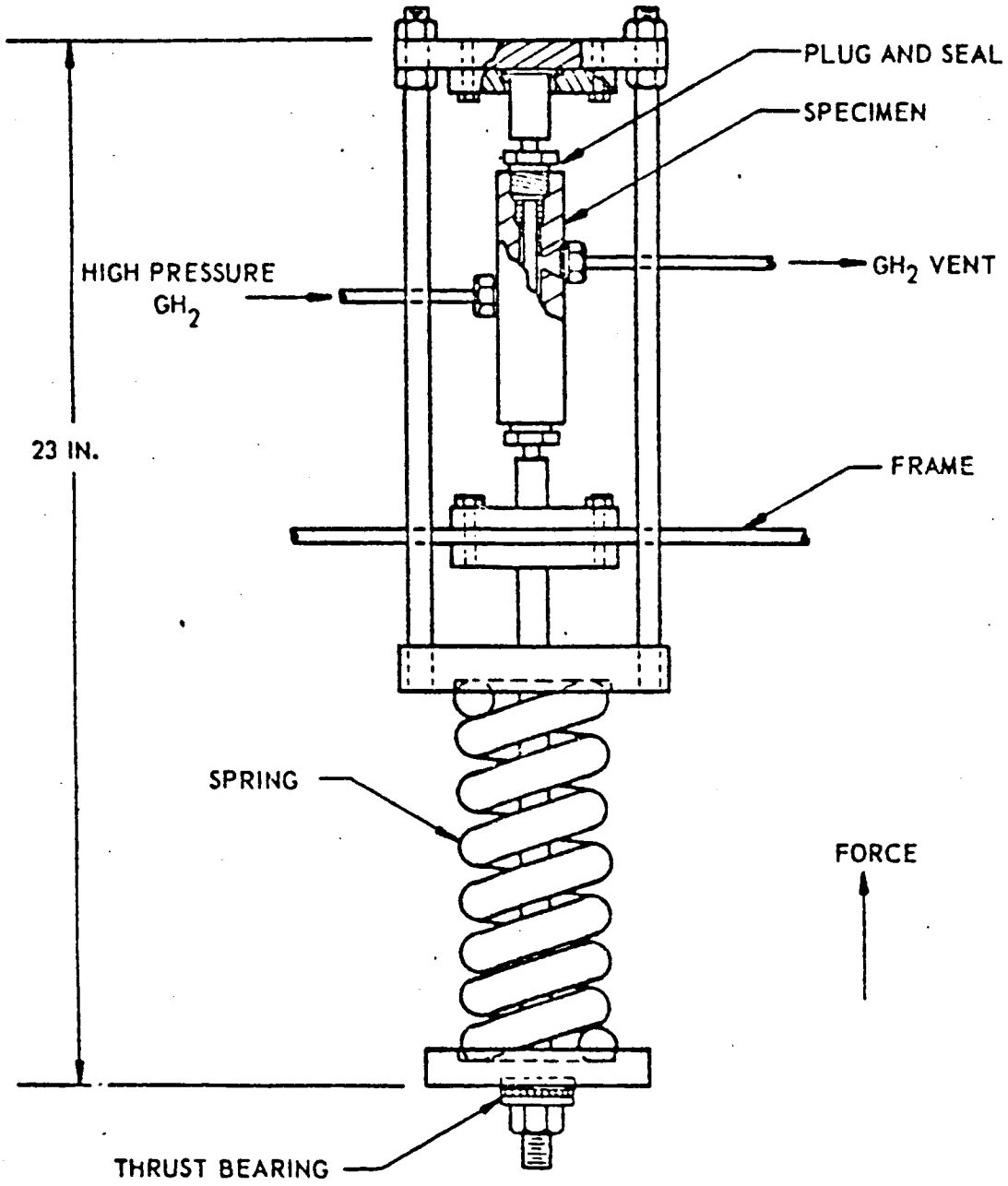

Figure 4. Test Vessel and Static Loading Device

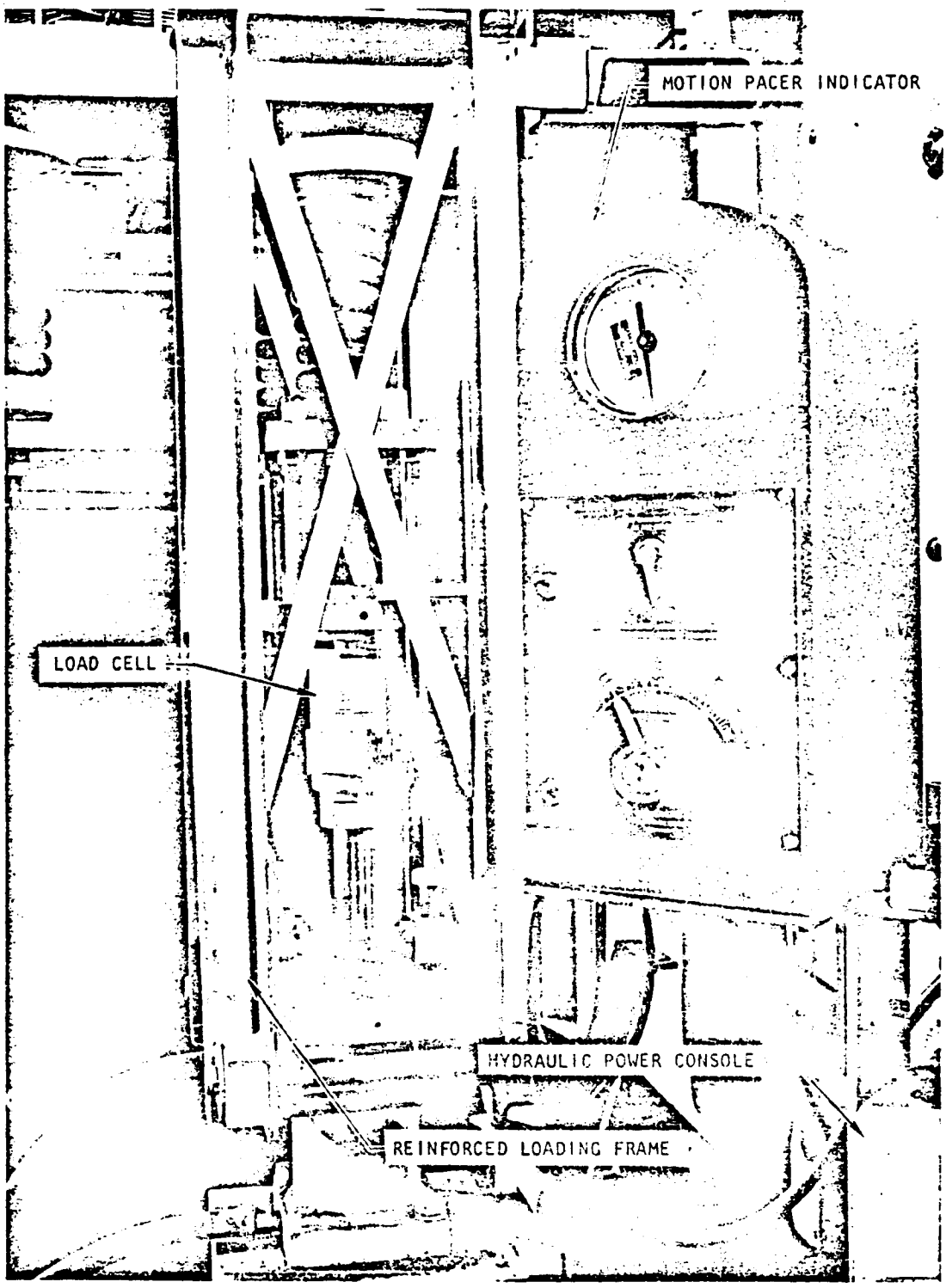

Figure 5. Hydraulic Loading Device

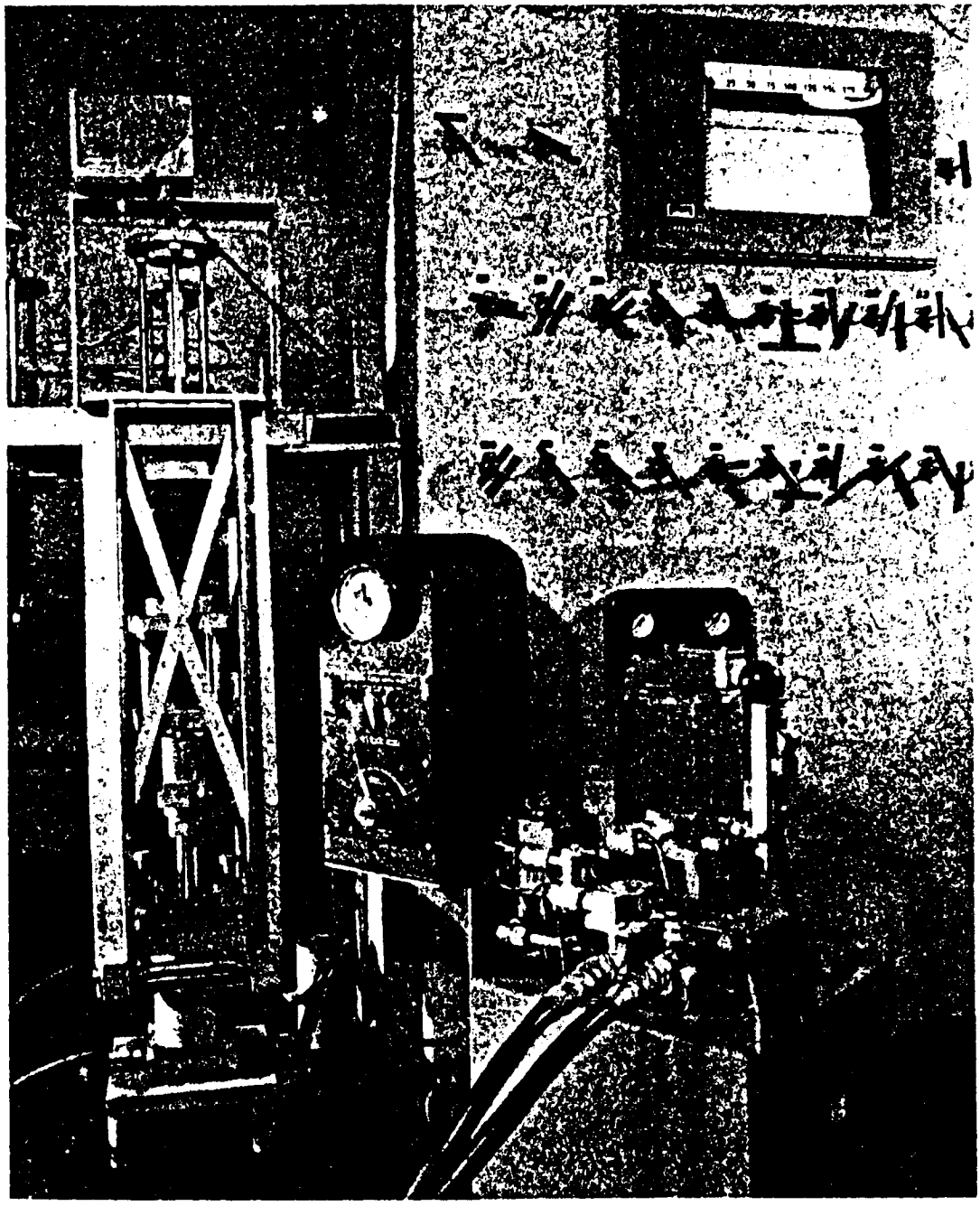

1CT91-2/11/69-C1A

Figure 6. Mechanical Testing System

be observed and controlled simultaneously; rate of movement is adjustable over a wide range. The motion pacer is attached to the lower spring bearing plate for load pacing or, as shown in Fig. 6, to the top of the plate which transmits the load to the upper end of the specimen for strain pacing.

In the previous program, load applied to a specimen was determined by measuring spring deflection. It was found that this was a source of considerable error. Therefore, as shown in Fig. 5, a load cell was added to the hydraulic loading system so that the load is applied to the spring through the load cell. This load cell was calibrated by using a calibrated load cell in place of a tensile specimen in the spring-loaded test frame. Tests showed that the relationship between the two load cell outputs was linear and that the load indicated on the load recorder was within 15 pounds of the true load indicated by the calibrated load cell. Load was recorded from the load cell on a strip chart recorder which had a 10,000 pound maximum load recording capability. Very few specimens required a greater load than 10,000 pounds to achieve failure; in these cases the load was determined by measuring the output from the load cell with a strain indicator. Yield strength of unnotched specimens was considered to be the point of departure from linearity of a load vs time recorder curve. For the high-strength specimens requiring the use of the strain indicator, an indication of yield strength was obtained by noting the point at which there was a considerable reduction of the rate at which the load was increasing. Yield strengths so obtained were considered to be of low accuracy.

The hydraulic loading frame used in the previous program had a tendency to tilt during loading because the ends of the loading springs were slightly out-of-parallel. This tilting led to small torque and bend strains on the test specimen. Although these strains were determined to be of approximately the same magnitude as those occurring when the same type of specimen was pulled in a Baldwin Universal Testing Machine, it was believed desirable to reduce them to as low a value as possible.

Therefore, for this program, the hydraulic loading frame was made considerably stronger and more rigid to minimize the tilting.

The tensile test devices used to perform the tests on the high-strength steel specimens had to be capable of transmitting up to 15,000 pounds load, and the basic testing frame was believed to be in danger of buckling under a load of this magnitude. Load capacity of six of the tensile test devices was therefore increased by increasing the diameter of the rods and bolt fasteners.

A second problem was the limited load-carrying capacity of the coil springs. Maximum load capacity coil springs obtainable in a size that would fit the load frame required only 10,000 pounds to effect maximum deflection. Belleville springs were the only springs available with adequate load capacity and a size small enough to fit the test frame. Thus, Belleville springs were installed on the six heavy duty tensile test devices. These springs have an advantage over the coil springs in that they effect better alignment between the top and bottom plates supporting the springs. Friction between the Belleville washers does not affect load transfer. However, any friction that exists between the Belleville springs and the rod extending through the spring center line would be transferred into the table frame instead of to the specimen and, thus, an error in the load measurement would occur. To prevent rubbing between the springs and the rod and still retain spring alignment, the springs were aligned in a surrounding cylinder.

Test Procedure

In this phase, unnotched and notched ($K_t \simeq 8.4$) specimens of ASTM A-302, AISI type 310 stainless steel, and Ti-6Al-4V were exposed to 10,000-psi hydrogen for various lengths of time and then were tensile tested to failure without removing them from that environment. No load other than that caused by the gas pressure was applied to the specimens during the periods of exposure to the 10,000-psi hydrogen. ASTM A-302 and AISI type

310 stainless steel specimens were exposed to the 10,000-psi hydrogen for 0, 1, 8, and 24 hours before tensile testing to failure. Ti-6Al-4V (annealed and solution-treated and aged) specimens were exposed to the 10,000-psi hydrogen for 0, 1 (only for unnotched, annealed specimens), and 24 hours before tensile testing to failure. Specimens of the three materials were also tensile tested to failure in 10,000-psi helium for comparison purposes.

Time of exposure to 10,000-psi hydrogen was measured from the time at which the high-purity 10,000-psi hydrogen environment was established in the test vessels. For the initial tests in this phase, air was purged from the test vessels by using three pressurization-depressurization cycles with hydrogen (or helium) from 10,000 psi to approximately 1 atmosphere; gas pressure was then brought up to 10,000 psi.

As a part of this phase, the effect of evacuation purging was investigated. This treatment consisted of evacuation of the test vessel to approximately 300 microns and back-filling to 100-psi hydrogen (or helium) three times, followed by the three-cycle pressurization-depressurization treatment described above.

Unnotched specimens were strain paced at 0.002/min from 0 load to yield and at 0.04/min from yield to ultimate. Notched specimens were load paced at a rate corresponding to a strain rate of 0.0007/min.

As noted in the previous Apparatus section, load measured by the load cell was recorded by a strip chart recorder. The yield strength of unnotched specimens was considered to be the point of departure from linearity on the load-versus-time curve.

Calculation of the tensile stress for tests conducted in high-pressure environments required that the sliding seal friction and tensile force obtained from the high-pressure gas be considered. Static and dynamic friction forces were 83 and 61 pounds, respectively. Static friction was

used to compute the notch strength and unnotched yield strength, and dynamic friction was used to calculate the unnotched ultimate tensile strength. These friction forces were subtracted from the applied load.

Load exerted by the gas pressure for notched specimens was equal to the pressure times the difference in specimen area at the sliding seals and at the base of the notch. For unnotched specimens, the maximum combined tensile load was assumed to occur prior to necking; thus the load exerted by the gas pressure was assumed equal to the gas pressure multiplied by the difference between the area at the seals and the area immediately adjacent to the necked-down region. Load exerted by the gas pressure was added to the load indicated by the load cell.

The percent elongation of the unnotched specimens was measured between punch marks placed two inches apart outside of and bridging the reduced section. In calculating the percent elongation, it was assumed that essentially all elongation took place in the reduced section. The reduction of area of the unnotched specimens was determined by measuring the cross section with a micrometer. The reduction of area of notched specimens was determined by using an optical comparator to measure the cross section of the notch before and after testing.

Tests were performed in triplicate in 10,000-psi hydrogen and in duplicate in 10,000-psi helium.

RESULTS AND DISCUSSION

Results of the Phase I tests are presented in Table 4. These data are the averages of three tests for the tests in hydrogen and two tests for the tests in helium. Data from the individual tests are contained in Appendix Tables I-1 and I-2 for ASTM A-302, I-3 and I-4 for AISI type 310 stainless steel, and I-5 and I-6 for Ti-6Al-4V.

For the AISI type 310 stainless steel, there was no observable difference between the strength and ductility of unnotched specimens in 10,000-psi hydrogen and that in 10,000-psi helium. Slightly lower strength and ductility was observed in notched specimens in 10,000-psi hydrogen compared to 10,000-psi helium. This small degree of hydrogen-environment embrittlement was not affected by the time of exposure. After testing, both the notched and unnotched AISI type 310 stainless steel specimens were checked with a fairly strong test magnet, and no indication of magnetism in the specimens was found. Thus, there was no gross phase transformation during straining, although some transformation to martensite could have occurred in localized regions.

Unnotched specimens of ASTM A-302 had approximately 50 percent lower reduction of area and slightly lower elongation in 10,000-psi hydrogen than in 10,000-psi helium. No significant difference were noted between the tensile strength of unnotched specimens in 10,000-psi hydrogen and in 10,000-psi helium. For all exposure times, the strength of notched ASTM A-302 specimens was approximately 22 percent lower in 10,000-psi hydrogen than in 10,000-psi helium. Ductility of the notched specimens was also considerably reduced in hydrogen. The degree of 10,000-psi hydrogen environment embrittlement of ASTM A-302 was not significantly different for the different hydrogen exposure times.

As noted in the Materials section, the ASTM A-302 specimens used in this phase were taken from the same plate as were the specimens tested in the previous program. It is instructive to compare the results of the tests

TABLE 4

EFFECT OF TIME OF EXPOSURE TO HYDROGEN ON THE TENSILE PROPERTIES OF THREE ALLOYS (ZERO HOLD STRESS)

Material	Unnotched or Notched	Hold Time, hours	Strength in 10,000-Psi Helium		Strength in 10,000-Psi Hydrogen		Ductility			
							Percent Elongation		Percent Reduction of Area	
			Yield, ksi	Ultimate, ksi	Ultimate, ksi	Percent Change from Helium	10,000-Psi Helium	10,000-Psi Hydrogen	10,000-Psi Helium	10,000-Psi Hydrogen
AISI Type 310 Stainless Steel	UN	0		77	78		56	56	64	62
		1			78			56		66
		8			79			56		68
		24			83			55		69
	N	0		116	108	-7			20	18
		1			112	-3				17
		8			119	+3				15
		24			113	-3				17
ASTM A-302 Gr.B Modified with Nickel	UN	0		119	116		19	17	66	33
		1			119			16		37
		8			118			16		37
		24			118			17		33
	N	0		227	176	-22			15	2.8
		1			173	-24				4.0
		8			179	-21				3.5
		24			182	-20				3.7
Ti-6Al-4V Annealed	UN	0	132	156	159		15	15	48	48
		1			158			16		48
		24			151			15		51
	N	0		243	183	-25			2.2	1.9
		24			220	-9				3.0
Ti-6Al-4V STA	UN	0	156	164	171		13	13	46	50
		24			167			11		46
	N	0[a]		227	230				2.2	2.3
		0[b]			158	-30				2.2
		0[c]			136	-40				1.1
		24[c]			192	-15				2.5

[a] First tests. Test vessels purged by 3-cycle pressurization (10,000 psi)-depressurization (1 atmosphere) hydrogen flushing
[b] Test vessels purged by 3- or 15-cycle pressurization (10,000 psi)-depressurization (1 atmosphere) hydrogen flushing
[c] Test vessels purged by evacuating to approximately 300 microns and backfilling with hydrogen to 100 psi 3 times followed by 3-cycle pressurization (10,000 psi)-depressurization (1 atmosphere) hydrogen flushing

on this material under the two programs. It should be recalled that the material used in this program was reheat treated, which resulted in higher tensile strength and lower ductility than the material tested in the previous program. Also, the specimens tested in the previous program were held under tensile load in high-pressure hydrogen prior to tensile testing to failure. However, the results from the previous program and from Phase III of this program indicate that the degree of hydrogen-environment embrittlement of specimens of low alloy steels such as ASTM A-302 is not affected by holding the specimens under load in hydrogen. Specimens tested in this phase were more embrittled by the 10,000-psi hydrogen environment than were specimens tested in the previous program. The percent reduction of tensile properties by the 10,000-psi hydrogen environment (compared to those in 10,000-psi helium) compare as follows between the specimens tested in the present program and those tested with a 1-day-hold period in the previous program:

Elongation: 13 percent reduction (present) and 0 percent reduction (previous)

Reduction of area: 47 percent (present) and 10 percent (previous)

Notch strength: 22 percent (present) and 13 percent (previous)

This greater degree of hydrogen-environment embrittlement found in the present program is believed due to the higher strength and lower ductility resulting from the reheat treatment of the material used in this program.

It can be seen from Table 4 that the tensile properties of unnotched, annealed Ti-6Al-4V specimens were the same in 10,000-psi hydrogen as in 10,000-psi helium for all hydrogen exposure conditions. However, the strength of notched, annealed specimens was considerably lower in 10,000-psi hydrogen, and the hydrogen-environment embrittlement was greater after zero exposure time (test run immediately upon establishing hydrogen environment) than after the 24-hour hold time in 10,000-psi hydrogen.

Tensile properties of unnotched Ti-6Al-4V STA specimens were the same in 10,000-psi hydrogen as in 10,000-psi helium. The strength of notched STA specimens was considerably lower in 10,000-psi hydrogen than in 10,000-psi helium. Results of the tests on the notched Ti-6Al-4V STA specimens were of particular interest because they showed that there was a large dependency of tensile properties in 10,000-psi hydrogen on the method of purging the test vessels. Thus, these results shown in Table 4 will be discussed in some detail.

First, two zero-exposure-time tests (marked 0[c] under hold time in Table 4) were performed on notched STA specimens in 10,000-psi hydrogen after using the 3-cycle pressurization-depressurization purging treatment, and there was no difference between the tensile properties of these specimens and specimens tested in 10,000-psi helium. Then, three zero-hold-time tests (marked 0[c] in Table 4) were conducted on notched STA specimens in 10,000-psi hydrogen after the test vessels were purged by evacuating to approximately 300 microns, backfilling with hydrogen to 100 psi three times, and followed by the 3-cycle pressurization (10,000 psi)-depressurization (1 atmosphere) hydrogen flushing. These specimens had a large reduction of strength compared to specimens tested in 10,000-psi helium.

To evaluate more thoroughly the effect of vacuum purging the test vessels prior to the pressurization-depressurization hydrogen flushing, three notched Ti-6Al-4V STA specimens were tested, each with a different purging technique as follows: Specimen 1, 3-cycle pressurization (10,000 psi)-depressurization (1 atmosphere) hydrogen flushing; specimen 2, 15-cycle pressurization (10,000 psi)-depressurization (1 atmosphere) hydrogen flushing; specimen 3, 3-cycle evacuation to approximately 300 microns and backfilling with hydrogen to 100 psi followed by 3-cycle pressurization (10,000 psi)-depressurization (1 atmosphere) hydrogen flushing. The results showed that the reduction of notch strength compared to specimens tested in 10,000-psi helium was 29, 31, and 45 percent, respectively, for specimens 1, 2, and 3. Thus, the evacuation treatment did

result in a considerable increase in the hydrogen-environment embrittlement. Increasing the number of pressurization-depressurization cycles had little effect and the results for specimens 1 and 2 above were averaged and included in Table 4 (marked 0[b] under hold time). In light of the results for these two specimens, it is now not clear why the first two notched Ti-6Al-4V STA specimens tested in 10,000-psi hydrogen were not embrittled.

Two explanations were considered for the increase in hydrogen-environment embrittlement of Ti-6Al-4V because of the prior evacuation purging treatment. The first was simply that the evacuation treatment served to improve the purity of the 10,000-psi hydrogen environment in the test vessel. The second explanation is that the evacuation treatment served to remove adsorbed gases, probably oxygen, from the surface of the specimens. An unambiguous choice between these two explanations is not possible on the basis of the Phase I results alone, although if purity of the hydrogen environment was the problem, then increasing the number of pressurization-depressurization cycles should have had some effect. In any case, some results from Phase III, as will be discussed in that section, tend to indicate that the removal of surface gases is the correct explanation.

Embrittlement of notched Ti-6Al-4V STA specimens by 10,000-psi hydrogen was less after the 24-hour exposure times than with zero hold time. This inverse effect of exposure time on hydrogen-environment embrittlement also occurred with the notched, annealed Ti-6Al-4V specimens and is believed to be a real effect. The reason for this inverse effect is not clear, although the following explanations have been considered. Hydrogen purity in the test vessel may be decreasing with hold time, and titanium alloys are very sensitive to the impurity content of the hydrogen. However, tests were being conducted on other alloys at the same time in the same type of equipment with exposure times of up to 100 days and no significant impurity increase in the hydrogen was indicated. The inverse exposure time effect for the notched Ti-6Al-4V STA specimens could be explained in terms of surface gas removal by the evacuation treatment and the re-establishment

with time of an adsorbed layer of impurities (probably oxygen) from the hydrogen. This will be discussed further under Phase III. However, this explanation is not applicable to the notched, annealed Ti-6Al-4V specimens because they were not subjected to the evacuation treatment. Finally, the inverse exposure time effect could be due to strain aging. There is evidence that at least the Ti-6Al-4V STA undergoes considerable strain aging.

As pointed out earlier, the purpose of this phase was to establish the procedure to be used in subsequent phases when performing tensile tests in high-pressure hydrogen. For the ASTM A-302, AISI type 310 stainless steel, and annealed Ti-6Al-4V and Ti-6Al-4V STA tested in this phase, it was found that the degree of hydrogen-environment embrittlement was either unaffected by the time of exposure to the hydrogen or was the greatest for zero exposure time, lessening with increased exposure time. Thus, it was decided that for subsequent phases (e.g., for screening materials), the basic procedure for performing tensile tests in high-pressure hydrogen would use a zero exposure time. That is, as soon as a bank of test vessels had been properly purged and the test pressure established, the tensile tests would be performed as rapidly as possible. It was also found in this phase that the degree of hydrogen-environment embrittlement was increased if evacuation of the test vessel was included as a part of the purging operation. Because the reason for the evacuation effect was not clear, it was decided to use vacuum purging in all subsequent tests. The purging treatment established was to evacuate the test vessels to approximately 20 microns and backfill with hydrogen to 100 psi three times, followed by three pressurization (to test pressure)-depressurization (1 atmosphere) cycles before raising the hydrogen to the test pressure. A few tests were performed in subsequent phases before the evacuation treatment was incorporated in the purging procedure.

SUMMARY

Tests were performed on ASTM A-302, AISI type 310 stainless steel, and annealed and Ti-6Al-4V STA to determine the effect of exposure time of unloaded (except for gas pressure) specimens to 10,000-psi hydrogen on the degree of embrittlement by that environment. The effect on hydrogen-environment embrittlement of including evacuation in the test vessel purging treatment was investigated for the Ti-6Al-4V alloy.

The degree of hydrogen-environment embrittlement was found to be considerable for ASTM A-302 and Ti-6Al-4V, but slight for AISI type 310 stainless steel. Degree of embrittlement was unaffected by the time of exposure to 10,000-psi hydrogen for ASTM A-302 and AISI type 310 stainless steel, but was greatest for zero exposure time and lessened with increasing time for Ti-6Al-4V. Evacuation of the test vessels considerably increased the hydrogen-environment embrittlement of Ti-6Al-4V.

Because of these results, the following basic test procedure was adopted for subsequent tensile tests in high-pressure hydrogen. A bank of test vessels are evacuated to approximately 20 microns and backfilled with hydrogen to 100 psi three times. This is followed by pressurizing with hydrogen to the test pressure and depressurizing to 1 atmosphere three times, after which the hydrogen pressure is brought up to the test pressure and the bank of tensile tests are performed one after the other as rapidly as feasible.

CONCLUSIONS

Based on the preceding test procedures, the following conclusions were reached.

1. ASTM A-302 and annealed Ti-6Al-4V and Ti-6Al-4V STA are considerably embrittled by a 10,000-psi hydrogen environment, but AISI type 310 stainless steel is only slightly embrittled.
2. The degree of embrittlement of ASTM A-302 and AISI type 310 stainless steel is unaffected by the time of exposure to the 10,000-psi hydrogen environment.
3. The degree of embrittlement of annealed Ti-6Al-4V and Ti-6Al-4V STA by a 10,000-psi hydrogen environment is greatest for zero time prior exposure to 10,000-psi hydrogen.
4. Prior evacuation of the test vessels considerably increases the embrittlement of Ti-6Al-4V by 10,000-psi hydrogen.

PHASE II: EFFECT OF A 10,000-PSI HYDROGEN ENVIRONMENT ON THE TENSILE PROPERTIES OF A VARIETY OF ALLOYS

INTRODUCTION

In previous investigations conducted at Rocketdyne and elsewhere into the effects of ambient-temperature, high-pressure hydrogen on metals, only a relatively few alloys (mainly steels) had been studied. Thus, the purpose of this phase was to determine the effect of a 10,000-psi ambient-temperature hydrogen environment on the tensile properties of a number of different type alloys.

Unnotched and notched ($K_t \simeq 8.4$) specimens of 25 alloys were tensile tested at ambient temperature in 10,000-psi hydrogen; for comparison, they were also subjected to 10,000-psi helium and ambient-pressure air. In accordance with the results of Phase I, the tensile tests were performed as soon as the test environment was established, without any hold period. Data on all tests conducted in this phase are initially presented and discussed. For completeness, data from other phases are also included in the discussion and the summary.

Alloys tested in this phase included the following:

Pure Iron:	Armco Iron
Carbon Steels:	AISI 1042 normalized
	AISI 1042 quenched and tempered
Low Alloy Steels:	AISI 4140
	HY-100
Forging Steel:	ASTM A-372 Class IV (API N-80)
High-Strength Steels:	Fe-9Ni-4Co-0.25C
	18 Nickel (250) maraging steel
Austenitic Stainless Steels:	AISI type 304L
	AISI type 305
	AISI type 316

Ferritic Stainless Steel:	AISI type 430F
Martensitic Stainless Steel:	AISI type 410
	AISI type 440C
Precipitation-Hardening Steels:	17-7 PH stainless steel
	A-286 stainless steel
Aluminum Alloys:	1100-0 commercially pure aluminum
	7075-T73
	6061-T6
Titanium Alloys:	Commercially pure titanium
	Ti-5Al-2.5Sn
Copper Alloys:	OFHC copper
	Beryllium-copper
Nickel Alloys:	Nickel 270
	Inconel 718
	Rene 41

EXPERIMENTAL PROCEDURE

Materials

Chemical compositions, heat treatments, and mechanical properties of the alloys tested in this phase are presented in Tables 5, 6, and 7, respectively.

Tensile Specimen Design

Design of the tensile specimens is described in detail under Phase I. The reduced sections of the unnotched, AISI type 304L stainless steel, AISI type 305 stainless steel, and OFHC copper specimens were 0.150 inch in diameter, instead of the 0.250-inch diameter of the other specimens. This change was necessary because loads sufficient to fracture a 0.250-inch-diameter reduced section of these alloys would also plastically

TABLE 5

CHEMICAL COMPOSITION OF PHASE II MATERIALS

Material	C	Mn	P	S	Si	Ni	Cr	Cu	Al	Ti	Mg	Mo	Fe	Co	Sn	V	Other
Armco Iron (3/8-inch rod)	0.033	0.036	0.007	0.015	0.001			0.000									
AISI 1042 (3/8-inch rod)	0.44	0.76	0.008	0.020	0.20												
AISI 4140 (3/8-inch rod)	0.405	0.83	0.009	0.014	0.31		0.93					0.20					
HY-100 (1/2-inch plate)	0.16	0.32	0.010	0.019	0.22	2.57	1.67	0.05		0.001		0.42				0.002	
ASTM 372 Class IV (API N-80) (24-inch OD, 0.817-inch-thick pipe)	0.46	1.60	0.010	0.022	0.21							0.22					
Fe-9Ni-4Co-0.25C (7/16-inch rod)	0.17	0.27	0.005	0.005	0.02	9.10	0.78					1.01		4.45		0.78	
18 Nickel (250) Maraging Steel (3-inch-square block)	0.006	0.02	0.003	0.007	0.02	18.70			0.15	0.40		4.80		7.58			B-0.002 Zr-0.012
AISI Type 304L Stainless Steel (3/8-inch rod)	0.020	1.78	0.014	0.011	0.49	9.78	18.50	0.10				0.09					Ca-0.05 C,O,B-0.15
AISI Type 305 Stainless Steel (3/8-inch rod)	0.07	0.86	0.025	0.025	0.68	11.99	18.19										
AISI Type 316 Stainless Steel (3/8-inch rod)	0.05	1.73	0.024	0.022	0.56	12.45	17.52	0.22				2.67					
AISI Type 430F Stainless Steel (3/8-inch rod)	0.096	1.07	0.015	0.293	0.63	0.24	16.33	0.07				0.40					
AISI Type 410 Stainless Steel (3/8-inch rod)	0.145	0.71	0.016	0.007	0.60	0.40	12.26	0.11	0.02			0.08			0.008		
AISI Type 440C Stainless Steel (3/8-inch rod)	0.96	0.48	0.013	0.024	0.33	0.36	17.33					0.48					
17-7 PH Stainless Steel (3/8-inch rod)	0.072	0.68	0.028	0.005	0.64	7.10	17.29		0.90								
A-286 Superstrength Alloy	0.052	1.47	0.019	0.010	0.61	25.58	15.07		0.13	1.93		1.35				0.30	B-0.0055
1100-0 Aluminum (3/8-inch rod)									99.0								
7075-T-73 Aluminum (3/8-inch rod)	Min						0.18		1.2		2.1						
	Max		0.30		0.50		0.40		2.0	0.20	2.9		0.7				Zn-5.1
6061-T-6 Aluminum (3/8-inch rod)	Min				0.40		0.15	0.15			0.8						Zn-6.1
	Max		0.15		0.8		0.35	0.40		0.15	1.2		0.7				Z-0.25 Other 0.15
Titanium, Commercially Pure (3/8-inch rod)	0.023												0.10				N_2-0.013 H_2-0.0058 O_2-0.10
Ti-5Al-2.5Sn ELI (15/16-inch rod)	0.011		0.02						5.47				0.09		2.70		N_2-0.006 H_2-0.0122 O_2-0.09
OFHC Copper (3/8-inch rod)								99.99									
Be-Cu Alloy 25 (3/8-inch rod)					0.09	0.04	0.005	Bal.	0.05				0.09	0.22	0.01		Zn-0.02 Be-1.86 Pb-0.05
Nickel 270 (3/8-inch rod)	0.01	0.001		0.001	0.001	Bal.	0.001		0.001	0.001	0.001		0.001	0.001			
Inconel 718 (3/8-inch rod)	0.04	0.16		0.007	0.33	51.11	18.37	0.12	0.52	0.92		3.13	19.81				Cb/Ta-5.39
Rene 41 (1/2-inch rod)	0.082	0.02		0.004	0.07	Bal.	18.88		1.51	3.09		9.79	0.64	10.9			B-0.006

Material	Heat Treatment by Supplier (As-Received Condition)	Hardness	Heat Treatment at Rocketdyne	Hardness
Armco Iron	Annealed		None	
AISI 1042	Annealed		One set of specimens normalized at 1650 F for 1 hour and air cooled; one set normalized as above, then annealed 1375 F for 1 hour, water quenched, tempered at 400 F for 2 hours, and air cooled	R_c 52 R_b 93.5
AISI 4140	Annealed	207 BHN	Anneal at 1550 F for 1 hour, water quench temper at 900 F for 2 hours	
HY 100	To MIL S-16216G dated 2-27-63		None	
ASTM 372 Class IV (API N-80)	Temper at 875 F		None	
Fe-9Ni-4Co-0.20C	Annealed		Anneal at 1550 F for 1 hour, oil quench; double temper at 1000 F for 2 hours	
18% Nickel (250) Maraging Steel	Annealed	R_c 30	Age at 900 F for 6 hours	
AISI Type 304L Stainless Steel	Annealed and cold drawn	170 BHN	Normalize at 1950 F for 1 hour, air cool	R_b 68
AISI Type 305 Stainless Steel	Annealed and cold drawn		None	
AISI Type 316 Stainless Steel	Annealed and cold drawn		None	
AISI Type 430F Stainless Steel	Annealed		None	
AISI Type 410 Stainless Steel	Annealed and cold drawn		Anneal at 1850 F for 1 hour, oil quench; temper at 1000 F for 1 hour	
AISI Type 440C Stainless Steel	Annealed and cold drawn	R_b 90	Heat slowly to 1900 F for 1 hour, oil quench; temper at 400 F for 2 hours	R_c 54.5
17-7 PH Stainless Steel	Annealed	214 BHN	Annealed at 1950 F for 1 hour; air cooled; austenitized at 1400 F for 1-1/2 hours; air cooled to 50 to 65 F; held 30 minutes; immediately aged at 1050 F for 1-1/2 hours	
A-286 Stainless Steel	Solution treated at 1650 F for 2 hours; water quenched; aged at 1325 F for 16 hours; air cooled	321 BHN	None	R_c 34.6
1100-0 Aluminum	0 temper		None	
7075 T-73 Aluminum	Heat treated to T-73 temper		None	
6061 T-6 Aluminum	Heat treated to T-6 temper		None	
Titanium, Commercially Pure	Hot rolled		None	
Ti-5Al-2.5Sn ELI	Rocketdyne Spec RB0170-079		Vacuum anneal at 1400 F for 4 hours; argon cool	
OFHC	Cold drawn		None	
Alloy 25 Be-Cu	Condition R		None	
Nickel 270	Hot Rolled		None	
Inconel 718	Annealed		Annealed at 1750 F for 1 hour; air cooled; reheated to 1325 F for 8 hours; furnace cooled to 1150 F at 100 F/hr; held for 10 hours; air cooled	
Rene 41	1975 F for 1 hour; water quenched	R_c 29	1975 F for 1 hour; water quenched; aged at 1400 F for 16 hours; air cooled	

TABLE 7

MECHANICAL PROPERTIES OF PHASE II MATERIALS
(Supplier Certification)

Material	Tensile Strength, ksi	Yield Strength, ksi	Percent Reduction of Area	Percent Elongation	Hardness
Armco Iron			Not Furnished		
AISI 1042			Not Furnished		
AISI 4140					207 BHN
HY 100	122.2	105.9	64.8	25.0	257 BHN
ASTM 372 Class IV (API N-80)	125.0	94.0	46.7	18.5	262 BHN
Fe-9Ni-4Co-0.25Cl			Not Furnished		
18% Nickel (250) Maraging Steel	259.0[a]	253.1		10.5	R_c 49.5
AISI Type 304L Stainless Steel	92.0	69.0	76.0	49.0	170 BHN
AISI Type 305 Stainless Steel	90.1				
AISI Type 316 Stainless Steel	94.1	70.0	70.4	44.0	R_b 98
AISI Type 430F Stainless Steel	93.0	78.0	62.0	20.0	
AISI Type 410 Stainless Steel	108.0	87.0	67.0	21.4	214 BHN
AISI Type 440C Stainless Steel					R_b 99
17-7 PH Stainless Steel	176.0[a]	161.7	46.2	15.0	363 BHN
A-286 Stainless Steel	161.2	118.9	42.2	24.1	321 BHN
1100-0 Aluminum			Not Furnished		
7075 T-73 Aluminum	77.0	66.0		7.0	
6061 T-6 Aluminum	42.0	35.0		10.0	
Titanium, Commercially Pure	69.5	62.0	53.0	29.5	
Ti-5Al-2.5Sn ELI	121.5	117.0	45.0	12.3	R_c 34
OFHC Copper	40.0(Min)			10.0	
Alloy 25 Be-Cu	97.7			20.5	30 N-59
Nickel 270	51.5				
Inconel 718	213.0[a]	187.0	15.0	15.0	R_c 47
Rene 41	214.0[a]	148.0	31.0	24.1	R_c 40

[a] The properties listed were determined by the supplier on material from the same heat as supplied to Rocketdyne and were heat treated in the same manner as the heat treatments conducted at Rocketdyne (shown in Table 3). The material was received in the annealed condition.

reduce the larger 0.306-inch-diameter section and cause leakage at the sliding seal.

Apparatus

The apparatus used for performing the tensile tests is also described in detail under Phase I.

Test Procedure

Tensile testing procedure used in this phase was essentially the same as described in Phase I. However, the notched specimens of AISI type 304L stainless steel, AISI type 430F stainless steel, and 6061-T6 aluminum alloy were paced at 0.005/minute instead of 0.0007/minute, and notched specimens of A-286 stainless steel were paced at 0.0014/minute. Tests were conducted in 10,000-psi helium on notched AISI 1042, AISI type 316 stainless steel, and AISI type 430F stainless steel, at both 0.005/minute and 0.0007/minute strain rates, with no difference in properties.

Whether or not evacuation was used in purging the test vessels is indicated for each alloy in the Results and Discussion section, which follows.

RESULTS AND DISCUSSION

Results

Results of the tensile tests on the 25 Phase II alloys are presented in Table 8; the tables within the Appendix that contain the data for the individual specimen are also referenced. Alloys are listed in Table 8 in the order of decreasing reduction of strength of notched specimens in 10,000-psi hydrogen.

High-strength steels tested in this program were quenched and tempered AISI 1042, AISI 4140, Fe-9Ni-4Co-0.25C, and 18 nickel (250) Maraging Steel. These steels were all extremely embrittled by gaseous hydrogen

TABLE 8

PHASE II TESTS ON VARIOUS ALLOYS IN 10,000-PSI HELIUM AND IN 10,000-PSI HYDROGEN

Material	Notched or Unnotched	Strength in 10,000-psi Helium		Strength in 10,000-psi Hydrogen		Ductility				Vacuum Purged	Appendix Table Number For Individual Specimen Data
						Elongation, percent		Reduction of Area, percent			
		Yield, ksi	Ultimate, ksi	Ultimate, ksi	Change From Helium, percent	10,000-psi Helium	10,000-psi Hydrogen	10,000-psi Helium	10,000-psi Hydrogen		
18 Nickel (250) Maraging Steel	UN	248	250	171	-32.0	8.2	0.2	55.0	2.5	Yes	II-1
	N		423	50	-88.0			2.5	0.0	Yes	
AISI Type 410 Stainless Steel	UN	192	211[a]	166	-21.0	15.0[b]	1.3	60.0[b]	12.0	Yes	II-2
	N		386[a]	82	-78.0			2.2[b]	0.6	Yes	
AISI 1042 Quenched and Tempered	UN	165	--	187	--	—	0	--	0	Yes	II-3
	N		236	53	-78.0			0.6	0.6	Yes	
17-7 PH Stainless Steel	UN	150	164[a]	151	-8.0	17.0[b]	1.7	45.0[b]	2.5	Yes	II-4
	N		302[a]	70	-77.0			0.6[b]	0.4	Yes	
Fe-9Ni-4Co-0.20C	UN	187	199	175	-12.0	15.0	0.5	67.0	15.0	Yes	II-5
	N		367	89	-76.0			6.3	0.2	Yes	
Rene 41	UN	163	196[a]	165	-16.0	21.0[b]	4.3	29.0[b]	11.0	Yes	II-6
	N		280[a]	77	-73.0			3.4[b]	0.2	Yes	
AISI 4140	UN	179	186	178	-4.0	14.0	2.6	48.0	8.8	Yes	II-7
	N		313	125	-60.0			2.8	0.9	Yes	
Inconel 718	UN	182	207	193	-7.0	17.0	1.5	26.0	0.8	Yes	II-8
	N		274	126	-54.0			1.7	0.2	Yes	
AISI Type 440C Stainless Steel	UN	236	293	119	-60.0			3.2	0	Yes	II-9
	N		149	74	-50.0			0.2	0	No	
AISI Type 430F Stainless Steel	UN	72	80	78	-2.5	22.0	14.0	64.0	37.0	No	II-10
	N		152	104	-32.0			1.9	0.6	No	
Nickel 270	UN		48[a]	50		56.0[b]	52.0	89.0[b]	67.0	Yes	II-11
	N		77	54	-30.0			23.0	6.9	Yes	
HY-100	UN	97	113	115		20.0	18.0	76.0	63.0	Yes	II-12
	N		224[a]	164	-27.0			7.3	3.8	Yes	
ASTM A-372 - Class IV	UN	82	118	116	-1.7	20.0	9.6	53.0	18.0	Yes	II-13
	N		200	148	-26.0			2.0	2.8	Yes	
AISI 1042 Normalized	UN	58	90	89		29.0	22.0	59.0	27.0	No	II-14
	N		153	115	-25.0			8.5	2.8	No	
Ti-5Al-2.5Sn	UN	106	113	114		20.0	18.0	45.0	39.0	Yes	II-15
	N		201	162	-19.0			3.1	1.8	Yes	
Armco Iron	UN	54	56	57		18.0	15.0	83.0	50.0	Yes	II-16
	N		121	105	-14.0			6.4	1.7	No	
AISI Type 304L Stainless Steel	UN	24[a]	77	76		86.0	79.0	78.0	71.0	No	II-17
	N		102	89	-13.0			21.0	11.0	No	
AISI Type 305 Stainless Steel	UN	51	90[a]	87	-3.0	63.0	65.0	78.0	75.0	Yes	II-18
	N		165[a]	147	-11.0			19.0	17.0	Yes	
Be-Cu Alloy 25	UN	79	94	93		22.0	22.0	72.0	71.0	Yes	II-19
	N		195	181	-7.0			12.0	13.0	Yes	
Titanium (Commercially Pure)	UN	53	63			32.0	31.0	61.0	61.0	Yes	II-20
	N		126	120	-5.0			10.0	7.3	Yes	
A-286 Stainless Steel	UN	123	158	162		26.0	29.0	44.0	43.0	No	II-21
	N		233	227	-3.0			5.6	6.2	No	
7075 T-73	UN	54	66	65		15.0	12.0	37.0	35.0	No	II-22
	N		116	114	-2.0			3.8	2.3	No	
6061 T-6 Al Alloy	UN	33	39	40		19.0	19.0	61.0	66.0	No	II-23
	N		72	78				9.5	11.0	Yes	
1100-0 Al	UN		16	16[c]		42.0	39.0	93.0	93.0	Yes	II-24
	N		18	25[c]				20.0	21.0	Yes	
OFHC Copper	UN	39	42	41		20.0	20.0	94.0	94.0	Yes	II-25
	N		87	86				20.0	24.0	Yes	
AISI Type 316 Stainless Steel	UN	64	94	99		59.0	56.0	72.0	75.0	No	II-26
	N		161	161				18.0	19.0	No	

[a] Strength in air minus 10,000 psi to compensate for effect of 10,000-psi pressure

[b] Ductility in air

[c] 5000-psi hydrogen or helium

as indicated by large reductions of notch strength and unnotched and notched ductility. Unnotched ductility of these specimens was reduced over 75 percent, and the notch ductility was essentially zero for all of the specimens tested in 10,000-psi hydrogen. Reduction of notch strength ranged from 60 percent for AISI 4140 to 88 percent for 18 nickel (250) Maraging Steel. The 18 nickel (250) Maraging Steel specimens were the most embrittled of all the materials tested in this program. This steel had a 32-percent reduction in unnotched strength, as well as an 88-percent reduction in notched strength.

Low alloy steels (Armco Iron, AISI 1042 normalized, HY-100, and ASTM A-372) are tough, ductile alloys, and the degree of embrittlement was about the same for all. Reduction of ductility of the unnotched specimen was greatest for ASTM A-372 class IV and least for HY-100. Reduction of notch strength was about 25 percent for HY-100 and ASTM A-372, and 14 percent for Armco Iron. Except for the ASTM A-372, the notched ductility of these steels was drastically reduced by the 10,000-psi hydrogen environment.

The 400 series stainless steels (AISI type 430F, 410, and 440C) were among the most hydrogen-environment-embrittled steels tested. Among these steels it appears the stronger the steel, the greater the hydrogen environment embrittlement, although the results for AISI type 440C are somewhat ambiguous because of its extreme notch sensitivity. The average reduction of notch strength of 440C attributable to 10,000-psi hydrogen was 50 percent. This is impressive because comparison was made to the notch strength in 10,000-psi helium, which was only 149,000 psi, because of the notch sensitivity of 440C.

There was also a reduction of strength of the unnotched specimens in high-pressure hydrogen. Strength reductions were 2.5 percent for AISI type 430F, 22 percent for AISI type 410, and 59 percent for AISI type 440C. Ultimate strength reduction of unnotched specimens of AISI type 440C was considerably greater than has been observed for any other material, including H-11 tool steel, tested in Phase III of this program.

Results of tests on 17-7 PH stainless-steel specimens show, as expected, that this steel was highly embrittled by 10,000-psi hydrogen.

A precipitation-hardened austenitic stainless steel (A-286 stainless steel) was also tested in this program. The data show that only slight embrittlement was caused by the 10,000-psi hydrogen environment, and there was no decrease in ductility of the unnotched and notched A-286 alloy specimens. Tensile strength of the notched specimen was approximately 7000 psi (2-1/2 percent) lower in hydrogen than it was in 10,000-psi helium.

These data indicate that the nickel-base alloys (Nickel 270, Inconel 718, and Rene 41) are at least as susceptible to embrittlement by gaseous hydrogen as are the iron-base alloys. Nickel 270, which is commercially pure nickel, was embrittled by 10,000-psi hydrogen to a greater degree than Armco Iron and most of the low-strength, high-toughness steels tested. Ductility of the unnotched specimens was reduced by 10,000-psi hydrogen and by hydrogen-contaminated helium (Table 8), but not by 10,000-psi helium containing 0.44 ppm hydrogen. All three of these hydrogen environments caused a reduction in strength and ductility of the notched specimens. Inconel 718, along with the previously discussed 18 nickel (250) Maraging Steel, had the greatest reduction in ductility of unnotched specimens in 10,000-psi hydrogen. The helium environment, in which the Inconel 718 specimens were tested, was contaminated with hydrogen, but only one of the four specimens tested was embrittled. That specimen had a 20-percent reduction of notch strength. Rene 41 also had one of the largest reductions of notch strength by high-pressure hydrogen. The average reduction of notch strength for this alloy was 73 percent.

These results have been corroborated by Forman on Inconel 718 (Ref. 5), who has shown a considerable reduction of $K_{IC(H_2)}$ values when testing in hydrogen environments with pressures of less than 1000 psi.

The 300 series stainless steels tested in this phase are AISI type 304L, 305, and 316. The reduction of area of unnotched AISI type 304L specimens was reduced approximately 10 percent by the 10,000-psi environment. The notched specimens had between approximately 10 and 17 percent strength reduction and 50 percent ductility reduction due to the hydrogen environment. All of the specimens were magnetic near the fracture after testing.

Specimens of AISI type 305 stainless steel were very slightly magnetic after testing; no surface cracking was observed, but there was slight indication of reduction of ductility of the unnotched and notched specimens. There was, however, a small reduction (about 4 percent) of unnotched strength and 11 percent reduction of notch strength. Thus, AISI type 305 stainless steel was somewhat less embrittled by 10,000-psi hydrogen than was AISI type 304L stainless steel, which had a reduction of ductility as well as strength in high-pressure hydrogen.

There was no indication of a reduction of strength or ductility of the unnotched and notched AISI type 316 specimens due to exposure to the high-pressure hydrogen environment. For some reason, the scatter in the ultimate strength results for the unnotched AISI type 316 stainless-steel specimens tested in hydrogen was larger than normally encountered. The results suggest a small increase of unnotched strength due to the hydrogen environment but, because of the scatter, this is not believed to be significant. The AISI type 316 stainless-steel specimens were not magnetic after testing. The degree to which the AISI type 300 series stainless steels are embrittled by 10,000-psi hydrogen appears therefore to be a function of degree of magnetism near the specimen fracture. This would suggest that the body-centered cubic structure is needed for these materials to be embrittled. Phase I tests on AISI type 310 stainless-steel specimens, however, indicated a slight degree of embrittlement caused by the 10,000-psi hydrogen environment.

Most of the tests for commercially pure titanium and Ti-5Al-2.5Sn were conducted on test vessels that had been previously evacuated. The unnotched

commercially pure titanium specimens were not embrittled by 10,000-psi hydrogen. However, there was a considerable decrease of notch ductility and a small decrease of notch strength of the two specimens tested in 10,000-psi hydrogen after prior test vessel evacuation. The notched specimen, which was tested in high-pressure hydrogen without prior evacuation of the test vessel, had no ductility decrease and only a slight strength decrease. The difference of strain rate at which the three tests were conducted is considered too small to affect the results significantly.

There was a reduction of notched strength and unnotched specimen ductility of the Ti-5Al-2.5Sn alloy. It is interesting to note that the unnotched Ti-5Al-2.5Sn specimens were embrittled by 10,000-psi hydrogen, while the Phase I tests on unnotched Ti-6Al-4V specimens showed no embrittlement for either the annealed or STA conditions. The determining factor is apparently whether vacuum purging was used prior to testing, because the test vessels were not evacuated for the Ti-6Al-4V tests, but were for the Ti-5Al-2.5Sn tests.

Unalloyed aluminum (1100 aluminum) was tested in 5000-psi hydrogen instead of 10,000 psi because the tensile stress exerted by the 10,000-psi hydrostatic pressure would break the specimen without applying an external load. There was no indication of embrittlement of the 1100-0 aluminum in 5000-psi hydrogen or of 6061-T6 aluminum alloy in 10,000-psi hydrogen. The tensile properties of 7075-T73 aluminum alloy were approximately the same in hydrogen and helium environments. However, the average ductility of the unnotched and notched specimens was slightly lower in 10,000-psi hydrogen than in 10,000-psi helium. Notched strength was somewhat decreased from the average strength in helium, but the strength of all three specimens tested in hydrogen was higher than the lowest strength obtained in 10,000-psi helium.

The test vessels were vacuum purged prior to pressurization with 10,000-psi hydrogen for the 1100 aluminum tests, but this procedure was not instituted before the tests were performed on the other two aluminum alloys. This is unfortunate because it is believed that aluminum alloy may possibly react similarly to titanium alloys for which prior vacuum purging led to considerably greater subsequent hydrogen-environment embrittlement. The fact that small amounts of embrittlement were encountered in this program should be viewed with caution because of the low $K_{IC}(H_2)$ values for aluminum observed by Forman (Ref. 5). He reported a 25 percent decrease of K_{IC} (air) values when testing in hydrogen at pressures less than 1000 psi. Results of tests on both unnotched and notched specimens of OFHC copper indicated no embrittlement from exposure to high-pressure hydrogen. All of the hydrogen tests were conducted after the test cells were vacuum purged.

Results of tests on Be-Cu alloy 25 indicated no embrittlement of the unnotched specimens by high-pressure hydrogen. There was, however, a 7-percent reduction of notched strength in 10,000-psi hydrogen and a 5-percent reduction in 10,000-psi helium containing 44 ppm hydrogen. The higher hydrogen contamination level in 10,000-psi helium did not reduce the notch strength. Notch ductility was not affected by high-pressure hydrogen.

Hydrogen-Contaminated Helium. Embrittlement occurred in a series of tests conducted with 10,000-psi helium contaminated with hydrogen. Those materials affected were HY-100, AISI type 305 stainless steel, AISI type 410 stainless steel, 17-7 PH stainless steel, Nickel 270, Inconel 718, Rene 41, and Be-Cu alloy 25. Embrittlement was indicated

by reduction in strength and ductility of the notched specimens compared to these properties in air after compensating for the effect of hydrostatic pressure. There was also evidence of embrittlement of some of the unnotched specimens from the helium environment.

The most obvious explanation for this embrittlement was that the helium had been contaminated with hydrogen. Thus, the high-pressure supply system was thoroughly flushed with helium and repressurized to 15,000-psi helium pressure. Tensile properties of Nickel 270 specimens were then measured in this helium environment over an 11-day period. The first tests that were performed gave no indication of embrittlement, but after 11 days there appeared to be a measurable reduction in strength of the notched and unnotched specimens and a small reduction in ductility. Degree of embrittlement was quite small compared to that obtained for the earlier tests in 10,000-psi helium contaminated with hydrogen.

At the end of this period (12 days after the system was pressurized), tests in 10,000-psi helium were performed on five of the notched Phase II materials. Following these tests, the helium was analyzed and found to contain 44 ppm hydrogen, which corresponds to a hydrogen partial pressure of 0.44 psi in the 10,000-psi helium.

Degree of embrittlement was markedly reduced by flushing the system thoroughly with helium prior to pressurization, but it was not eliminated. The source of the hydrogen is unclear but there were indications that hydrogen accumulation occurs by evolution from the high-pressure components. This deduction is based mainly on the apparent increase of embrittlement of the Nickel 270 specimens with an increase in exposure

time to high-pressure helium within the system. To eliminate this possible source of hydrogen, the gas purification unit and the high-pressure side of the testing system were held under vacuum for several days. The system was then refilled with helium to 15,000 psi and a gas sample taken. Analysis of the helium sample showed 0.9 ppm hydrogen. There was no indication of embrittlement in subsequent Phase II tests in 10,000-psi helium.

Data obtained from the tests in hydrogen-contaminated helium were enlightening because they showed that embrittlement can occur at very low hydrogen pressures, and that dilution with high-pressure helium did not prevent the effect. Unfortunately, the degree of hydrogen contamination was not ascertained for the original contaminated helium. Results of tests performed in the original hydrogen-contaminated helium, in the helium containing 44 ppm hydrogen, and in 10,000-psi hydrogen are summarized in Table 9. Hydrogen contamination in the helium was certainly an effective embrittling environment. There is no explanation as to why there was indication of a small degree of embrittlement of the Be-Cu alloy in 10,000-psi helium contaminated with 0.44 psi hydrogen, while hydrogen contamination believed to be greater did not result in embrittlement. The test vessels for all of the tests performed with hydrogen-contaminated helium had been evacuated prior to pressurizing with 10,000-psi helium.

Discussion. As an aid to assessing whether any relationship exists between the mechanical properties in air and the propensity toward embrittlement by gaseous hydrogen, properties of all materials including those from other phases are listed in Table 10 in decreasing order of reduction of notch strength, along with their air environment mechanical properties. Other criteria, rather than reduction of notch strength (e.g., reduction of ductility of unnotched specimens) could be used to

TABLE 9

REDUCTION OF NOTCHED STRENGTH FROM HYDROGEN CONTAMINATION IN 10,000-PSI HELIUM

Material	Percent Reduction of Strength (Average)		
	Helium Plus 44 ppm Hydrogen	Hydrogen-Contaminated Helium	10,000-psi Hydrogen
HY-100		7	27
AISI Type 305 Stainless Steel	0	11	11
AISI Type 410 Stainless Steel	13	50	79
17-7 PH Stainless Steel	8	53	77
Nickel 270	3	20	31
Inconel 718		10	54
Rene 41	4	20	72
Be-Cu Alloy 25	5	0	7

TABLE 10

ARRANGEMENT OF MATERIALS IN ORDER OF PERCENT REDUCTION OF NOTCH STRENGTH IN 10,000-PSI HYDROGEN

Material	Air Yield Point, ksi	Air Ultimate, ksi		UN Yield/Ultimate	Percent Reduction of N Strength	Percent Elongation	Ductility in Air		Vacuum Purged
		UN	N				Percent Reduction of Area UN	Percent Reduction of Area N	
18 Nickel (250) Maraging Steel	190[a]	261	436	0.72	88	7.9	53	3.1	Yes
AISI Type 410 Stainless Steel	158[a]	221	396	0.71	79	15	60	1.4	Yes
AISI 1042 (Quenched and Tempered)	(b)	—		—	78	--	—	2.3	Yes
17-7 PH Stainless Steel	163	174	236	0.94	77	17	45	0.6	Yes
H-11 Tool Steel	165[a]	294	252[b]	0.56	76	11	30	0.0	Yes
9Ni-4Co-0.20C	154[a]	208	373	0.74	76	16	66	6.8	Yes
Rene 41	166	206	290	0.80	73	21	29	3.4	Yes
AISI 4140	186	197	318	0.94	60	14	57	3.9	Yes
Inconel 718	193	213	284	0.90	54	16	27	1.7	Yes
AISI Type 440C Stainless Steel	236	301	149[c]	0.78	50	3.5	3.1	0.6[c]	No
Ti-6Al-4V STA	156[c]	164[c]	227[c]	0.95	45	13[c]	46[c]	2.2[c]	Yes
ASTM A-212 (K_t = 4.2)	38	73	112	0.52	33	37	56	12	No
AISI Type 430F Stainless Steel	85	89	166	0.96	32	22	64	2.8	No
Nickel 270	22	59	85	0.37	30	56	90	24	Yes
ASTM A-515	49	73	106[c]	0.67	30	39	66	8	Yes
HY-100	110	123	234	0.89	27	21	71	7.3	Yes
ASTM A372 Class IV	95	127	207	0.75	26	19	50	2.9	Yes
Ti-6Al-4V Annealed	154	162	243[c]	0.95	25	16	45	2.2[c]	No
AISI 1042 Normalized	67	97	161	0.69	25	30	58	8.3	No
ASTM A-302	—	120[c]	227[c]		22	19[c]	66[c]	15	No
HY 80	93	107	189[c]	0.87	21	26	64	8.6	Yes
AISI 1020	54	71	114	0.76	20	32	65	13	Yes
Ti-5Al-2.5Sn	116	121	205	0.96	19	18	46	3.7	Yes
Armco Iron	31	66	133	0.47	14	19	79	5.9	No
AISI Type 304L Stainless Steel	24	80	102	0.30	13	79	81	15	No
ASTM A-517 (K_t = 4.2)	109	118	204	0.92	11	18	49	3	No
AISI Type 305 Stainless Steel	62	100	175	0.62	11	67	78	16	Yes
Be-Cu	92	104	200	0.88	7	18	67	11	Yes
Titanium (Commercially Pure)	57	70	141	0.81	5	25	53	11	No
AISI Type 310 Stainless Steel	41[c]	77[c]	116[c]	0.53	3	56[c]	64[c]	20[c]	No
A-286 Superstrength Alloy	126	169	250	0.75	3	27	45	4.2	No
7075 T-73	66	74	119	0.89	2	13	32	2.8	No
6061 T-6	40	46	91	0.87	0	17	56	6.1	No
1100 Al	6	12	21	0.50	0	37	90	20	Yes
OFHC Copper	37	52	98	0.71	0	14	89	22	Yes
AISI Type 316 Stainless Steel	79	95	177	0.83	0	48	73	17	No

(a) Yield point in hydrogen plus 10,000 psi

(b) The unnotched mechanical properties of 1042 (quenched and tempered) were not measured in inert environments because these specimens fractured in the threaded grip region

(c) Helium

rate materials as to their susceptibility of embrittlement. However, there is generally a close correlation between reduction of ductility and reduction of notch strength for most of the materials tested. The last column in Table 10 indicates whether the test vessels were vacuum purged prior to pressurizing with hydrogen. Evacuation of the test vessel was also performed prior to conducting the tests in 10,000 psi helium. Those materials tested in hydrogen after prior test vessel evacuation were in most cases, also tested in helium using the evacuation procedure.

Figure 7 shows the relationship between the degree of embrittlement and strength and ductility of the materials tested in 10,000-psi hydrogen. There is considerable scatter, but it is evident that embrittlement is greatest for the higher strength, low-ductility metals. There appears to be a discontinuity in the relationship between yield strength and embrittlement. Specimens with yield strengths above 150 ksi had greater than 50 percent reduction of notch strength in 10,000-psi hydrogen and specimens with a yield strength less than 150 ksi had less than 35 percent reduction of notch strength in 10,000-psi hydrogen.

On the average, there was about 50 percent less decrease of elongation than decrease in reduction of area of the unnotched specimen due to the 10,000-psi hydrogen environment. This difference of embrittlement between the two types of measurements is consistent with the observation that surface cracking in high-pressure hydrogen is generally associated with the necked region, indicating that the majority of the elongation occurred prior to cracking. On the other hand, the majority of the area reduction may occur after initiation of necking, and this parameter would thus be more affected by surface cracking than would the elongation. As will be discussed in more detail in Phase X, fracture of the extremely embrittled specimens proceeded from a single surface crack, which ordinarily formed and propagated prior to necking. Thus, the elongation as well as reduction of area of the extremely embrittled specimens was reduced by 10,000-psi hydrogen.

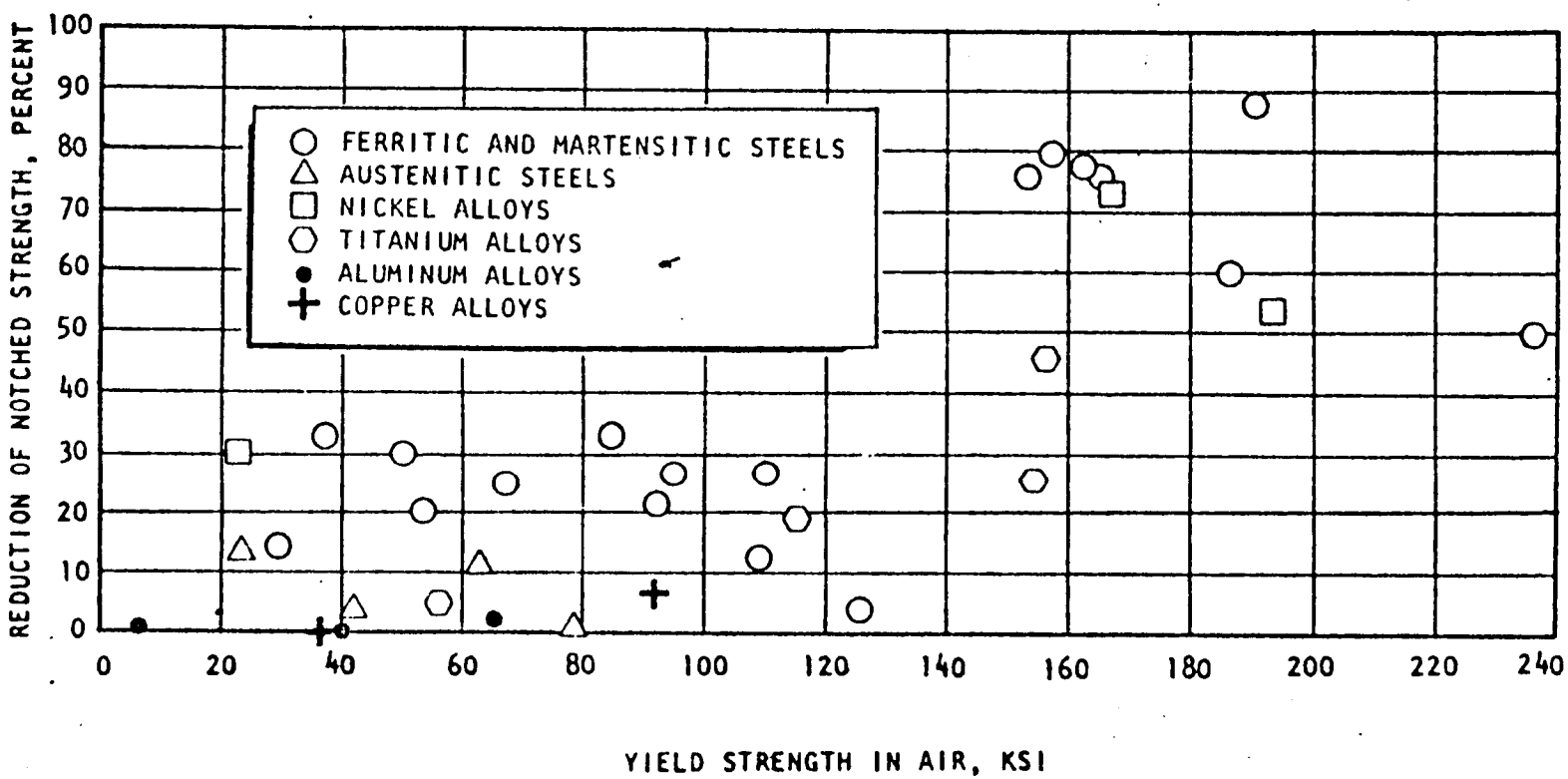

Figure 7. Relationship Between Yield Strength and Reduction of Notched Strength by 10,000-psi Hydrogen for Various Alloys

It has been postulated (Ref. 3) that the degree of embrittlement, as measured by strength reduction, may be a function of the yield strength/ultimate strength ratio. This is based on the theory that rupture of the surface oxide occurs during plastic deformation and this precedes embrittlement. There is experimental evidence that embrittlement proceeds only after a critical degree of deformation. It has been noted that surface cracking in "severely" embrittled specimens is frequently limited to the necked-down region (region of maximum plastic deformation) of the specimen. Secondly, it has been observed that failure of the unnotched high-strength metal specimens frequently occurred soon after deviation from linearity of the load-versus-time curve. This would suggest that embrittlement of the extremely embrittled specimens is associated with a small but critical amount of plastic deformation being obtained. There appears to be no relationship between embrittlement and the yield strength/ultimate strength ratio included in Table 10. Therefore it is suggested that the chemical compositions and toughness are important parameters affecting the degree of embrittlement of metals, as well as the yield strength/ultimate strength ratio. In Phases III and VII this ratio will be shown to be an important embrittlement parameter when the chemistry and structure remain approximately constant.

Relation Between Internal Hydrogen Embrittlement and Hydrogen-Environment Embrittlement. It is of interest to compare the relative susceptibilities of metals to hydrogen-environment embrittlement and internal hydrogen embrittlement. Groeneveld, Fletcher, and Elsea (Ref. 6) compared the susceptibility of various metals to different electrolytic charging conditions ranging from "severe" to "very mild." The specimens were subjected to stress-rupture tests while being charged with hydrogen. Based on their results, the metals can be divided into four categories, ranging from not susceptible to susceptible for all charging conditions. Table 11 compares their results and the results of ambient-temperature tests on similar metals in 10,000-psi hydrogen.

TABLE 11

SUSCEPTIBILITY OF VARIOUS MATERIALS TO INTERNAL HYDROGEN EMBRITTLEMENT AND HYDROGEN-ENVIRONMENT EMBRITTLEMENT

Degree of Embrittlement	Internal Hydrogen Electrolytically Charged	Gaseous Hydrogen Environment
Extreme (Mild charging conditions)	H-11 Tool Steel 17-4 PH Stainless Steel	18 Nickel (250) Maraging Steel AISI Type 410 Stainless Steel H-11 Tool Steel 17-7 PH Stainless Steel Rene 41 Inconel 718
Severe (Medium charging conditions)	AM 355 PH Stainless Steel 18 Nickel (250) Maraging Steel AISI E 8740	HY-100 Nickel 270
Slight (Severe charging conditions	17-7 PH Stainless Steel	AISI Type 304L Stainless Steel
Negligible	Inconel 718	A-286 Stainless Steel AISI Type 316 Stainless Steel

There appears to be very little correlation between embrittlement resulting from internal hydrogen introduced by electrolytic charging and that resulting from a hydrogen environment. Inconel 718 and Rene 41 are two of the materials most embrittled by high-pressure hydrogen, but were classified by Groenevald et al. as not susceptible to embrittlement.

Effect of Pressure on Mechanical Properties. The large volume of tensile data obtained in ambient air and in 10,000-psi helium environments on a wide variety of alloys gave, in spite of considerable scatter, a good indication of the effect of pressure on the mechanical properties of metals. Yield strength in 10,000-psi hydrogen and helium should be approximately 10,000 psi less than in 1 atmosphere air. The 10,000-psi strength reduction would occur for slip on the plane of maximum shear stress, which is oriented 45 degrees to the specimen axis. The difference of yield strength between tests conducted in air and in 10,000-psi helium ranged between 3000 and 22,000 psi, with an average difference of 10,500 psi and a mean difference of 11,000 psi. The difference of yield strength between tests conducted in air and in 10,000-psi hydrogen ranged between 3000 and 16,000 psi, with an average difference of 10,100 psi and a mean difference of 10,000 psi. In all cases, the yield strength was lower in 10,000-psi gaseous environments than in air at 1-atmosphere pressure. Thus, although the results are scattered, there appears to be on an average good correlation between the predicted and experimental yield strength reduction from 10,000-psi environments.

There was also a reduction of the ultimate strength of unnotched specimens and the strength of notched specimens because of the high pressure in high-pressure helium tests. Ultimate strength was between 1000 and 12,000 psi lower in tests conducted in 10,000-psi helium than in tests conducted in air. The average difference was 8500 psi and the mean difference was 9000 psi. It is interesting that the two materials with the least strength reductions were the very ductile AISI type 316 and 304L stainless steels, with 1000 and 4000 psi lower strength in 10,000-psi helium than in air. It is possible that preferred orientation,

resulting from the large plastic deformation, caused final failure or shear lip formation to occur at other than the 45-degree plane of maximum shear stress. If this was the case, then the hydrostatic pressure would have less influence on the strength.

Notched strength varied similarly between that obtained in air and in 10,000-psi helium. Notched strength was between 3000 and 16,000 psi lower in tests conducted in 10,000-psi helium than in tests conducted in air. The average difference was 9500 psi and the mean difference was 8500 psi.

For most of the metals tested, the ductility of the notched and unnotched specimens was essentially the same in air and in 10,000-psi helium environments. Exceptions were AISI type 304L and 316 stainless steels, 1100-0 aluminum, 6061 T-6 and 7075 T-73 aluminum alloys, commercially pure titanium, Ti-5Al-2.5Sn, OFHC copper, and Be-Cu Alloy 25. Unnotched specimens of these alloys had significantly higher ductility in 10,000-psi helium than in air. The parameter most affected was elongation, which was increased from 79 to 86 percent for AISI type 304L stainless steel and from 25 to 37 percent for commercially pure titanium. This corresponded to an increase of ductility, which ranged from 9 percent for AISI type 304L stainless steel to 48 percent for commercially pure titanium.

Of these metals, there were only two (commercially pure titanium and 7075 T-73 aluminum alloy) that had significant increases in reduction of area because of high-pressure helium. The percent reduction of area increased from 53 to 61 for commercially pure titanium and from 32 to 37 for 7075 T-73 aluminum alloy.

Metals that showed a significant increase of notch ductility from air to 10,000-psi helium, as measured by reduction of area of the notch, were AISI type 304L stainless steel (which increased from 15 to 21 percent), AISI type 305 stainless steel (which changed from 16 to 19 percent), and 6061 T-6 aluminum alloy (which changed from 5.5 to 9.5 percent).

An increase of ductility from hydrostatic pressure was also observed by Davidson and Ansell (Ref. 7) on various plain carbon steels in the annealed and spheroidized conditions. They found that there was an increase of elongation with increasing hydrostatic pressure between 1 and 22 kilobars (15,000 and 330,000 psi). Their investigation indicates only about 1 to 2 percent increase of elongation from 10,000-psi pressure. This correlated well with the results from this program that indicate no measurable increase of elongation of the low alloy and plain carbon steels due to 10,000-psi helium.

SUMMARY

Unnotched and notched iron, nickel, titanium, aluminum, and copper-base tensile specimens were tensile tested in air (1 atmosphere), 10,000-psi helium, and 10,000-psi hydrogen environments. From the results of these tests, the metals have been classified, according to their relative degree of embrittlement (based on reduction of notched strength) in 10,000-psi hydrogen, into the following categories of embrittlements; Extreme, Severe, Slight, and Negligible.

1. Extreme Embrittlement. The high-strength steels and high-strength nickel-base alloys fall into this category. These materials had a large decrease of notch strength and ductility, and some decrease of unnotched strength in 10,000-psi hydrogen. Reduction of ductility was between 84 and 92 percent for all three ductility categories (elongation and reduction of area of the unnotched specimens, and reduction of area of the notched specimens). The materials in this category are summarized in Table 12.

2. Severe Embrittlement. The majority of the metals tested are in this category and are listed in Table 13. The ductile, lower-strength steels (Armco Iron), pure nickel, and the titanium base alloy were severely embrittled. These materials had a considerable reduction of notch strength and ductility,

TABLE 12

MATERIALS EXTREMELY EMBRITTLED BY 10,000-PSI HYDROGEN

Material	Reduction of Strength, percent		Reduction of Notch Ductility (Reduction of Area), percent	Reduction of Unnotched Ductility	
	Notched	Unnotched		Reduction of Area, percent	Elongation, percent
18 Nickel (250) Maraging Steel	88	32	100	95	98
AISI Type 410 Stainless Steel	79	21	73	80	91
AISI 1042 (Quenched and Tempered)	78	--	0[a]	100	100
17-7 PH Stainless Steel	77	8	33	95	90
H-11 Tool Steel	76	43	100	100	100
9Ni-4Co-0.20C	76	12	97	78	97
Rene 41	73	16	94	62	80
AISI 4140	60	4	68	81	81
Inconel 718	54	7	88	97	91
AISI Type 440C Stainless Steel	50	60	100	100	100

[a] Two of the three specimens tested in hydrogen had 0.0 ductility; however, the third had sufficient ductility so that there was no ductility on an average between helium and hydrogen environments

TABLE 13

MATERIALS SEVERELY EMBRITTLED BY 10,000-PSI HYDROGEN

Material	Reduction of Strength, percent		Reduction of Notch Ductility (Reduction of Area), percent	Reduction of Unnotched Ductility	
	Notched	Unnotched		Reduction of Area, percent	Elongation, percent
Ti-6Al-4V STA	45	0	9.1	—	—
A-212 (K_t = 4.2)	33	3.3	79.0	40	28
AISI Type 430F Stainless Steel	32	2.5	68.0	42	36
Nickel 270	30	0	70.0	25	7
ASTM A-515	30	0	58.0	48	31
HY-100	27	0	48.0	17	10
ASTM A-372 Class IV	26	0	+7.7	66	52
Ti-6Al-4V Annealed	25	0	+9.1	—	—
AISI 1042 Normalized	25		67	54	24
ASTM A-302	22		81	50	11
HY-80	21		55	14	13
AISI 1020	20		35	34	18
Ti-5Al-2.5Sn	19		42	14	10
Armco Iron	14		73	40	16
ASTM A-517 (K_t = 4.2)	11		61	49	11

but no reduction of unnotched strength. The criterion most affected by the high-pressure hydrogen environment was notch ductility

3. Slight Embrittlement. The non-stable AISI type 300 series stainless steels (AISI types 304L and 305), beryllium copper, and commercially pure titanium fall into this embrittlement category. These materials had a small decrease of notch strength and small or negligible decrease of unnotched ductility. Both AISI type 304L and commercially pure titanium also had a moderate (48 to 27 percent, respectively) reduction of notch ductility. The materials in this category are summarized in Table 14.

4. Negligible Embrittlement. Alloys in this category are listed in Table 15 and include the aluminum alloys, stable austenitic stainless steels, A-286 (a precipitation-hardened austenitic stainless steel), and OFHC copper.

A series of tests were conducted in a hydrogen-contaminated 10,000-psi helium environment. Hydrogen content was 44 ppm, or 0.44-psi partial pressure. Specimens from metals in the slight, severe, and extreme embrittlement categories were tested, and a measurable reduction of notch strength was observed on specimens in each category. Thus, embrittlement by gaseous-hydrogen environments is not restricted to high-pressure hydrogen even for the materials in the slight embrittlement category.

A comparison was made between the relative susceptibilities of metals to hydrogen-environment embrittlement and internal hydrogen embrittlement. There appeared to be very little correlation between embrittlement resulting from internal hydrogen induced by electrolytic charging and that resulting from a hydrogen environment. The poorest correlation was for the two nickel alloys (Inconel 718 and Rene 41), which were not embrittled by electrolytic charging but were extremely embrittled when tested in 10,000-psi hydrogen.

TABLE 14

MATERIALS SLIGHTLY EMBRITTLED BY 10,000-PSI HYDROGEN

Material	Reduction of Notch Strength, percent	Reduction of Notch Ductility (Reduction of Area), percent	Reduction of Unnotched Ductility	
			Reduction of Area, percent	Elongation, percent
AISI Type 304L Stainless Steel	13	48	9	8.0
AISI Type 305 Stainless Steel	11	11	3.8	+3.2
Be-Cu Alloy 25	7	+8	1.4	0
Titanium (Commercially Pure)	5	27	0	5.0

TABLE 15

MATERIALS NEGLIGIBLY EMBRITTLED BY 10,000-PSI HYDROGEN

Material	Reduction of Notch Strength, percent	Reduction of Notch Ductility (Reduction of Area), percent	Reduction of Unnotched Ductility	
			Reduction of Area, percent	Elongation, percent
AISI Type 310 Stainless Steel	3	10.0	3.1	0
A-286 Stainless Steel	3	11.0	2.3	+11.0
7075 T-73 Al Alloy	2	39.0	5.4	20.0
6061 T-6 Al Alloy	0	16.0	+8.0	0
1100-0 Al	0	5.0	0	7.0
OFHC Copper	0	+20.0	0	0
AISI Type 316 Stainless Steel	0	+5.6	+4.2	5.1

The large volume of tensile data obtained in ambient air and in 10,000-psi helium on a wide variety of alloys gave, in spite of considerable scatter, a good indication of the effect of pressure on the mechanical properties of metals. The yield and ultimate strengths of the unnotched specimens and the strength of the notched specimens were reduced approximately 10,000 psi from exposure to the 10,000-psi helium environment. This strength reduction was caused by the 10,000-psi shear component on the specimens from hydrostatic pressure. It was also observed that the weaker metals (OFHC copper, commercially pure titanium, aluminum alloys, and the AISI type 300 series stainless steels) had significantly higher ductility in 10,000-psi helium than in ambient air. The parameter most affected was elongation.

CONCLUSIONS

Metals studied in this phase and other phases were classified into the following categories with regard to their susceptibility to embrittlement in 10,000-psi hydrogen:

1. Extreme Embrittlement (large reduction of notched and unnotched strength and ductility): High-strength steels and high-strength nickel-base alloys
2. Severe Embrittlement (considerable reduction of notched strength and unnotched ductility): Ductile, lower-strength steels, Armco Iron, pure nickel, and the titanium-base alloys
3. Slight Embrittlement (small reduction of notched strength): Non-stable AISI type 300-series stainless steels, beryllium-copper, pure titanium
4. Negligible Embrittlement: Aluminum alloys, stable austenitic stainless steels, copper

PHASE III: EFFECT OF LONG-TIME EXPOSURE OF STRESSED SPECIMENS TO HIGH-PRESSURE HYDROGEN ON THE DEGREE OF EMBRITTLEMENT

INTRODUCTION

In this phase it was determined what influence holding specimens under load in high-pressure hydrogen had on the degree of embrittlement by the hydrogen environment. Both unnotched and notched ($K_t \simeq 8.4$) specimens of AISI 1020, ASTM A-515, HY-80, and H-11 tool steel were tested in tension to failure in 10,000-psi hydrogen following exposure to the environment for various periods of time and at various loads.

Unnotched specimens were held under sustained loads of either 75 percent of yield strength or midway between yield and ultimate strength. Sustained loads were based on the yield and ultimate strengths of the alloys tested in 10,000-psi hydrogen with a prior hydrogen exposure time of zero. Yield strength in 10,000-psi hydrogen was taken to be the stress at which plastic deformation was first observed. Sustained loads used for the notched specimens were either 80 or 90 percent of the strength of notched specimens of the particular alloy in 10,000-psi hydrogen with a prior hydrogen exposure time of zero. Hydrogen exposure times were 1 and 100 days for all conditions plus the zero hold time tests to develop baseline properties mentioned above. For comparison with the hydrogen test results, tests were also performed in air with zero hold time and in 10,000-psi helium with 0-, 1-, and 10-day hold times.

Specimens of AISI 1020 were prestrained under tension in air immediately prior to testing to investigate the role of strain or stress aging during the long-duration tests. Unnotched specimens were strained 1 percent across the reduced section; notched specimens were prestrained 0.001 inch across the notch, which was equal to a 50-percent elongation across the 0.001-inch root radius of the notch.

In addition to the previously described tests on the four steels, similar tests were conducted on Ti-6Al-4V specimens but with only a 1-day hold period.

Preceding page blank

EXPERIMENTAL PROCEDURE

Many of the procedures employed in this phase of the program were identical to those in Phase I. Both Tensile Specimen Design and Apparatus are two such areas; hence, they are eliminated from this discussion.

Materials

Chemical composition, heat treatments, and mechanical properties of the alloys tested in this phase are presented in Tables 16, 17, and 18, respectively.

Test Procedure

In most respects the tensile testing procedure used in this phase was the same as described under Phase I. Except for a few of the earliest tests, the test vessel purging included evacuation treatment. The test vessel purging technique used in each case is indicated in the Results and Discussion sections of this report.

In contrast to Phase I, the tests in Phase III involved much longer hold times. During these hold periods, the specimens were stressed as described in the introduction of this phase.

Phase III test sequence was as follows. The test vessel was purged, the 10,000-psi hydrogen or helium environment was established, and the desired tensile load was applied to the specimen, using the hydraulic loading devise. The load was maintained on the specimen by spring tension for the desired hold time, and the hydraulic loading device was used to tensile test the specimen to failure.

TABLE 16

CHEMICAL COMPOSITIONS OF PHASE III MATERIALS

Material	C	Mn	P	S	Si	Ni	Cr	Al	Ti	Mo	Fe	V	Other
AISI 1020 (3/8-inch-diameter rod)	0.17	0.47	0.011	0.037							Bal.		
ASTM A-515 Gr.70 (3/8-inch-thick plate)	0.27	0.71	0.011	0.018	0.19						Bal.		
HY-80 (1/2-inch-thick plate)	0.13	0.30	0.016	0.021	0.22	2.49	1.46	0.05	0.001	0.43	Bal.	0.002	
H-11 (1-inch-diameter rod)	0.42	0.40	0.021	0.005	0.80		5.01			1.27	Bal.	0.53	
Ti-6Al-4V Annealed (3/8-inch-diameter rod)	0.24							6.0	Bal.		0.15	4.1	N_2, 0.0241 H_2, 0.0081 O_2, 0.191
Ti-6Al-4V STA (1/2-inch-diameter rod)	0.023							6.4	Bal.		0.15	4.2	N_2, 0.014 H_2, 0.008 O_2, 0.140

TABLE 17

HEAT TREATMENTS OF PHASE III MATERIALS

Material	Heat Treatment by Supplier (As-Received Condition)	Hardness	Heat Treatment at Rocketdyne	Hardness
AISI 1020	Hot Rolled	---	None	---
ASTM A-515 Gr.70	Hot Rolled	---	None	---
HY-80	To MIL S-16216G (Ships)	---	None	---
H-11 Tool Steel	Annealed	---	Annealed at 1850 F for 40 mintues; air cooled; triple tempered at 1000 F for 2 hours; air cooled	R_c 55
Ti-6Al-4V Annealed	Annealed	R_c 35	None	---
Ti-6Al-4V STA	Solution treated at 1750 F for 1 hour; water quenched; aged for 4 hours at 1000 F	R_c 40	None	---

TABLE 18

MECHANICAL PROPERTIES OF PHASE III MATERIALS
(SUPPLIER CERTIFICATION)

Material	Tensile Strength, ksi	Yield Strength, ksi	Reduction of Area, percent	Elongation, percent
AISI 1020		Not Furnished		
ASTM A-515 Gr.70	76.1	46.4		27.5
HY-80	106.6	90.0	68.9	27.0
H-11 Tool Steel		Not Furnished		
Ti-6Al-4V Annealed	159.0	140.0	50.0	18.0
Ti-6Al-4V STA	173.0	163.0	47.0	17.0

RESULTS AND DISCUSSION

Unnotched Steel Specimens

Results of the Phase III tests on unnotched AISI 1020, ASTM A-515, HY-80, and H-11 tool steel specimens are given in Table 19. Individual specimen test data are contained within Appendix Tables III-1 through III-4.

The most evident effect of the duration of the hold period on the unnotched steel specimens was an increase in yield strength of AISI 1020, ASTM A-515, and HY-80. For AISI 1020 the yield strength was higher after the longer hold times and with the higher hold stress; the yield strength increase was approximately the same in 10,000-psi helium as in 10,000-psi hydrogen. For the 35,500-psi hold stress tests, the yield strength increase was 6000 psi for the 1-day hold times in helium and hydrogen and 12,000 psi for the 100-day hold times in hydrogen. When the AISI 1020 specimens were held at the higher stress which was above the zero hold time yield strength in hydrogen, a new yield point was found in the subsequent tensile test. This will be discussed in more detail later in this section.

The new yield strength was 11,000 psi above the hold stress for the 1-day hold tests in both hydrogen and helium, 18,000 psi above the hold stress for the 10-day hold period in helium, and 19,000 psi above the hold stress for the 100-day hold period in hydrogen. Ultimate tensile strengths of AISI 1020 specimens were essentially unchanged by holding at the lower hold stresses, but were significantly increased by holding at the higher hold stress in either hydrogen or helium. The increase in yield and ultimate tensile strength during the hold periods of unnotched AISI 1020 specimens was not a function of the environment, because the increase was the same in helium as in hydrogen.

Elongation of AISI 1020 specimens was not significantly affected by hold time or hold stress, but generally was slightly lower for tests in 10,000-psi hydrogen than for tests in 10,000-psi helium. Reduction of area of

TABLE. 19

TENSILE PROPERTIES OF UNNOTCHED SPECIMENS OF AISI 1020, ASTM A-515, HY-80, AND H-11 TOOL STEEL IN 10,000-PSI HYDROGEN, 10,000-PSI HELIUM, AND AIR

Material	Environment	Pressure, psig	Hold Time, days	Hold Stress, ksi	Strength		Ductility	
					Yield, ksi	Ultimate, ksi	Elongation, percent	Reduction of Area, percent
AISI 1020 (Prestrained 1 Percent)	Air	0	0	0	54	71	—	65
	Helium	10,000	0	0	41	63	40.0	68
	↓	↓	1[a]	0	43	66	39.0	69
			1	35.5	47	64	34.0	68
			1	53.0	63	67	37.0	71
			10	53.0	71 45[b]	72	31.0	69
	Hydrogen		0	0	40	62	32.0	45
	↓		1	35.5	46	63	33.0	45
			100	35.5	52	66	25.0	49
			1	53.0	64	65	30.0	45
			100	53.0	72	73	30.0	54
ASTM A-515 Gr.70	Air	0	0	0	49	73	—	66
	Helium	10,000	0	0	≈40[b]	65	42.0	67
	Hydrogen	10,000	0	0	≈43[b]	64	29.0	35
	↓	↓	1	32.3	44	67	28.0	34
			100	32.3	45	66	27.0	38
			1	54.0	63	67	29.0	36
			100	54.0	69	71	27.0	47
HY-80	Air	0	0	0	93	107	—	64
	Helium	10,000	0	0	≈82[b]	98	23.0	70
	Hydrogen	10,000	0	0	85	99	20.0	60
	↓	↓	1	64.4	85	99	22.0	52
			100	64.4	85	101	22.0	66
			1	92.5	98	101	20.0	58
			100	92.5	102	105	17.0	58
H-11 Tool Steel	Air	0	0	0	165	299	13.0	30
	Helium	10,000	0	0	---	299	8.8	30
	Helium	10,000	0	0	---	277	1.4	1.2
	Hydrogen	10,000	0	0		171	0	0
	↓	↓	1	128.0	153	172	0	0
			100	128.0	146	167	0	0

[a] Allowed to stand for 24 hours in air after prestraining before testing to failure in 10,000-psi helium

[b] Calculated from strain indicator reading [c] Hydrogen-contaminated helium

AISI 1020 in helium was virtually the same for all test conditions. Reduction of area was considerably lower in hydrogen than in helium for all test conditions, and there appears to have been a tendency in the hydrogen tests for the reduction of area to increase with hold time and hold stress although the relationships are somewhat obscured by data scatter (see Appendix Table III-1).

Yield strength of unnotched specimens of ASTM A-515 was unaffected by holding in hydrogen at the lower hold stress, which was below the yield strength. However, as with AISI 1020, when the ASTM A-515 specimens were held at a stress above the yield strength, a new yield point was found in the subsequent tensile test. This yield point was 9000 and 15,000 psi above the hold stress for the 1- and 100-day tests in hydrogen, respectively. Ultimate tensile strength was essentially the same for all hold conditions in hydrogen. Yield and ultimate tensile strength for zero hold time tests in hydrogen were the same as in helium.

Elongation of unnotched ASTM A-515 specimens was definitely lower in 10,000-psi hydrogen than in 10,000-psi helium, but it was unaffected by hold time or hold stress. Reduction of area was considerably lower in hydrogen than in helium, and there was some tendency for it to increase with an increase in hold time and hold stress.

Yield strength of HY-80 was not affected by holding at a stress below the yield strength. After holding in hydrogen at a stress above the yield strength, a yield point was found that was 5500 psi and 9500 psi above the hold stress for 1- and 100-day hold tests, respectively. Ultimate tensile strength of unnotched HY-80 specimens was unaffected by hold time or hold stress. Yield and ultimate tensile strengths were the same in hydrogen as in helium for zero hold time tests. Elongation of unnotched HY-80 specimens was essentially the same under all test conditions. Reduction in area was lower in hydrogen than in helium, but not as much as for AISI 1020 and ASTM A-515, while it was essentially the same for all test conditions in hydrogen.

Hydrogen exposure tests on H-11 were performed with only one hold stress. From the zero hold time tests, it was found that H-11 had zero ductility in 10,000-psi hydrogen. Thus, H-11 had no true yield strength in 10,000-psi hydrogen. The single hold stress used was 75 percent of ultimate strength in 10,000-psi hydrogen with zero hold time. Yield strengths listed in Table 19 for H-11 were determined as described under the Phase I Test Procedure section, i.e., they were the points where any deviation from linearity occurred in the load versus time curves and are thus more like proportional limits. It is interesting that throughout the different phases of this program the high-strength materials such as H-11 tended to fail in 10,000-psi hydrogen shortly after deviation from linearity occurred. Ultimate tensile strength of H-11 in hydrogen was not significantly influenced by hold time, but it was greatly reduced from the strength in helium. Elongation and reduction of area were both reduced to zero for H-11 in 10,000-psi hydrogen. The extreme effect of hydrogen on H-11 tool steel is further attested to by the results (Table 19) of tests on two unnotched H-11 tool-steel specimens in helium that was contaminated with hydrogen. The amount of hydrogen in the helium is believed to have been less than 1 ppm, yet the ultimate tensile strength and ductility were significantly reduced by this small partial pressure of hydrogen. Unnotched specimens of HY-80 and ASTM A-515 were not embrittled by the same contaminated helium.

Thus, for the same test conditions, yield and ultimate tensile strengths of unnotched AISI 1020, ASTM A-515, and HY-80 specimens were the same in both 10,000-psi hydrogen and 10,000-psi helium. The lower ultimate strength of H-11 tool steel in hydrogen can probably be attributed to the extreme brittleness of this material in 10,000-psi hydrogen. The ductility of all four steels were lower in 10,000-psi hydrogen than in 10,000-psi helium, but the ductility reduction varied from the relatively modest reduction for HY-80 to the extreme reduction, to zero ductility for H-11. There was some indication that the ductility of AISI 1020 and ASTM A-515 increased with increased hold stress or hold time in hydrogen, but the effect was small.

Thus, there was no significant effect of hold time or hold stress on the effect of the 10,000-psi hydrogen environment on the tensile properties of the unnotched specimens of the four steels. There were effects of hold stress and hold time on tensile properties of AISI 1020, ASTM A-515, and HY-80 specimens, irrespective of environment, and these are discussed below.

The increase in yield strength of the unnotched AISI 1020 specimens, prestrained and held at a stress below the yield strength, appears to have been typical carbon strain aging. Holding unstressed in air after prestraining before testing in helium resulted in an increase in yield strength, although smaller than that which resulted from holding specimens under stress for the same time. These very limited results indicate that holding under stress accelerates strain aging. Yield strength was essentially the same after holding 1 day in helium as after holding 1 day in hydrogen. Thus, the environment apparently had no affect on the yield strength. The fact that the yield strength was essentially the same after holding 10 days in helium as after holding 100 days in hydrogen indicates that the strain aging was complete within the 10-day period. Since the ASTM A-515 and HY-80 specimens were not prestrained, no strain aging could occur in the specimens held below yield strength, and thus yield strength was not affected by hold time for these specimens. For specimens held above yield strength, enough plastic deformation occurred in loading to the hold stress to eliminate completely any effect of prior prestraining.

Re-establishment of a yield point after holding above the normal yield strength for AISI 1020, ASTM A-515, and HY-80 is described in greater detail for clarity. Figure 8 shows a load-versus-time curve from a load recorder chart for a test of an unnotched AISI 1020 specimen in helium. As described in Phase I, the hydraulic loading device was used to perform the tensile test. A hold test in hydrogen with a stress above

yield strength proceeded as follows. After establishment of the 10,000-psi hydrogen environment, the hydraulic loading device was used to load the specimen in the same manner as if a tensile test were being performed, except loading was stopped at a stress midway between yield and ultimate tensile strengths. Up to this point the load-versus-time curve appeared the same as in Fig. 8. The nut was tightened against the lower plate of the spring loading system (refer to Fig. 6, Phase I), and the hydraulic loading device was removed. Thus, the spring maintained the load on the specimen. After the hold period the hydraulic loading device was replaced, the ram was brought up against the lower spring plate, and a tensile test was performed.

Figure 9 shows a load-versus-time curve for an unnotched AISI 1020 specimen after a 100-day hold period in hydrogen. The curve begins at the point at which the hydraulic loading device began receiving the load from the spring. Once the loading device assumed the load, the load-versus-time curve was linear and had the same slope as the elastic portion of the preloading curve. That is, after the hold period, when the load was again increased, the specimen behaved elastically until a yield point was reached and the load dropped abruptly, as shown in Fig. 9. The load measured from the load cell by the recorder remained at this lower level for the majority of the plastic deformation and increased only slightly at failure. Although the measured load remained relatively constant between the lower yield point and failure, the stress was increasing during this period. This occurred because the difference between the area at the necked region and at the sliding seals was increasing which, in turn, increased the tensile load exerted by the pressure. As noted above, this behavior was typical for unnotched AISI 1020, ASTM A-515, and HY-80 specimens held above the zero hold time yield strength, and the difference between the upper yield point and the hold stress was greater after holding 100 days than after 1 day. The increase in upper and lower yield points as a result of holding above the normal yield strength appears to have been a stress or strain-aging effect. A brief review of the literature on this phenomenon appears below.

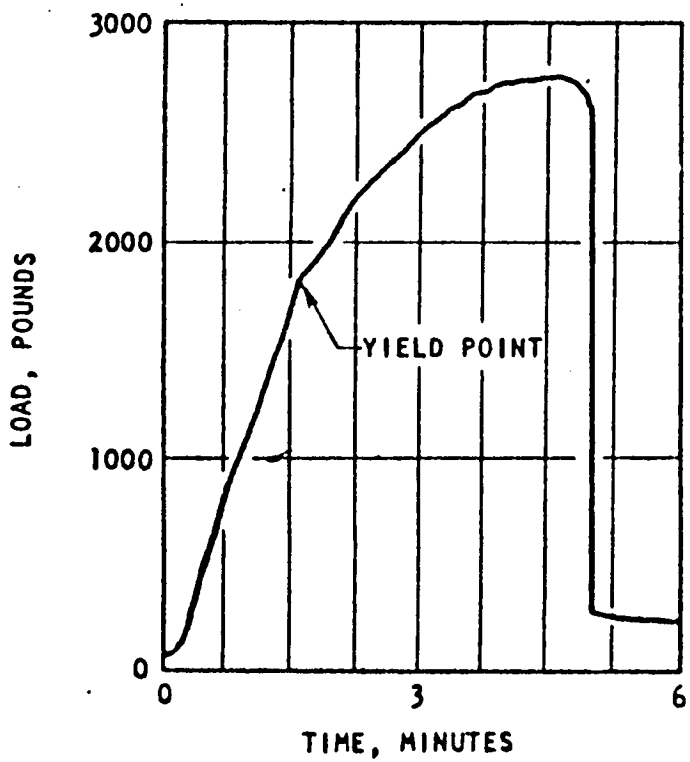

Figure 8. Typical Load-Versus-Time Curve for Unnotched AISI 1020 Specimen; Tested to Failure in 10,000-psi Helium (No Hold Time)

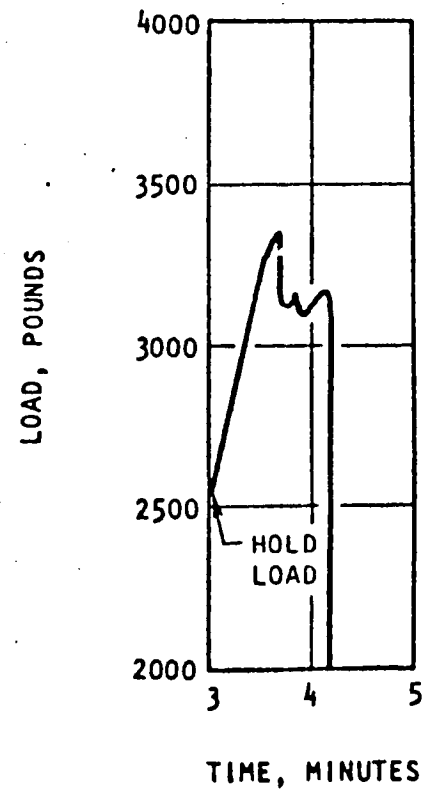

Figure 9. Typical Load-Versus-Time Curve for Unnotched AISI 1020 Specimen; Held Above the Yield Strength in 10,000-psi Hydrogen for 100 Days; then Tested to Failure in 10,000-psi Hydrogen

Wilson and Russell (Ref. 7) studied the tensile properties between the lower yield strength and the fracture stress of low-carbon steels that were prestrained and aged for various periods of time at 60 C, and observed three stages of aging. During the first stage, the Luders strain increased with greater aging duration, but there was only a slight increase in the lower yield strength. The second aging stage was characterized by an increase in the lower yield strength, and the third stage by an increase of flow stress, strain hardening coefficient, and ultimate strength. Times for these stages to occur were about 0 to 20 minutes for the first stage, 20 to 200 minutes for the second stage, and over 200 minutes for the third.

Further work by Wilson and Russell (Ref. 9) indicated that first-stage aging resulted from migration of interstitials to dislocations, and at the end of the first stage all of the disclocations were pinned. The second stage of aging was caused by the clustering of interstitials around dislocation and was thus the first stage of precipitation. These pre-precipitates do not affect flow stress after Luders strains have occurred. Wilson and Russell suggested that the third stage resulted from the formation of stable precipitates which acted as barriers to dislocation motion and so increased the flow and ultimate stresses.

A similar increase of yield and ultimate strengths has been found to occur after aging prestrained, high-strength, low alloy steels. Goel, Busch, and Zackay (Ref. 10) showed that the yield strength ultimate strength ratio of H-11 tool steel was increased to near unity by prestraining and aging at 900 F. The ductility of the specimens was approximately the same after the different mechanical-thermal treatments. Similar results were also observed by Stevenson and Cohen (Ref. 11) from the prestraining and retempering of AISI 4340. They observed for certain tempering treatments that the yield strength corresponded to the maximum tensile load and following yielding there was almost a complete lack of stable elongation, i.e., plastic elongation at maximum stress. Stevenson and Cohen also observed that a reduction of ductility accompanied the increase in strength which occurred during strain aging.

Both of these investigations (Ref. 10 and 11) indicated that during tempering there was a re-solution of the carbide particles and then a re-formation of finer precipitates. Goel, Busch, and Zackay calculated that the change in the carbide spacing alone could not account for the higher yield strength from aging. They suggested, however, that the large particle density "would be expected to cause an increase in the rate of dislocation multiplication. This would account for the strength increase on the basis of an increased dislocation density."

No references were found on the influence of tensile stress during strain aging. There are, however, recent investigations by Harrington (Ref. 12 and 13) on stress aging. In the experiments, Harrington's specimens were held for short periods at elevated temperatures under a tensile stress less than the yield strength. His investigations showed that a large increase of proportional limit, yield strength and ductility, and a smaller increase of ultimate strength resulted from aging (at 600 to 800 F for less than 1/2 hour) high-strength steels held at a stress below the elastic limit. Strain aging also increased the electrical conductivity. Harrington explained these results by postulating that stress- or strain-induced precipitation occurred from the solid solution, which reduced the solute content of the solid solution matrix. In this respect, stress aging would have similar characteristics to strain aging, but stress aging is not dependent upon pre-straining.

This brief review of strain and stress aging indicates that properties similar to those obtained in this program by holding the low alloy steels under stress at room temperature are also obtainable from strain aging prestrained specimens or from elevated-temperature stress aging. The Phase III steels have greater similarity to the low carbon steels used in the investigations of Wilson and Russell than the low alloy steels used in the other investigations reviewed. Aging temperature used in their work was also relatively low (60 C). In this program, holding above the yield strength evidently resulted in second-stage aging according to the classification of Wilson and Russell, and the 10-day hold period for AISI 1020 specimens resulted in third-stage aging.

To explain the strength increase observed during the Phase III tests, it can be postulated that the applied stress accelerated the aging reaction. The aging reaction probably resulted from interstitial clustering and/or precipitation as postulated in all strain and stress aging theories.

Notched Steel Specimens

Results of the Phase III tests on notched AISI 1020, ASTM A-515, HY-80, and H-11 tool-steel specimens are given in Table 20. Tables of individual specimen test data are contained in Appendix Tables III-5 through III-8.

In accordance with the hydrogen-environment embrittlement classification used in Phase II, AISI 1020, ASTM A-515, and HY-80 were severely embrittled while H-11 tool steel was extremely embrittled by the 10,000-psi hydrogen compared to 10,000-psi helium environment. The results show that holding under stress in 10,000-psi hydrogen did not increase the degree of hydrogen-environment embrittlement and, in fact, the notch strength and ductility were in some cases higher after holding in hydrogen.

Strain aging probably occurred during the long-duration tests on the notched AISI 1020 specimens because they were prestrained 0.001 inch across the notch prior to testing in high-pressure helium and hydrogen. There was no change of notch strength or ductility during the 1- and 10-day exposure tests in 10,000-psi helium. Nevertheless, it is probable that yielding occurred at a higher stress after the 1- and 10-day tests than after the zero hold duration tests because of strain aging.

Reduction of notch strength in 10,000-psi hydrogen compared to that in 10,000-psi helium decreased from about 14 percent at zero hold time to 4 percent and 1 percent after 1-day and 100-day hold durations in 10,000-psi hydrogen. This decrease of embrittlement due to holding under stress

TABLE 20

TENSILE PROPERTIES OF NOTCHED SPECIMENS OF AISI 1020, ASTM A-515, HY-80, AND H-11 TOOL STEEL IN 10,000-PSI HYDROGEN, 10,000-PSI HELIUM, AND AIR

Material	Test Conditions				Test Results		
					Strength		Ductility
	Environment	Pressure, psig	Hold Time, days	Hold Stress, ksi	Ultimate, ksi	Percent Change From Helium	Percent Reduction of Area
AISI 1020	Air	0	0	0	114		12.0
	Helium	10,000	0	0	105		14.0
	Helium		1[a]	0	104		16.0
	Helium		1	76	101		19.0
	Helium		10	76	103		14.0
	Hydrogen		0	0	90	14	8.3
	Hydrogen		1	72	101	4	9.2
	Hydrogen		100	72	104	1	9.4
	Hydrogen[b]		0	0	84	20	8.2
	Hydrogen[b]		1	76	101	4	8.7
	Hydrogen[b]		100	76	104	1	8.4
ASTM A-515 Gr.70	Helium		0	0	106		8.1
	Hydrogen		0	0	81	24	2.3
	Hydrogen		1	65	82	23	3.2
	Hydrogen		100	65	83	22	3.8
	Hydrogen[b]		0	0	74	32	3.4
	Hydrogen[b]		1	67	83	22	3.4
	Hydrogen[b]		100	67	83	22	3.7
HY-80	Helium		0	0	190		8.6
	Hydrogen		0	0	155	18	3.6
	Hydrogen		1	124	160	16	3.5
	Hydrogen		100	124	154	19	3.4
	Hydrogen[b]		0	0	151	20	3.9
	Hydrogen[b]		1	136	161	15	4.2
	Hydrogen[b]		100	136	155	18	4.3
H-11 Tool Steel	Helium		0	0	252		0.0
	Hydrogen		0	0	63	75	0.0
	Hydrogen		100	50	95	62	0.1
	Hydrogen[b]		0	0	57	77	0.0
	Hydrogen[b]		1	54	78	69	0.0
	Hydrogen[b]		100	54	112	56	0.0

[a] Allowed to stand for 24 hours in air after prestraining before testing to failure in 10,000-psi helium

[b] Test cells evacuated prior to testing

parallels the increase of yield strength in the unnotched specimens and is believed associated with an increase in the yield strength and thus the yield strength/ultimate strength ratio of the notched specimens due to strain aging. This effect will be discussed in greater detail in Phase VII.

There was no significant effect of hold stress on notch strength or ductility; however, the two hold stresses were nearly the same because of a change of test procedure during notched specimen testing. For the first set of tests performed, the test vessels were purged, using only a pressurization-depressurization treatment. During these tests it was found that evacuation prior to the pressurization treatment resulted in more severe hydrogen-environment embrittlement (see Discussion under Phase I); therefore, the evacuation treatment was used for the second set of tests.

Hold stress used during the first tests was 80 percent of the zero time hold notch strength in hydrogen without the evacuation treatment For the second set of tests, the hold stress was raised to 90 percent of the zero time hold notch strength in hydrogen, but based on the lower strength which resulted from the use of prior evacuation.

Zero hold time notch strength of AISI 1020 and ASTM A-515 was significantly reduced by prior test vessel evacuation. However, after a hold time in hydrogen of even 1 day (as well as 100 days), there was no difference in notch strength between tests performed with and without prior evacuation. This does not seem to have been merely an improvement of test vessel hydrogen purity, which reverted because of leakage to purity levels without prior evacuation. If such were the case, then the notch strengths of all of the steels should have increased with hold time, and considerably between 1 and 100 days, for both evacuation and non-evacuation purging. However, this was not so. Although the amount of hydrogen in an individual test vessel was not sufficient for an accurate gas analysis, the hydrogen in the storage vessel (receiver) was analyzed after the 100-day tests and no increase in impurity content was found.

It is suggested that evacuation of the test vessels removes adsorbed gases, most importantly oxygen, from the surface of the specimens, and that this reduced concentration of adsorbed oxygen on the surface is below the concentration which would be in equilibrium with hydrogen of the purity used in the tests. To elaborate, the vacuum obtained during test vessel evacuation is approximately 20 microns (4×10^{-4} psi) gas pressure or, since air is being removed, approximately 1×10^{-4} psi oxygen pressure. The oxygen content in the test hydrogen is 0.5 ppm or 5×10^{-3} psi oxygen partial pressure in the 10,000-psi hydrogen. Thus, the oxygen partial pressure was lower during evacuation than during exposure to 10,000-psi hydrogen and, consequently, the concentration of adsorbed oxygen on the surface of the specimen would be lower during evacuation than when equilibrium was attained with the 10,000-psi hydrogen.

After evacuation and upon exposure to the 10,000-psi hydrogen, the hydrogen can more effectively adsorb on the metal surface because of the lower adsorbed oxygen concentration, resulting in greater embrittlement. Upon holding in 10,000-psi hydrogen, the oxygen from the hydrogen preferentially adsorbs on the metal surface; this reduces the degree to which hydrogen can adsorb on the surface, thus reducing the embrittlement. In particular for the ASTM A-515 specimens, the hydrogen-environment embrittlement was the same after the 1-day hold period as after the 100-day hold period. This indicates that equilibrium between the adsorbed oxygen concentration on the metal surface and the oxygen in the 10,000-psi hydrogen was attained within the 1-day hold time.

The effect of adsorbed nitrogen was not considered in the above hypothesis because Hofmann and Rauls (Ref. 14) showed that argon and purified nitrogen additions to high-pressure hydrogen did not affect the degree of embrittlement of steels, but the addition of 1 percent oxygen to hydrogen at 1910 psi completely eliminated the embrittling effect of the hydrogen.

COMPARISON OF RESULTS FOR STEELS WITH RESULTS FROM PREVIOUS PROGRAM

It is of interest to correlate the results of the long-duration tests in this program with those performed previously (Ref. 2) on ASTM A-212, ASTM A-517, and ASTM A-302 low-alloy ductile steels. The effect of hold stress on the degree of embrittlement was evaluated in the previous program for ASTM A-302, and it was observed that embrittlement decreased with increasing hold stress for both unnotched and notched specimens. The main effect of hold duration found in the previous program was a few failures that occurred during the hold period in ASTM A-212 parent metal specimens and ASTM A-517 weld metal specimens.

Decrease in embrittlement of ASTM A-302 unnotched specimens with increasing hold stress correlates well with the results from the current program; however, hold stress did not influence the degree of embrittlement of the notched specimens. No failures occurred during the hold period in the current program, and failures during the hold period in the previous program may be related to temperature fluctuations during the tests. These fluctuations occurred because the temperature of the laboratory was not controlled, and many variations in temperature were noted during the long-duration tests. Temperature fluctuations cause pressure changes in the test vessels and consequently changes in the load applied to the specimen by the pressure. Therefore, increased load and load cycling because of the temperature fluctuations could have contributed to the failures in the long-duration tests in the previous program. A laboratory temperature control was installed during the present program and uniformity of test results was found to improve.

Ti-6Al-4V Specimens

Results of the Phase III tests on Ti-6Al-4V specimens are given in Table 21. Tables of individual specimen test data are contained in Appendix Tables III-9 and III-10. Test vessel purging included the evacuation treatment for all tests on Ti-6Al-4V in this phase.

TABLE 21

TENSILE PROPERTIES OF Ti-6Al-4V IN 10,000-PSI HYDROGEN AND 10,000-PSI HELIUM

Heat Treatment	Unnotched or Notched	Test Conditions				Test Results				
						Strength			Ductility	
		Environment	Pressure, psig	Hold Time, hours	Hold Stress, ksi	Yield, ksi	Ultimate, ksi	Percent Change From Helium	Percent Elongation (1.25-Inch Gage Length)	Percent Reduction of Area
Solution Treated and Aged (STA)	U	He	10,000	0	0		164		13	46.0
	U	H_2		24	115	153	169	--	12	47.0
	U	H_2		24	162	140[a], 168[b]	169		12	45.0
	N	He		0	0		227			2.2
	N	H_2		0[c]	120		120	-47		1.4
	N	H_2		0	0		166[d]	-27		1.7
Annealed	N	He					243			2.2
	N	H_2		0	0		156	-36		1.9
	N	H_2		(e)	140		140	-42		0.6
	N	H_2		(e)	125		125	-49		2.0
	N	H_2		(f)	(f)		241	-1		3.9
	N	H_2		(g)	205		205	-16		3.2

(a) Yield strength found on loading to hold stress
(b) Yield strength found on testing after hold period
(c) One specimen failed on preloading just before reaching hold stress; one failed seconds after reaching hold stress
(d) Specimen loaded at faster strain rate than other specimens
(e) Specimen failed seconds after reaching hold stress
(f) Specimen stressed in 10,000-psi hydrogen to 67 ksi, unloaded, and examined in air; re-exposed to 10,000-psi hydrogen and held unloaded for 3 days, loaded to 96,000 psi and then in 11,000-psi increments to failure at 241 ksi
(g) Specimen preloaded to occurrence of first crack step; loading stopped; specimen failed within seconds

As can be seen from Table 21, there was no indication of any hydrogen-environment embrittlement of unnotched Ti-6Al-4V STA specimens. Some surface cracking similar to that found in Phase I occurred in the necked region of the specimens tested in hydrogen. This will be discussed in Phase X.

The only significant change in properties of unnotched STA specimens was an increase in yield strength, which resulted from holding the specimens under load for 24 hours in 10,000-psi hydrogen. It is not believed that the hydrogen affected the yield strength or played any role in its increase. The normal yield strength, i.e., without the hold period, was determined during the preloading of the specimens that were held at a stress above the yield strength. A load recorder determined the yield strength from the load-versus-time curve to be 140 ksi. It should be noted that the hold stresses used in this phase were based on the yield strength determined in Phase I for Ti-6Al-4V STA, using a strain indicator. That value was higher than the 140 ksi reading given above. Yield strength determined from the load-versus-time curve is more accurate.

Thus, the average yield strength of unnotched Ti-6Al-4V STA specimens increased from 140 to 153 ksi as a result of holding for 24 hours at a stress below the yield strength. When unnotched Ti-6Al-4V STA specimens were tensile tested after holding for 24 hours at a stress above the yield strength, a new yield strength was found. That is, as described earlier for the steels tested in this phase, when the load on the specimen was increased above the hold stress, the specimen behaved elastically until yielding occurred. The yield strength thus determined was almost as high as the ultimate strength, which was not affected by the hold period. Thus, as for the steels, it appears that some strain or stress aging occurred in the unnotched Ti-6Al-4V STA specimens during the 1-day hold period.

Strength of notched Ti-6Al-4V specimens was considerably reduced in 10,000-psi hydrogen compared to 10,000-psi helium. In both this phase and Phase I, the results of tests in hydrogen on notched Ti-6Al-4V specimens were quite erratic. As a consequence, the data in Table 21 for notched specimens tested in hydrogen represent individual specimen test results.

Notched Ti-6Al-4V STA specimens were scheduled to be held 1 day at a stress of 120 ksi, i.e., 90 percent of the notched strength in 10,000-psi hydrogen with zero hold time determined in Phase I. One specimen failed within a few seconds after reaching that stress level. A second specimen broke during preloading at a stress 1400 psi below the scheduled hold stress. As noted above, the results of the zero hold time tests in Phase I were erratic and one of those specimens failed at 120 ksi. Thus, 120 ksi may be the most accurate ultimate strength for notched Ti-6Al-4V STA specimens in 10,000-psi hydrogen. A third notched Ti-6Al-4V STA specimen was tested in 10,000-psi hydrogen at a fast strain rate (0.050/minute), and its strength was 25 percent higher than the strength in hydrogen at the normal strain rate of 0.007/minute. The main characteristic observed for the tests of notched Ti-6Al-4V STA specimens was the very rapid crack propagation in hydrogen once a crack had been initiated.

Results for the notched, annealed Ti-6Al-4V specimens tested in hydrogen were also erratic. The first test specimen failed within a few seconds after reaching a hold stress of 140 ksi, which was 90 percent of the notched strength in 10,000-psi hydrogen with no hold period. The second specimen failed within a few seconds after reaching a hold stress of 80 percent of the notched strength in the same environment.

A third specimen was stressed to 62 percent of the strength in hydrogen with zero hold time. No cracks were observed when the specimen was removed from the test vessel and examined. The specimen was returned to the test vessel, held unstressed in 10,000-psi hydrogen for 4 days, and then loaded in increments over a 3-day period until final failure occurred

at 155 percent of the notched strength in 10,000-psi hydrogen. This is about the same value as found in 10,000-psi helium. The specimen also failed within a few seconds after having established the last hold stress.

Electrical resistivity was monitored on a fourth specimen during loading in the hydrogen environment. It was planned to hold the load constant at the first indication of crack initiation; however, failure occurred almost immediately after the first indication of a crack.

Thus, in almost all cases, both annealed and STA notched Ti-6Al-4V specimens failed within moments after a hold stress was established. Why the failures did not occur more often during the relatively slow rate of loading is not clear.

SUMMARY

The four steels tested in Phase III were considerably embrittled by a 10,000-psi hydrogen environment as compared to 10,000-psi helium. The steels listed in order of increasing hydrogen-environment embrittlement included HY-80, AISI 1020, ASTM A-517, and H-11 tool steel, which had zero ductility in the hydrogen. No effect on the degree of hydrogen-environment embrittlement of the steels could be attributed to holding specimens under stress in 10,000-psi hydrogen for periods up to 100 days before tensile testing. Yield strengths of unnotched AISI 1020 specimens increased with hold time when held at a stress below the yield strength; however, specimens were prestrained and the yield strength increase was attributed to strain aging. Yield strengths of unnotched HY-80 and ASTM A-515 specimens, which were not prestrained, were not affected by holding at a stress below the yield strengths. When unnotched AISI 1020, ASTM A-515, and HY-80 specimens were tensile tested after holding at a stress above the yield strength, a new yield point was found that increased with a longer hold time. This increase in yield strength was attributed to strain or stress aging.

The degree of hydrogen-environment embrittlement, as measured by reduction of notch strength in 10,000-psi hydrogen compared to that in 10,000-psi helium, decreased with increasing exposure duration for the prestrained, notched AISI 1020 specimens. It was suggested that this embrittlement decrease related to an increase of yield strength/ultimate strength ratio, resulting from strain aging during the hold period. Evacuation of the test vessels prior to pressurization-depressurization purging led to increased embrittlement from the 10,000-psi hydrogen environment in tests involving no hold period. The increased embrittlement was attributed to a reduction in the concentration of oxygen adsorbed on the specimen surface. After holding for 1 day or longer, the embrittlement in 10,000-psi hydrogen was the same whether or not the test vessels had been evacuated.

The strength of notched Ti-6Al-4V specimens was considerably lower in 10,000-psi hydrogen as compared to 10,000-psi helium. In almost all cases, both annealed and STA notched Ti-6Al-4V specimens failed in hydrogen shortly after a hold stress was established, rather than while the specimens were being loaded. Once cracking was initiated in hydrogen, failure was rapid. There was no indication of hydrogen-environment embrittlement f unnotched Ti-6Al-4V STA specimens, but an increase of yield strength occurred during the hold period and was attributed to strain or stress aging.

CONCLUSIONS

Based on the preceding tests the following conclusions were drawn:

1. HY-80, AISI 1020, ASTM A-515, and H-11 tool steel are considerably embrittled by a 10,000-psi hydrogen environment, with the increasing degree of embrittlement in that order.
2. Holding unnotched or notched HY-80, AISI 1020, ASTM A-515, or H-11 tool steel under stress in 10,000-psi hydrogen has no effect on the degree of hydrogen-environment embrittlement.

3. The notch strength of both annealed and STA Ti-6Al-4V is considerably reduced in 10,000-psi hydrogen as compared to 10,000-psi helium, but there is no embrittlement of unnotched Ti-6Al-4V specimens by 10,000-psi hydrogen.

PHASE IV: INFLUENCE OF HYDROGEN PRESSURE ON THE DEGREE OF EMBRITTLEMENT

INTRODUCTION

Phase IV tests were conducted to better evaluate the influence of hydrogen pressure on hydrogen-environment embrittlement. Unnotched and notched specimens of ASTM A-302 and AISI type 310 stainless steel were tested to failure under tension in a hydrogen environment at pressures of 1 atmosphere, 100 psig, 1000 psig, and 10,000 psig, and, for comparison, in a helium environment at 1000 and 10,000 psig. In accordance with the results of Phase I, the tensile tests were performed as soon as the test environment was established without any hold period.

EXPERIMENTAL PROCEDURE

Both the tensile specimen design and apparatus were identical to those described in Phase I. Therefore, no further discussion of these areas appears in this section.

Materials

Chemical composition, heat treatment, and mechanical properties of the alloys tested in this phase are presented in Tables 22, 23, and 24, respectively.

Test Procedure

Tensile testing procedures were described in Phase I. The test vessel purging procedure included initial evacuation for all tests in this phase. For tests conducted in 1-atmosphere-pressure hydrogen, backfilling after evacuation was to 1 atmosphere hydrogen pressure rather than the 100 psi used for the tests at all other hydrogen pressures.

Preceding page blank

TABLE 22

CHEMICAL COMPOSITION OF PHASE IV MATERIALS

Material	C	Mn	P	S	Si	Ni	Cr	Cu	Al	Ti	Mo	Fe	Sn	V	Other
ASTM A-302 Gr.B Modified With Nickel (5-1/2-inch plate)	0.25	1.31	0.016	0.021	0.27	0.63						Bal.			
AISI Type 310 Stainless Steel (3/8-inch-diameter rod)	0.05	1.34	0.013	0.014	0.64	20.39	24.83	0.11			0.14	Bal.	0.010		
ASTM A-212-61T Gr.B-FB (4-inch-thick plate)	0.32	0.75	0.016	0.020	0.23	<0.10	<0.05	0.06			0.02	Bal.		0.06	
Inconel 718	0.04	0.16		0.004	0.07	Bal.	18.86		1.51	3.09	3.13	19.81			Cb/Ta, 5.39

TABLE 23

HEAT TREATMENT OF PHASE IV MATERIALS

Material	Heat Treatment by Supplier (As-Received Condition)	Hardness	Heat Treatment by Rocketdyne	Hardness
ASTM A-302 Gr.B Modified With Nickel	Stress-relieved plate		Annealed at 1650 F for 1 hour; water quenched; tempered at 1270 F for 1 hour; air cooled	
AISI Type 310 Stainless Steel	Annealed	R_b 79	None	R_b 79
ASTM A-212-61T Gr.B-FB	Normalized; stress relieved at 1100 F for 4 hours		None	
Inconel 718	Annealed	R_c 24	Annealed at 1850 F for 1 hour; air cooled; reheated to 1360 F for 10 hours; furnace cooled to 1175 F; held for 10 hours; air cooled	R_c 44

TABLE 24

MECHANICAL PROPERTIES OF PHASE IV MATERIALS

Material	Tensile Strength, ksi	Yield Strength, ksi	Reduction of Area, percent	Elongation, percent	Hardness
ASTM A-302 Gr.B Modified With Nickel	114[a]	98	68.0	21.0	
AISI Type 310 Stainless Steel	86	34	60.6	45.7	R_b 79
ASTM A-212-61T Gr.B-FB	38	73	56.0	37.0	
Inconel 718	213[b]	187	15.0	15.0	R_c 47

(a) Properties determined at Rocketdyne prior to heat treatment (Ref. 2)

(b) The properties listed were determined by the supplier on material from the same heat as supplied to Rocketdyne and were heat treated in the same manner as the heat treatments conducted at Rocketdyne (shown in Table 23). The material was received in the annealed condition.

RESULTS AND DISCUSSION

Results for all of the tests in this phase are given in Table 25. The individual specimen test data are contained in Appendix Tables IV-1 and IV-2 for AISI type 310 stainless steel, IV-3 and IV-4 for ASTM A-302, IV-5 for ASTM A-212, and IV-6 for Inconel 718.

There is no evidence of any reduction of strength or ductility of the unnotched AISI type 310 stainless steel because of the hydrogen environment. However, there appears to be a small decrease of strength and ductility of the notched specimens, and the degree of embrittlement lessens with decreasing pressure. Data at hydrogen pressures less than 10,000 psi are possible within experimental scatter of the expected properties in inert environments. The notch ductility at lower hydrogen pressures is somewhat lower on an average than the ductility in 10,000-psi helium, but this difference may be due to an increase of ductility in the 10,000-psi helium due to pressure per se as has been discussed in Phase II.

Interpretation of the data for ASTM A-302 is somewhat difficult because the ASTM A-302 specimens were given two different heat treatments. Initially, a sufficient number of bars were prepared to perform all the tests, but examination after heat treatment revealed that some of these contained cracks. Replacement bars were then prepared and these bars were slightly harder than the original group. The small difference in hardness and strength may have been due to the different location in the large forging from which the bars were removed or may have been due to a small difference between the two heat treatments.

Strength and ductility of the unnotched ASTM A-302 specimens are shown in Fig. 10 and 11. There may be a slight reduction of strength of the specimens tested in 10,000-psi hydrogen, but there was no strength reduction for specimens tested in hydrogen at lower pressures. A substantial loss

TABLE 25

TENSILE PROPERTIES OF NOTCHED AND UNNOTCHED SPECIMENS OF AISI TYPE 310 STAINLESS STEEL, ASTM A-302, ASTM A-212, AND INCONEL 718 IN HYDROGEN, HELIUM AND AIR AT VARIOUS PRESSURES

Test Conditions						Test Results				
				Strain Rate/Minute		Strength			Ductility	
Material	Notched or Unnotched	Environment	Pressure, psig	0 Load to Yield	to Ultimate	Yield, ksi	Ultimate, ksi	Helium Change, percent	Elongation, percent (1.25-inch gage length)	Reduction of Area, percent
AISI Type 310 Stainless Steel	U	Helium	0	0.0020	0.0400	33.5	89	—	55.0	66.50
			1,000			35.0	90	—	54.0	67.50
			10,000			—	77	—	56.0	64.00
		Hydrogen	0	0.0020	0.0400	35.0	87	-2.2	53.5	65.50
			100			36.3	87	-2.2	52.3	66.00
			1,000			34.0	89	-1.1	55.0	67.00
			10,000				78	+1.3	56.0	63.30
	N	Helium	10,000	0.0007	0.0007	—	116	—	—	19.80
		Hydrogen	0	0.0007	0.0007	—	124	-1.6[a]	—	18.70
			100			—	123	-2.4[a]	—	18.00
			1,000			—	123	-1.6[a]	—	16.00
			10,000			—	108	-6.9[a]	—	18.00
ASTM A-302	U	Helium	0	0.0020	0.0400	118.0	118	—	28.0	70.00
			1,000			119.5	116	—	23.5	71.50
			10,000			—	120	—	19.5	67.50
		Hydrogen	0	0.0020	0.0400	115.0	118	0	21.0	68.30
			100			118.0	120	+1.7	22.3	67.30
			1,000			113.5	117	+0.9	20.0	57.70
			10,000			36.0	116	-3.2	16.7	32.70
	N	Helium	0	0.0007	0.0007	—	216[b]	—	—	12.00
			1,000			—	215[b]	—	—	14.00
			10,000			—	227	—	—	11.00
		Hydrogen	0	0.0007	0.0007	—	235	-0.9[a]	—	7.10
			100			—	212[b]	-1.8	—	7.40
			1,000			—	218	-7.6[a]	—	4.20
			10,000			—	176	-22.5[a]	—	2.90
ASTM A-212	N	Hydrogen	1,000	0.0007	0.0007	—	105	-20.5	—	4.15[c]
			3,000			—	104	-19.5	—	6.20[c]
			5,000			—	103	-19.5	—	4.40[c]
			7,500				90	-28.5	—	3.80[c]
Inconel 718	U	Air	0	0.0020	0.0400	187.5	217	—	16.0	31.00
		Helium	1,000			194.0	216	—	16.5	32.00
		Hydrogen	1,000			186.3	215	-0.5	17.3	28.00
	N	Air	0	0.0007	0.0007	—	284	—	—	1.45
		Helium	1,000			—	282	—	—	1.40
		Hydrogen	1,000				169	42.0	—	1.30

(a) Based on 1000 psi strength decrease for each 1000 psi increase of pressure for helium comparisons

(b) Second heat treatment

(c) Percent reduction of area in 10,000-psi helium = 12.0 percent

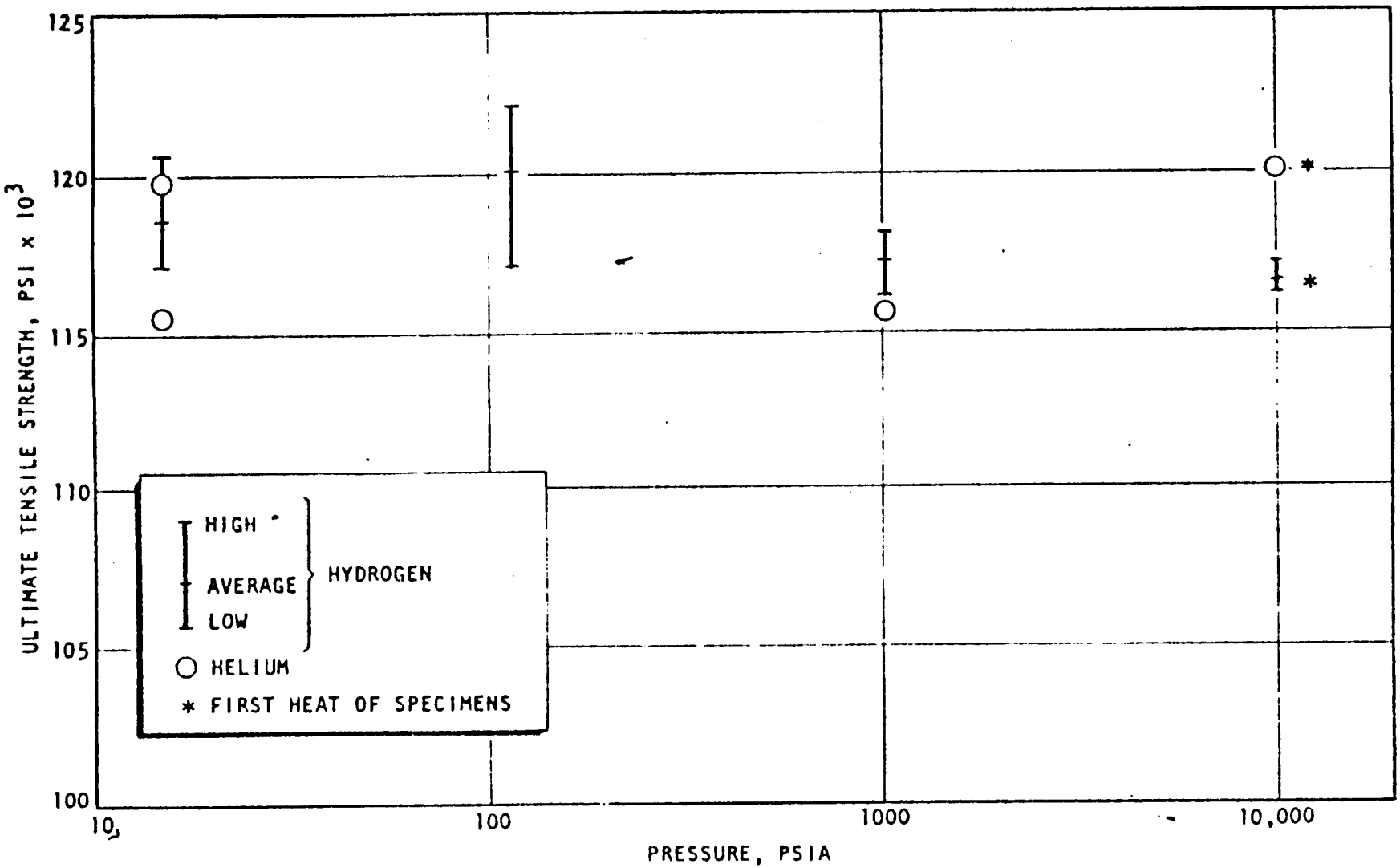

Figure 10. Effect of Hydrogen Pressure on the Strength of Unnotched ASTM A-302 Specimens

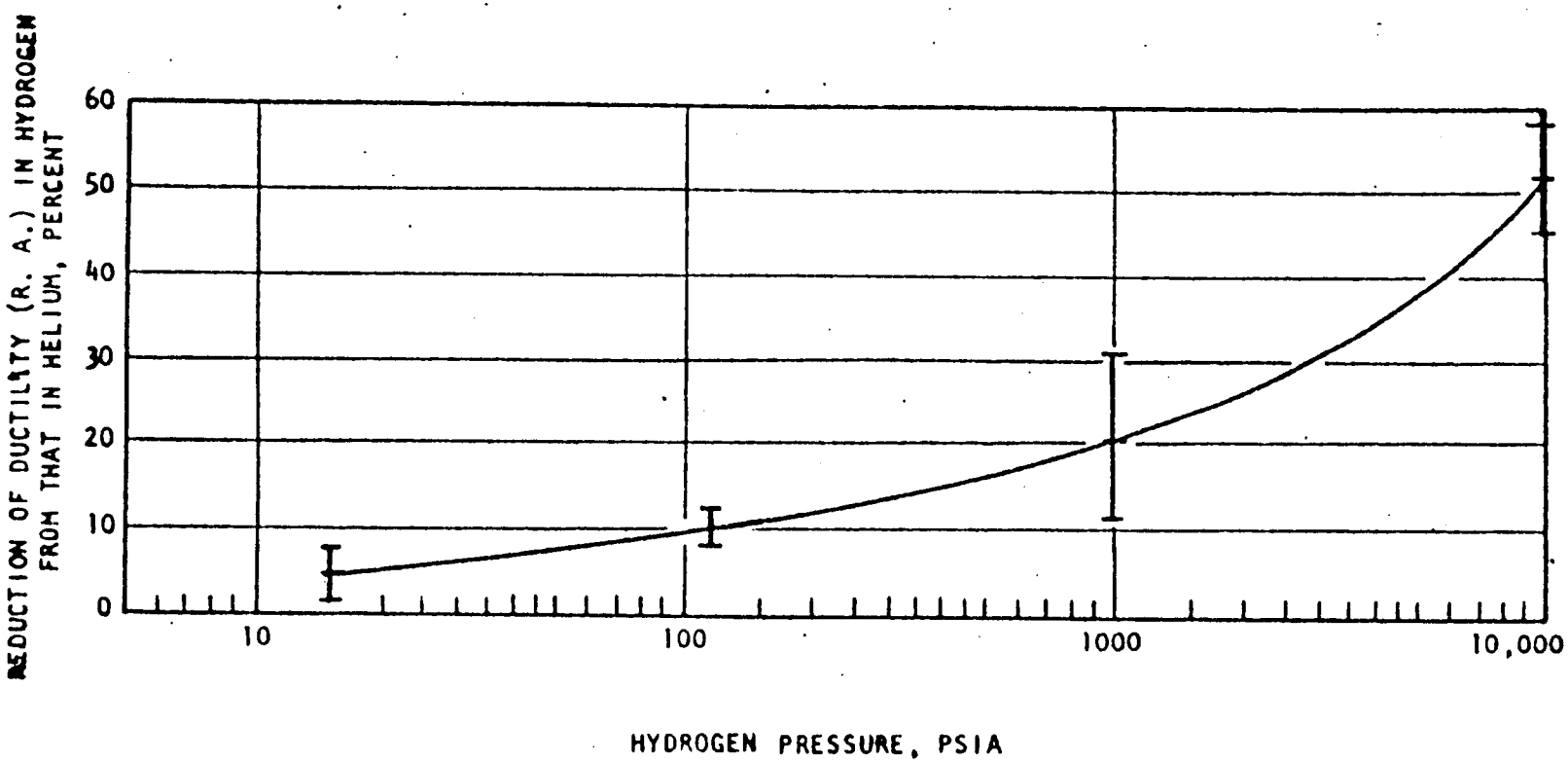

Figure 11. Reduction of Ductility in Hydrogen From That in Helium for Unnotched ASTM A-302 Specimens as a Function of Hydrogen Pressure

of ductility was noted in the unnotched ASTM A-302 specimens tested in hydrogen at 1000- and 10,000-psig pressures (Fig. 11). The loss of ductility lessened with decreasing hydrogen pressure, and there appeared to be almost no embrittlement of specimens tested in hydrogen at 100 psig and none at 1-atmosphere pressure. However, surface cracking occurred on unnotched ASTM A-302 specimens tested at all hydrogen pressures, including 1 atmosphere.

The decrease of notched tensile strength of ASTM A-302 as a function of hydrogen pressure is illustrated in Fig. 12. The minimum hydrogen pressure for which there is a notch strength reduction is somewhat difficult to determine because the tests at 100-psig hydrogen pressure were conducted on a different heat of material. Strength of the specimens tested at 100-psi hydrogen was about the same or slightly lower than the strength of this material in helium. Thus, from these data it appears that the hydrogen environment caused a measurable strength decrease of the ASTM A-302 notched ($K_t \approx 8.4$) specimens at pressures greater than 100 psi.

The decrease in ductility of the notched specimens as a function of hydrogen pressure is illustrated in Fig. 13. Degree of embrittlement lessened with decreasing hydrogen pressure: but even at 1 atmosphere, the percent reduction of area was considerably lower than obtained in an inert environment.

Two notched ($K_t = 4.2$) ASTM A-212 parent metal specimens from the previous program (Ref. 2) were tested in 1000-psi hydrogen to determine whether the decrease of embrittlement with decreasing hydrogen pressures observed in the previous program between 3000 and 10,000 psi extended down to 1000-psi hydrogen pressure. It can be seen from Table 25 that there was no significant difference between the tensile properties in 1000-psi hydrogen and in 3000-psi hydrogen.

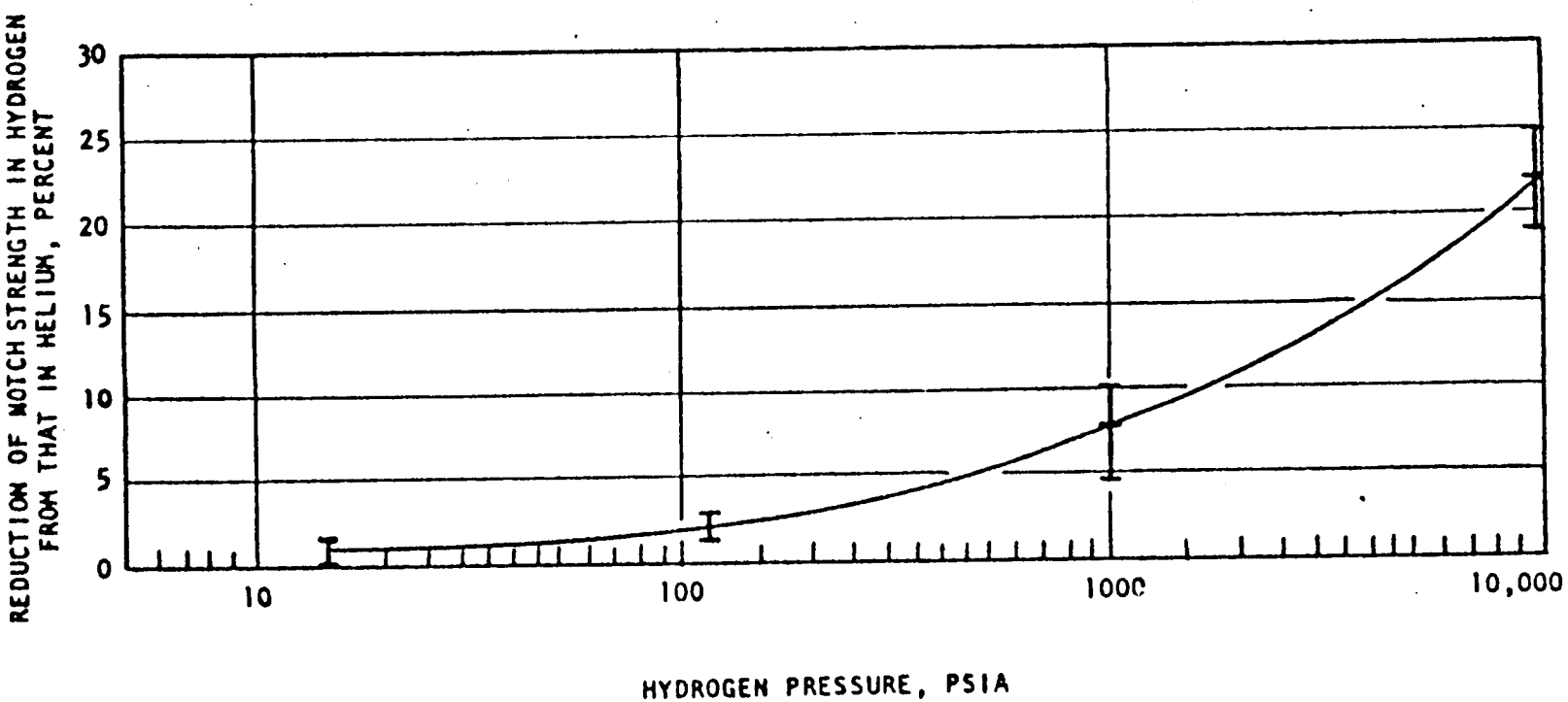

Figure 12. Reduction of Strength In Hydrogen From That in Helium For Notched ASTM A-302 Specimens as a Function of Hydrogen Pressure

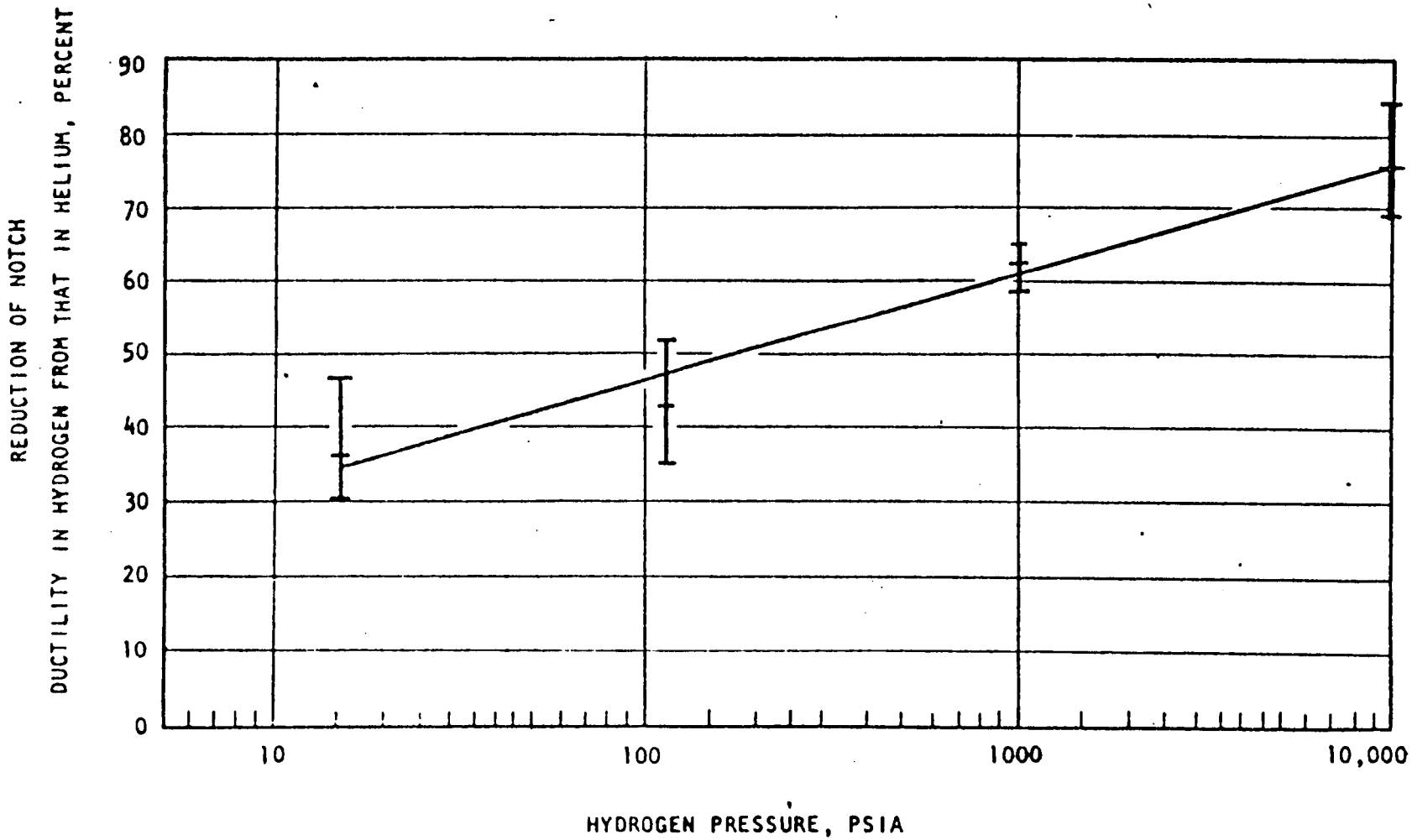

Figure 13. Reduction of Ductility In Hydrogen From That in Helium For Notched ASTM A-302 Specimens as a Function of Hydrogen Pressure

The influence of pressure was also determined to a limited extent on Inconel 718. In this phase, a series of tests were run on Inconel 718 in 1000-psi hydrogen; the results appear in Table 25. In Phase II, a series of tests were run on Inconel 718 in 10,000-psi hydrogen; those results appear in Table 8. There were small differences in the heat treatments given the two sets of specimens, but the mechanical properties in air were quite similar (refer to Tables 6, 7, 23, and 24).

The results in Table 25 indicate a small reduction of ductility, as measured by reduction of area, of the unnotched specimens because of exposure to 1000-psi hydrogen. This is a considerable difference from the almost zero ductility resulting from tests conducted in 10,000-psi hydrogen (Table 8). It is interesting that the reduction of area for the individual specimens in 1000-psi hydrogen was directly proportional to the size of the surface crack causing fracture. The fact that a surface crack was formed was indicated by the absence of a shear lip over a small distance at the surface. The fracture of a specimen with a 24-percent reduction of area was initiated by a short surface crack. The fracture of a specimen with a 29-percent reduction of area was also initiated by a surface crack, but the crack was of vanishingly short length. There was no indication of surface cracking of a specimen with a 31-percent reduction of area.

Notched strength was reduced 35 to 40 percent in 1000-psi hydrogen, compared to 51 to 55 percent in 10,000-psi hydrogen. There was a small reduction in ductility of the notched specimens from exposure to 1000-psi hydrogen, while the notched specimens tested in 10,000-psi hydrogen had almost zero ductility.

SUMMARY

Embrittlement of AISI type 310 stainless steel was limited to the 10,000-psi hydrogen environment. Embrittlement of ASTM A-302 lessened with decreasing pressure, and for most properties was negligible at hydrogen

pressures equal to or less than 100 psig. Exceptions were the notch ductility, which was considerably reduced by 1-atmosphere hydrogen pressure, and surface cracking, which was observable on unnotched specimens tested in 1 atmosphere hydrogen. The degree of hydrogen-environment embrittlement of ASTM A-212 was found to be approximately the same in 1000-psi hydrogen as in 3000-psi hydrogen in a previous program.

The tests conducted on Inconel 718 in 1000-psi hydrogen indicated that the unnotched specimen ductility was reduced to a much smaller degree by 1000-psi hydrogen than by 10,000-psi hydrogen. The notched strength was reduced 35 to 40 percent in 1000-psi hydrogen, compared to 51 to 55 percent in 10,000-psi hydrogen.

CONCLUSIONS

Results of the testing indicated that the degree of hydrogen-environment embrittlement lessens with decreasing hydrogen pressure, but there are embrittlement effects at the lowest hydrogen pressures investigated (1 atmosphere for ASTM A-302 and 1000-psi for ASTM A-212 and Inconel 718).

PHASE V: INFLUENCE OF NOTCH SEVERITY ON HYDROGEN-ENVIRONMENT EMBRITTLEMENT

INTRODUCTION

All prior programs in which specimens were tested to failure in high-pressure hydrogen showed the importance of the presence of notches. The investigation by Steinman, et al. (Ref. 15) indicated that the reduction of notched tensile strength of AISI 4140 steel was greater the sharper the notch. However, the two notches used in that investigation were both rather dull, as was the notch used in the previous Rocketdyne program (Ref. 2).

Thus, Phase V was conducted to determine the influence of notch severity on the degree of hydrogen-environment embrittlement of steels of interest as pressure vessel structural or protective liner materials. This phase consists of two separate tasks:

A. Influence of Notch Severity on Hydrogen-Environment Embrittlement of Tensile Specimens.

B. Influence of Hydrogen Environments on Fracture Toughness.

Experimental work on Task B was extended past the time which would have allowed that task to be covered in this report. Thus, Task B is reported upon in a supplement to this report. The discussion of Task A follows.

ASTM A-302, ASTM A-517, and AISI type 310 stainless-steel specimens with various notch geometries were tested in tension to failure in 10,000-psi hydrogen and, for comparison, in 10,000-psi helium and one-atmosphere air. There was no prior hold period before testing to failure. Notch geometries were approximately 4.0, 6.0, and 8.4 K_t.

EXPERIMENTAL PROCEDURE

Materials

Chemical compositions, heat treatments, and mechanical properties of the materials tested in this phase are given in Tables 26, 27, and 28, respectively.

Tensile Specimen Design

Only notched specimens were tested in this phase. The basic specimen design was described in Phase I. The 0.306-inch diameter specimens contained a 60-degree V notch. The specimen diameter at the bottom of the notch was 0.150 ± 0.001 inch. Three root radii were used for this phase; 0.0046 ± 0.0001 inch to give a K_t of approximately 4.0, 0.0020 ± 0.0001 inch to give a K_t of approximately 6.0, and 0.00095 ± 0.0001 to give a K_t of approximately 8.4. Of course, there are nominal radii and K_t values; the actual radius was measured and K_t calculated according to Peterson (Ref. 4) for each specimen. These K_t values are reported in the Results and Discussion section for each specimen.

Apparatus

The apparatus used for the tensile tests was described in detail in Phase I.

Test Procedure

The tensile testing procedure was described in detail in Phase I. Test vessel purging did not include prior evacuation for any of the tests in this phase.

RESULTS AND DISCUSSION

Results of the tensile tests performed on ASTM A-302, ASTM A-517, and AISI type 310 stainless-steel specimens with various notch geometries

TABLE 26

CHEMICAL COMPOSITIONS OF PHASE V MATERIALS

Material	C	Mn	P	S	Si	Ni	Cr	Cu	Mo	Fe	Other
ASTM A-302 Gr.B Modified With Nickel (5-1/2-inch Plate)	0.25	1.31	0.016	0.021	0.27	0.63					
ASTM A-517 Br.F (3/8-inch Plate)	0.16	0.80	0.010	0.016	0.21	0.79	0.54	0.25	0.43	Balance	0.04 V 0.002 B
AISI Type 310 Stainless Steel (3/8-inch Diameter Rod)	0.05	1.34	0.013	0.014	0.64	20.39	24.83	0.11	0.14	Balance	

TABLE 27

HEAT TREATMENT OF PHASE V MATERIALS

Material	Heat Treatment by Supplier (As-Received Condition)	Hardness	Heat Treatment by Rocketdyne	Hardness
ASTM A-302 Gr.B Modified With Nickel	Stress relieved plate	----	Annealed at 1650 F for 1 hour; waterquenched; tempered at 1270 F for 1 hour; air cooled	----
ASTM A-517 Gr.F	Annealed at 1625 F for 1/2 hour; water quenched; tempered at 1225 F for 1 hour	----	None	----
AISI Type 310 Stainless Steel	Annealed	R_b 79	None	R_b 79

TABLE 28

MECHANICAL PROPERTIES OF PHASE V MATERIALS
(Supplier Certification)

Material	Tensile Strength, ksi	Yield Strength, ksi	Reduction of Area, percent	Elongation, percent
ASTM A-302 Gr.B Modified With Nickel	114.0[a]	98.0	68.0	21.0
ASTM A-517 Gr.F	76.1	46.4		27.5
AISI Type 310 Stainless Steel	86.0	34.0	60.6	45.7

[a] Properties determined at Rocketdyne prior to heat treatment

are presented in Table 29. The Appendix tables containing data for individual specimens of each alloy are identified in Table 29. Results in Table 29 are an average of three tests for tests in hydrogen and two for tests in helium and air.

Results shown in Table 29 for AISI type 310 stainless steel indicate that embrittlement by the 10,000-psi hydrogen environment was limited to those specimens with the sharpest of the three notches, and even in those specimens the embrittlement was slight.

Reduction of notch strength in 10,000-psi hydrogen compared to the notch strength in 10,000-psi helium versus the stress concentration factor is plotted for ASTM A-302 and ASTM A-517 in Fig. 14 and 15, respectively. Each point in these figures represent an individual specimen test. In addition to the data obtained in this phase, Fig. 14 and 15 contain results for precracked specimens from Phase VI and for unnotched ($K_t = 1$) specimens from Phase I, for ASTM A-302, and Phase VI, ASTM A-517. The K_t value for the fatigue crack was arbitrarily assumed to be between 19 and 20. Helium used for the tests in 10,000-psi helium on the $K_t \simeq 8.4$ ASTM A-517 specimens was contaminated with hydrogen; consequently, the reduction of notch strength in hydrogen of those specimens was determined by comparison with tests in air (with compensation for pressure effects).

Figures 14 and 15 show that the precracked specimens of both ASTM A-302 and ASTM A-517 were not as embrittled by 10,000-psi hydrogen as were the specimens with $K_t \simeq 6.0$ and 8.4 notch geometries. Thus, hydrogen-environment embrittlement apparently does not increase indefinitely with decreasing notch radius, at least for these low alloy steels. At low values of K_t, the degree of hydrogen-environment embrittlement appeared to increase almost linearly with increasing K_t. The degree of hydrogen-environment embrittlement as a function of K_t passed through a maximum at approximately 9 (estimated) for ASTM A-302 and 6 for ASTM A-517.

TABLE 29

EFFECT OF NOTCH SEVERITY ON DEGREE OF EMBRITTLEMENT BY 10,000-PSI HYDROGEN

Material	Test Conditions: Approx. Stress Concentration Factor	Test Conditions: Environment	Test Conditions: Pressure, psi	Test Conditions: Strain Rate/Min	Test Results: Strength: Ultimate, ksi	Test Results: Strength: Change from Helium, percent	Test Results: Ductility: Reduction of Area, percent	Appendix Table Number for Individual Specimen Data
AISI Type 310 Stainless Steel	8.27	He	10,000	0.0007	116	---	20	V-1
	8.54	H_2	10,000		108	-7	18	
	5.90	Air	0		125	---	27	
	5.90	He	10,000		112	---	29	
	5.90	H_2	10,000		112	0.0	29	
	4.08	Air	0		112	---	37	
	4.08	He	10,000		112	---	32	
	4.08	H_2	10,000		111	-1	32	
	8.27	Air	0		220	---	15	
	8.00	He	10,000		227	---	11	
ASTM A-302 Gr.B Modified with Nickel	7.50	H_2	10,000		176	-23	2.7	V-2
	5.95	Air	0		221	---	15	
	5.95	He	10,000		212	---	16	
	5.90	H_2	10,000		168	-21	4.9	
	3.97	Air	0		221	---	19	
	4.00	He	10,000		207	---	19	
	4.00	H_2	10,000		177	-15	4.8	
	1.0	He	10,000		120	---	---	
	1.0	H_2	10,000		116	-3.3	67	
ASTM A-517 Gr.F	8.27	Air	0		236	---	7.4	V-3
	8.70	He[a]	10,000		222	---	5.7	
	8.50	H_2	10,000		173	-23	2.1	
	5.79	Air	0		243	---	11	
	5.76	He	10,000		230	---	12	
	5.79	H_2	10,000		172	-25	2.0	
	3.77	Air	0		243	---	13	
	3.76	He	10,000		227	---	12	
	3.76	H_2	10,000		181	-20	2.8	
	1.0	Air	0		128	---	65	
		H_2	10,000		121	-6	63	

[a] Hydrogen contaminated helium. Reduction of strength based on strength in air - 10,000 psi.

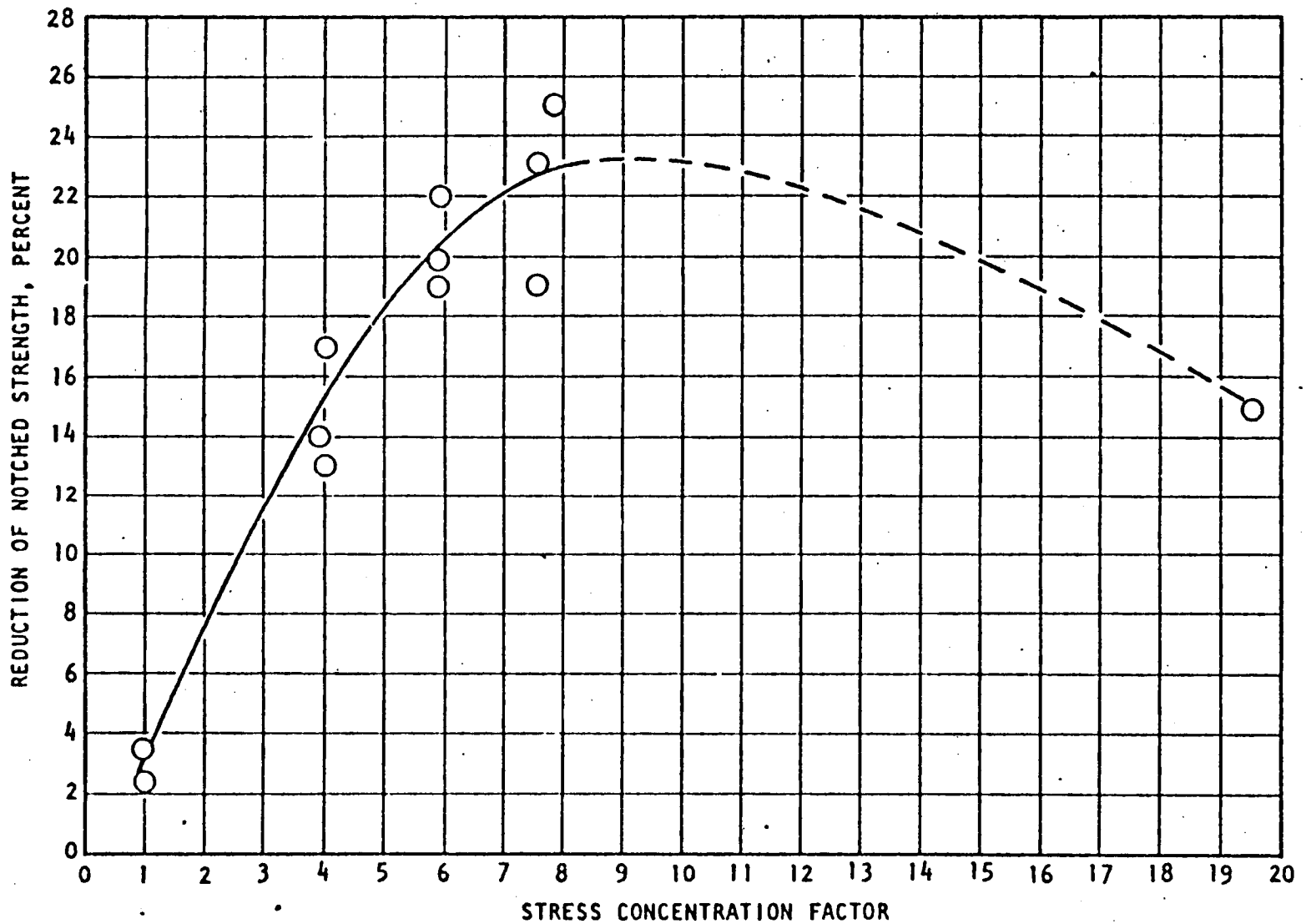

Figure 14. Effect of Notch Severity on Reduction of Notch Strength of ASTM A-302 in 10,000-psi Hydrogen Compared to 10,000-psi Helium

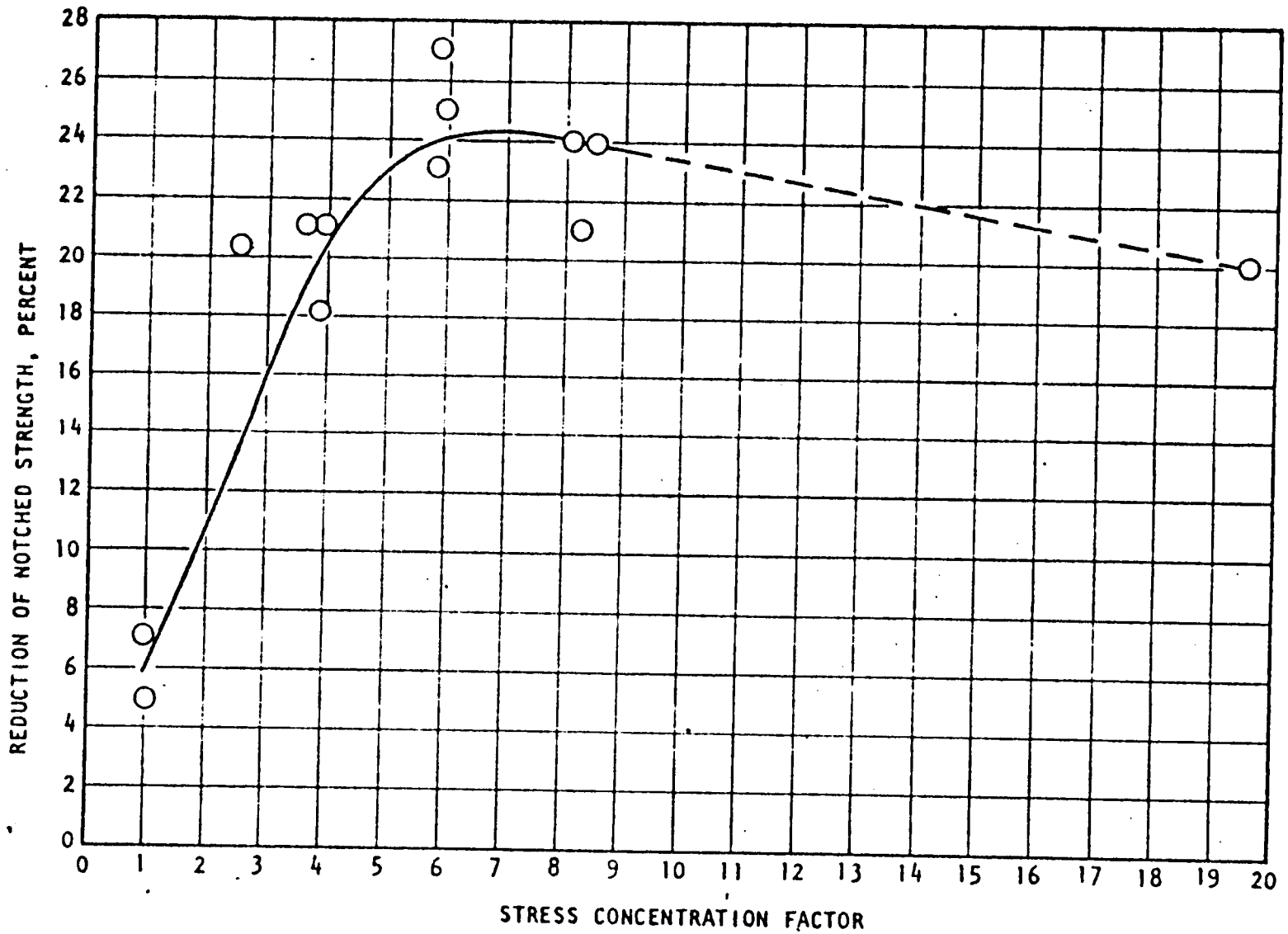

Figure 15. Effect of Notch Severity on Reduction of Notch Strength of ASTM A-517 in 10,000-psi Hydrogen Compared to 10,000-psi Helium

SUMMARY

The degree of embrittlement by 10,000-psi hydrogen of ASTM A-302 and ASTM A-517 was found to increase linearly with stress concentration factor (K_t) at low values of K_t, pass through a maximum at approximately $K_t = 9$ for ASTM A-302 and $K_t = 6$ for ASTM A-517, and then decrease with further increase in K_t. For both steels, the degree of embrittlement by 10,000-psi hydrogen was lower for fatigue precracked specimens than for specimens with $K_t \simeq 6$ or 8.4.

There was no embrittlement by 10,000-psi hydrogen of AISI type 310 stainless-steel specimens with $K_t \simeq 4.0$ and 6, and only slight embrittlement of specimens with $K_t \simeq 8.4$.

CONCLUSIONS

The hydrogen-environment embrittlement of low alloy steels is a function of stress concentration factor (K_t), increasing with K_t at low K_t, passing through a maximum for $K_t \simeq 6$ to 9, and then decreasing with K_t for the higher K_t values.

PHASE VI: INFLUENCE OF HYDROGEN ENVIRONMENT ON LOW CYCLE FATIGUE PROPERTIES OF ALLOYS

INTRODUCTION

A likely mechanism of failure of high-pressure gas storage vessels and other engineering structures is low cycle fatigue. Because even low-pressure hydrogen environments have been shown to accelerate crack growth in statically loaded steel specimens (Ref. 16 and 17), it was expected that a hydrogen environment, particularly a high-pressure hydrogen environment, would tend to accelerate propagation of a fatigue crack and might also accelerate crack initiation. Thus, Phase VI was conducted to determine the load for 1000-cycle fatigue failure in hydrogen and inert environments for steels considered for use as structural or liner materials in pressure vessels. Unnotched and notched-and-precracked-in-air specimens of ASTM A-302, ASTM A-517, and AISI type 310 stainless steel were fatigue tested to failure in air, 10,000-psi helium, and 1000- and 10,000-psi hydrogen.

EXPERIMENTAL PROCEDURE

Materials

Chemical compositions, heat treatments, and mechanical properties of the alloys tested in this phase are presented in Tables 30, 31, and 32, respectively.

Fatigue Specimen Design

Design of the unnotched specimens tested in fatigue in this phase was identical to that of the tensile specimens tested in other phases and is described in detail under Phase I. For testing in this phase, notched specimens with the same design as the tensile specimens described in Phase I, were precracked by high-cycle tension fatigue in air. These fatigue cracks were quite shallow and uniform around the periphery of the specimen.

TABLE 30

CHEMICAL COMPOSITION OF PHASE VI MATERIALS

Material	C	Mn	P	S	Si	Ni	Cr	Cu	Mo	Fe	Other
ASTM A-302 Gr.B Modified with Nickel (5-1/2-inch plate)	0.25	1.31	0.016	0.021	0.27	0.63				Bal.	
ASTM A-517 Gr.F (3/8-inch plate)	0.16	0.80	0.010	0.016	0.21	0.79	0.54	0.25	0.43	Bal.	0.04V 0.002B
AISI Type 310 Stainless Steel (3/8-inch diameter rod)	0.05	1.34	0.013	0.014	0.64	20.39	24.83	0.11	0.14	Bal.	

TABLE 31

HEAT TREATMENT OF PHASE VI MATERIALS

Material	Heat Treatment by Supplier (As-Received Condition)	Hardness	Heat Treatment by Rocketdyne	Hardness
ASTM A-302 Gr.B Modified with Nickel	Stress-relieved plate	--	Annealed at 1650 F for 1 hour; water quenched; tempered at 1270 F for 1 hour; air cooled	--
ASTM A-517 Gr.F	1625 F for 1/2 hour; water quenched; 1225 F for 1 hour	--	None	--
AISI Type 310 Stainless Steel	Annealed	R_b 79	None	R_b 79

TABLE 32

MECHANICAL PROPERTIES OF PHASE VI MATERIALS
(SUPPLIER CERTIFICATION)

Material	Tensile Strength, ksi	Yield Strength, ksi	Reduction of Area, percent	Elongation, percent
ASTM A-302 Gr.B Modified with Nickel	114.0[a]	98.0	58.0	21.0
ASTM A-517 Gr.F	76.1	46.4	--	27.5
AISI Type 310 Stainless Steel	86.0	34.0	60.6	45.7

[a] Properties determined at Rocketdyne prior to heat treatment (Ref. 2)

Apparatus

The tensile testing apparatus described in detail under Phase I was used for the fatigue tests in this phase. Low-cycle fatigue tests were performed using the hydraulic ram shown in Fig. 5 and 6 . A solenoid-operated valve automatically controlled the hydraulic ram movement, while a recorder was used to record the load from the load cell signal. When the load reached a preset value, the solenoid valves were triggered and the hydraulic ram moved either up or down, according to the indicated signal.

It was desirable to follow the crack propagation during cyclic loading. The method judged most feasible was to measure the change of electrical resistivity of the specimen while the crack was propagating. This method required that the specimen be electrically isolated from the test apparatus; a design that accomplished this requirement is shown in Fig. 16. The steel plate that houses the ball joint is separated electrically from the remainder of the apparatus by the micarta plate, and the ball stem passes through a sufficiently large opening so that it does not touch the steel frame.

A second location of possible electrical contact between the tensile specimen and test apparatus was at the sliding seals. The sliding seal design used in the previous program (Ref. 2) contained brass backup rings that tended to contact the tensile specimen after the seal plug was torqued into the pressure vessel to compress the Teflon O-rings. This metal-to-metal contact increased the friction forces as well as prevented electrical isolation. To eliminate this problem, hardened-steel backup rings were designed to fit tightly into the pressure vessel cavity and not touch the tensile specimen. This improved sliding seal design was then used for all the tests on the No. 1 system, which was the system used for conducting all except the long-duration Phase III tests.

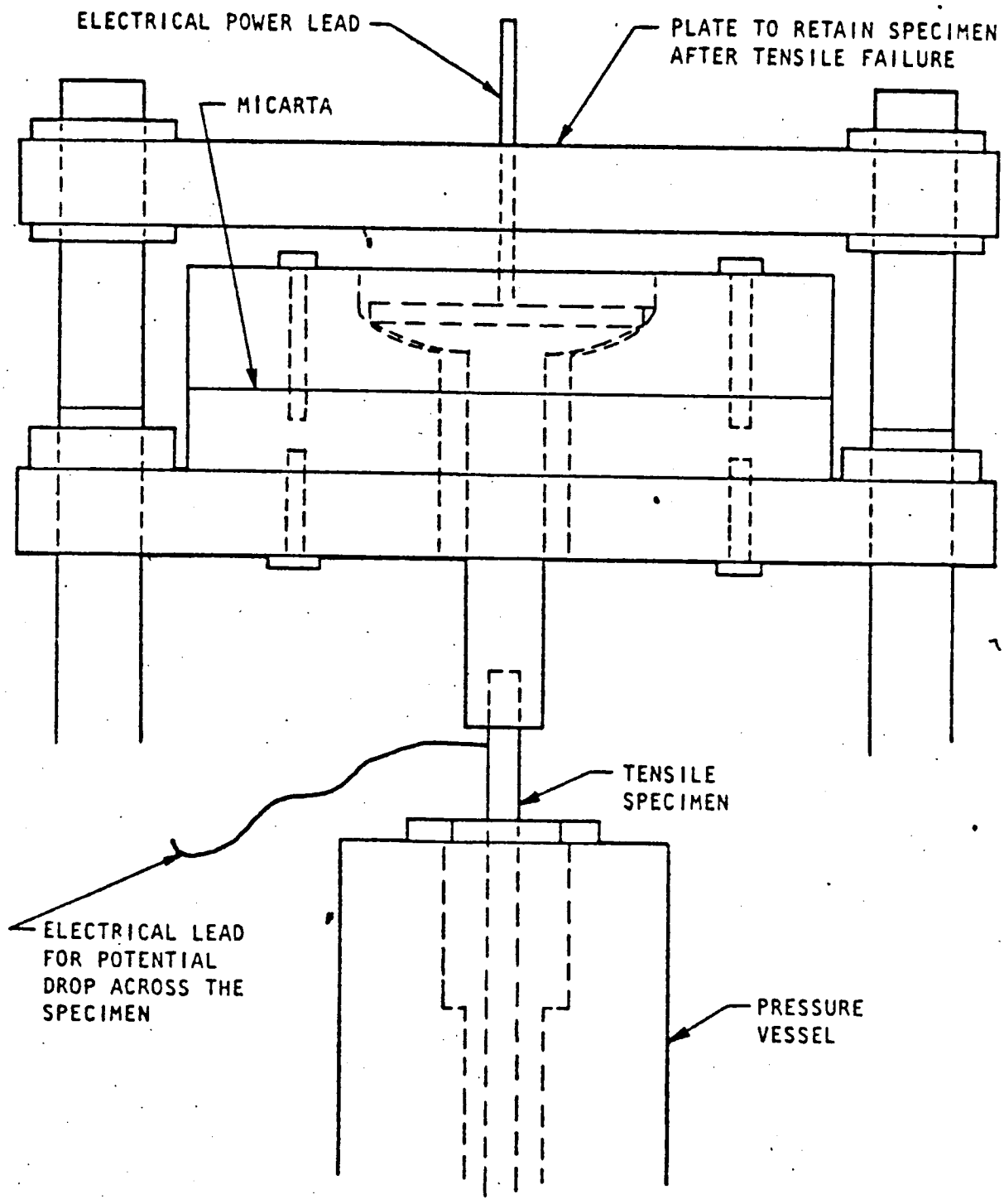

Figure 16. Test Apparatus for Measuring Crack Propagation by Electrical Resistivity Measurements

A schematic of the system for electrical resistivity measurement is shown in Fig. 17. The millivolt recorder was adjusted to indicate change of potential rather than absolute potential. It was impractical to measure the absolute potential across the specimen, because the potential change during the test was relatively small as compared to the absolute value. Change of potential due to crack growth prior to specimen failure was between 0.05 and 0.15 millivolts and physically spanned only 1/2 to 1-1/2 inches on the millivolt recorder. This sensitivity was sufficient to resolve all the individual crack steps which occurred in hydrogen, but not the smaller initial ones which occurred in inert environments. Attempts to improve the sensitivity were unsuccessful. Considerable effort was made to amplify the voltage drop across the crack prior to recording the potential. Unfortunately, the d-c amplifiers amplified stray signals generated from the loading apparatus, which made the record impossible to interpret. An EMF of unknown origin occurred, which had an amplitude directly proportional to the rate of loading. The source of this signal could not be ascertained, although it appeared to come from the specimen itself. Strangely, the EMF was in a direction so as to indicate resistance decrease during loading and increase during unloading. This phenomenon had to be damped out to measure the crack growth and, thus, it was not possible to use a d-c amplifier.

Test Procedure

Except for the type of loading, i.e., load cycling rather than tensile testing, the procedures for the fatigue tests in this phase are similar to the tensile test procedures described in detail in Phase I. Test vessel purging included evacuation for all the hydrogen and helium tests in this phase.

The specimens were load cycled by means of the hydraulic ram as described in the previous Apparatus section. Tests were conducted by load cycling between zero applied load and a constant maximum applied

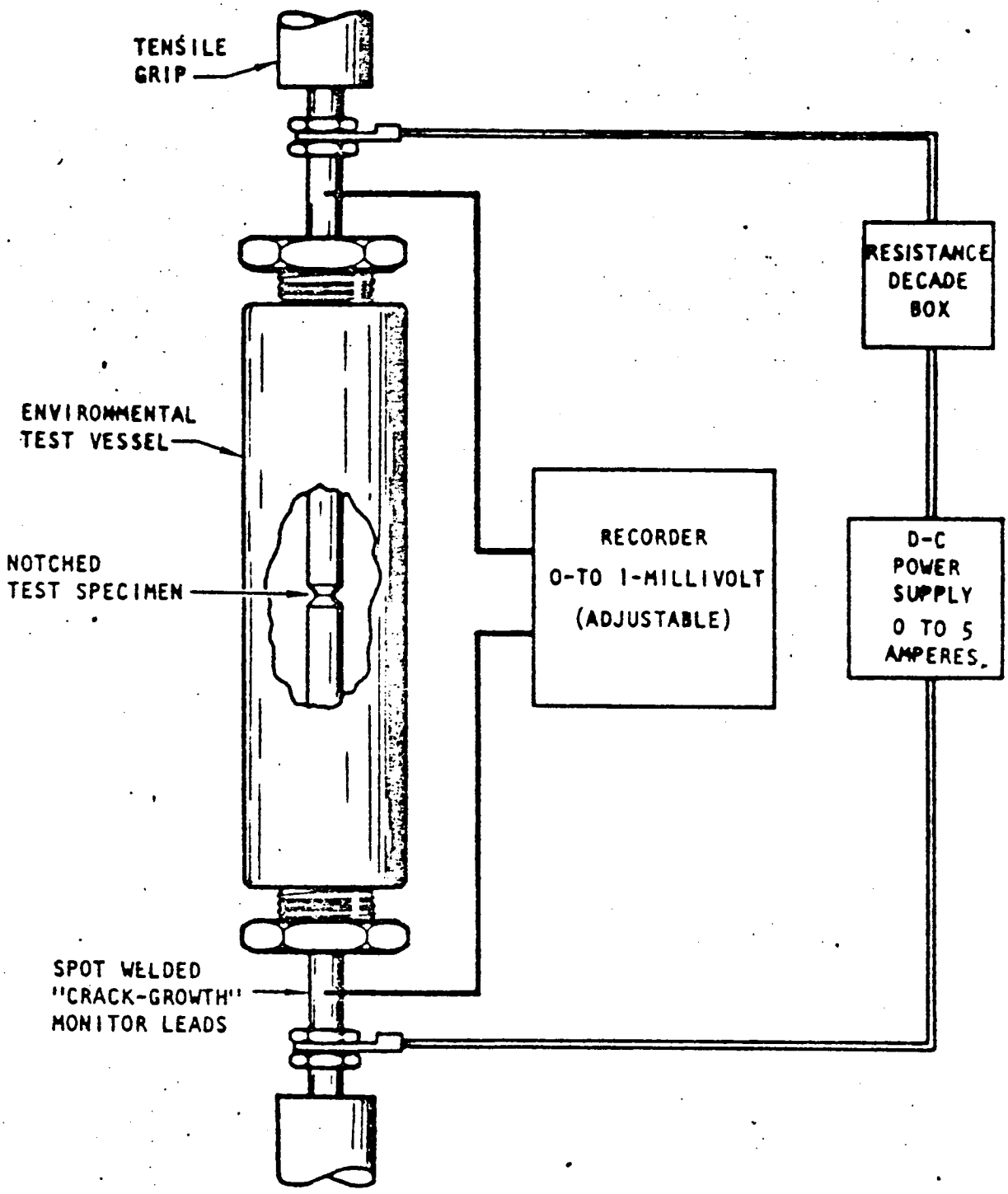

Figure 17. Schematic of System for Following Crack Growth by Electrical Resistivity

load, which resulted in a stress between the yield and ultimate strengths. The actual load, however, included the load exerted by the gas pressure. The pressure component was equal to the difference of area of the specimen at the sliding seal and at the precracked or reduced section multiplied by the pressure. A third force, which influenced the specimen stress was friction. During loading, the friction stress of 83 pounds acts to decrease the load; during unloading, the friction force acts to prevent unloading. The minimum tensile stress exerted by the pressure in 10,000-psi environments was about 31,000 psi for the precracked specimens and 3250 psi for the unnotched specimens. The maximum tensile load during cycling was the sum of the applied load plus the pressure component minus the 83 pounds of friction force.

As the specimen cross section decreased during cyclic loading, the pressure component to the load increased. Thus, the load or force exerted on the specimen increased with increasing cycles. The difference between the maximum and minimum tensile forces, however, remained constant, since the pressure component does not vary with applied load. Therefore, the stress amplitude during cyclic loading was equal to the applied stress minus two times the friction stress.

RESULTS AND DISCUSSION

Almost all the data presented in this section are in the form of figures. The points plotted in these figures represent individual specimen data. Tables of data for individual specimens are contained in Appendix Tables VI-1 for unnotched ASTM A-302 specimens, VI-2 for unnotched ASTM A-517 specimens, VI-3 for precracked AISI typs 310 stainless steel specimens, VI-4 for precracked ASTM A-302 specimens, and VI-5 for precracked ASTM A-517 specimens.

Unnotched Specimens

Results of tests on unnotched ASTM A-302 specimens (Fig.18) are rather widely scattered. One of the reasons for this scatter is probably

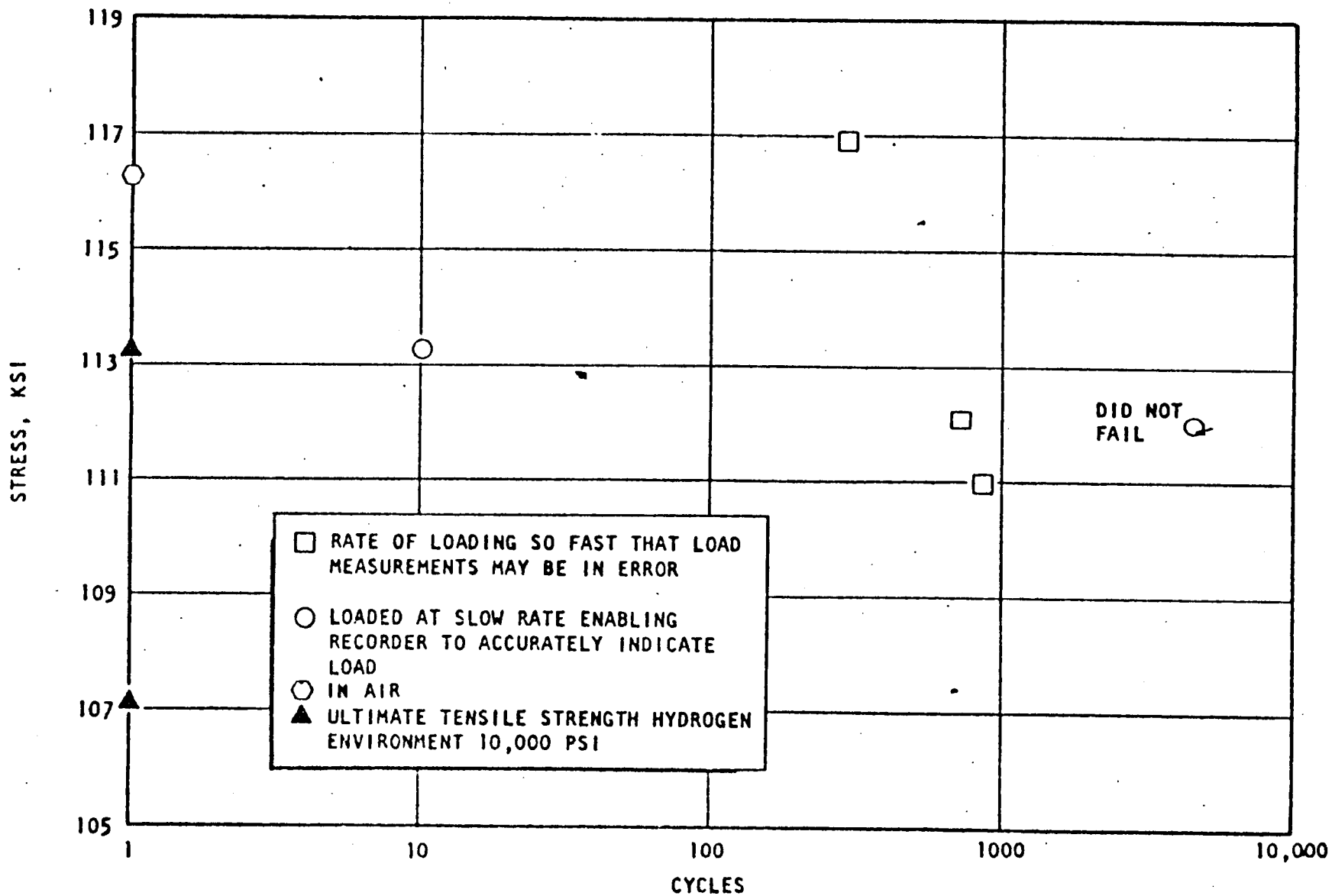

Figure 18. Results of Cyclic Loading Tests on ASTM A-302 Unnotched Specimen

errors in load measurements because of the rapid loading rate used during the first three tests (shown as square points in Fig. 18). Nevertheless, it is apparent that the strengths of the unnotched specimens in 10,000-psi hydrogen were approximately identical in low cycle fatigue as the ultimate tensile strength obtained in 10,000-psi hydrogen without load cycling.

Applied loads at the yield and ultimate strengths of this material were approximately identical when tested in a 10,000-psi hydrogen environment, and this made it difficult to conduct the tests in the region between yield and ultimate strength. It is interesting to note that the ASTM A-302 specimen with the largest number of cycles to failure (one specimen did not fail) also underwent the least elongation, only 5.3 percent. Visual examination of the specimens indicated that the fracture origin extended most of the distance around the perimeter for the specimens tensile tested to failure in 10,000-psi hydrogen. Fracture origins of specimens that failed during cyclic loading, however, appeared as a small semicircular region that extended from a short crack at the surface.

During macroscopic examination, a few striations were observed near the inside extensions of the fracture origins for the two specimens that failed with the greatest number of cycles. It is believed that striations of this type were caused by fatigue, because they were not noticed during examination of a large number of low alloy steel specimens tensile tested in 10,000-psi hydrogen. Tensile specimens were not, however, examined with this in mind. Electron microscopy examination of precracked specimens fractured in fatigue in 10,000-psi hydrogen did not show fatigue striations although the striations were present in specimens fractured in fatigue in air and in 10,000-psi helium environments. It is possible, therefore, that the fatigue striations which form in 10,000-psi hydrogen occur only on a macroscopic but not a microscopic scale.

Two fatigue tests were performed on unnotched ASTM A-517 specimens with stresses which ranged between 3250 and 113,000 psi; test results are

shown in Table 33. Load versus deflection was monitored for the first cycle to ensure that plastic deformation was achieved. Maximum stress was only 7000 psi below the tensile strength, but neither specimen failed because of cyclic loading.

After 3000 cycles had elapsed, one of the two specimens was loaded to failure. The yield and ultimate strengths of this specimen were evidently not affected by the previous cycling in the 10,000-psi hydrogen environment, but the ductility was measurably reduced. The second specimen, failed at the threaded specimen end after 3099 cycles. It therefore appears that the 1000-cycle fatigue strength in 10,000-psi hydrogen of the unnotched ASTM A-517 specimens is not appreciably different from the tensile strength in 10,000-psi hydrogen.

The tests on ASTM A-302 and ASTM A-517 specimens were conducted by maintaining a constant maximum load, and it is possible, that had the tests been conducted in such a way so as to maintain a constant strain increment per cycle, the 1000-cycle strength would be considerably lower than the tensile strength of the materials. A factor that also influences the fatigue strength is change of mechanical properties of the material during the tests. Cyclic loading is known to harden "soft" materials and soften "hard" materials. Ham (Ref. 18) states that initially "soft" materials (typically with ultimate tensile strength σu and yield strength σy such that $\sigma u/\sigma y > 1.4$) show cyclic hardening in that they require an increase (by as much as 500 percent) in stress amplitude to maintain a constant strain amplitude. Hard materials (typically $\sigma u/\sigma y < 1.2$) are softened and the stress amplitude required to maintain a constant strain amplitude falls by as much as 50 percent. The $\sigma u/\sigma y$ values for ASTM A-302, ASTM A-517 and AISI type 310 stainless steel are 1.16, 1.05, and 2.5, respectively. Therefore, fatigue softening would be predicted for ASTM A-302 and ASTM A-517 specimens, with fatigue hardening for AISI type 310 stainless steel.

TABLE 33

RESULTS OF LOW CYCLE FATIGUE TESTS ON UNNOTCHED ASTM A-517 SPECIMENS IN 10,000-PSI HYDROGEN

Test Conditions					Test Results			
Strain Rate/Minute		Rate, cycles per minute	Cycle		Strength		Ductility	
Load to Yield	Yield to Ultimate		Load Amplitude, psi	Number	Yield, ksi	Ultimate, ksi	Percent Elongation (1.25-Inch Gage Length)	Percent Reduction of Area
0.003	0.04	8.5			111	122	18.3	64.7
↓	↓	↓			111	120	17.6	61.3
			3250[a] to 113,000	3000	Did not fail; strain paced to failure			
					108	122	13.2	52.3
			3250[a] to 113,000	3099	Specimen failed at threaded end; test aborted			

[a] Load from 10,000-psi gas pressure minus seal friction

Precracked Specimens

A series of low cycle fatigue tests were conducted on notched ($K_t \simeq 8.4$) specimens which were precracked by high cycle tension fatigue in air prior to testing in low cycle fatigue. Resulting fatigue cracks were quite shallow and uniform around the perimeter of the specimen. The results of tests conducted on the precracked AISI type 310 stainless-steel specimens are plotted in Fig. 19 and 20. The precracked diameter could not be determined with any degree of certainty on the AISI type 310 stainless-steel specimens, thus the original notch diameter prior to precracking was used to calculate the stress. Figure 19 is a plot of maximum stress versus cycles to failure. It can be seen that the 1000-cycle fatigue strength of the precracked specimens is about the same as the notch tensile strength of precracked specimens, and there is no difference between the fatigue strength in 10,000-psi hydrogen and in 10,000-psi helium. Figure 20 is a plot of stress amplitude versus cycles to failure. The data do not extrapolate to the tensile strength. It would appear that the stress amplitude is not useful in the analysis of tension-tension fatigue data when the maximum stress is very close to the tensile strength.

Low cycle fatigue tests were not performed on the unnotched AISI type 310 stainless-steel specimens. It is quite unlikely that the unnotched AISI type 310 stainless-steel specimens would be affected by hydrogen in low cycle fatigue when there is no effect of 10,000-psi hydrogen on the unnotched tensile properties and 10,000-psi hydrogen did not reduce the low cycle fatigue strength of precracked AISI type 310 stainless-steel specimens.

Results of tests on precracked ASTM A-302 specimens are plotted in Fig. 21, 22 and 23. Figure 21 is an S-N (S = maximum stress) plot, using the notch specimen diameters prior to precracking. Figure 22 is the same as Fig. 21 except that the maximum stress was calculated using the diameter after the specimen was precracked. The diameter after the

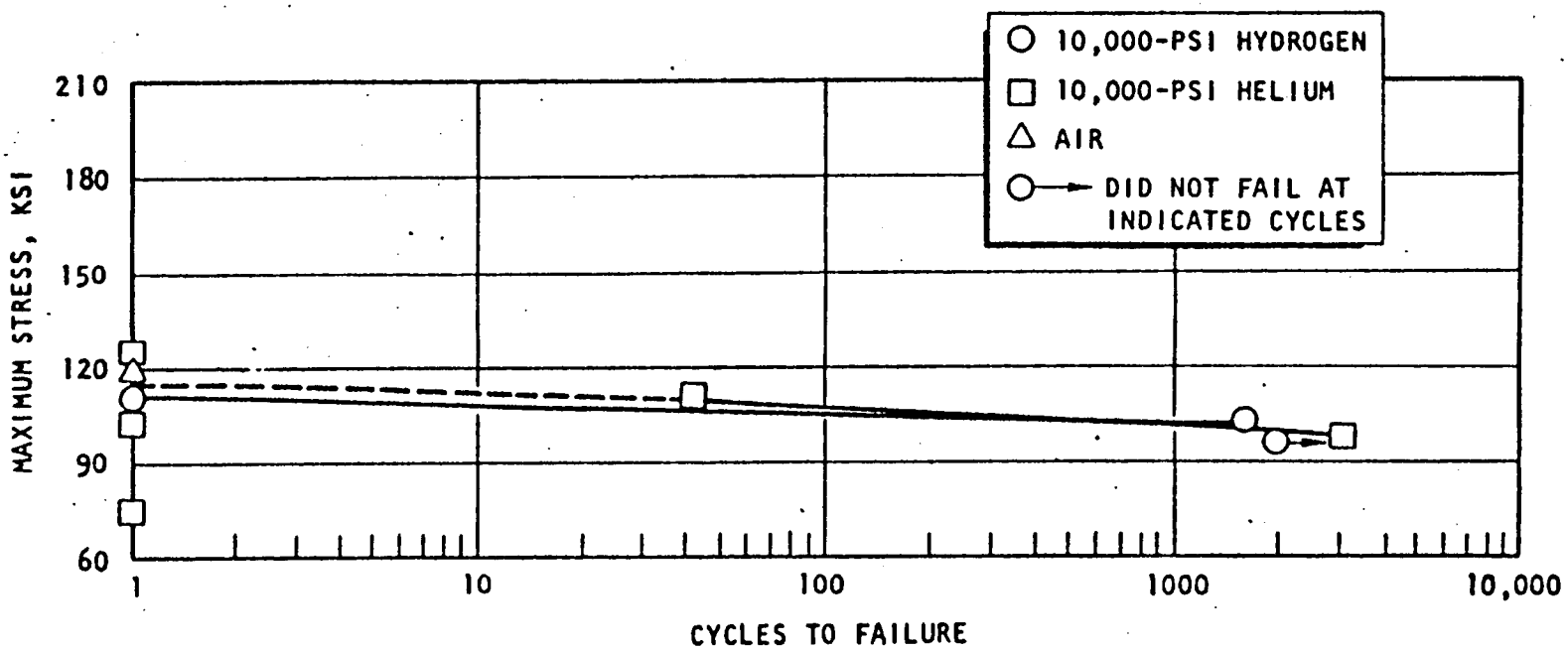

Figure 19. Effect of High-Pressure Hydrogen Environment on Low-Cycle Fatigue Strength of Precracked AISI Type 310 Stainless-Steel Specimens (Stress Calculated Using Diameter of Notched Specimens Prior to Precracking)

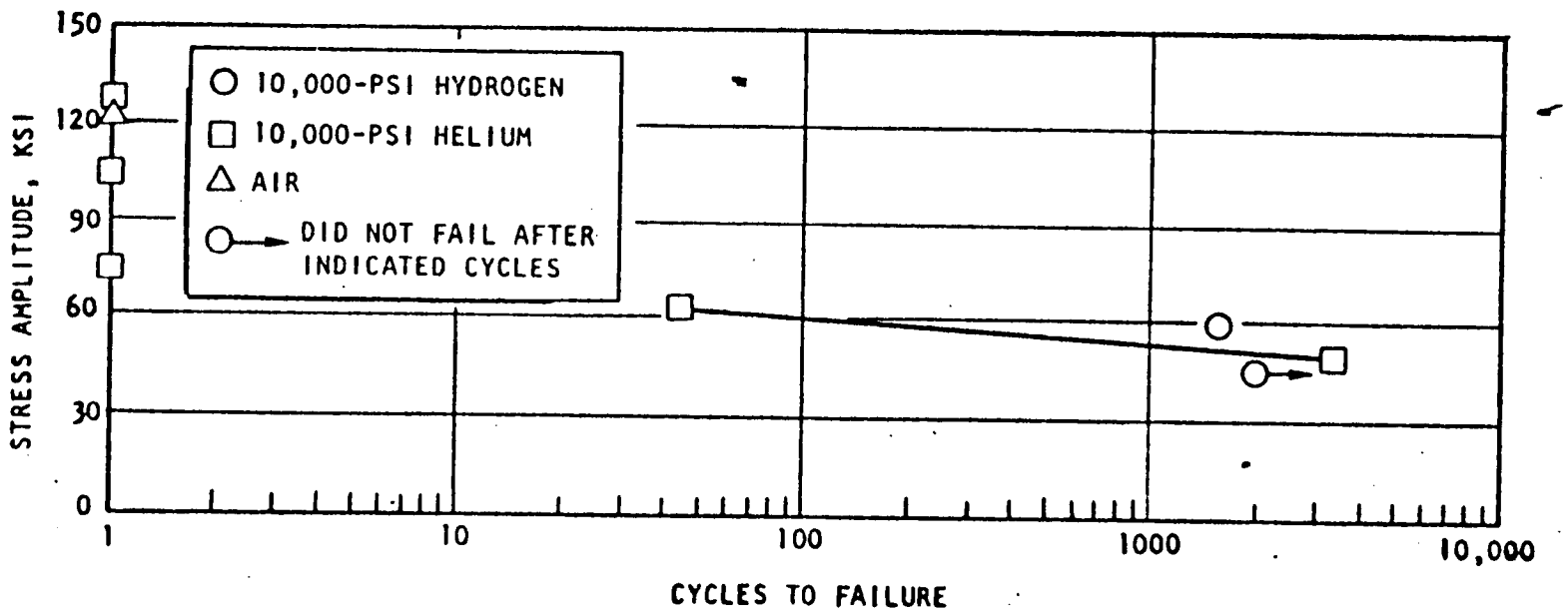

Figure 20. Effect of High-Pressure Hydrogen Environment on Low-Cycle Fatigue Strength of Precracked AISI Type 310 Stainless-Steel Specimens (Stress Calculated Using Diameter of Notched Specimens Prior to Precracking)

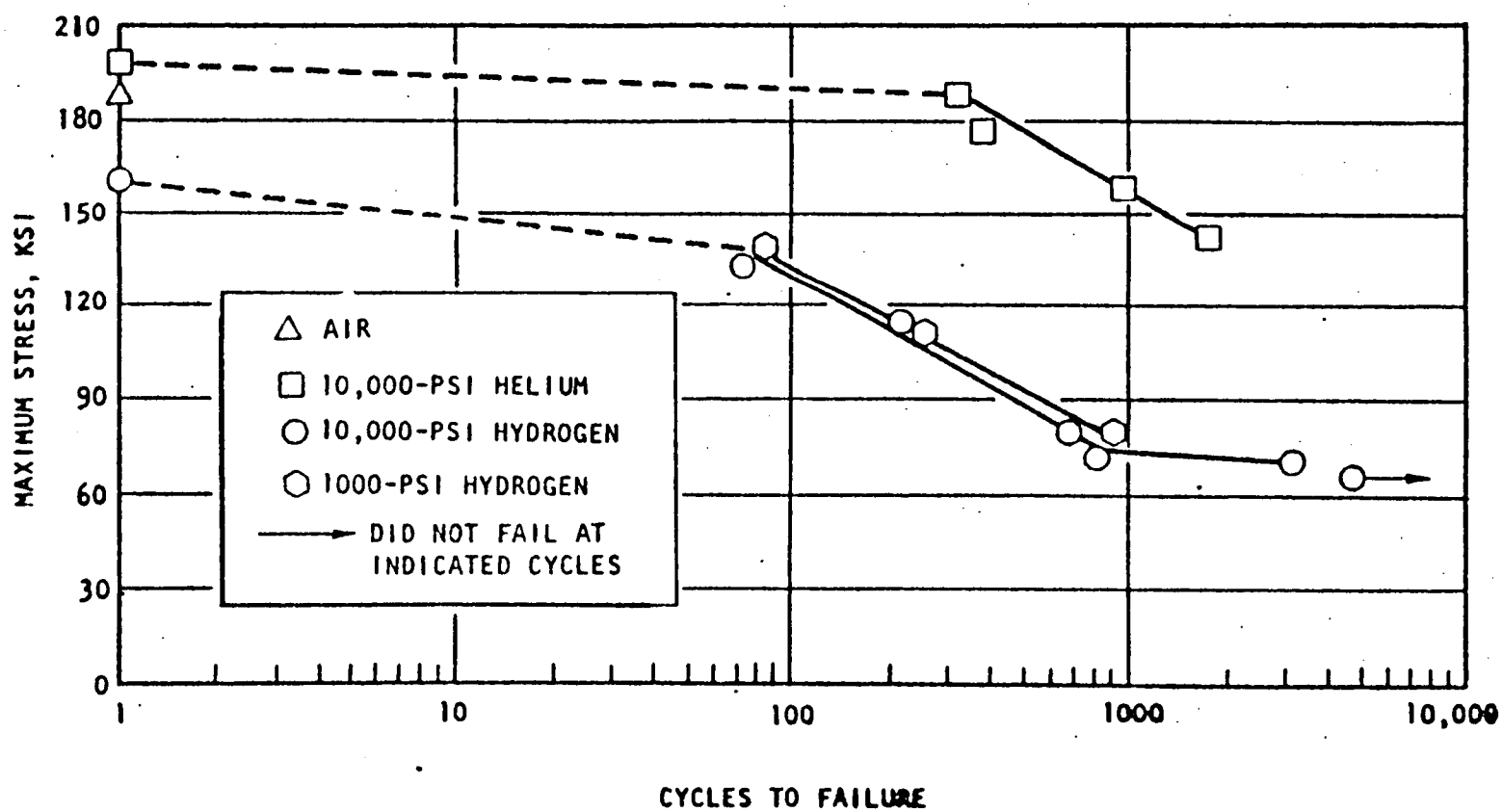

Figure 21. Effect of High-Pressure Hydrogen Environment on Low-Cycle Fatigue Strength of Precracked ASTM A-302 Specimens (Stress Calculated Using Diameter of Notched Specimen Prior to Precracking)

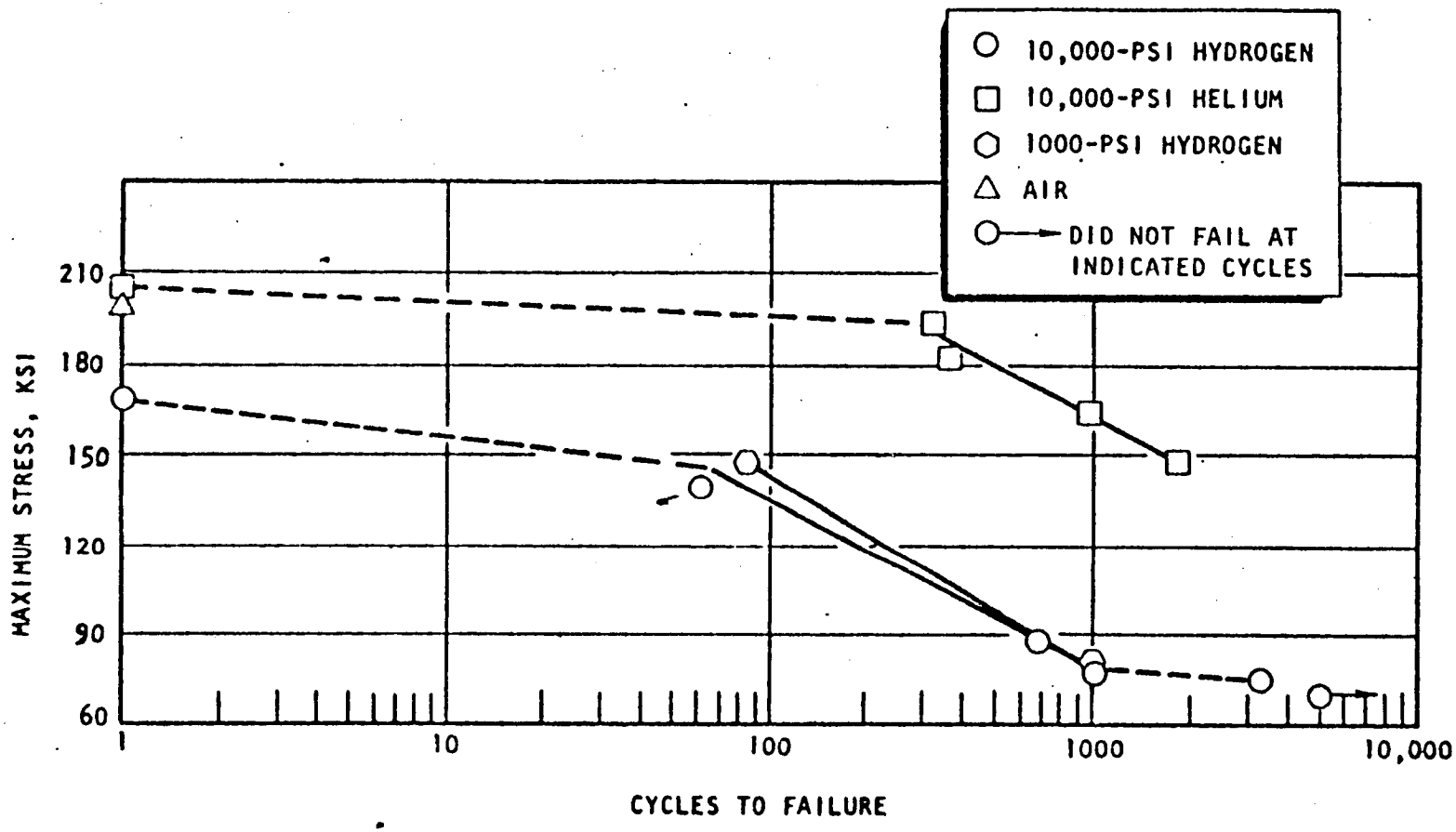

Figure 22. Effect of High-Pressure Hydrogen Environment on Low-Cycle Fatigue Strength of Precracked ASTM A-302 Specimens (Stress Calculated Using Diameter After Specimen was Precracked)

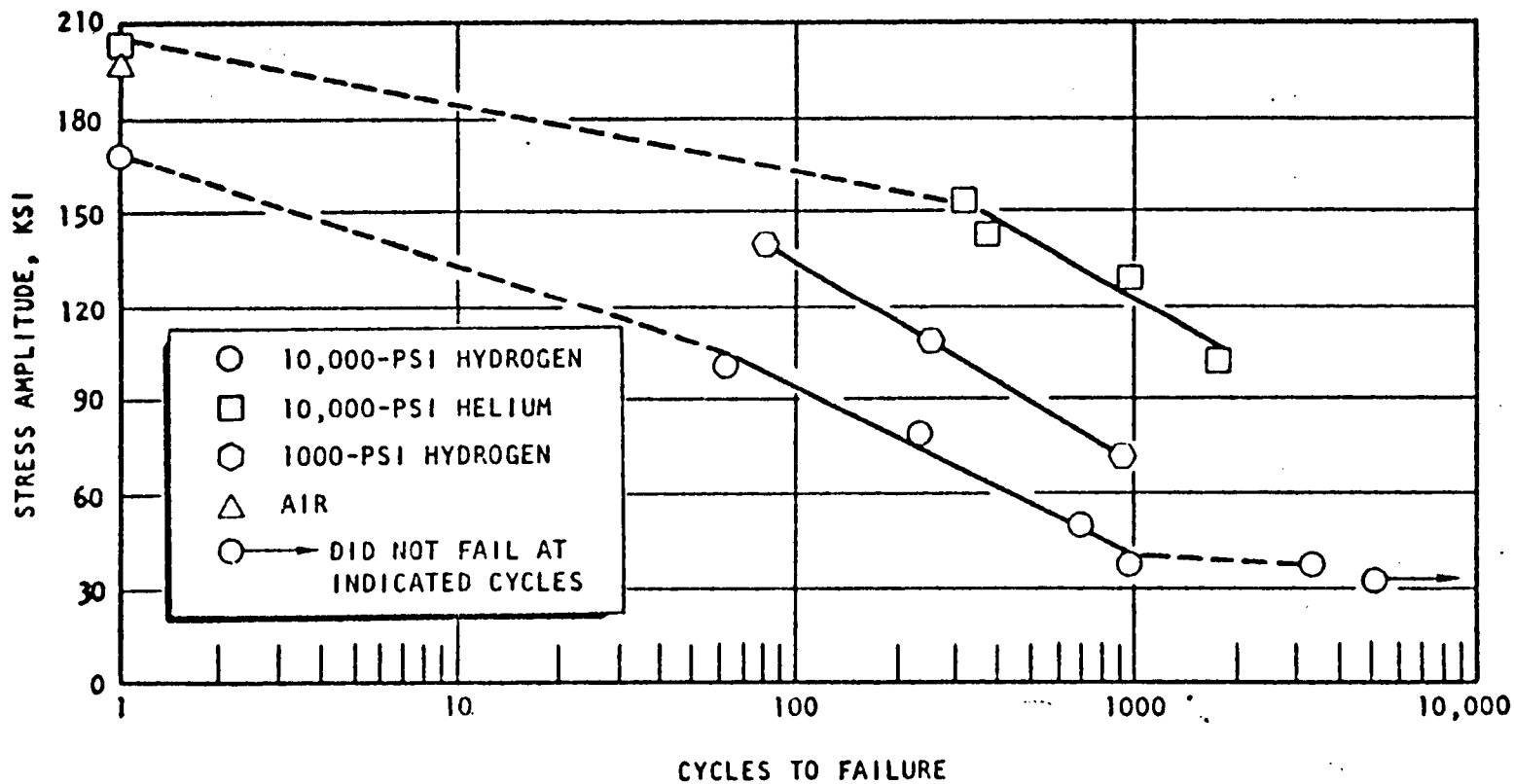

Figure 23. Effect of High-Pressure Hydrogen Environment on Low-Cycle Fatigue Strength of Precracked ASTM A-302 Steel Specimens (Stress Calculated Using Diameter After Specimen was Precracked)

specimen was precracked was only slightly less than the notch diameter, and it was somewhat difficult to measure. The choice of diameters did not affect the relation between the results in hydrogen and in inert environments.

Figures 21 and 22 show that the low cycle fatigue strength is much less in 10,000-psi hydrogen than in 10,000-psi helium. There is also indication of a low cycle fatigue limit in 10,000-psi hydrogen at about 65 ksi. The data appear to be almost without scatter, which is probably because the specimens were fatigue cracked in air prior to the environmental cyclic loading tests. Thus, it would seem that the apparent fatigue limit is real and not due to data scatter.

Figure 23 is a plot of the cycles to failure versus the stress amplitude over which the tests were conducted. In this plot, there is considerable difference in the stress amplitude to cause failure in 1000 cycles in 1000-psi and 10,000-psi hydrogen. The 1000-cycle strength (amplitude) is 30 ksi in 10,000-psi hydrogen, 70 ksi in 1000-psi hydrogen, and 122 ksi in 10,000-psi helium. The plot of stress amplitude versus cycles to failure appears to give a much better representation of the low cycle fatigue data than the plot of maximum stress versus cycles to failure. Except for the apparent fatigue limit in 10,000-psi hydrogen, the S-N curves apparently have about the same slope in the three environments.

Results of the tests on the precracked ASTM A-517 specimens are plotted in Fig. 24, 25 and 26. Figures 24 and 25 are plots of maximum stress versus cycles to failure. In Fig. 24 the strength is calculated on the basis of the diameter prior to precracking the specimens by high cycle fatigue. In Fig. 25 the data are plotted using the precracked diameter. Precracked diameter could not be adequately discerned in about half of the tests, thus there are fewer points in Fig. 25 than in Fig. 24. Figure 24 shows that the maximum stress to failure was about the same in 1000- and 10,000-psi hydrogen, and the 1000-cycle strength in the

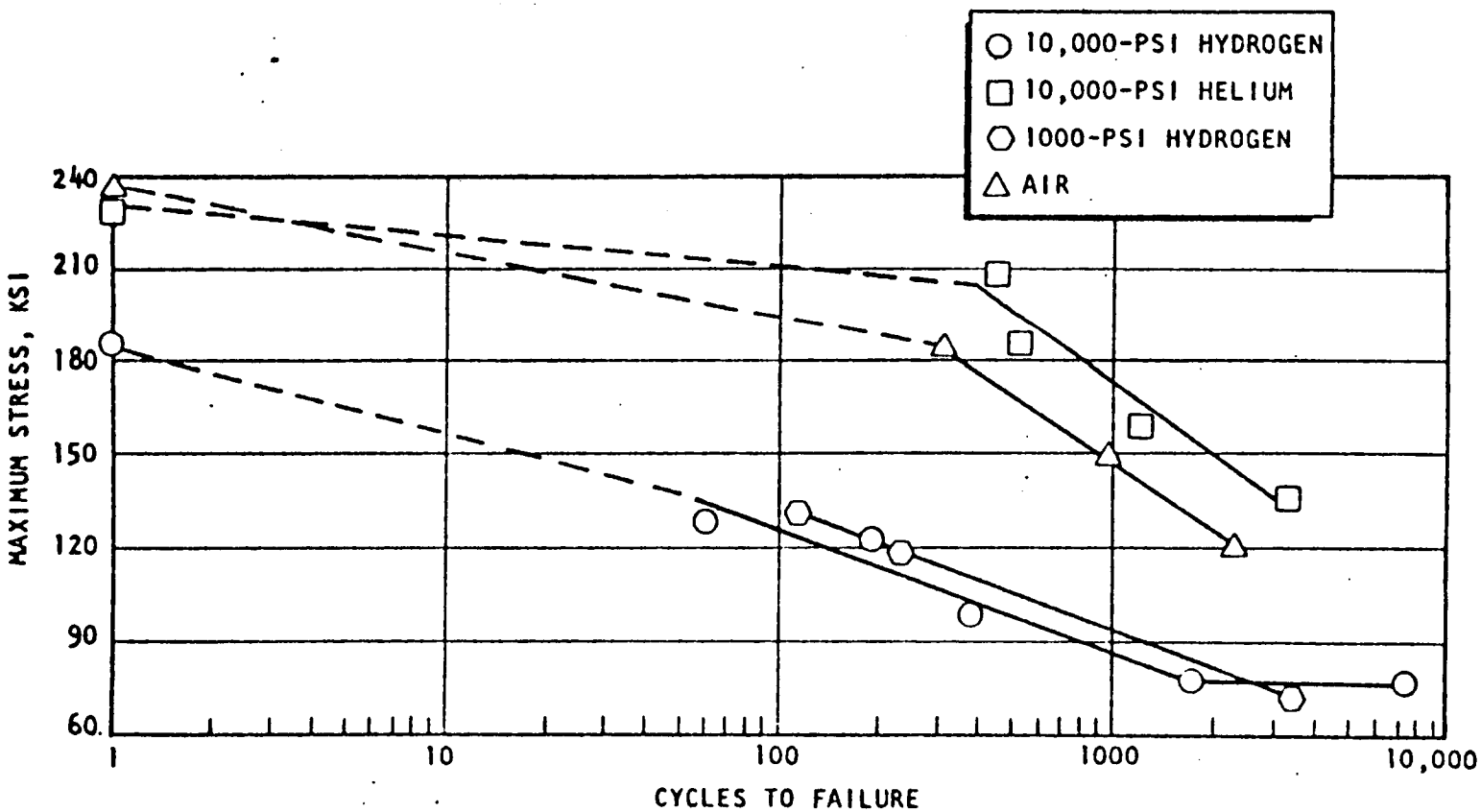

Figure 24. Effect of High-Pressure Hydrogen Environment on Low-Cycle Fatigue Strength of Precracked ASTM A-517 Specimens (Stress Calculated Using Diameter of Notched Specimen Prior to Precracking)

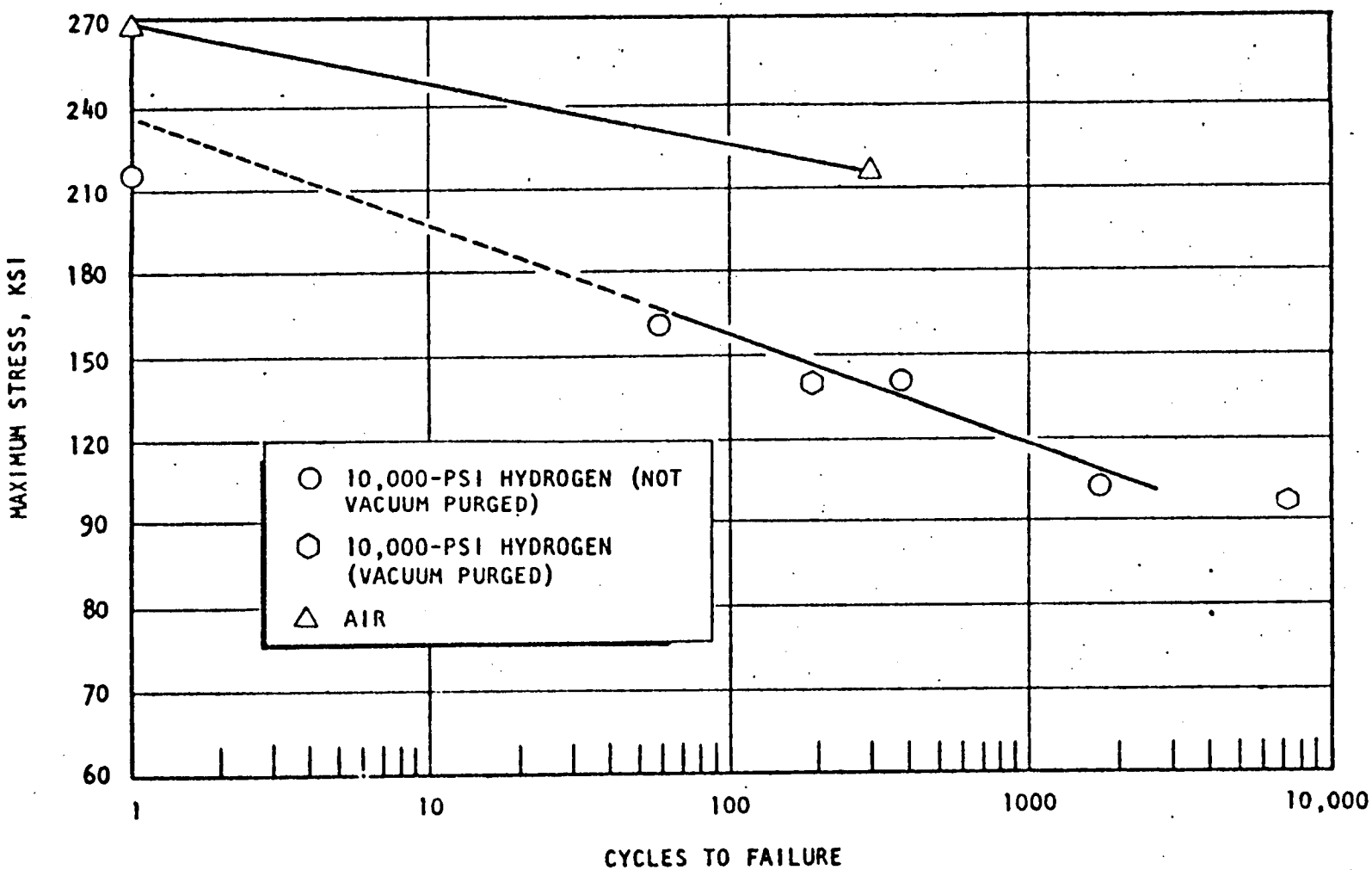

Figure 25. Effect of High-Pressure Hydrogen Environment on Low-Cycle Fatigue Strength of Precracked ASTM A-517 Specimens (Stress Calculated Using Diameter After Specimen was Precracked)

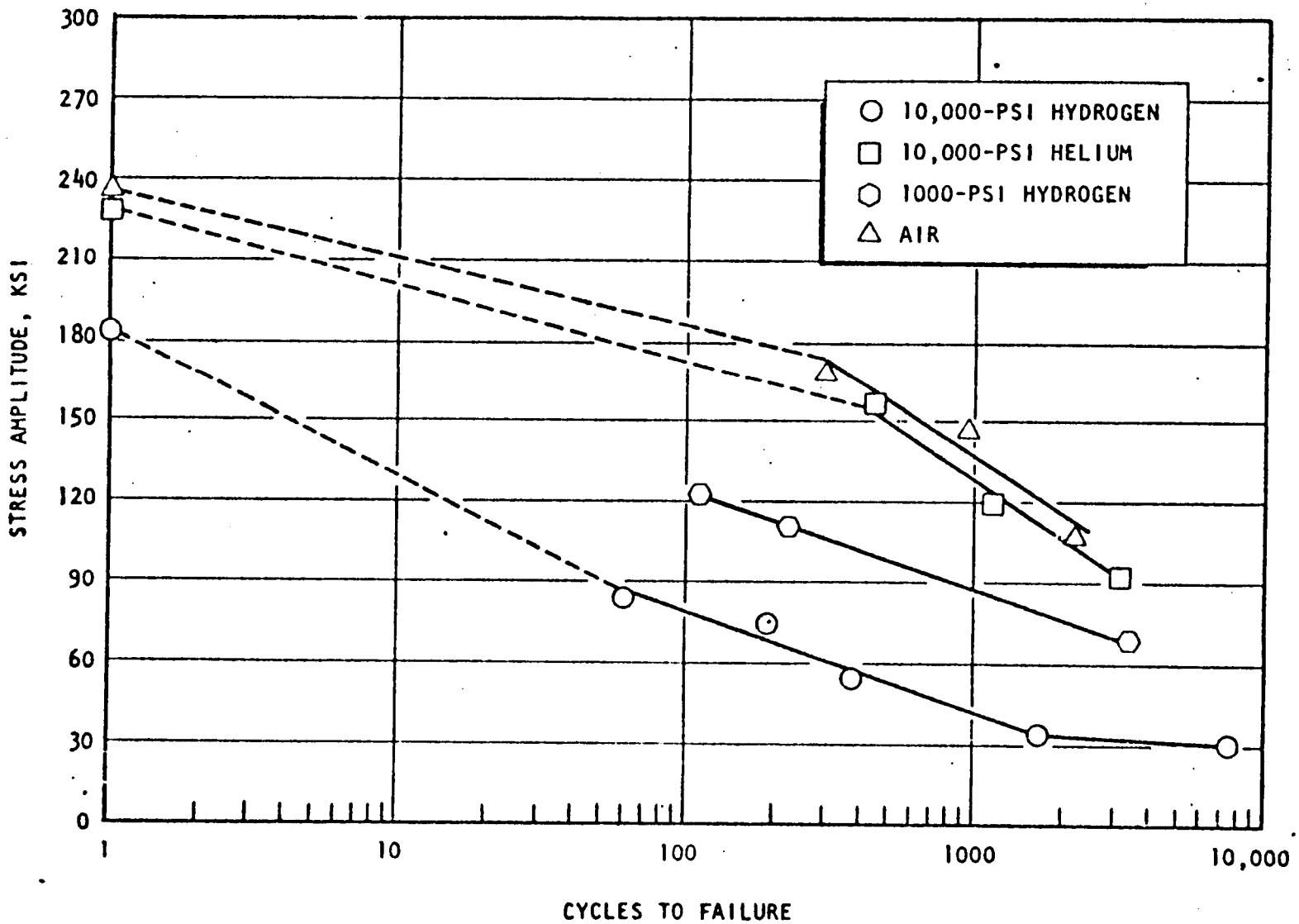

Figure 26. Effect of High-Pressure Hydrogen Environment on Low-Cycle Fatigue Strength of Precracked ASTM A-517 Specimens (Stress Calculated Using Diameter of Notched Specimen Prior to Precracking)

hydrogen environments was about 50 percent of that in 10,000-psi helium. Fatigue strength in 10,000-psi helium was higher than in air, but this difference was mainly due to the difference of the lower stress between these two environments as will be dexcribed below. As with ASTM A-302, the 10,000-psi hydrogen data for ASTM A-517 suggests a low cycle fatigue limit at about 75 ksi.

A plot of the stress amplitude over which the ASTM A-517 fatigue tests were conducted versus cycles to failure is shown in Fig. 26. The stress amplitude to cause failure in 1000 cycles is considerably lower in 10,000-psi hydrogen than in 1000-psi hydrogen. A second difference between Fig. 24 and 25 is that in Fig. 26 the stress amplitude to cause failure in a given number of cycles in 10,000-psi helium is about 10,000 psi lower than in air. This is equal to the increase of shear stress due to 10,000-psi hydrostatic pressure. Therefore, the fatigue strength in air and in 10,000-psi helium was the same within the accuracy of the measurements.

There was a problem, during the period in which the helium tests were conducted, of obtaining hydrogen-free helium, and the purification train was circumvented during this period to eliminate it as a source of hydrogen contamination. As a consequence, the impurity contents range from 1.1 to 1.4 ppm O_2 and 5.0 to 6.9 ppm N_2 compared to less than 50 percent of these contents obtained for purified helium. Thus the O_2 partial pressure in 10,000-psi helium was about 0.01 psi (0.5 mm Hg). This oxygen partial pressure is many orders of magnitude higher than in a reasonable vacuum. Therefore, the large increase of fatigue life experienced in vacuum environments would not likely be observed in helium containing oxygen at that partial pressure.

The stress amplitude to cause failure in 1000 cycles according to Fig. 26 is about 45, 85, 130, and 135 ksi in 10,000-psi hydrogen, 1000-psi hydrogen, air (1 atmosphere) and in 10,000-psi helium, respectively. The slope of the stress amplitude versus cycles to failure curves are steeper in

air and helium than in the hydrogen environments, and it appears that convergence would occur at about 10^6 cycles.

Therefore, the low cycle fatigue strengths of ASTM A-302 and ASTM A-517 are quite similar. The lower tensile stress during cycling in the 10,000 psi environments was sufficiently high that the stress amplitude rather than maximum stress was the better stress criterion for representing the fatigue results. For both materials, the 1000 cycle fatigue strength in 10,000-psi hydrogen was about 1/3 that in 10,000-psi helium. For both materials, there appears to be a low cycle fatigue limit in 10,000-psi hydrogen, which occurred between 1000 to 2000 cycles. The lack of scatter of all the data obtained on the precracked specimens would suggest that this fatigue limit is real. Correlation was made with 10,000-psi helium environment tests; the data obtained in air at 1 atmosphere pressure indicates that the fatigue strength in 10,000-psi helium was about the same as that in air (1 atm). The fatigue strength in 1000-psi hydrogen was about midway between the strength in 10,000-psi hydrogen and that in 10,000-psi helium for both materials.

Tensile strength was plotted in the figures as 1 cycle. A good argument could be made for plotting these data as 1/2 cycle since the stress cycle in tension-tension fatigue is 1/2 of the total cycle. At any rate, extrapolation to the tensile strength was poor in most instances regardless of where the tensile data were plotted.

Crack growth was followed by resistivity measurements for most of the low-cycle fatigue tests. Resistivity measurements could resolve a crack step of about 0.001 inch in length. From electron microscopy, the initial fatigue steps in 10,000-psi helium and air were found to be about 0.00007 inch. Thus, the first crack steps probably were not resolved in these environments and the change in resistivity was gradual rather than stepwise. The first crack step was assumed to occur at the point that the resistivity increased from the value prior to testing.

The resistivity measurements indicated that crack growth in all environments was not uniform. Even at high stresses for which virtually every crack step could be recorded, there were many cycles for which no crack growth was noted. Often, a region of no crack growth would separate regions in which crack movements of various lengths occurred during each cycle.

A definite crack step occurred during the first cycle for all of the tests conducted on precracked AISI type 310 stainless-steel specimens. The number of cycles at which the first crack step was noted was a function of cyclic stress and environment for the two low alloy steels. Figure 27 and 28 show that the first crack step was observed at fewer cycles on the ASTM A-302 and ASTM A-517 specimens in the hydrogen environments than in the inert environments. As would be expected, the higher the stress, the lower the number of cycles for appearance of the first crack step. It would appear, therefore, that the hydrogen environment affects crack initiation as well as propagation. This conclusion is tentative, however, because of the comparative lack of resolution particularly at the beginning of the tests where the stress is the lowest because the cross section has not been reduced by propagation of the crack.

There were considerably fewer resolved crack steps than fatigue cycles as is illustrated in Fig. 29, 30 and 31 for AISI type 310 stainless steel, ASTM A-302 and ASTM A-517, respectively. Figures 30 and 31 show that fewer crack steps occurred in the hydrogen environments than in inert environments for the low-alloy steel specimens. Crack steps were observed during tensile testing (1 cycle) on AISI 310 stainless steel for all environments and on the ASTM A-302 and ASTM A-517 specimens tensile tested in 10,000-psi hydrogen. The fact that crack growth is stepwise in hydrogen in the low-alloy steel specimens may be helpful in clarifying the embrittlement mechanisms.

Figures 32 and 33 show that the average distance each crack grew was indeed greater in hydrogen than in inert environments.

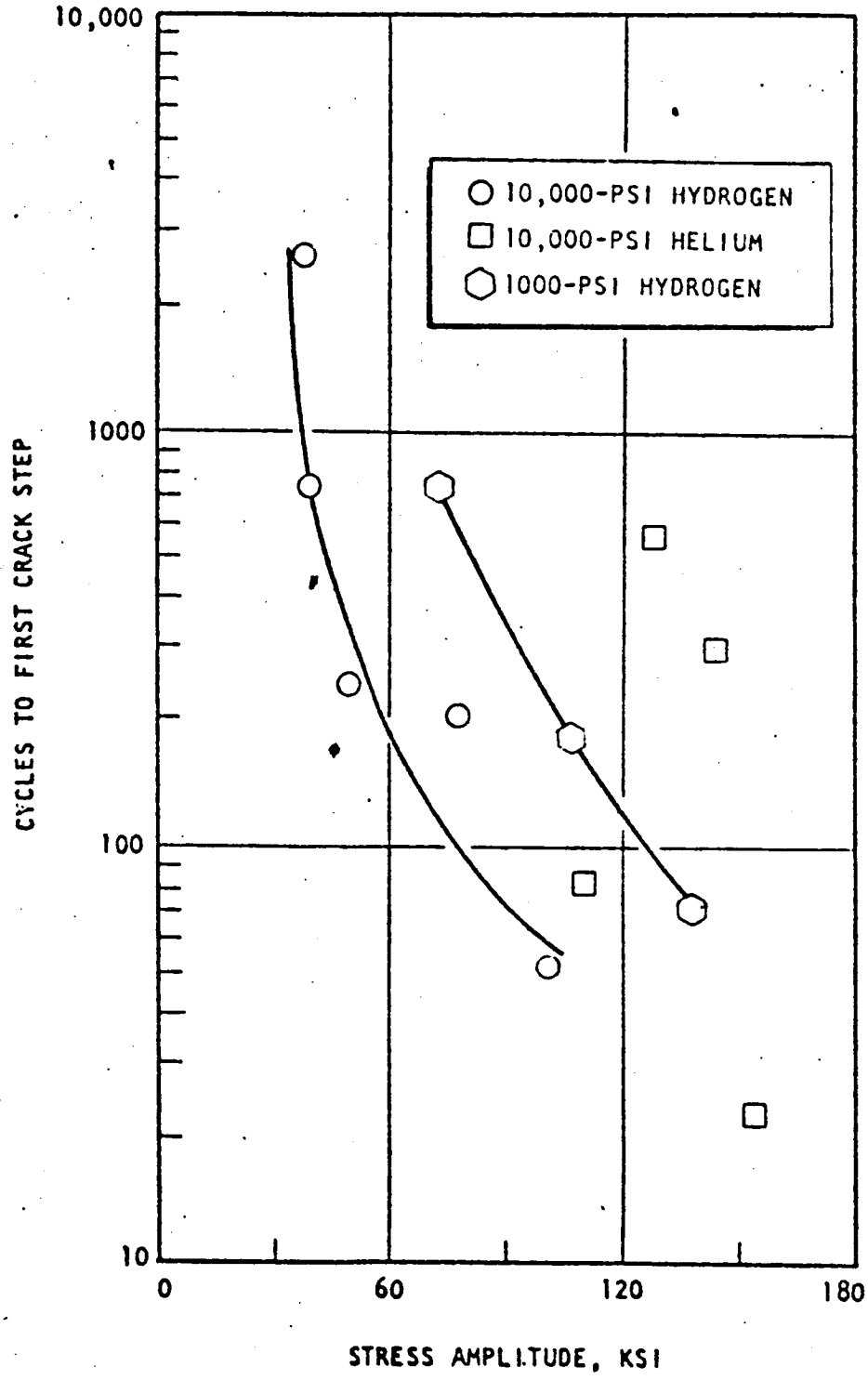

Figure 27. Cycles at Which First Crack Step Occurred in Precracked ASTM A-302 Specimens

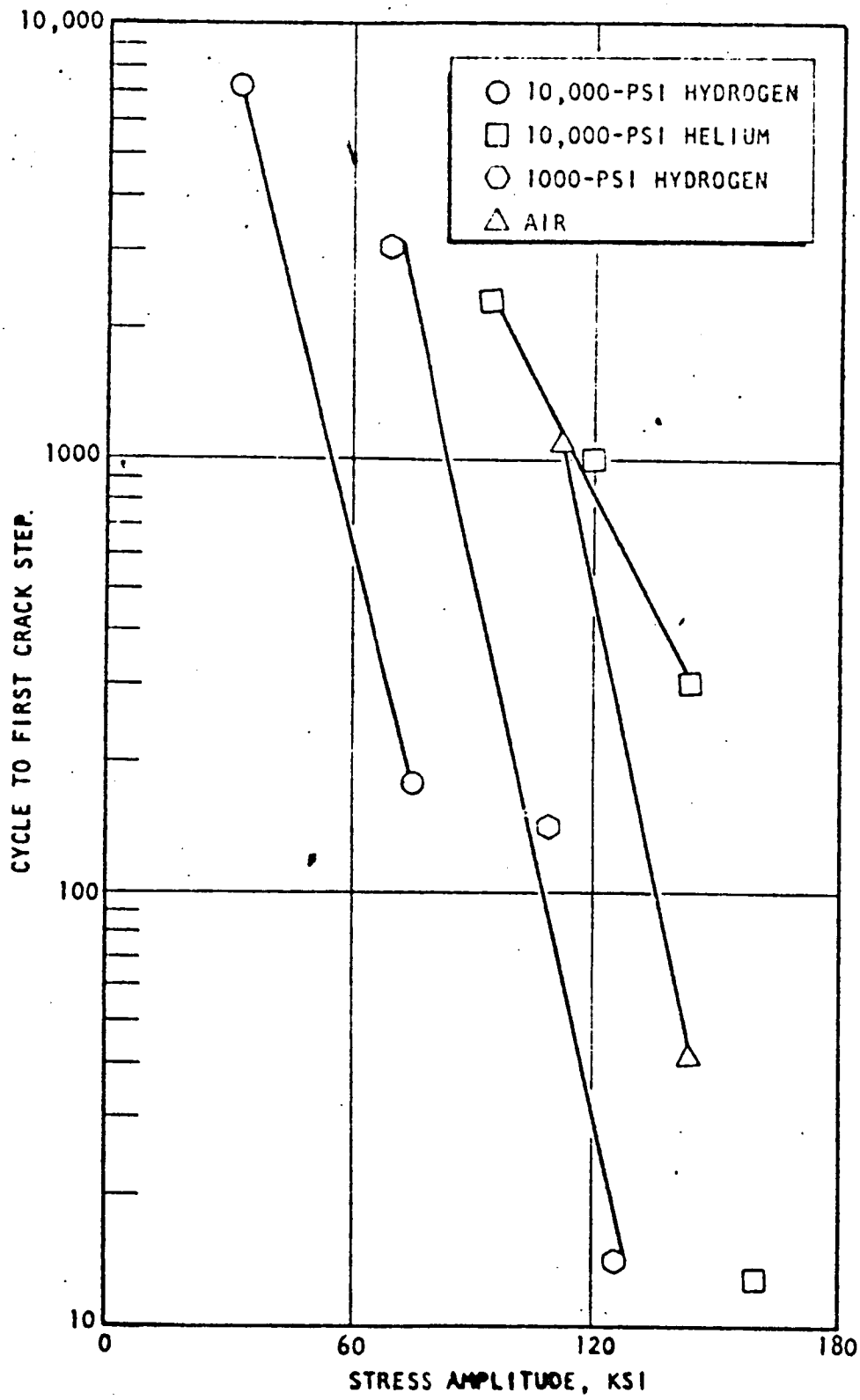

Figure 28. Cycles at Which First Crack Step Occurred in Precracked ASTM A-517 Specimens

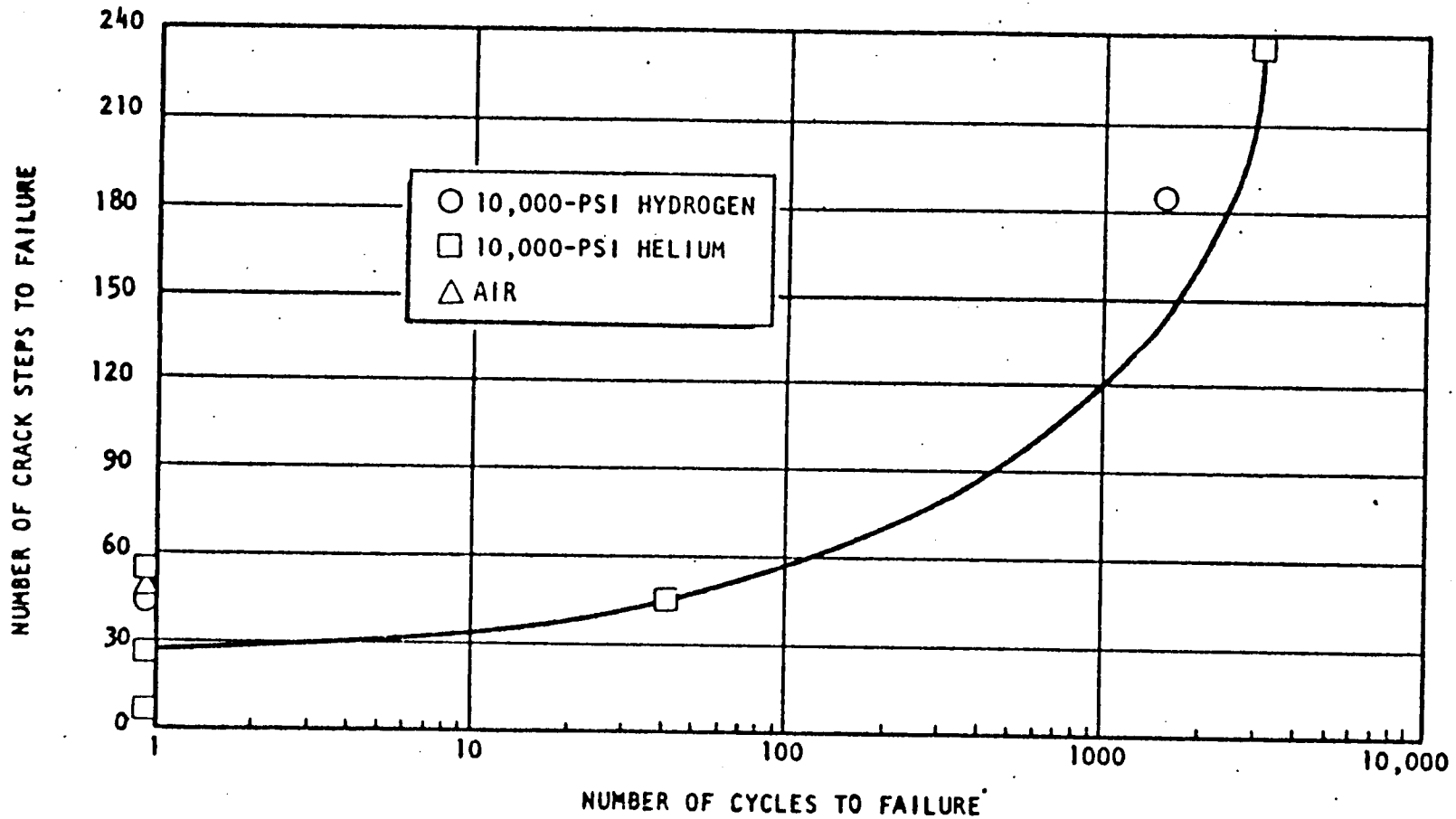

Figure 29. Crack Steps Versus Cycles to Failure of Precracked AISI Type 310 Stainless Steel Specimens

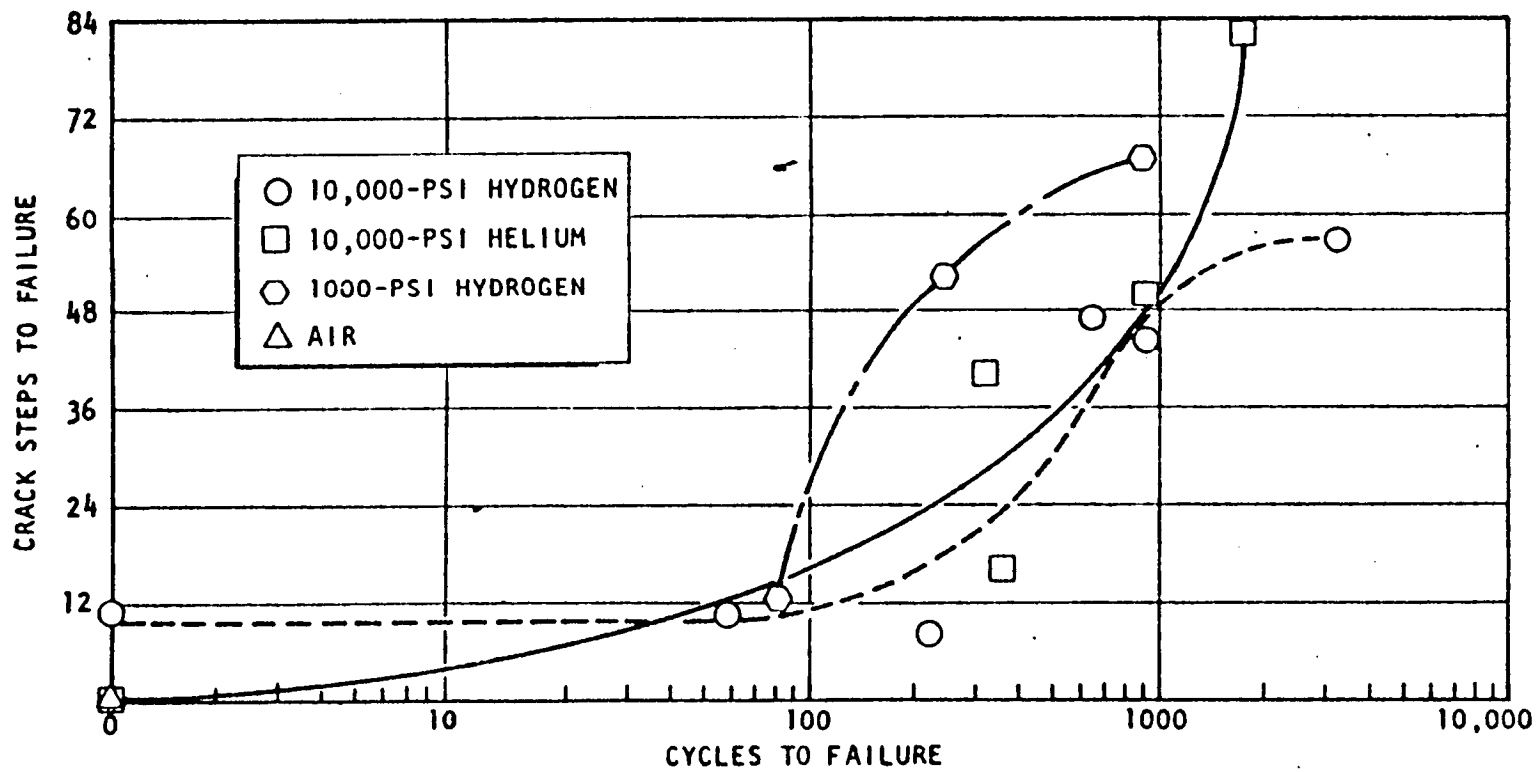

Figure 30. Crack Steps Versus Cycles to Failure of Precracked ASTM A-302 Specimens

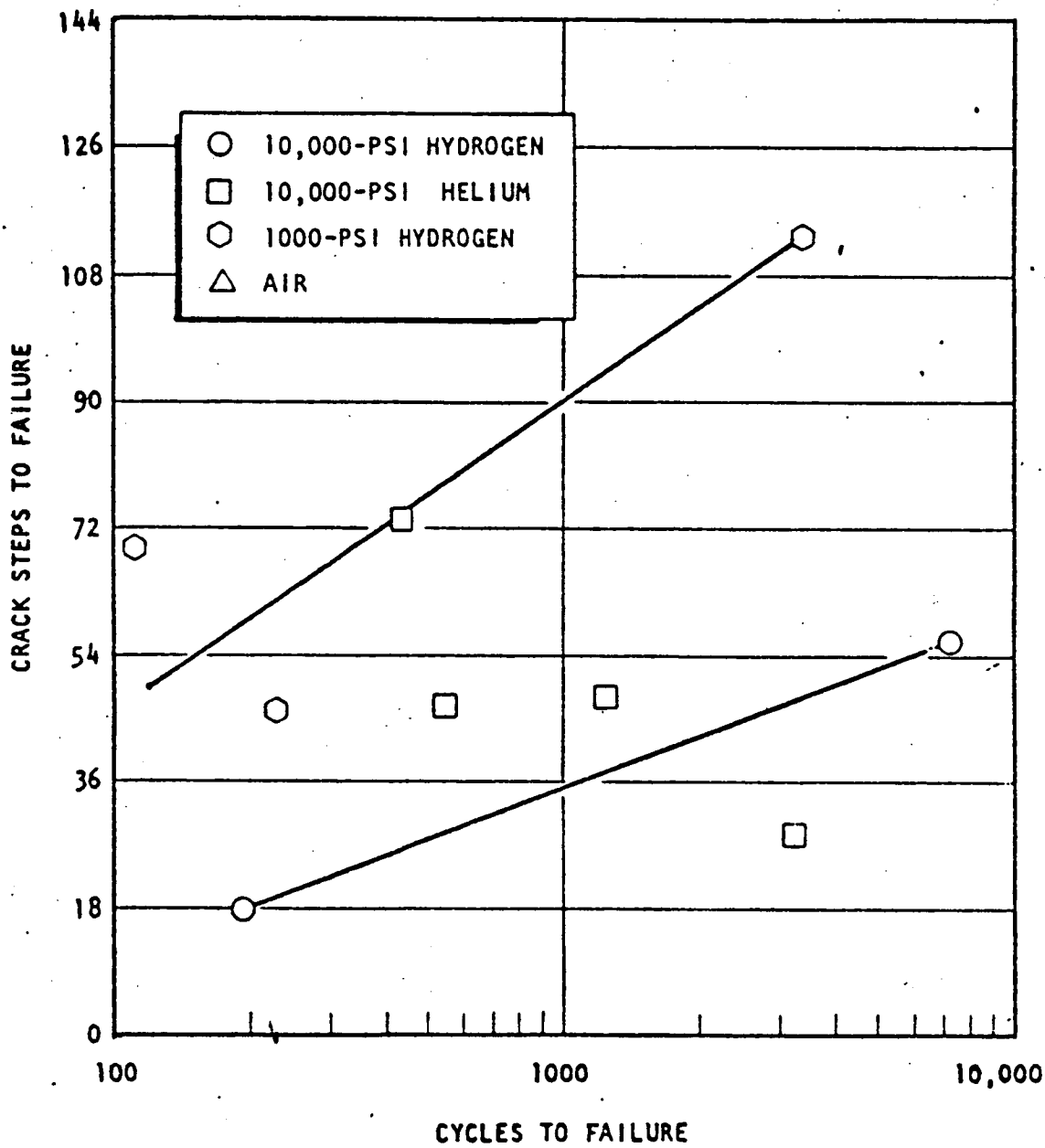

Figure 31. Crack Steps Versus Cycles to Failure of Precracked ASTM A-517 Specimens

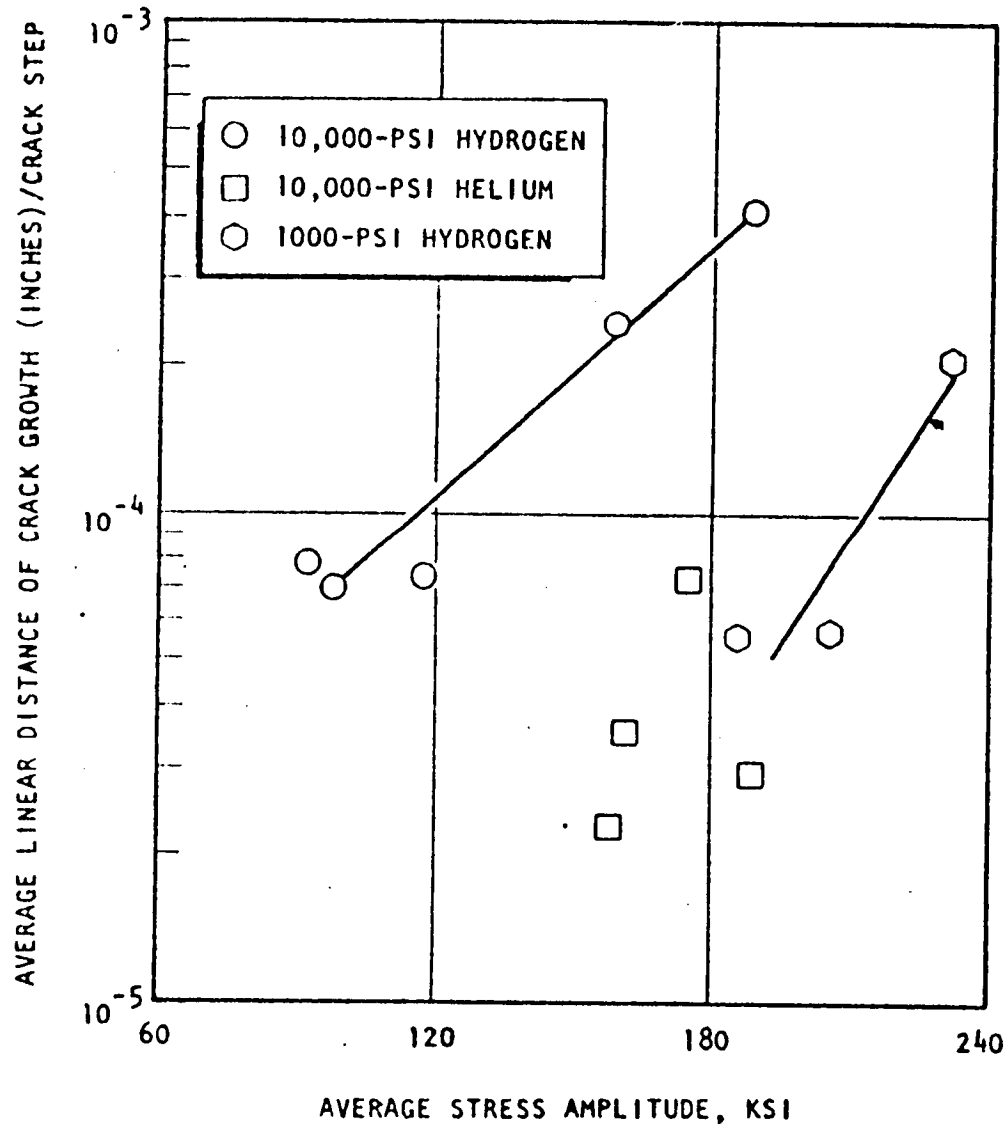

Figure 32. Average Linear Distance of Crack Growth in Precracked ASTM A-302 Specimens (Inches) Crack Step

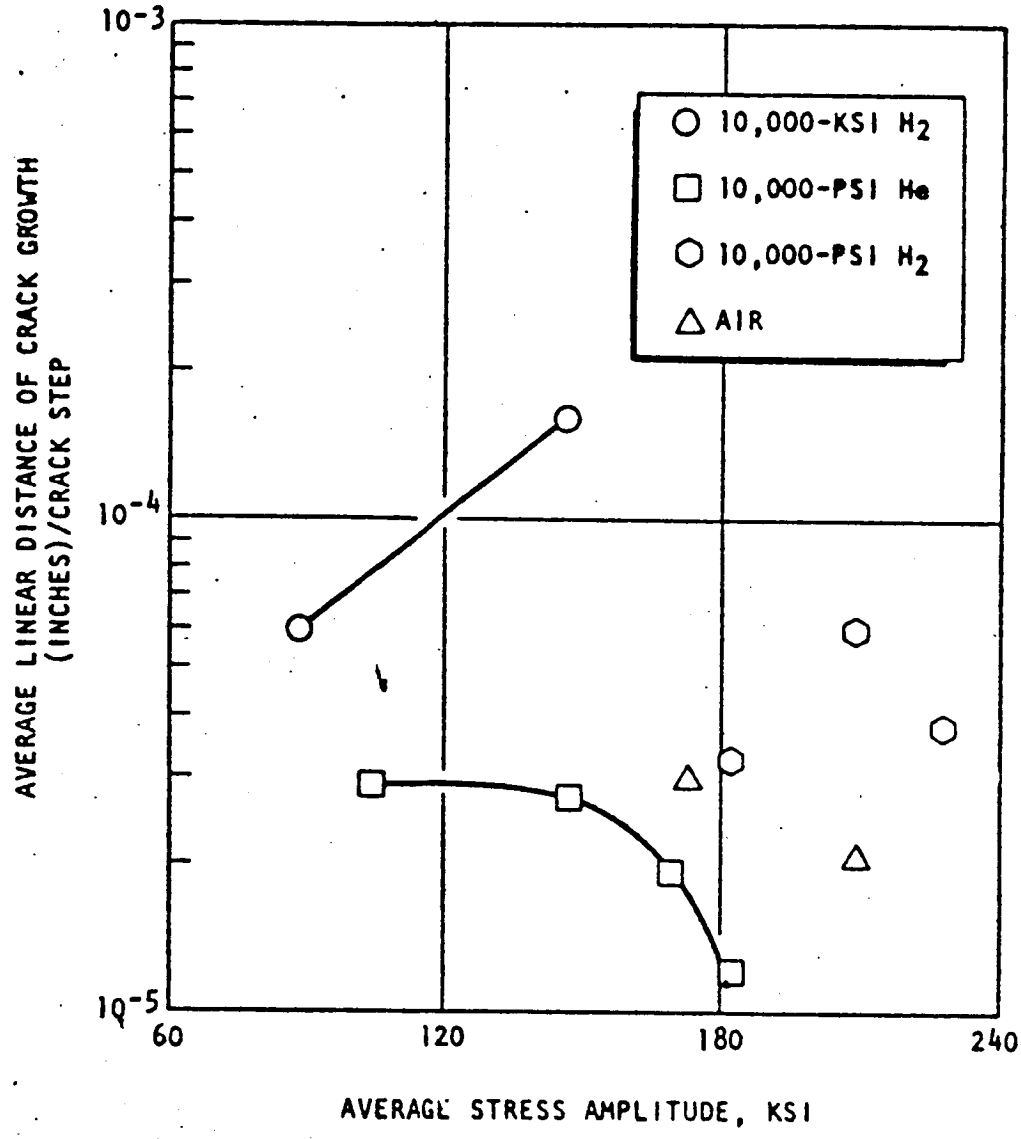

Figure 33. Average Linear Distance of Crack Growth in Precracked ASTM A-517 Specimens

The rate of crack growth during fatigue is important in predicating the life of parts subject to fatigue. This rate as a function of stress amplitude was calculated for several of the specimens tested in low-cycle fatigue. Calculations were made by relating the initial specimen cross section, and the cross section immediately prior to catastrophic failure to the overall resistivity change. Resistivity was recorded on a strip chart recorder and therefore the resistivity change per cycle could be measured. This analysis was not subject to the limitation of nonresolvable crack steps because the calculations were based on the average resistivity change over various stress increments or fatigue cycle span increments.

Crack growth per cycle is plotted as a function of stress amplitude (difference between maximum and minimum stress) for the ASTM A-302 and ASTM A-517 specimens in Fig. 34 and 35. The overall environmental effect on crack propagation is that the rate of propagation is considerably faster in 10,000-psi hydrogen than in 10,000-psi helium, and the rate in 1000-psi hydrogen is near that in 10,000-psi hydrogen initally (that is at low stress amplitudes at the beginning of the tests) but falls off to slower rates compared to that in 10,000-psi hydrogen as the crack propagates.

An explanation of the variation of the hydrogen environment rate data is that there was a critical combination of minimum hydrogen pressure and maximum crack depth, so that the rate of crack propagation is dependent upon the rate at which hydrogen gas reached the crack tip, when that rate fell below a certain minimum value. Comparison between the 10,000-psi hydrogen data for ASTM A-302 and ASTM A-517 shows that the curves extrapolate so that they lie essentially on top of each other. But the 1000-psi ASTM A-302 curve and the low-cycle, 1000-psi ASTM A-517 curve deviate from the 10,000-psi hydrogen curves at about the same relative positions from the start of the test. Thus it appears that the crack rate in 1000-psi hydrogen is determined by both the distance the crack propagated and the stress amplitude.

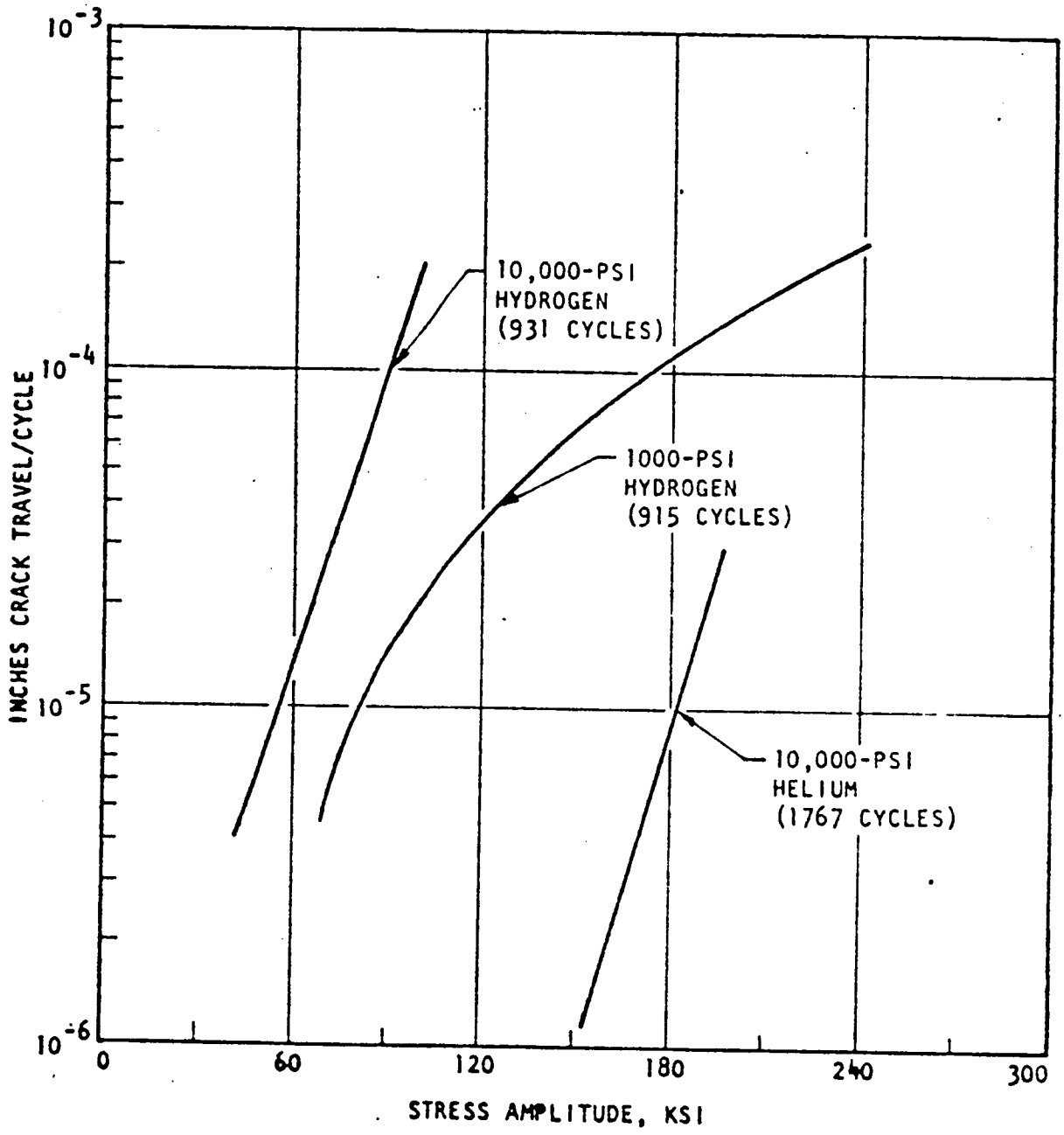

Figure 34. Crack Growth per Cycle Versus Stress Amplitude of ASTM A-302 Precracked Specimens

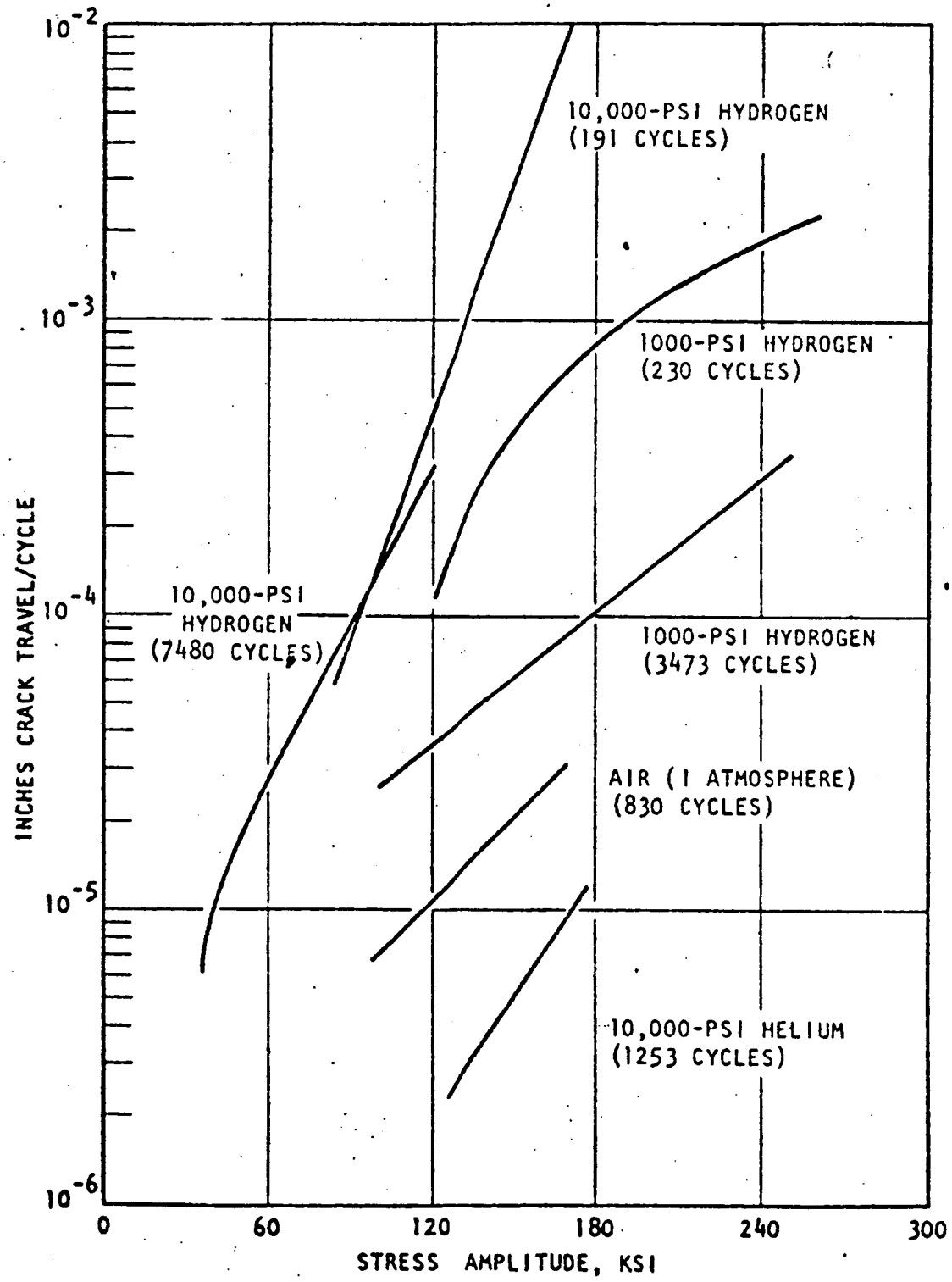

Figure 35. Crack Growth per Cycle Versus Stress Amplitude of ASTM A-517 Precracked Specimens

The shallow slope obtained from the higher cycle data on ASTM A-517 specimens in 1000-psi hydrogen can be explained in the same manner. Stress amplitude of this test was initially 68 ksi. The specimen area at the same stress amplitudes was about 50 percent less for the higher cycle tests than for the lower; and thus the crack depth at similar stress amplitude was considerably deeper for the higher cycle tests. It is suggested that crack depth during the high-cycle hydrogen test was so deep over the portion of the test analyzed that the rate of crack propagation was limited by the rate of hydrogen transport to the crack tip. If the analysis could be extended to lower stress amplitudes, the rate of crack growth should compare with the rate obtained from the lower cycle tests.

The above analyses assume that the crack growth of the cylindrical precracked specimens can be expressed as a semi-log function of crack displacement versus stress amplitude. Generally, the crack growth is expressed as either a semi-log or log-log function of crack displacement versus stress intensity. The small specimens used for these tests do not readily lend themselves to stress intensity analysis.

SUMMARY

Low-cycle fatigue strengths in various environments of unnotched specimens of all three materials and of precracked, AISI type 310 stainless-steel specimens were about the same as their tensile strengths in the same environment. The low-cycle fatigue properties of the precracked ASTM A-302 and ASTM A-517 specimens were quite similar to each other in all environments. For both materials, the 1000-cycle fatigue strength in 10,000-psi hydrogen was about 1/3 that in 10,000-psi helium; and for the 10,000-psi hydrogen tests there appeared to be a low-cycle fatigue limit that occurred between 1000 and 2000 cycles. The fatigue strengths of precracked ASTM A-302 and ASTM A-517 specimens in 1000-psi hydrogen were about midway between the strengths in 10,000-psi hydrogen and that in 10,000-psi helium.

Crack growth measurements indicated that crack initiation occurred at fewer cycles in hydrogen than in inert environments. There were fewer crack steps in hydrogen and the distance the crack traveled per crack step was greater in hydrogen than in the inert environments. The relationship between stress amplitude and logarithm of crack growth per cycle was linear for the 10,000-psi hydrogen and 10,000-psi helium environments. Curves in 1000-psi hydrogen deviated from linearity to slower rates of crack growth with increasing crack depth, and it is suggested that the rate of crack propagation was dependent upon the rate at which 1000-psi hydrogen gas reached the crack tip.

CONCLUSIONS

1. The stress amplitude to cause failure in 1000 cycles of precracked ASTM A-302 is approximately 40, 70, and 120 ksi in 10,000-psi hydrogen, 1000-psi hydrogen, and in 10,000-psi helium, respectively.

2. The stress amplitude to cause failure in 1000 cycles of precracked ASTM A-517 is approximately 35, 75, 105, and 120 ksi in 10,000-psi hydrogen, 1000-psi hydrogen, 10,000-psi helium and air at 1 atmosphere pressure, respectively.

3. The low-cycle fatigue strengths in various environments of unnotched specimens of all three materials and of precracked AISI type 310 stainless-steel specimens is about the same as their tensile strengths in the same environment.

PHASE VII: RELATION BETWEEN THE MECHANICAL PROPERTIES OF STEELS IN AIR AND SUSCEPTIBILITY TO HYDROGEN-ENVIRONMENT EMBRITTLEMENT

INTRODUCTION

In the previous program conducted at Rocketdyne, the three low-alloy steels investigated (ASTM A-302, ASTM A-517, and ASTM A-212) exhibited the following characteristics: (1) the strength and ductility of notched specimens and reduction of area of unnotched specimens was considerably reduced by a 10,000-psi hydrogen environment, (2) the strength and elongation was little affected by the hydrogen environments, and (3) surface cracking occurred in the necked-down region of unnotched specimens tested in hydrogen. These observations suggested that hydrogen-environment embrittlement required the occurrence of a certain critical plastic strain and further that the reduction of notch strength in hydrogen might be related to the normal yield strength/ultimate strength ratio; other variables being constant. It was also found in the previous program that ASTM A-212, which was the lowest strength steel of the three investigated, had the largest reduction of notch strength in high-pressure hydrogen. In conformance with the above suggestions, this was explained on the basis that ASTM A-212 had the lowest yield strength/ultimate strength ratio of the three steels.

Thus, this phase was conducted to determine if the reduction of notch strength of steels in 10,000-psi hydrogen, as compared to that in 10,000-psi helium, increases as the normal (in air) yield strength/ultimate strength ratio decreases. A review of the mechanical properties of many steels was made in an effort to find two with similar compositions, structures, and ultimate strengths, but with as greatly different yield strengths as possible. Unfortunately, one or both of the most optimum combinations of steels were unavailable except in mill-run quantities. The combination of steels finally selected was AISI 1042 and AISI 4140, both quenched and tempered to an ultimate strength of 110 ksi.

EXPERIMENTAL PROCEDURE

During the course of this program, several phases employed similar procedures. Such is the case with Tensile Specimen Design, Apparatus, and Test Procedure. Identical to their Phase I counterparts, these three are discussed in detail in that section of the report and, thus, eliminated here. Test vessel purging included evacuation in this phase.

Materials

Chemical compositions, heat treatments, and mechanical properties of the AISI 1042 and AISI 4140 steels used in this phase are presented in Tables 34, 35, and 36. The mechanical properties of the AISI 1042 specimens were found to be variable from specimen to specimen and this is discussed in the Results and Discussion section.

RESULTS AND DISCUSSION

Results of the tests performed in this phase are presented in Table 37. The hardness and other mechanical properties were very consistent from specimen to specimen for AISI 4140. Thus, the results given for AISI 4140 in Table 37 are averages of three tests in hydrogen, two in helium, and two in air for both unnotched and notched specimens. Individual specimen data for AISI 4140 is contained in Appendix Table VII-1.

In testing the AISI 1042 specimens, the mechanical properties were found to be significantly different from specimen to specimen, and it was necessary to interpret the results in terms of individual specimens. Thus, the results for individual AISI 1042 specimens are given in Table 37. Essentially the same table is repeated in the Appendix (Table VII-2).

Variability of properties from specimen to specimen for AISI 1042 led to two problems when attempting to relate the degree of hydrogen-environment embrittlement to the yield strength/ultimate strength ratio.

TABLE 34

CHEMICAL COMPOSITION OF PHASE VII MATERIALS

Material	C	Mn	P	S	Si	Cr	Mo	Fe
AISI 1042 3/8-inch-diameter rod	0.44	0.76	0.008	0.020	0.20			Balance
AISI 4140 3/8-inch-diameter rod	0.405	0.83	0.009	0.014	0.31	0.93	0.20	Balance

TABLE 35

HEAT TREATMENT OF PHASE VII MATERIALS

Material	Heat Treatment by Supplier (As-Received Condition)	Heat Treatment by Rocketdyne
AISI 1042	Annealed	Heat treated at 1575 F for 1 hour; oil quenched; tempered at 1000 F for 2 hours; air cooled; re-tempered at 1150 F for 2 hours; air cooled
AISI 4140	Annealed	Heat treated at 1550 F for 1 hour; oil quenched; tempered at 1300 F for 2 hours; air cooled

TABLE 36

MECHANICAL PROPERTIES OF PHASE VII MATERIALS

Material	Tensile Strength, ksi	Yield Strength, ksi	Reduction of Area, percent	Elongation, percent
AISI 1042	98 to 110	63 to 82	69	24 to 29
AISI 4140	108	93	68	29

TABLE

TENSILE PROPERTIES OF QUENCHED AND TEMPERED AISI 1040 AND AISI 4140 IN 10,000-PSI HYDROGEN, 10,000-PSI HELIUM, AND AIR

Material	Specimen	Stress Concentration Factor	Test Conditions				Test Results						
					Strain Rate/Minutes		Strength			Ductility			
			Environment	Pressure, psig	0 Load to Yield	Yield to Ultimate	Yield, ksi	Ultimate, ksi	Change from Helium,[a] percent	Elongation (1.25-inch Gage Length), percent	Reduction of Area, percent	Yield Strength to Ultimate Strength Ratio	Hardness, R_b
AISI 1042 Quenched and Tempered	UN		Air	0	0.002	0.04	82	110		24	68	0.75	95
	UN		Air	0	0.002	0.04	63	98		29	62	0.64	86
	N	8.28	Air	0	0.0007	0.0007		169			11		84
	N	8.27	He	10,000	↓	↓		188			16		95.5
	N	8.28	He	↓	↓	↓		164			11		90
	N	8.28	He	↓	↓	↓		151			16		87.5
	N	8.92	H_2	↓	↓	↓		109	-30		6.7	0.67[a]	88
	N	8.90	H_2	↓	↓	↓		148	-19		5.1	0.74[a]	94
	N	8.29	H_2	↓	↓	↓		107	-29		5.0	0.66[a]	87
AISI 4140 Quenched and Tempered	UN		Air	0	0.002	0.04	93	107.5		29	68	0.87	
	N	8.77	Air	0	0.0007	0.0007		195			10.5		92.7
	N	8.63	He	10,000	↓	↓		182.5			14		94
	N	8.81	H_2	10,000	↓	↓		155.6	-15		7.1		92.3

[a] Determined from specimen hardness and from data for two specimens tested in air and 10,000-psi helium assuming a linear relationship between strengths and hardness.

First, the notch strength of a specimen in 10,000-psi hydrogen must be compared to the notch strength of a similar specimen in 10,000-psi helium. Secondly, the yield strength/ultimate strength ratio in air must be the ratio appropriate to the specimen tested in 10,000-psi hydrogen. Therefore, it was necessary to use hardness when interpreting the AISI 1042 results. The hardness of each AISI 1042 specimen was determined. The notch strength in 10,000-psi helium was found to be a linear function of hardness as shown in Fig. 36. The reduction of notch strength of a specimen because of the 10,000-psi hydrogen environment was determined by comparing the notch strength in hydrogen to the notch strength in 10,000-psi helium (from Fig. 36) for a hardness the same as that of the specimen tested in hydrogen.

It was also assumed that the yield strength and ultimate strength of unnotched AISI 1042 specimens varied linearly with hardness. The yield strength, ultimate strength, and yield strength/ultimate strength ratio in air, appropriate to a specimen tested in 10,000-psi hydrogen, was determined from the hardness of that specimen and from the data for the two specimens tested in air, assuming the linear relationship between strength and hardness.

Figure 37 shows a plot of the yield strength/ultimate strength ratio versus percent reduction of notch strength in 10,000-psi hydrogen as compared to the notch strength in 10,000-psi helium. The points in Fig. 37 for AISI 1042 represent single specimens, as discussed above, while the AISI 4140 point represents the average for three specimens. Thus, Fig. 37 does indeed show, as predicted, that the hydrogen-environment embrittlement increases with a decreasing yield strength/ultimate strength ratio.

Ultimate strength, as well as the yield strength, varied for the AISI 1042 specimens because of nonuniformity of the mechanical properties following heat treatment. It might therefore be argued that the change of embrittlement with yield strength/ultimate strength ratio was a

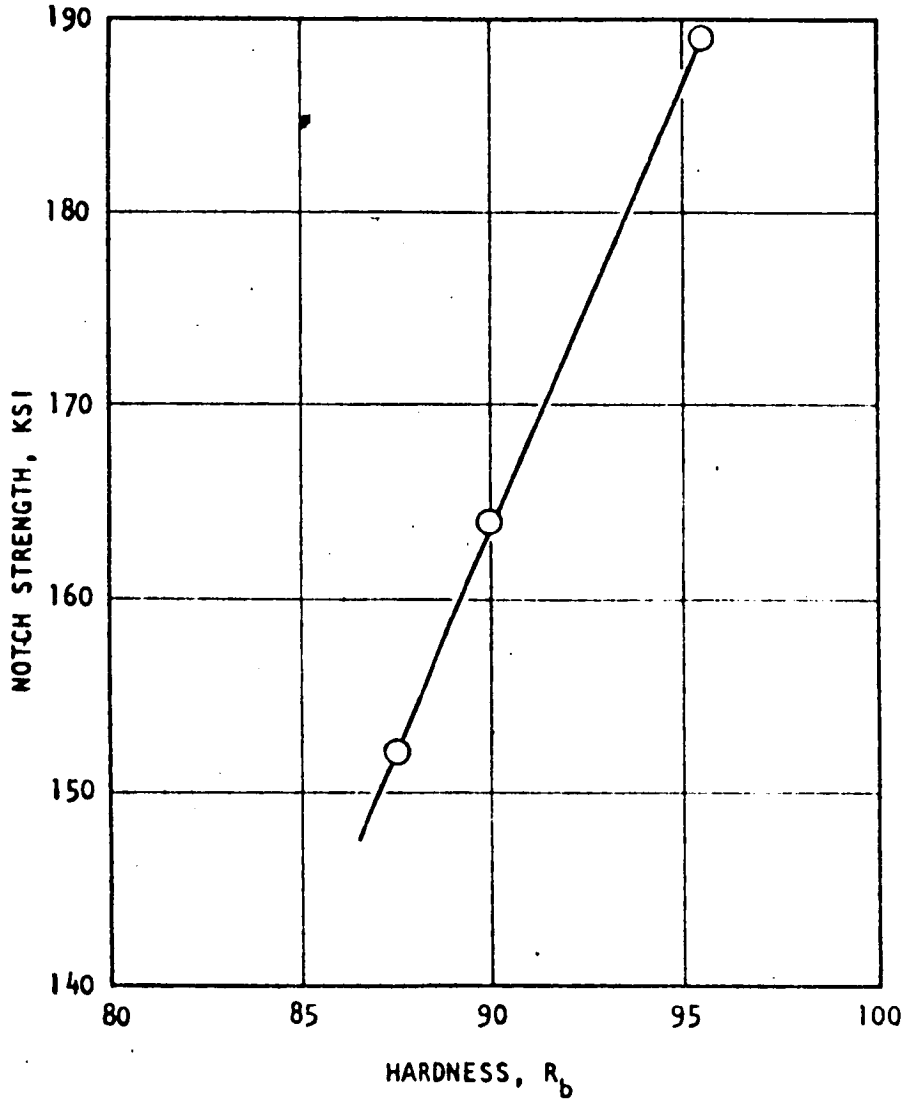

Figure 36. Notch Strength in a 10,000-psi Helium Environment versus Specimen Hardness for AISI 1042 and AISI 4140 Steels

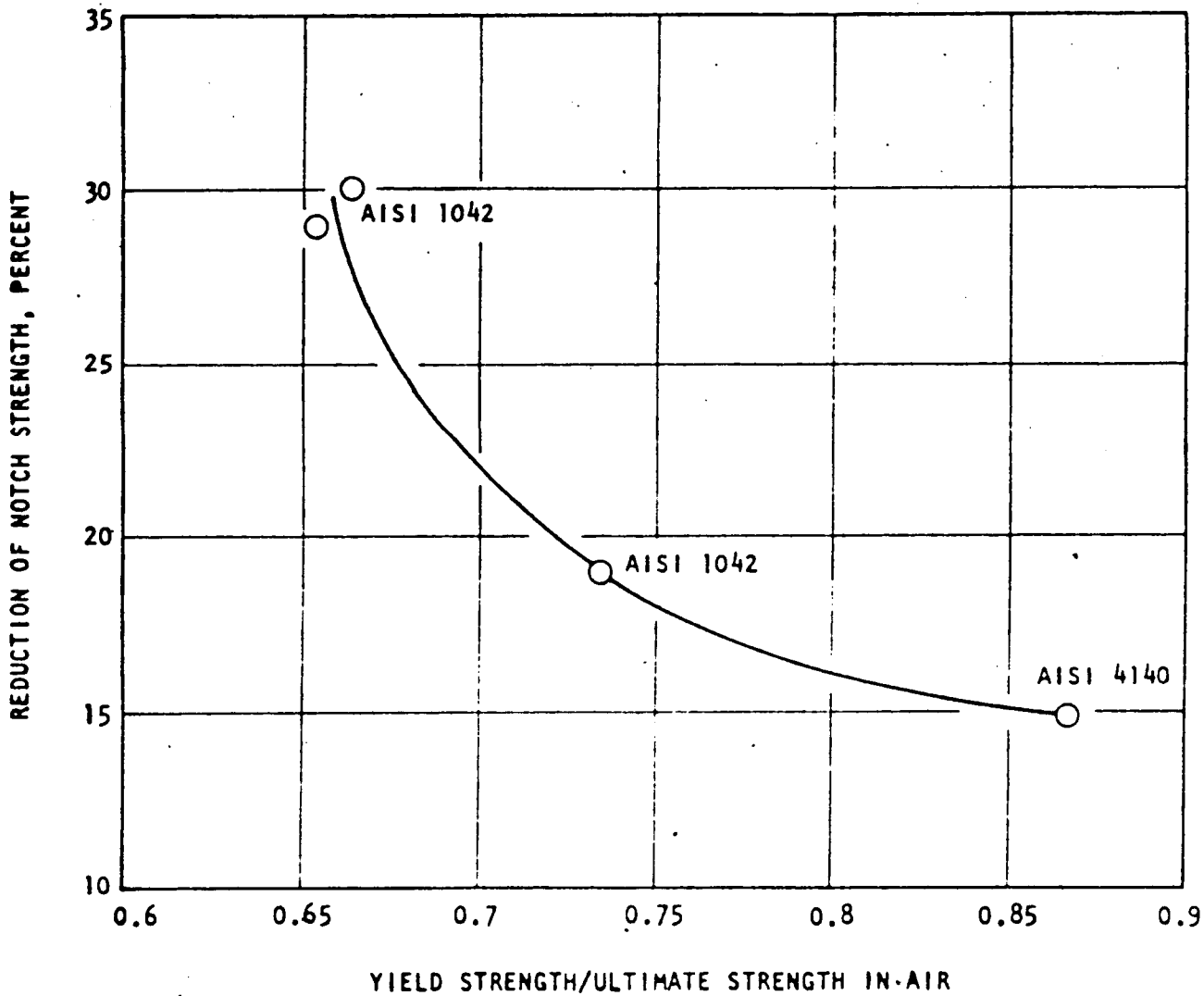

Figure 37. Percent Reduction of Notch Strength in a 10,000-psi Hydrogen Environment Versus Yield Strength/Ultimate Strength Ratio for AISI 1042 and AISI 4140 Steels

result of different ultimate strengths rather than the difference between the yield and ultimate strengths. Figure 38 is a plot of reduction of notch strength versus both the yield and ultimate strengths in air of unnotched specimens. It can be seen that the ultimate strength varies comparatively little among the specimens. However, there is a wide variation of yield strength, which of course is reflected in the variation of the yield strength/ultimate strength ratio. According to Fig. 38 embrittlement increases with decreasing yield and ultimate strengths. Such dependency is, of course, contrary to the Phase II results, which showed that the high-strength metals were the most embrittled of all of the materials tested. Therefore, it appears from these results that hydrogen-environment embrittlement is indeed a function of the yield strength/ultimate strength ratio.

The most definitive experiments conducted in this program into the effect of yield strength/ultimate strength ratio on embrittlement were performed on prestrained AISI 1020 specimens in Phase III. Because of strain aging, holding under stress increased the yield strength; however, the ultimate strength in most cases remained essentially constant. After 100 days of exposure, the yield and ultimate strengths were almost the same, and the yield strength/ultimate strength ratio increased to nearly 1.0 during the hold period. Reduction of notch strength of the AISI 1020 specimens was about 14, 4, and 1 percent after 0, 1, and 100 days of exposure to 10,000-psi hydrogen under tensile stresses of 80 and 90 percent of their strength.

Other variables such as chemistry and microstructure remained constant for the AISI 1020 specimens, and the only material change was caused by interstitial clustering around dislocations, which increased the yield strength. Thus, the decrease of embrittlement during the hold period was evidently associated with the increase of yield strength/ultimate strength ratio.

Phase VII tests and the sustained load tests on AISI 1020 specimens therefore indicate that embrittlement is a function of the yield strength/ultimate strength ratio. In the Phase II screening tests, all materials

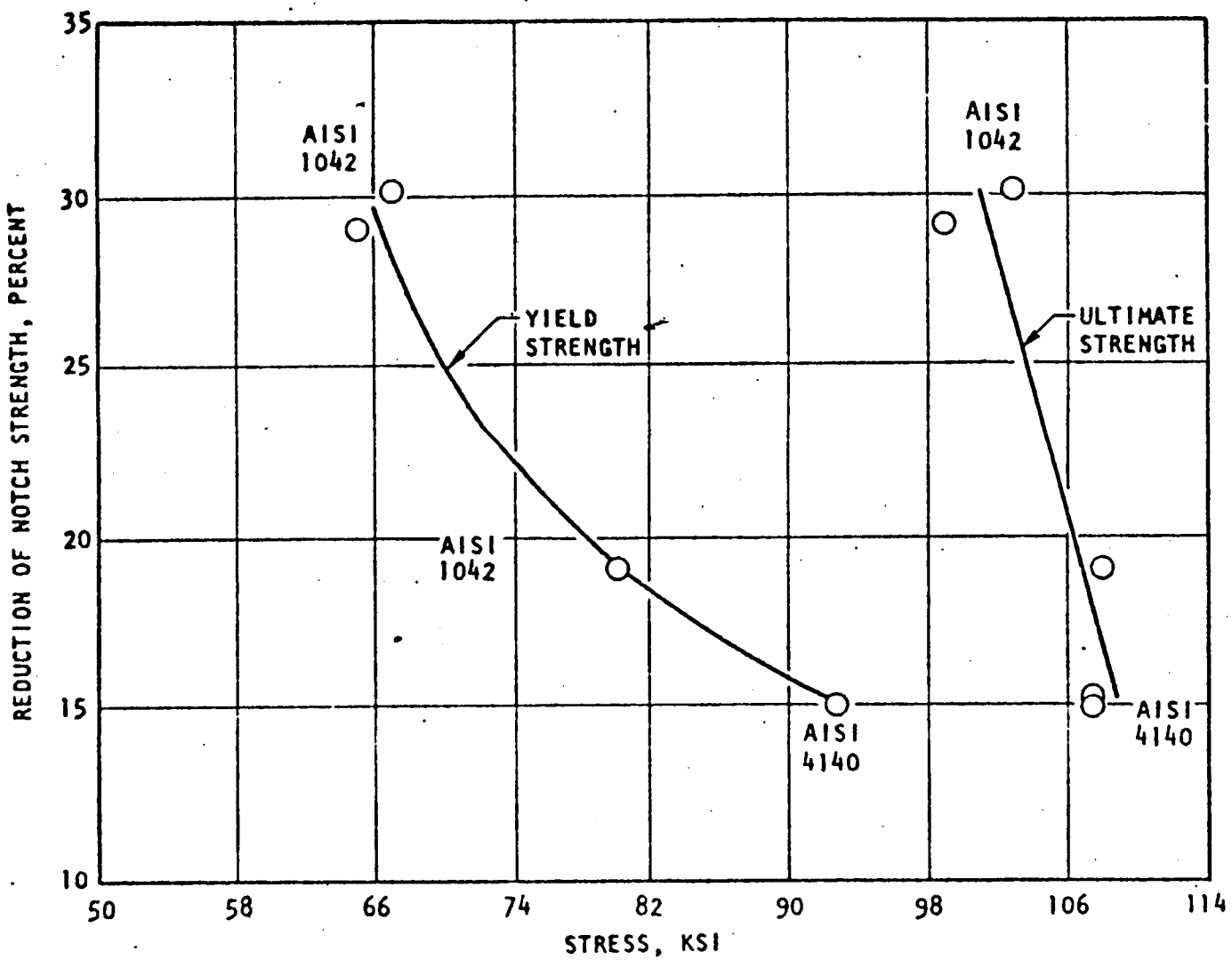

Figure 38. Percent Reduction of Notch Strength in 10,000-psi Hydrogen versus Unnotched Yield Strength and Ultimate Strength in Air for AISI 1042 and AISI 4140 Steels

tested in the program were arranged in order of their degree of embrittlement (as indicated by percent reduction of notch strength). Embrittlement of these metals did not appear to be a function of the yield strength/ultimate strength ratios. The only relationship observed between embrittlement and mechanical properties was that embrittlement tended to increase with increasing yield and ultimate strength levels. The results in this program therefore indicate that embrittlement is a function of yield strength/ultimate strength ratio, providing that other variables such as chemistry, microstructure, and ultimate strength remain constant.

SUMMARY

Results of the Phase III tests on the prestrained AISI 1020 specimens and the Phase VII tests on AISI 1042 and AISI 4140 indicated that hydrogen-environment embrittlement is a function of the yield strength/ultimate strength ratio. That is, plastic deformation is required before the hydrogen environment reacts with the metal surface; the lower the yield strength/ultimate strength ratio, the greater the decrease of notch strength possible from exposure to high-pressure hydrogen.

Phase II screening tests, however, indicate that the relative degree of embrittlement was probably not a function of yield strength/ultimate strength ratio, unless the other variables such as chemistry, microstructure, and ultimate strength remain constant.

CONCLUSIONS

Embrittlement as measured by reduction of notch strength in hydrogen environments is a function of yield strength/ultimate strength ratio, providing that other variables such as chemistry, microstructure, and ultimate strength remain constant.

PHASE VIII: PROTECTION FROM HYDROGEN-ENVIRONMENT EMBRITTLEMENT

Investigations prior to this, including the previous study at Rocketdyne, had established that at least certain steels were highly susceptible to high-pressure hydrogen-environment embrittlement. Other phases of this program have now revealed that a wide variety of alloys are embrittled by high-pressure hydrogen environments. Whatever the case, in planning this program it was believed that the hydrogen-environment embrittlement of metals was sufficiently serious that some consideration should be given to the prevention of such embrittlement. Thus, Phase VIII was designed to investigate the prevention of high-pressure hydrogen-environment embrittlement by the use of inhibiting additives to the hydrogen or hydrogen barrier coatings. Hofmann and Rauls (Ref. 14) had shown that the addition of 1 percent oxygen eliminated the embrittling effect of 1900-psi hydrogen. In this program, it was proposed to investigate the potential of such additives as oxygen, carbon dioxide, and water vapor to inhibit the embrittlement by hydrogen at pressures up to 10,000 psi. It was further planned to investigate gold and cadmium as hydrogen barrier coatings.

During the course of the overall program, certain unexpected findings in other phases, in particular the extreme embrittlement of the high-strength nickel-base alloys, led to the requirement for additional, unplanned work in those areas. To compensate, further effort in this phase was dropped. Before work was diverted from this phase, equipment was purchased for an apparatus designed so that precise pressures of inhibitor gases could be added to the high-pressure hydrogen.

A schematic of the apparatus is shown in Fig. 39. The system would initially be evacuated; the desired quantity of impurity gas would then be added to a large (4 liter), 5000-psi storage vessel. The quantity of impurity gas would be measured by means of a manometer or by the 0- to 100-psi pressure gage. Purified hydrogen would then be added to obtain the

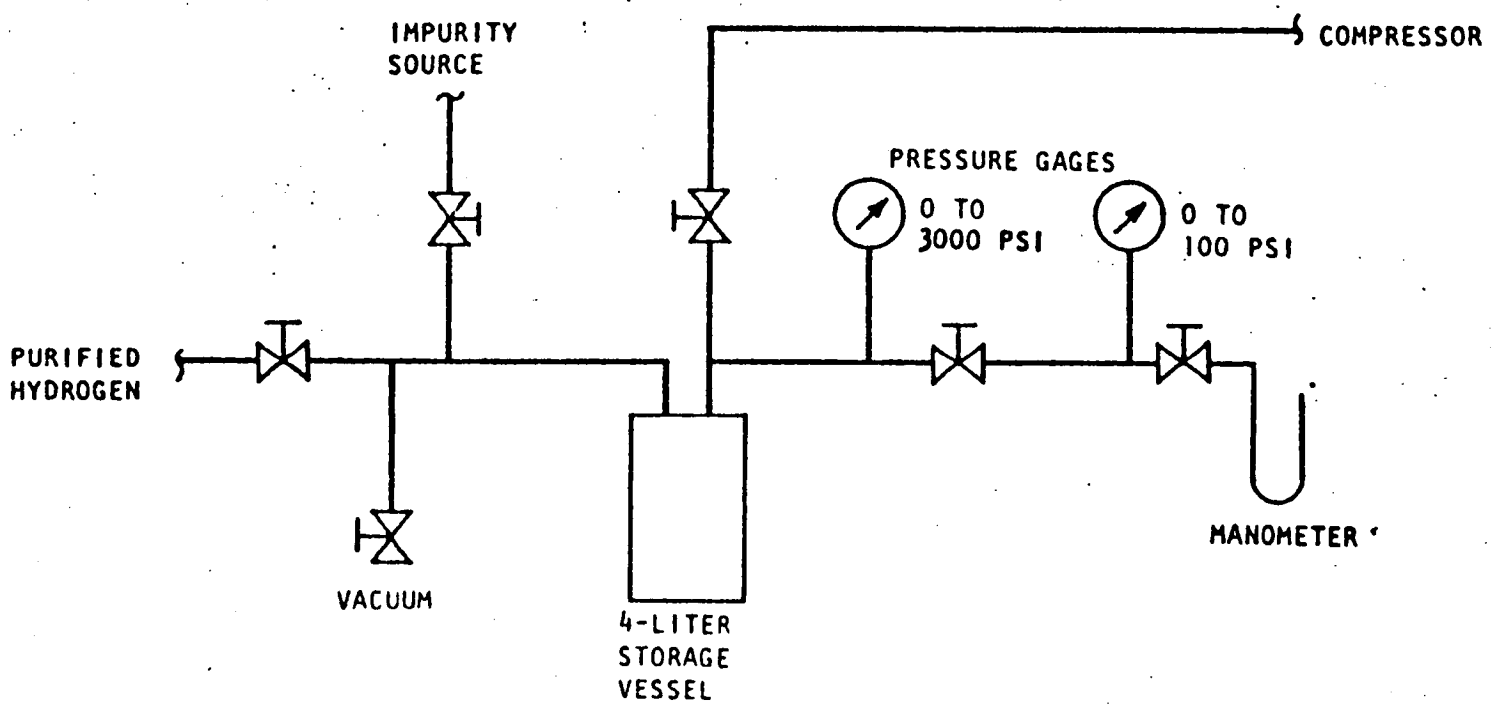

Figure 39. Equipment for Obtaining Various Hydrogen Purity Levels

desired hydrogen partial pressure, and the total pressure measured by the 0- to 2000-psi gage. The hydrogen-impurity gas mixture would then be compressed into the 15,000-psi storage vessel of one of the high-pressure gas supply systems. The gas supply systems are described in detail in Phase I.

PHASE IX: EFFECT OF SURFACE ABRASION IN HYDROGEN ON HYDROGEN-ENVIRONMENT EMBRITTLEMENT

INTRODUCTION

Surface cleanliness is expected to influence hydrogen-environment embrittlement of metals because of its effect on adsorption and/or absorption of hydrogen by the metal. It was postulated (Ref. 2) that hydrogen does not react with a metal until a critical amount of plastic deformation has occurred, and that the critical amount is that deformation required to rupture surface protective layers, usually natural oxides, and expose a fresh metal surface to the hydrogen. Accordingly, the greater effect of a high-pressure hydrogen environment on notched rather than on smooth specimens may, in part, be associated with the early, but highly localized, deformation at the base of the notch. In any case, there are a number of applications (e.g., high-pressure hydrogen compressors) in which parts rubbing together could produce clean metal surfaces exposed to high-pressure hydrogen. Therefore, it was believed to be important practically, as well as enlightening as to the mechanism of hydrogen-environment embrittlement, to conduct investigations into the effect of producing a clean metal surface in hydrogen on hydrogen-environment embrittlement.

In Phase IX, unnotched tensile specimens of ASTM A-517 were abraded in 10,000-psi hydrogen, and examined for surface cracking or tensile tested to failure in this environment to determine the effect of producing a clean metal surface in hydrogen on the hydrogen-environment embrittlement.

EXPERIMENTAL PROCEDURE

Materials

Specimens of ASTM A-517 Gr. F (T-1) steel used in this phase were fabricated from 3/8-inch plate. The chemical composition of the material was as follows: 0.16 carbon, 0.80 manganese, 0.010 phosphorus, 0.010 sulfur,

0.21 silicon, 0.79 nickel, 0.54 chromium, 0.25 copper, 0.43 molybdenum, 0.04 vanadium, 0.002 boron, and the balance iron. The plate was received in the following heat treatment condition: annealed at 1625 F for 1/2 hour, water quenched, tempered at 1225 F for 1 hour, and air cooled. There was no additional heat treatment at Rocketdyne. The supplier certified mechanical properties were: 46.4 ksi yield strength, 76.1 ksi ultimate strength, and 27.5 percent elongation.

Tensile Specimen Design

Design of the tensile specimens used in this phase is the same as described in detail in Phase I.

Apparatus

A special pressure vessel (Fig. 40) was constructed to abrade tensile specimens in high-pressure environments. The specimen extends through sliding seals on both ends of the vessel. An abrading tool located at the longitudinal center of the vessel extends from the side into the middle of the vessel to contact the tensile specimen. The abrading tool has interchangeable tips for abrading unnotched or notched specimens. The tool for abrading unnotched specimens is about 3/16-inch wide; and for abrading notched specimens, a tool with a carbide tip was designed to fit exactly into the root of the standard $K_t \simeq 8.4$ notch. In each case, after the tool was placed in contact with the specimen, the specimen was rotated 180 degrees. Abrading can be performed while the specimen is under an applied tensile stress. Electrical conductors extend through the vessel wall and can be spot welded to the tensile specimens to follow by resistivity measurements surface crack formation and propagation during abrasion. However, it was not found necessary for the potential leads to be attached to the specimen inside the vessel to make these measurements. Instead, the potential leads were fastened to the specimen outside the vessel in the same manner that was used to follow crack growth during cyclic loading (Phase VI).

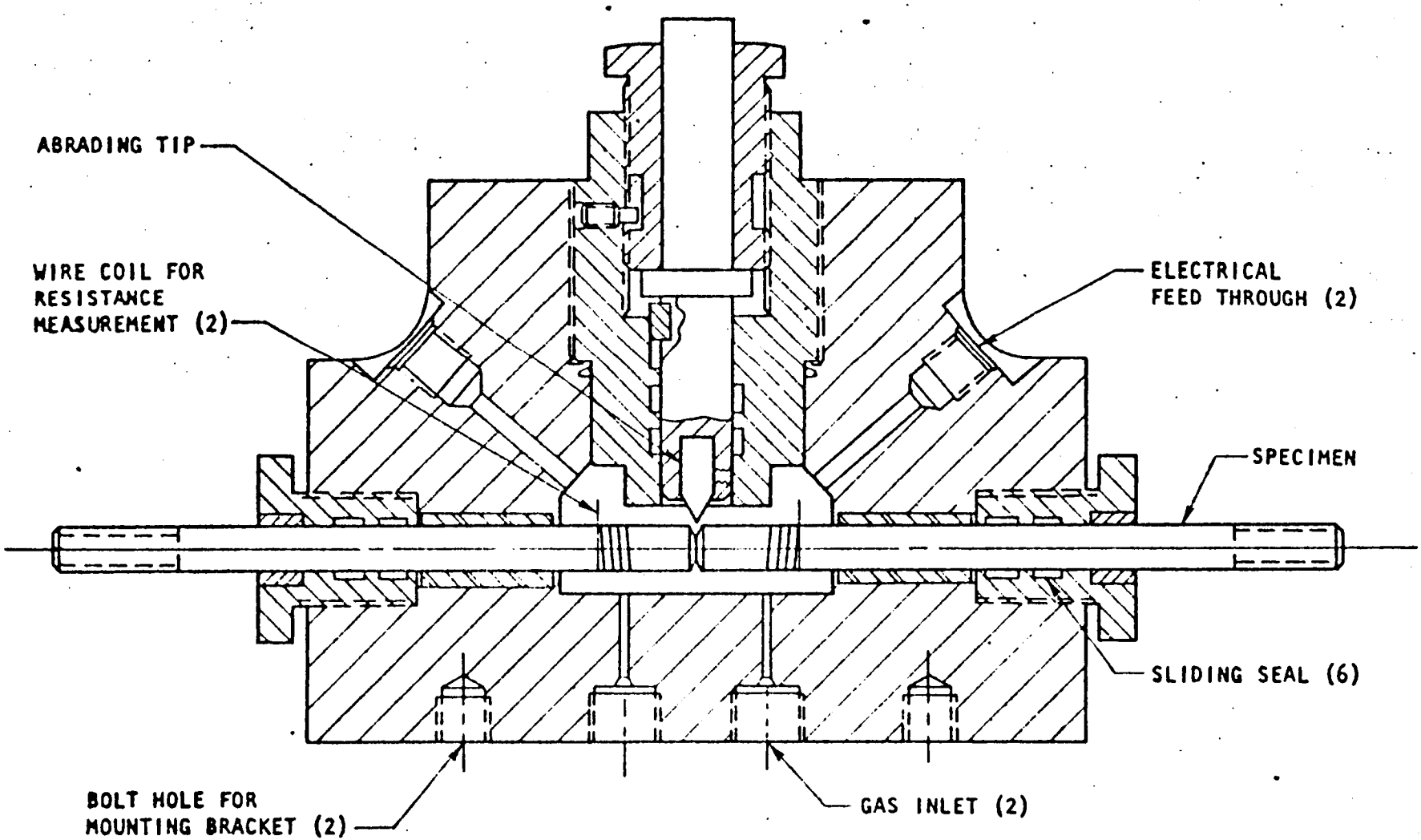

Figure 40. Device for Abrading Tensile Specimens in High-Pressure Hydrogen

The abrading device was substituted for the smaller test vessels used to perform the tensile tests in high-pressure environments in the other phases of this program. The tensile load was applied by the same loading apparatus as that described in Phase I. The high-pressure hydrogen supply system employed in this phase has also been previously described in Phase I.

TEST PROCEDURE

Unloaded and loaded unnotched specimens were abraded while in 10,000-psi hydrogen. Following abrasion, the specimens were either removed from the environment and examined for surface irregularities (for instance surface cracking) or tested to failure in the high-pressure hydrogen environments. Control tests were also conducted in air and in 10,000-psi helium. General features of the tensile testing procedure were the same as described in Phase I. In Phase IX, test vessel purging did not include evacuation.

RESULTS AND DISCUSSION

When the unnotched, ASTM A-517 specimens were abraded with the carbide-typed tool, a 3/16-inch-wide cut was made around the middle of the reduced section, reducing the diameter by approximately 0.002 inch. The effects of abrading on mechanical properties are summarized in Table 38, and individual specimen test data are given in Appendix Table IX-1.

The unabraded ASTM A-517 specimens were not embrittled by the 1000-psi hydrogen environment. This same lack of hydrogen-environment embrittlement of unnotched specimens of this alloy was observed in Phase VI. Small surface cracks were present in the unabraded specimens tested in hydrogen, but there was a shear lip completely around the periphery of the fracture, indicating that the surface cracks had not initiated fracture. Abraded or not, all the specimens tested in hydrogen had very nearly the same yield strengths and ultimate strengths. The differences between the strengths in 10,000-psi hydrogen and those in air are due to the effect

of hydrostatic pressure which reduces the strength of a specimen in a 10,000-psi environment by that pressure when the failure is by shear. This effect was discussed in detail in Phase II.

TABLE 38

AVERAGE PROPERTIES OF ABRADED AND NONABRADED UNNOTCHED A-517 SPECIMENS TESTED IN AIR (1 ATMOSPHERE) AND 10,000-PSI HYDROGEN

Test Environment			Strength		Ductility	
Abrading Environment	Time After Abrading Before Hydrogen Contact	Tensile Testing Environment	Yield, ksi	Ultimate, ksi	Elongation, percent	Reduction of Area, percent
Unabraded		Air	121	130	11	67
Air		Air	121	129	11	64
Unabraded		H_2	108	122	11	65
Air	1/2 hour	H_2	111	124	7.5	39
Air	2 days	H_2	106	121	8.8	46
H_2		H_2	107	119	7.9	43

Although abrading did not affect the yield or ultimate strengths, it did result in a substantial decrease in ductility for specimens tested in hydrogen. Ductility as measured by either elongation or reduction in area was reduced approximately 35 percent by abrading. However, there was no difference in the effect on ductility in 10,000-psi hydrogen between abrading in hydrogen and abrading in air.

An important part of this phase was to determine the effect of abrading on surface crack formation. A summation of the surface appearance of specimens abraded but not tested to failure is tabulated in Appendix Table IX-2. Parallel, shallow, circumferential grooves, rounded at the

bottom, were present in the specimens first abraded in air and then immediately examined. Also, the surface abraded in air contained very small irregularities that appeared to be oriented parallel to the specimen's axis. The appearance of specimen surfaces abraded in air was the same for those abraded without an applied load as for those abraded while under a tensile stress of 90 percent of yield strength. The abraded region of specimens that were both abraded and tested in air appeared rather smooth with the grooves less pronounced than before testing to failure. Failure, of course, occurred in the abraded region.

Deep surface cracks formed in a few of the abrasion-produced grooves of specimens abraded in air and tested in 10,000-psi hydrogen. These surface cracks initiated fracture and were responsible for the reduction of ductility in these specimens. It was rather apparent that there would have been no added embrittlement because of abrading in air if abrasion was performed in a manner that permitted the surface to remain smooth.

Two specimens, abraded in air and tested in hydrogen, were exposed to air for 1/2 hour prior to being exposed to 10,000-psi hydrogen, and a third specimen was exposed to air for 2 days prior to testing in 10,000-psi hydrogen. The specimen held 2 days in air before testing was slightly more ductile in 10,000-psi hydrogen. In addition, there were fewer surface cracks on this specimen, and a shear lip was present about one-half way around the fracture as compared to no shear lip on the other specimens. Thus, there may be an influence of time in air which builds up a protective self-oxide. The abraded surface of the specimen held 2 days in air still appeared bright and rust free.

One specimen was abraded in 10,000-psi helium and examined immediately thereafter. The abraded region contained broad circumferential grooves and the abrasion markings appeared smeared as compared to specimens abraded in air. The abraded region of specimens, abraded in 10,000-psi hydrogen and then removed from the vessel without testing to failure, was similar in appearance to the abraded regions in specimens abraded in air. There

was, however, one difference; the longitudinal irregularities were somewhat larger on the specimens abraded in hydrogen. Comparing the appearance of the regions abraded in air, 10,000-psi helium, and 10,000-psi hydrogen, therefore, indicates that the environment affects the cutting characteristics of the tool.

Specimens were abraded in 10,000-psi hydrogen under the following applied stresses, unloaded (except for pressure), stressed to 90 percent of the yield strength, and stressed slightly above the yield strength. There were no indications of surface cracks on any of these specimens.

The abraded region of specimens abraded in 10,000-psi hydrogen and tested to failure in that medium contained surface cracks. A surface crack was present in nearly every groove. Surface cracking was not limited to the grooves, but followed the longitudinal irregularities as well.

An effort was made to determine by resistivity the stress at which surface cracks were initiated. The resistivity of all specimens increased immediately after yielding, and it was not possible to separate the contributions of crack propagation and plastic deformation on the resistivity increase.

Comparison between the surface cracking of specimens abraded in air and in 10,000-psi hydrogen showed the major effect of abrading in hydrogen to be on the formation of surface cracks when the abraded specimens were tested to failure. A much larger number of surface cracks were formed on specimens abraded in hydrogen than on specimens abraded in air. Thus, the main effect of producing a clean surface in a 10,000-psi hydrogen environment on the unnotched ASTM A-517 specimens was to promote the formation of surface cracks. However, the type of surface cracking that initiated fracture occurred, not from abrading, but from loading above the yield strength. Evidently there is a critical plastic strain connected with this type of surface cracking, even when the specimens are abraded in a hydrogen environment.

The greater number of cracks formed on specimens abraded in hydrogen did not increase the degree of embrittlement of these specimens over that of specimens abraded in air and tested in hydrogen. It is believed that, if abrading was performed without groove formation, there would have been a considerable difference in degree of embrittlement between specimens abraded in air and those abraded in hydrogen. The lack of increased embrittlement in the specimens abraded in hydrogen is, however, meaningful because it indicates that embrittlement is more associated with crack propagation than with crack initiation. The importance of resistance to crack propagation within hydrogen environments in determining the relative degree of hydrogen-environment embrittlement is discussed in greater detail in Phase X.

SUMMARY

Unnotched ASTM A-517 specimens were abraded in air and 10,000-psi hydrogen environments. The abraded surfaces contained circumferential grooves, which were initiation sites for surface cracking when the specimens were abraded in air and tensile tested to failure in 10,000-psi hydrogen. The major effect of abrading in hydrogen was to increase the formation of surface cracks when the abraded specimens were tested to failure in hydrogen. There was a much larger number of surface cracks formed on specimens abraded in hydrogen than those abraded in air.

Specimens abraded in 10,000-psi hydrogen, while stressed slightly above the yield strength, did not contain surface cracks, so it was assumed that a certain amount of plastic deformation was needed for surface crack formation even on specimens preabraded in hydrogen.

The greater number of cracks formed on specimens abraded in hydrogen did not increase the degree of embrittlement of these specimens over that of specimens abraded in air and tested in hydrogen. The lack of increased embrittlement would seem to indicate that embrittlement is more associated with crack propagation than crack nucleation.

CONCLUSIONS

The following conclusions can be drawn from the results of this phase:

1. Surface cracking in ASTM A-517 is promoted by the formation of a clean surface in 10,000-psi hydrogen.
2. The degree of embrittlement of ASTM A-517 is not increased by abrading in 10,000-psi hydrogen, as compared to abrading in air and testing in 10,000-psi hydrogen.

PHASE X: POSTTEST METALLOGRAPHIC ANALYSIS (SPECIMENS FROM PHASES I THROUGH IX)

INTRODUCTION

Considerable posttest metallographic examination of specimens from Phases I through IX was performed to further identify the characteristics and clarify the mechanism of hydrogen-environment embrittlement. It was decided that posttest metallography was a coherent study in itself and, for greatest clarity, should be combined and covered in a separate phase rather than dispersed throughout the other sections.

EXPERIMENTAL PROCEDURE

Selected specimens tested in this program were examined visually for surface cracking, and representative specimens were examined by optical microscopy and electron fractography. Conventional metallographic procedures were used for optical microscopy. The etchants used are listed in each figure in the Results and Discussion section, where appropriate. For electron fractography the standard two-stage plastic-carbon technique was used. Initial carbon deposition was followed by shadowing with Pt-C pellets.

RESULTS AND DISCUSSION

Unnotched Specimens

Results of visual examination of unnotched specimens tested in 10,000-psi hydrogen are summarized in Table 39. The materials are arranged in order of decreasing embrittlement in terms of the decrease of ductility, as measured by reduction of area, in 10,000-psi hydrogen as compared to 10,000-psi helium. Results in Table 39 suggest that metals with similar degrees of embrittlement in high-pressure hydrogen also have similar

Preceding page blank

Material	Percent Ductility Decrease In 10,000-Psi Hydrogen(a)	Description of Surface Cracking	Shear Lip	Obvious Point of Fracture Initiation
M-41 Tool Steel	100	One crack approximately 1/8 inch long which initiated fracture; faint indication of cracks in the shear lip oriented parallel to the longitudinal specimen axis	Yes, except at fracture origin	Yes
AISI Type 440C Stainless Steel	100	No surface cracks	No	Yes, small region on the periphery
AISI 1042 Quenched and Tempered	100	One small crack which initiated fracture	Yes, except at fracture origin	Yes
Inconel 718	97	One small crack which initiated fracture	Yes, except at fracture origin	Yes
17-7 PH Stainless Steel	95	One crack approximately 1/8 inch long which initiated fracture	Yes except at fracture origin	Yes
18 Nickel (250) Maraging Steel	95	Two or three deep 45-degree cracks that appear more like brittle cleavage cracks than hydrogen-induced surface cracks	No	One fracture face oriented perpendicular to specimen axis appeared darker and intergranular (this may have been the origin)
AISI 4140	81	Three deep surface cracks	No	No
AISI 410 Stainless Steel	80	A 1/4-inch-long crack initiated fracture; also, some large 45-degree cracks and a few very small cracks in slightly necked region	No	Yes
Fe-0Ni-4Co-0.20C	78	Some deep cracks, one of which initiated fracture; fracture stepwise along periphery because of crack branching	No	One major and several minor initiation sites
ASTM 372 Class IV (API N-80)	66	Surface cracks along entire reduced section	No	Numerous
Rene 41	62	One short crack which initiated fracture; also, about two extra surface cracks per specimen	Yes, except at fracture origin	Yes
AISI 1042 Normalized	54	Fairly small cracks which are not particularly numerous; practically all cracks in necked-down region	Partial formation in some specimens	No, for most specimens
ASTM A-302 Gr.B Modified With Nickel	50	Many deep cracks in necked-down region	No	No
ASTM A-515 Gr.70	48	Deep cracks in necked-down region; fine cracks outside of necked-down region which follow machining markings	No	Partial double ring indicating fracture initiated around almost entire periphery
AISI Type 430F Stainless Steel	42	Numerous deep cracks in necked-down region	No	Double ring
Armco Iron	40	A large number of deep cracks	No	Numerous origins did not link up to form double ring
AISI 1020	34	Numerous and deep cracks in necked-down region; a few very small cracks outside necked-down region	No	Numerous
Nickel 270	25	Numerous short cracks over entire reduced section; necked-down region contains deepest cracks; cracks are shallow outside necked-down region	No	No
HY-100	17	Large number of cracks which are almost entirely restricted to necked-down region	No	One obvious origin and indications of other smaller origins
HY-80	14	Fairly deep cracks restricted to necked-down region	Cracks did not affect shear lip as much as expected; shear lip mostly intact	No
Ti-5Al-2.5Sn	13	Large number of very small cracks, mostly restricted to necked-down region	Yes, surface cracks distorted outer edge of shear lip	No
AISI Type 304L Stainless Steel	9.0	Numerous small surface cracks along entire reduced section; the depth of the cracks increased in necked-down region; cracks observable only with aid of magnification	No	No
7075 T-73 Al Alloy	5.4	None	Inconclusive	No
AISI Type 305 Stainless Steel	3.8	None	Yes	No
ASTM A-517 Gr.F (T-1)	3.1	Small shallow cracks	Yes	No
ASTM A-286 Stainless Steel	2.3	None	Inconclusive	No
Be-Cu Alloy 25	1.4	None	Inconclusive	No
1100-0 Al	0	None	A large void on both fracture faces; very ductile fracture	No
Titanium (Commercially Pure)	0	Large number of very short cracks in necked-down region	Yes	No
OFHC Copper	0	None	Necked to a point	No
Ti-6Al-4V Annealed	0	Very small cracks in necked-down region	Yes	No
Ti-6Al-4V STA	0	Very small cracks in necked-down region	Yes	No
AISI Type 316 Stainless Steel	-4.2(b)	None	Inconclusive	No
6061 T-6 Aluminum	-8.0(b)	None	Inconclusive	No

(a) Calculated as follows: $\frac{\text{percent reduction of area in air or helium} - \text{percent reduction of area in hydrogen}}{\text{percent reduction of area in (air or helium)}}$

(b) Reduction of area increased in hydrogen

TESTED IN 10,000-PSI HYDROGEN

R-7780-1

192-B

192-A

surface cracking characteristics. In Phase II the metals were grouped into the following four categories: Extreme embrittlement, Severe embrittlement, Slight embrittlement, and Negligible embrittlement.

1. Extreme embrittlement: These metals are extremely embrittled by hydrogen in the notched and unnotched condition, as shown by a large decrease of notch strength and ductility and some decrease of unnotched strength.

2. Severe embrittlement: These metals are considerably embrittled in both unnotched and notched conditions, as shown by a considerable reduction of notch strength and ductility and no reduction of unnotched strength.

3. Slight embrittlement: These metals have a small decrease of notch strength and a negligible decrease of unnotched ductility.

4. Negligible embrittlement: These metals are relatively nonembrittled by hydrogen in both notched and unnotched conditions.

These categories will be used throughout this section to denote the degree of hydrogen-environment embrittlement. The least embrittled metals, i.e., those placed in category 4, were the aluminum alloys, stable austenitic stainless steel (e.g., A-286 stainless steel), and OFHC copper. There were no surface cracks observed in specimens of those metals.

Metals in category 3 are Be-Cu Alloy 25, titanium, and AISI types 304L and 305 stainless steels. These metals either had no surface cracks, as found for Be-Cu Alloy 25 and AISI type 305 stainless steel, or contained a large density of very small shallow cracks, as observed on titanium and AISI type 304L stainless steel. The cracks were generally so small that they required low-power magnification to be observed. Figures 41 and 42 illustrate these small surface cracks on commercially pure titanium and AISI type 304L stainless-steel specimens. There appears to be no association between fracture and surface cracking for the metals in this category. Shear lips were well formed, indicating that fracture initiated within the specimen.

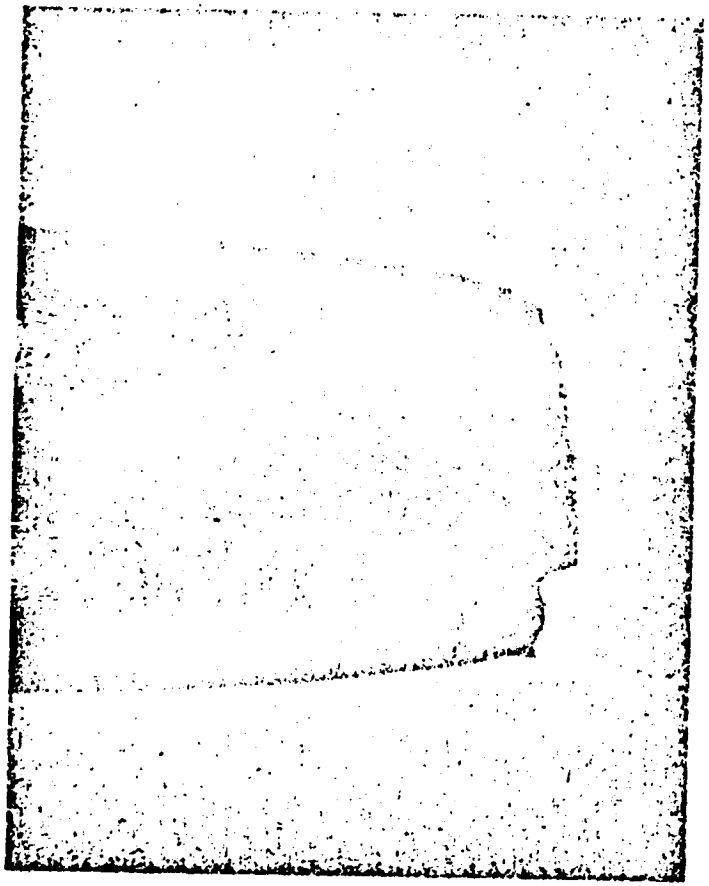

No. 981 Photomacrograph 10X

Tested in Air: 1 Atmosphere

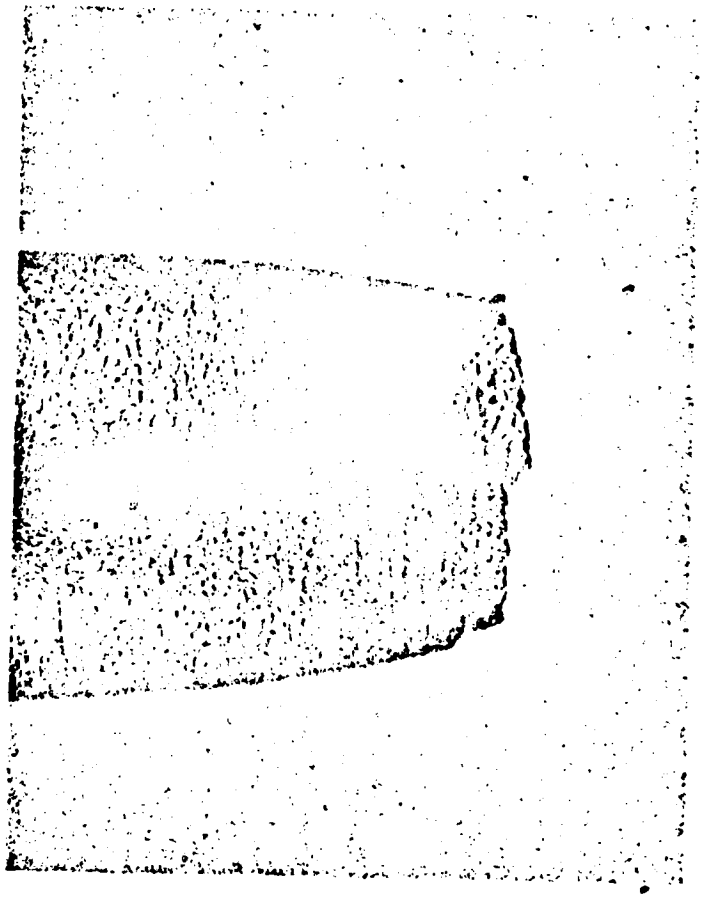

No. 979 Photomacrograph 10X

Tested in 10,000-psi Hydrogen (note multitude of small surface cracks)

Figure 41. Commercially Pure Titanium Unnotched Specimens

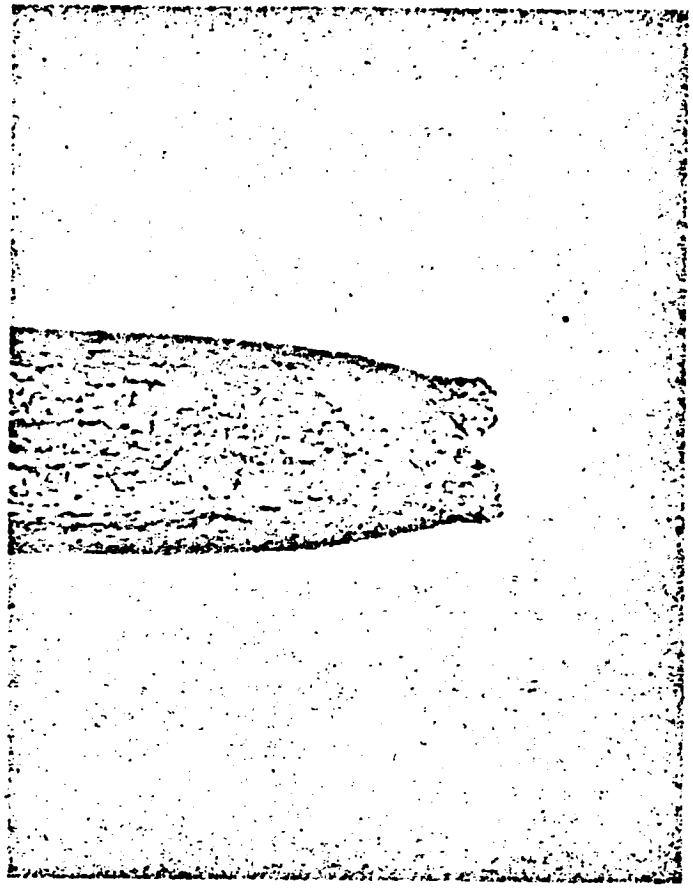

No. 429 Photomacrograph 10X

Figure 42. AISI Type 304L Stainless-Steel Unnotched Specimen Tested in 10,000-psi Hydrogen (note small cracks along entire reduced section)

The majority of metals tested in this program fall in category 2, which includes the ductile, low- and moderate-strength steels, pure nickel, and titanium alloys. Reduction of notch strength of the titanium alloys was sufficiently severe to place them in this category. However, the reduction of unnotched ductility was small and the surface cracking was characteristic of category 3.

Unnotched steel and nickel-base alloy specimens which were tested in hydrogen contained surface cracks that are visible without magnification. The density and size of the cracks increased with the degree of plastic strain, i.e., there were few (if any) cracks located outside of the necked-down region; close to the fracture, the cracks were numerous and sufficiently deep to initiate fracture. Shear lips were not formed and visual examination showed that surface cracks formed around the entire fracture periphery.

Fracture origins were usually easily recognized on those specimens that were "severely" embrittled (category 2) by hydrogen. Frequently, there were numerous apparent fracture origins. These origins appeared as small areas oriented perpendicular to the tensile axis and intersected the specimen surface in a manner indicated that they originated at the surface. Figures 43 and 44 illustrate multiple fracture origins on AISI 1020 and ASTM A-302 specimens. On the other hand, the origins of some specimens were continuous at the periphery as is illustrated in Fig. 45, a photomacrograph of an AISI type 430F stainless-steel specimen tested in 10,000-psi hydrogen. For some specimens, the fracture origin(s) were not particularly apparent as is illustrated in Fig. 46, which contains photomacrographs of AISI 1042 specimens tested in air and 10,000-psi hydrogen. Although the fracture origin(s) in 10,000-psi hydrogen was not readily distinguishable, it was evident that the fracture in air initiated within the specimen while the fracture in hydrogen probably initiated at the surface.

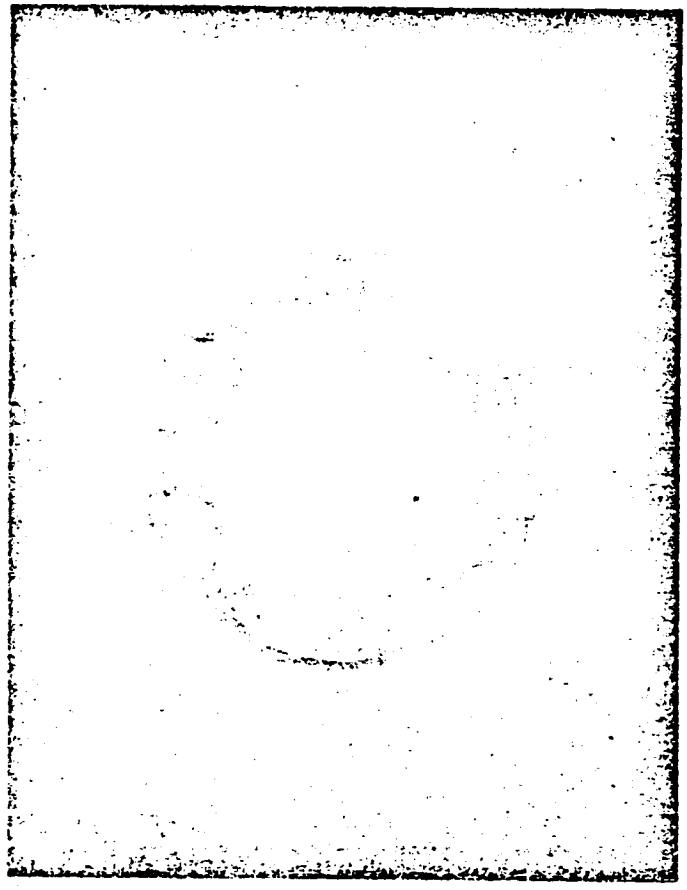

No. F255 Photomacrograph 10X

Figure 43. AISI 1020 Unnotched Specimen Tested in 10,000-psi Hydrogen (note the multiple fracture origins around the specimen periphery)

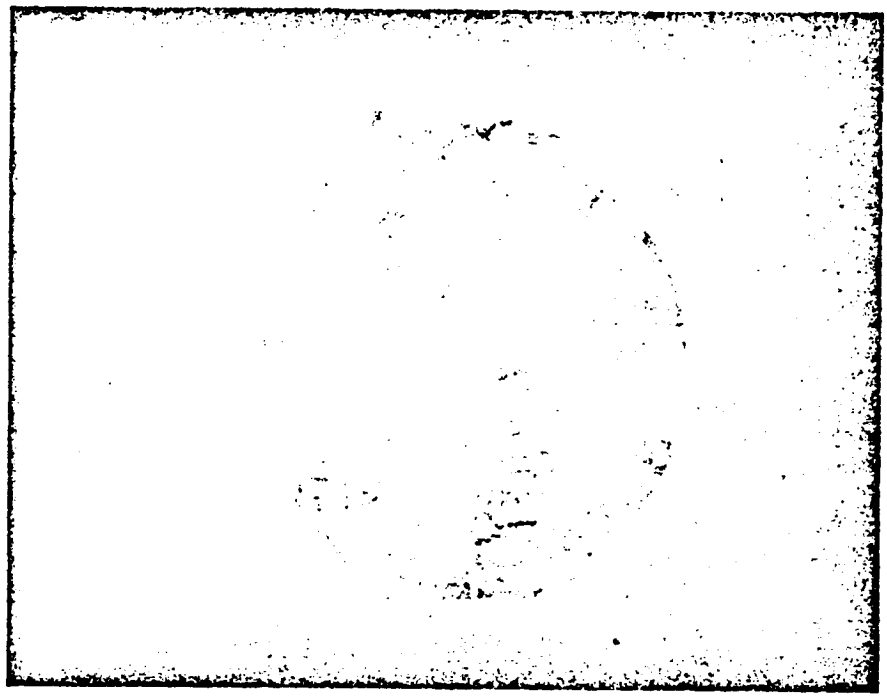

No. A306 Photomacrograph 10X

Figure 44. ASTM A-302 Unnotched Specimen Tested in 10,000-psi Hydrogen (note the multiple fracture origins around the specimen periphery)

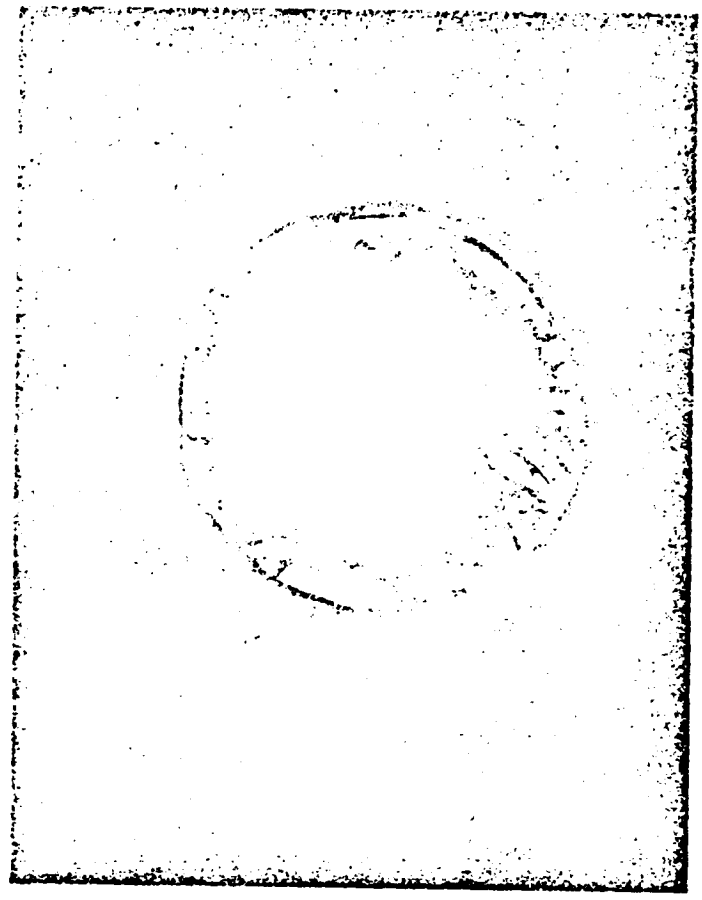

No. 580 Photomacrograph 10X

Figure 45. AISI Type 430F Stainless-Steel Unnotched Specimen Tested in 10,000-psi Hydrogen (note fracture origin continuous at the surface)

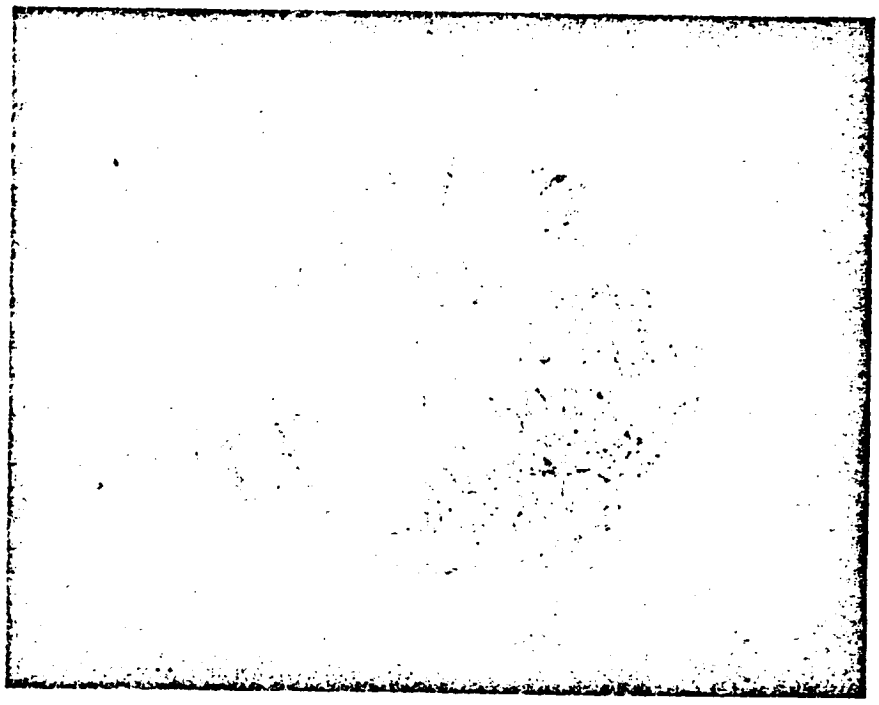

No. 78 Photomacrograph 10X

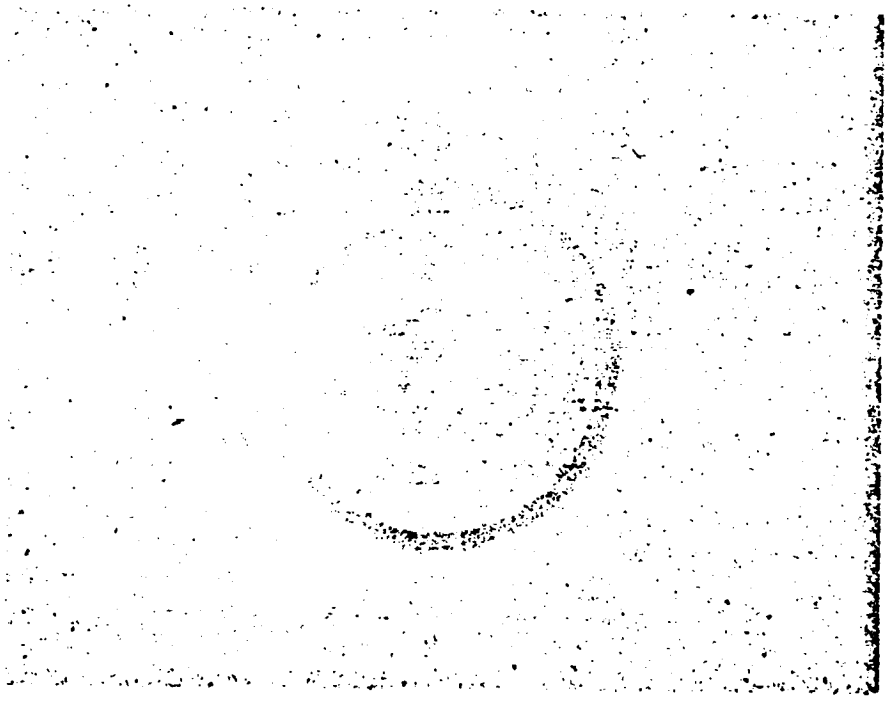

No. 81 Photomacrograph 10X

Figure 46. AISI 1042 Normalized Unnotched Specimens Tested in 10,000-psi Hydrogen (Top), and Tested in Air (Bottom)

Metals in category 1, which were highly embrittled by hydrogen, were likely to have only one crack, and this crack initiated catastrophic failure. Included within this category are the high-strength steels and high-strength nickel-base alloys. Fractures in Inconel 718, Rene 41, AISI 1042 quenched and tempered, H-11 tool-steel, AISI type 410 stainless-steel, AISI type 440C stainless-steel, and 17-7 PH stainless-steel specimens tested in 10,000-psi hydrogen originated from a single surface crack. In the specimens of each of these alloys, the thin shear lips were complete except for a short region, and this region appeared to be a surface crack that initiated failure. Figure 47 illustrates this type of crack on an Inconel 718 specimen tested in hydrogen.

In some instances, other surface cracks were present on specimens of these alloys, but these extra cracks were generally few in number and appeared to have occurred during the specimen fracture. For example, the shear lip on the H-11 tool-steel specimens contained short vertical (parallel to the specimen axis) cracks that appeared to be the result of buckling of the shear lip during fracture. There were small cracks in a slightly indented area present on one side of the fracture of an AISI type 410 stainless-steel specimen. This indented area appeared to have occurred while the specimen was failing.

It is interesting to note that the type of surface cracking is evidently independent of hydrogen pressure. Figure 48 is a photomacrograph of one of the unnotched ASTM A-302 specimens tested in 1 atmosphere hydrogen pressure. The scratches that are oriented at approximately 45 degrees to the tensile axis have been noticeably enlarged during the tests. However, specimens tested in 10,000-psi helium have smooth surfaces up to the fracture as illustrated in Fig. 49. The dark mark in Fig. 49 that has the appearance of a crack is not a crack but a scratch made on the surface by the caliper while measuring the reduction of area.

Figures 50, 51, and 52 are photomacrographs of unnotched ASTM A-302 specimens tested in 100-, 1000-, and 10,000-psi hydrogen, respectively. Inspection of Fig. 48 and 50 through 52 shows that the surface cracks were

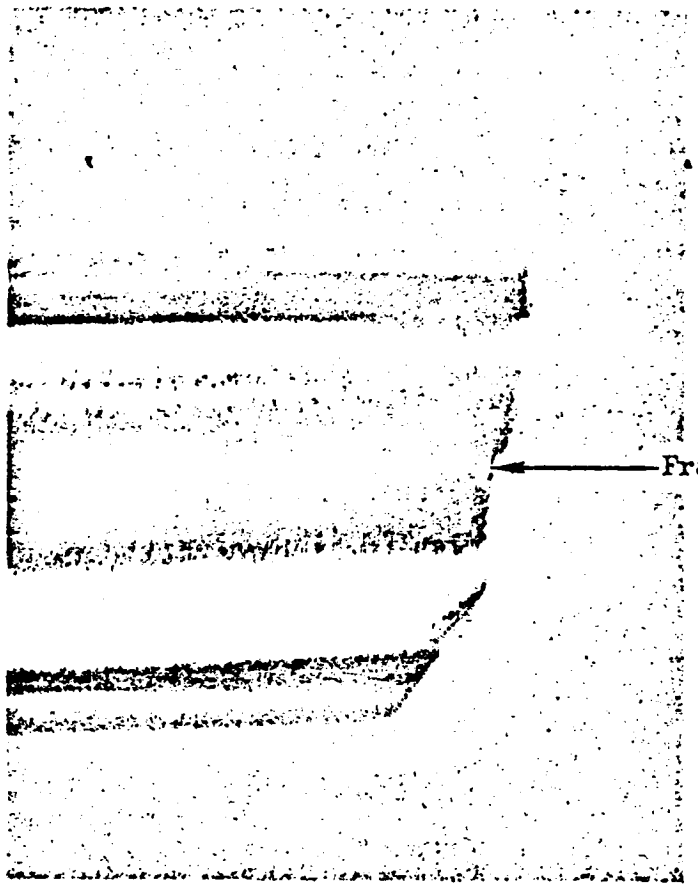

No. 1227 Photomacrograph 10X

Figure 47. Inconel 718 Unnotched Specimen Tested in 10,000-psi Hydrogen (the straight region at the middle of the photo is the surface crack that initiated fracture)

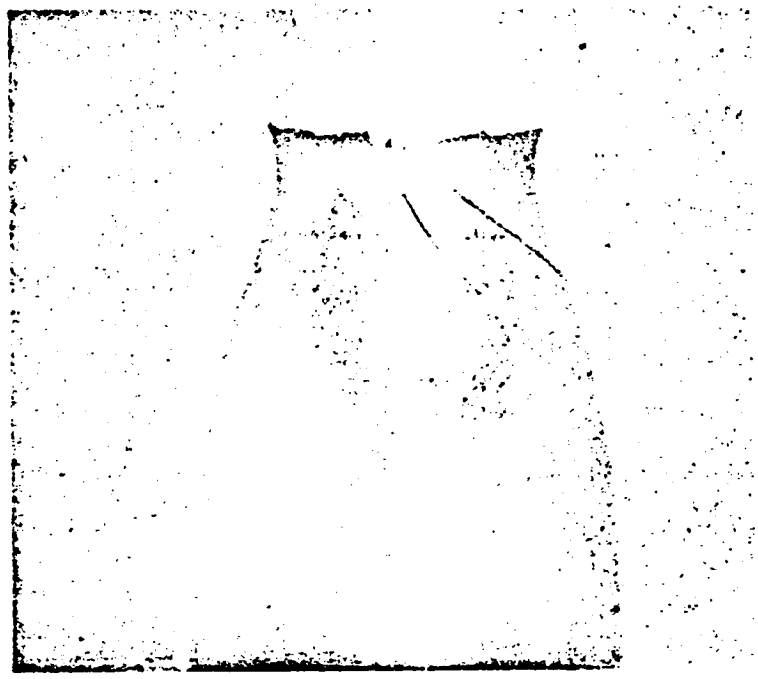

No. A327 Photomacrograph 10X

Figure 48. ASTM A-302 Unnotched Specimen Tested in Hydrogen at 1 Atmosphere Pressure

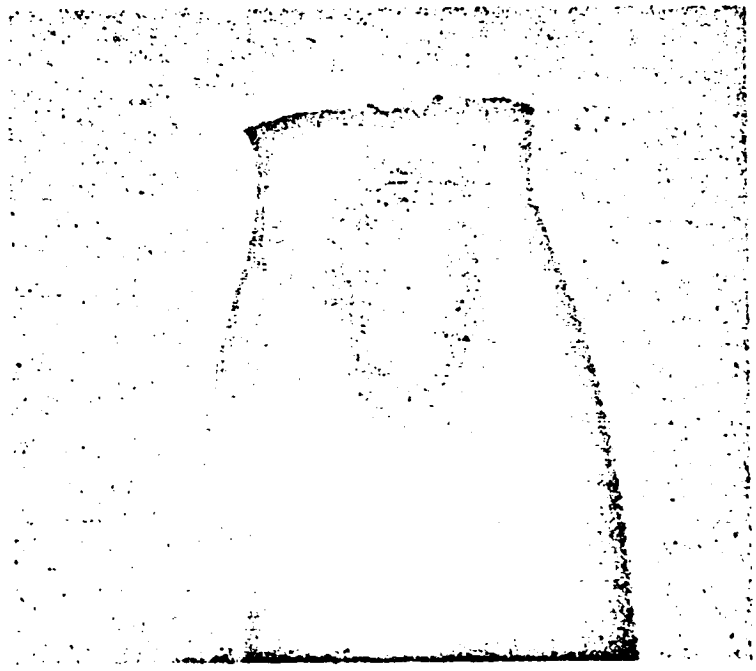

No. A302 Photomacrograph 10X

Figure 49. ASTM A-302 Unnotched Specimen Tested in 10,000-psi Helium

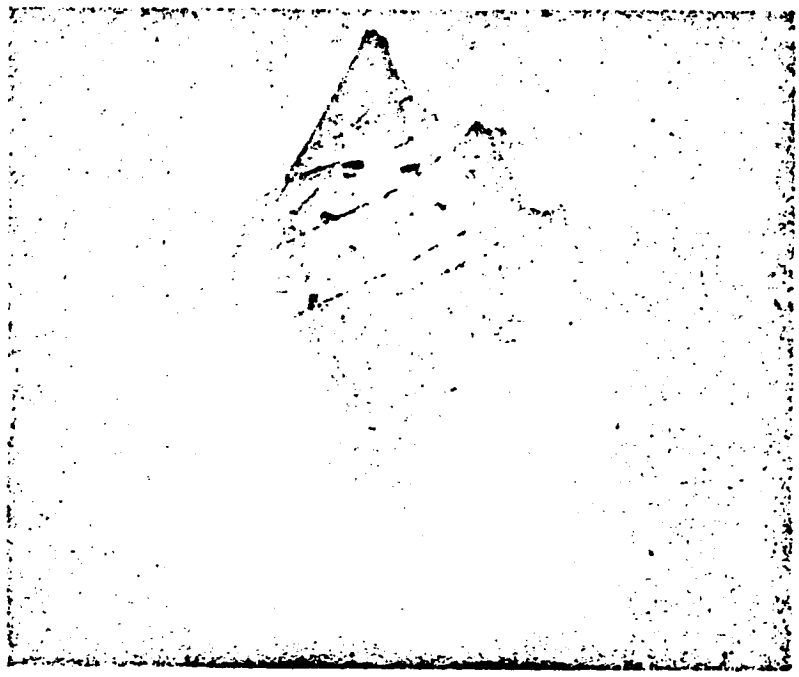

No. A332 Photomacrograph 10X

Figure 50. ASTM A-302 Unnotched Specimen Tested in 100-psi Hydrogen

No. A330 Photomacrograph 10X

Figure 51. ASTM A-302 Unnotched Specimen Tested in 1000-psi Hydrogen

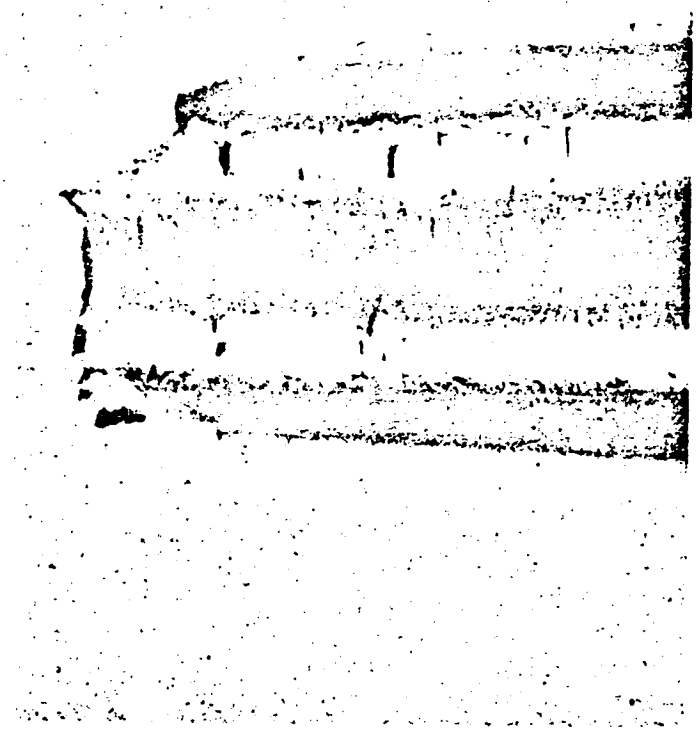

No. A306 Photomacrograph 10X

Figure 52. ASTM A-302 Unnotched Specimen Tested in 10,000-psi Hydrogen

essentially the same for all four hydrogen pressures. Cracks were less numerous at low hydrogen pressures, but their size did not decrease appreciably.

Tests conducted on Inconel 718 showed that the specimens tested in 1000-psi hydrogen were considerably more ductile than the specimens tested in 10,000-psi hydrogen. However, fracture of these specimens initiated from a single surface crack in the same manner as fracture in 10,000-psi hydrogen. The only difference was that the cracks that initiated fracture in 1000-psi hydrogen were much shorter than the cracks that initiated fracture in 10,000-psi hydrogen. This was described in greater detail in Phase IV.

Examination by optical microscopy was made on representative unnotched specimens from the three classes of materials embrittled by hydrogen. Figure 53 and 54 are photomicrographs, respectively, of a titanium specimen and an AISI type 304L stainless-steel specimen, both tested in 10,000-psi hydrogen. Surface cracks are shallow and very blunt.

Surface cracking of the severely embrittled group of alloys (category 2) was examined with AISI 1020 and AISI type 430F stainless-steel specimens. Figure 55 is a photomicrograph of an AISI 1020 specimen. The cracks are not as blunt as in the slightly embrittled specimens, and branching is observed in the deeper fissures. Figure 56 shows that the fracture is mostly transgranular. Branching had the effect of widening the crack tip and thus blunting the crack. It is interesting to note that the crack terminated soon after branching.

Surface cracks are somewhat sharper on the AISI type 430F stainless-steel specimen (Fig. 57). Longitudinal branching appears to have occurred immediately below the surface, but the crack propagation continued normal to the surface. Branching, however, appears to hinder propagation of the deeper cracks shown in Fig. 57 and 58. It caused the cracks to change

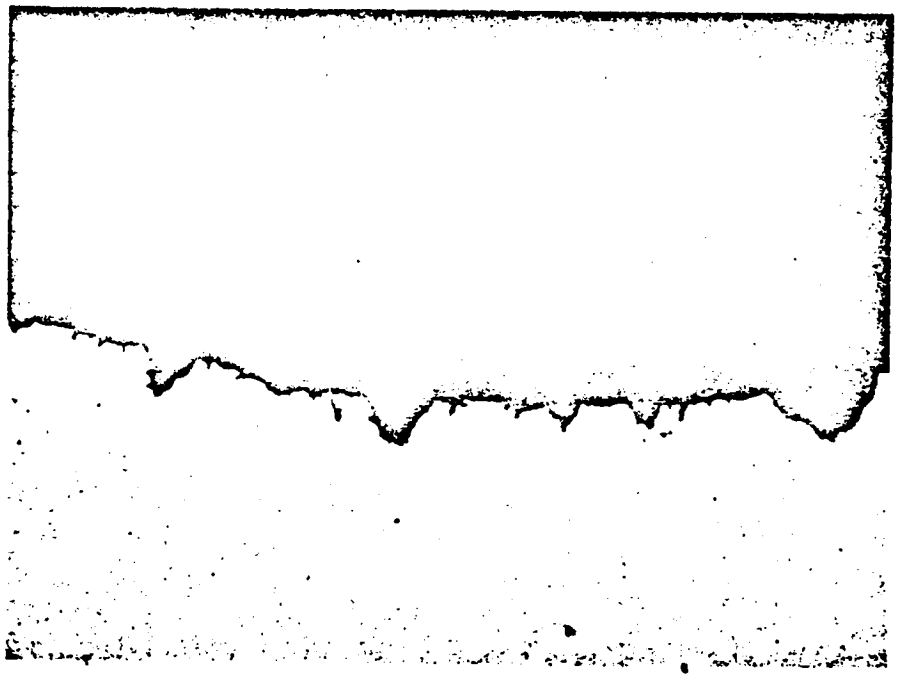

No. 979 Photomicrograph 110X

Figure 53. Commercially Pure Titanium Unnotched Specimen Tested in 10,000-psi Hydrogen

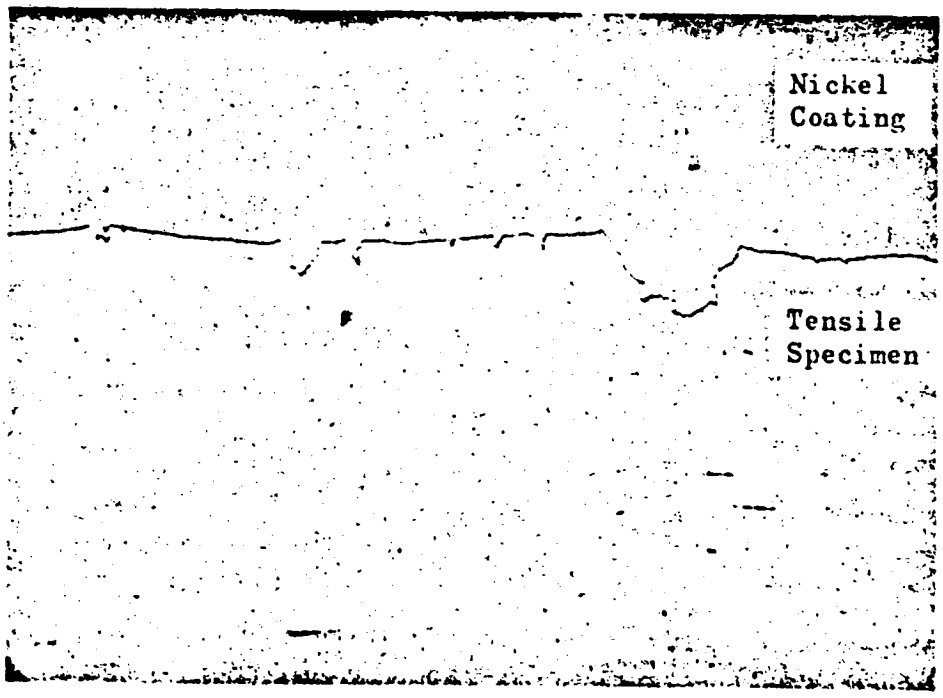

No. 429 Photomicrograph 100X

Figure 54. AISI Type 304L Stainless-Steel Unnotched Specimen Tested in 10,000-psi Hydrogen (note blunting of surface cracks)

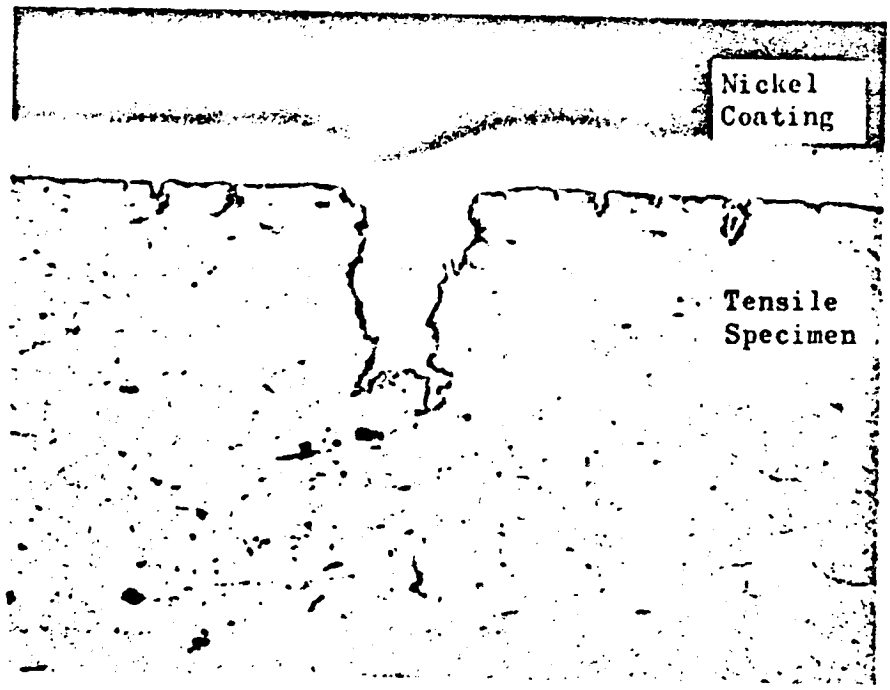

No. F264 Photomicrograph 150X

Figure 55. AISI 1020 Unnotched Specimen Tested in 10,000-psi Hydrogen (noteblunting of larger crack)

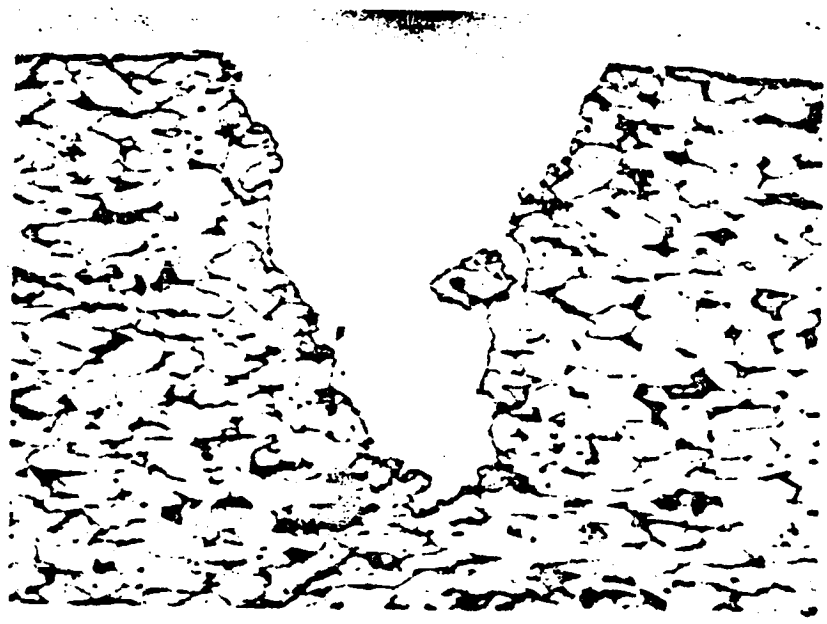

No. F264 Photomicrograph 250X

Figure 56. AISI 1020 Unnotched Specimen Tested in 10,000-psi Hydrogen (Etchant, Nital)

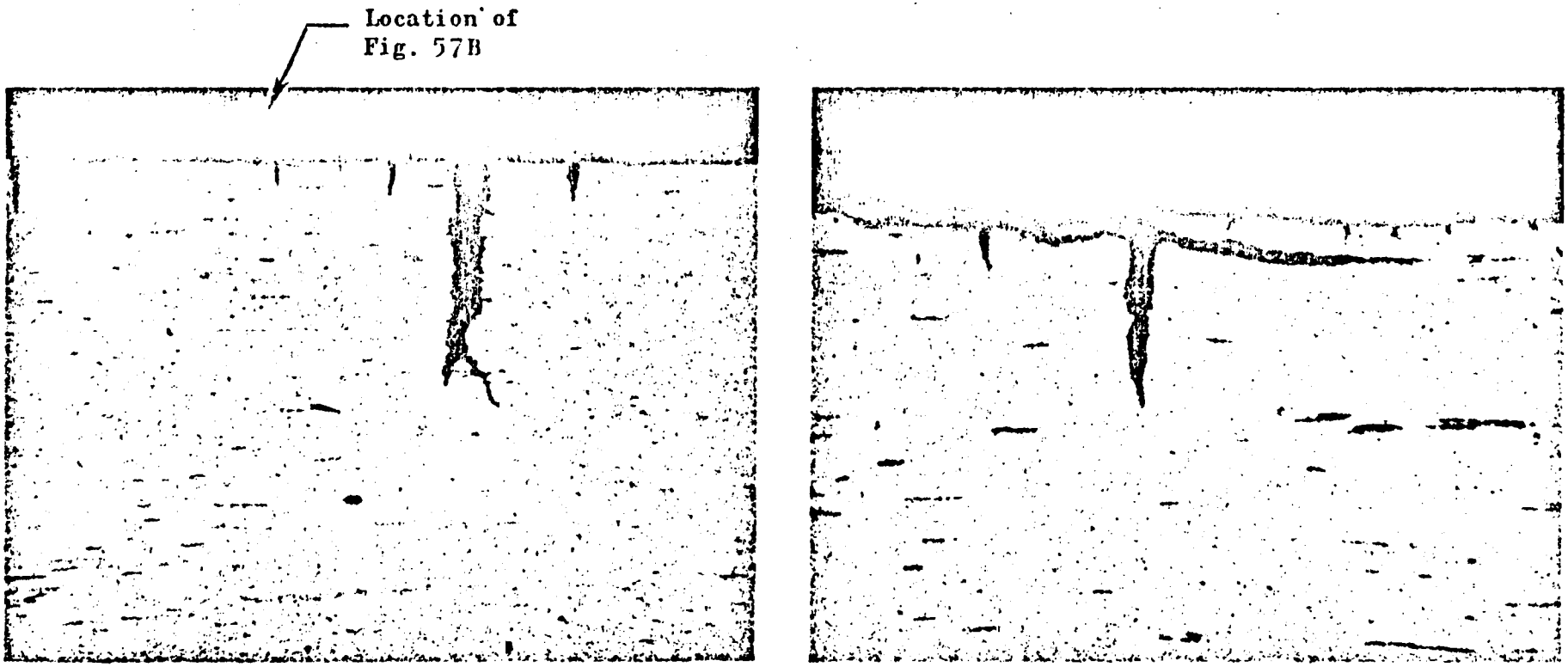

100X B 800X

Photomicrographs

Figure 57. AISI Type 430F Stainless-Steel Unnotched Specimen Tested in 10,000-psi Hydrogen (photo at right is an enlargement of the middle of the surface region of photo at left)

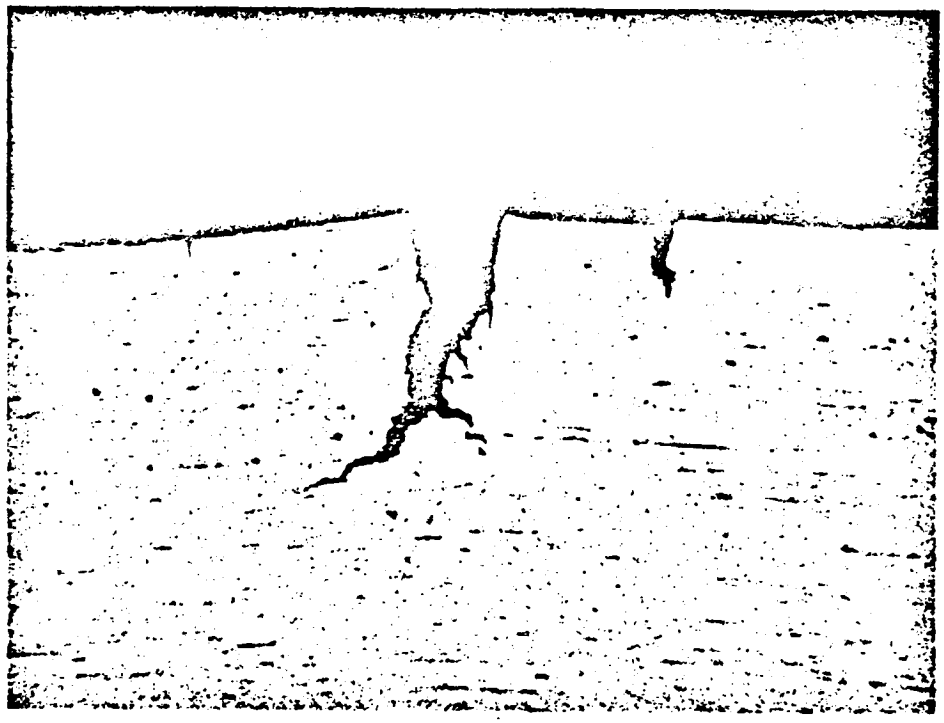

No. 580 Photomicrograph 100X

Figure 58. AISI Type 430F Stainless-Steel Unnotched Specimen Tested in 10,000-psi Hydrogen (note branching caused crack to change direction but did not stop crack propagation)

direction toward the tensile axis, which decreased the stress intensity on the crack tips, and the cracks ceased to propagate.

Surface cracks of the severely embrittled specimens are therefore characterized by branching of the deeper cracks. This blunts the cracks and causes them to change direction into the tensile axis, terminating their propagation.

Few surface cracks were found in specimens of the extremely embrittled alloys because cracks in these alloys, once formed, tended to propagate to failure. Two cracks in an AISI 4140 specimen are shown in Fig. 59. The cracks appear to be fairly broad initially, but then narrow and remain sharp, despite branching, and continue to propagate perpendicular to the tensile axis. A high-magnification photomicrograph of a region of a long crack is shown in Fig. 60. The markings observed in the crack may be optical fringes or cleavage facets.

The surface crack on an Fe-9Ni-4Co-0.25C specimen (Fig. 61) is quite sharp, as were the cracks on the AISI 4140 specimen. There are many fine branches radiating from the crack, but most of them did not appear to influence crack propagation. The two branches at the end of the crack do, however, appear to have been responsible for halting crack growth. Surface cracks on the extremely embrittled specimens are therefore sharp and propagate apparently unimpeded into the material. Branching does not significantly impede crack propagation in these materials.

Nickel-Base Alloys

Because the extreme embrittlement of Inconel 718 and Rene 41 in 10,000-psi hydrogen was unexpected and of considerable concern, a more comprehensive metallographic examination (Ref. 6) was made on these alloys. The microstructure of the Inconel 718 specimens tested in 10,000-psi hydrogen environment (Fig. 62) is considered normal (Ref. 7) for the heat treatment given the alloy.

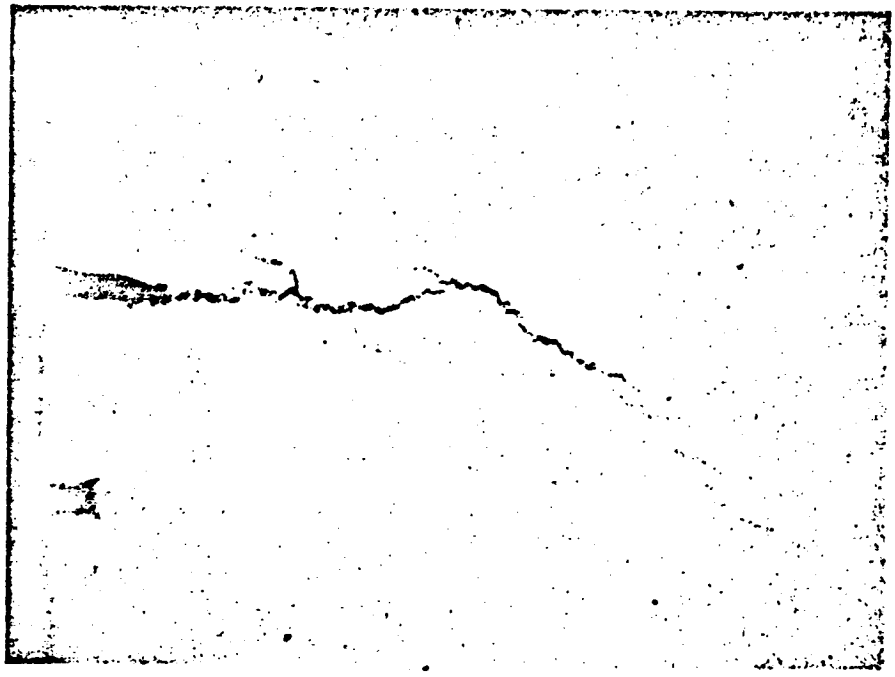

Photomicrograph 37.5X

Figure 59. AISI 4140 Unnotched Specimen Tested in 10,000-psi Hydrogen (note lack of blunting of crack after it propagates about 0.010 inch into specimen)

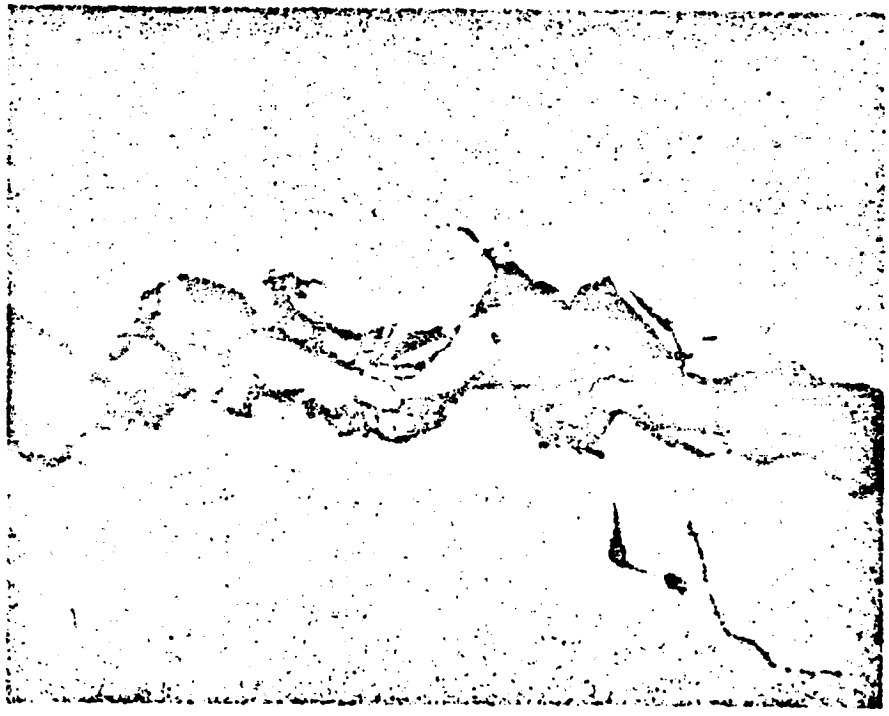

Photomicrograph 800X

Figure 60. AISI 4140 Unnotched Specimen Tested in 10,000-psi Hydrogen

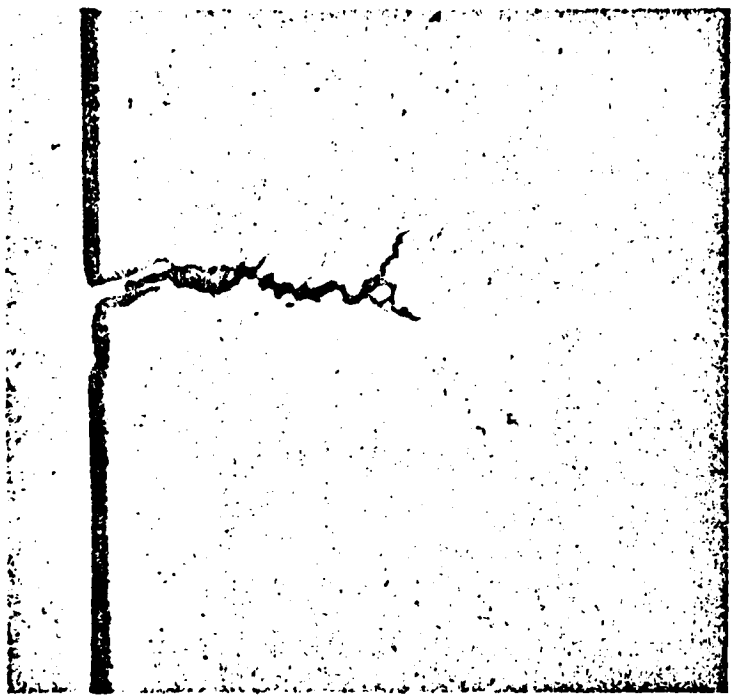

No. 330 Photomicrograph 100X

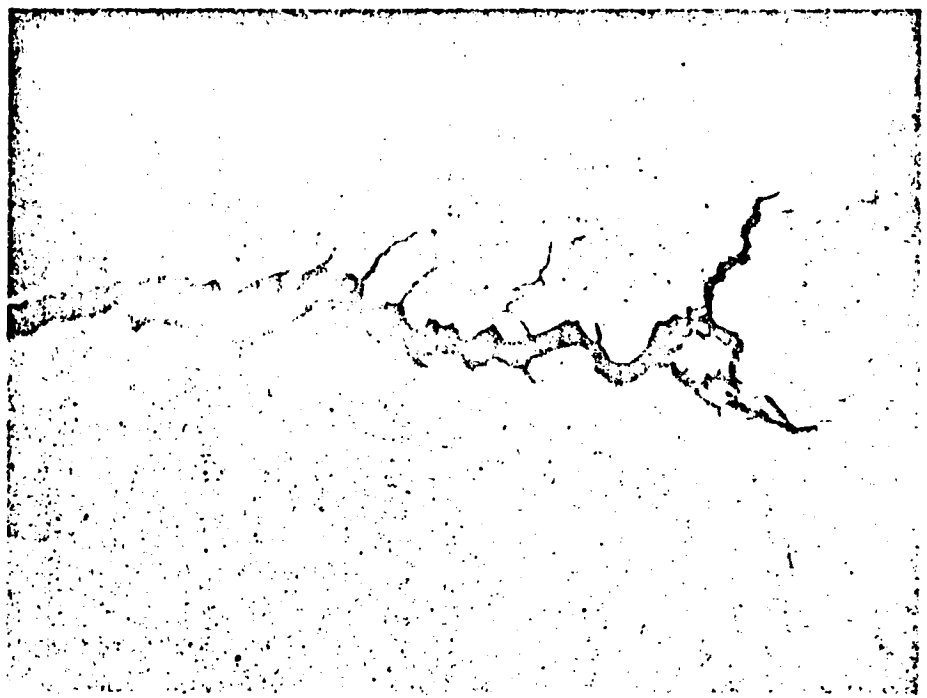

No. 330 Photomicrograph 300X

Figure 61. Fe-9Ni-4Co-0.25C Unnotched Specimen Tested in 10,000-psi Hydrogen (photo at right is same area at higher magnification)

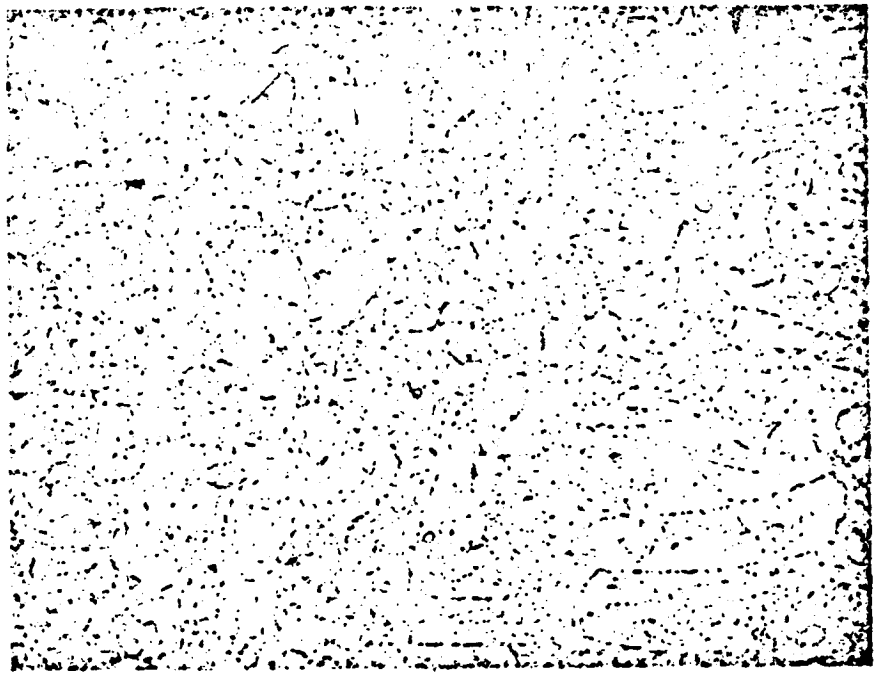

a. Transverse 500X

Photomicrograph

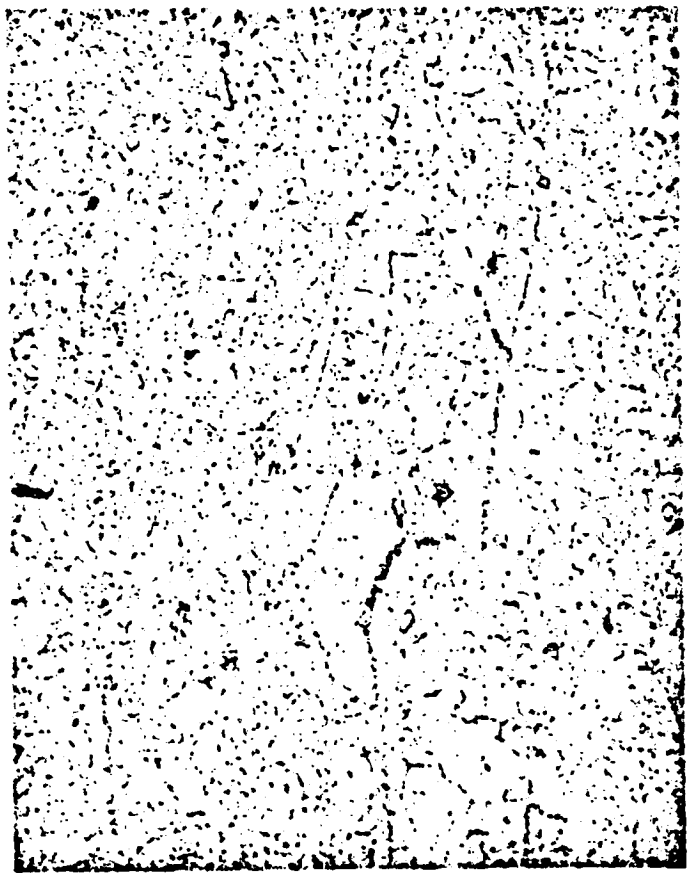

b. Longitudinal 500X

Photomicrograph

Figure 62. Inconel 718 Bar Stock, As-Received (electrolytically etched with oxalic acid; see Table 6 for heat treatment)

Fracture surfaces of unnotched specimens tested in 10,000-psi helium and 10,000-psi hydrogen are shown in Fig. 63 and 64, respectively. It can be seen that the shear lip was complete around the fracture periphery for the specimen tested in helium, but was missing over a small portion of the specimen fracture in 10,000-psi hydrogen. The region without the shear lip was the fracture origin.

The fracture in 10,000-psi helium was transgranular (Fig. 65). The white area was the nickel plate that preserved the fracture edge during metallographic preparation. Conversely, the fracture in 10,000-psi hydrogen was largely intergranular at the origin as shown in Fig. 66. The degree of intergranular fracture decreased with increasing distance from the origin, and was largely transgranular near the shear lip across from the origin as shown in Fig. 67.

Electron fractographic examination of the unnotched specimen tested in 10,000-psi hydrogen was performed by means of the scanning electron microscope at the Jet Propulsion Laboratory. Figure 68 shows the fracture origin, which appears intergranular with secondary intergranular cracking.

The small dimples on the grains may be second-phase particles located in the grain boundary. Center of the fracture is quite ductile (Fig. 69), and the shear lip opposite the fracture origin appears extremely ductile (Fig. 70).

Metallographic examination also was performed (Ref. 6) on an unnotched Rene 41 specimen tested in 10,000-psi hydrogen. Figure 71 is a photomacrograph of the fracture. Origin of the fracture is at the bottom of the photomacrograph, which is the only part of the specimen periphery without a shear lip. The fracture was intergranular (Fig. 72 and 73) and in Fig. 73b the intergranular cracks are shown to extend for a considerable distance into the specimens.

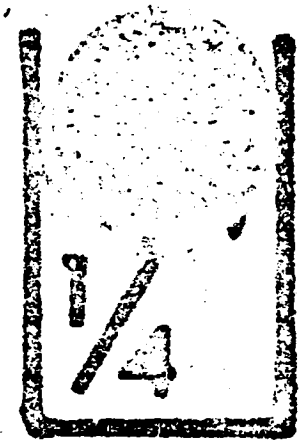

Photomacrograph

Figure 63. Inconel 718 Unnotched Specimen Tested in 10,000-psi Helium (fracture initiated inside of the specimen)

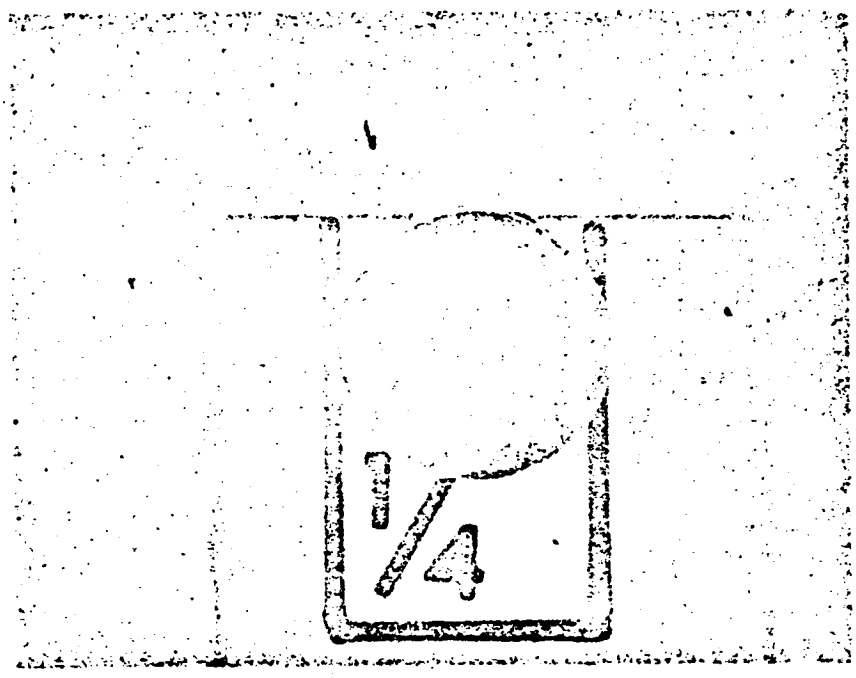

Photomacrograph

Figure 64. Inconel 718 Unnotched Specimen Tested in 10,000-psi Hydrogen (shear lip is missing at the dark area at bottom of photomacrograph; fracture initiated at the surface in this location)

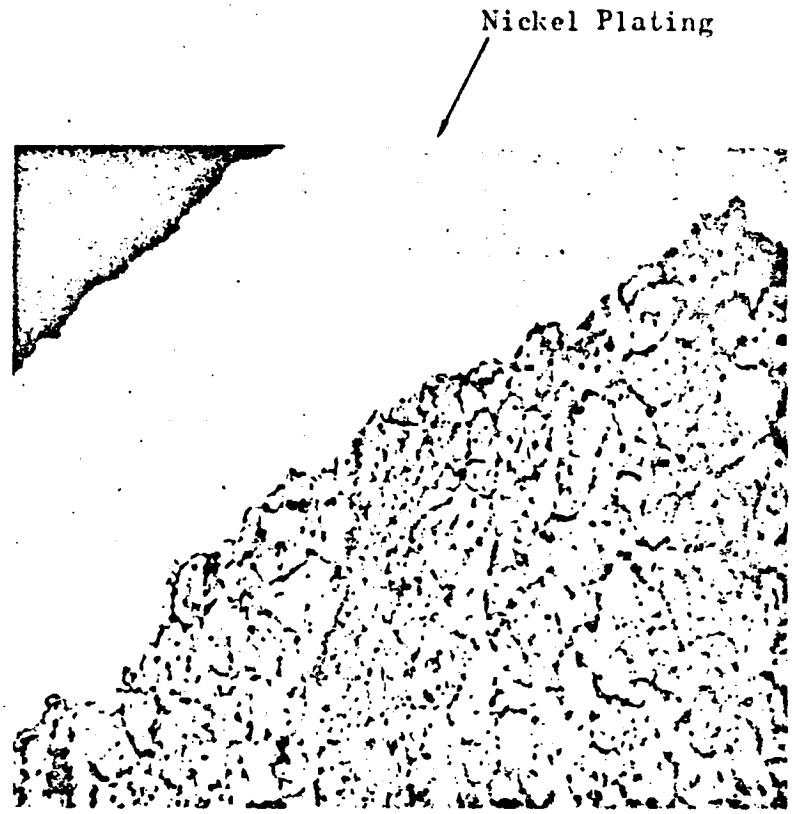

Photomicrograph 500X

Figure 65. Inconel 718 Fracture Surface For Specimen Tested in Helium (electrolytically etched with oxalic acid; see Table 6 for heat treatment)

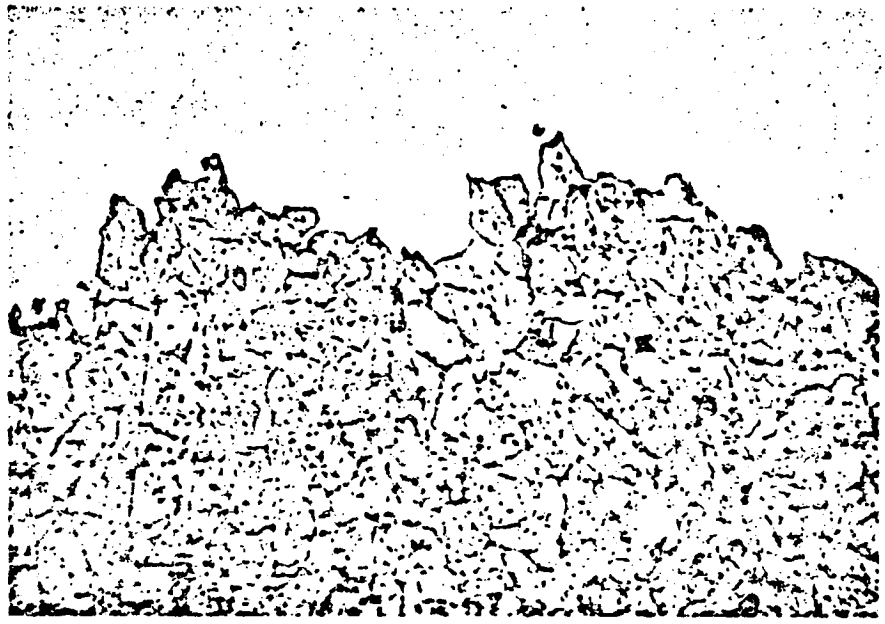

Photomicrograph 500X

Figure 66. Initiation Area of Fracture Surface Formed in Inconel 718 Specimen Tested in 10,000-psi Hydrogen Showing Intergranular Nature of Fracture (electrolytically etched with oxalic acid; see Table 6 for heat treatment)

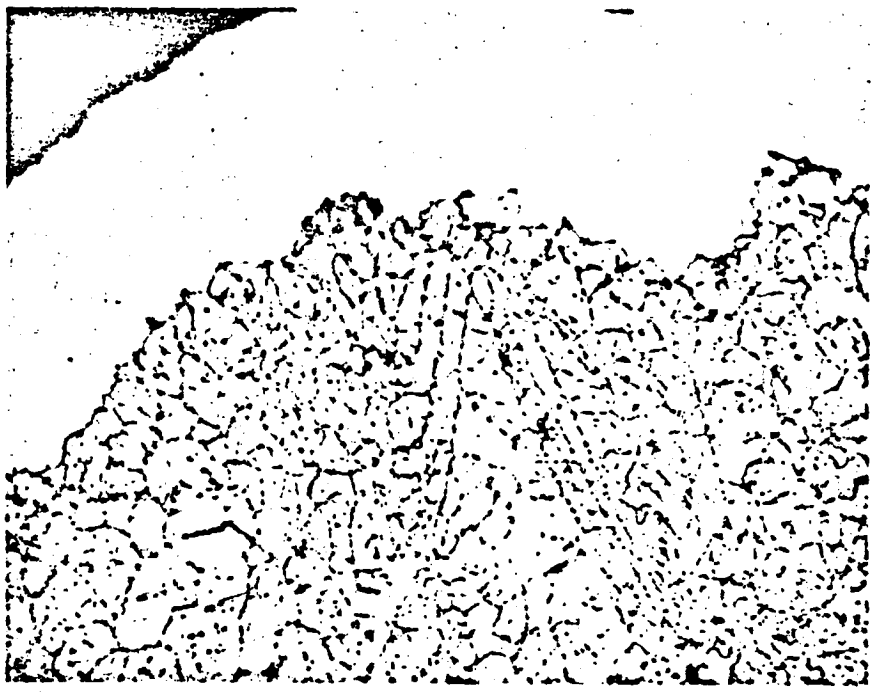

Photomicrograph 500X

a. Center of bar

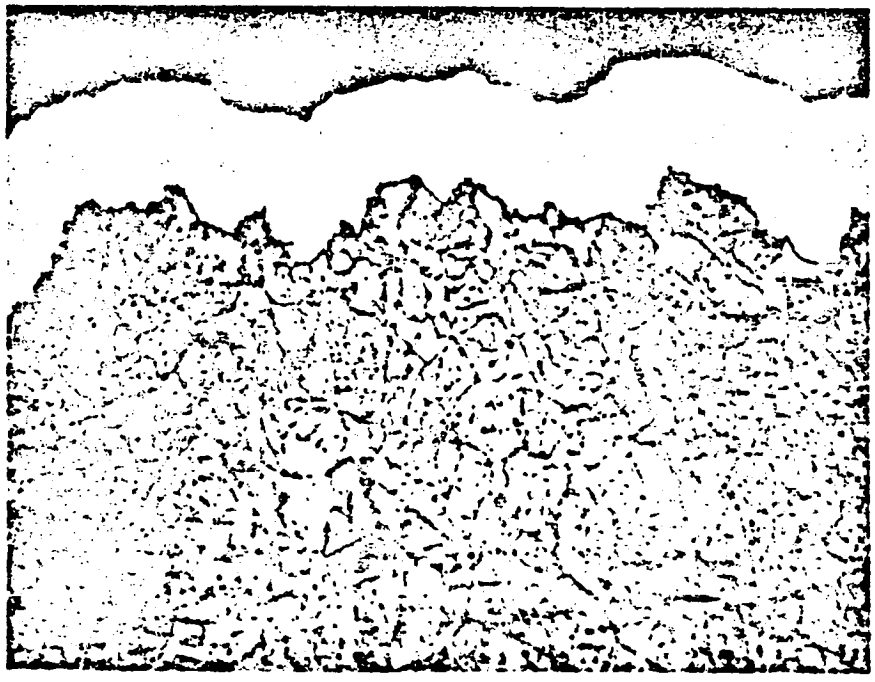

Photomicrograph 500X

b. Close to start of shear lip but still on flat portion, 180 degrees from origin

Figure 67. Sections Through Inconel 718 Fractured Under Hydrogen (electrolytically etched with oxalic acid; see Table 6 for heat treatment)

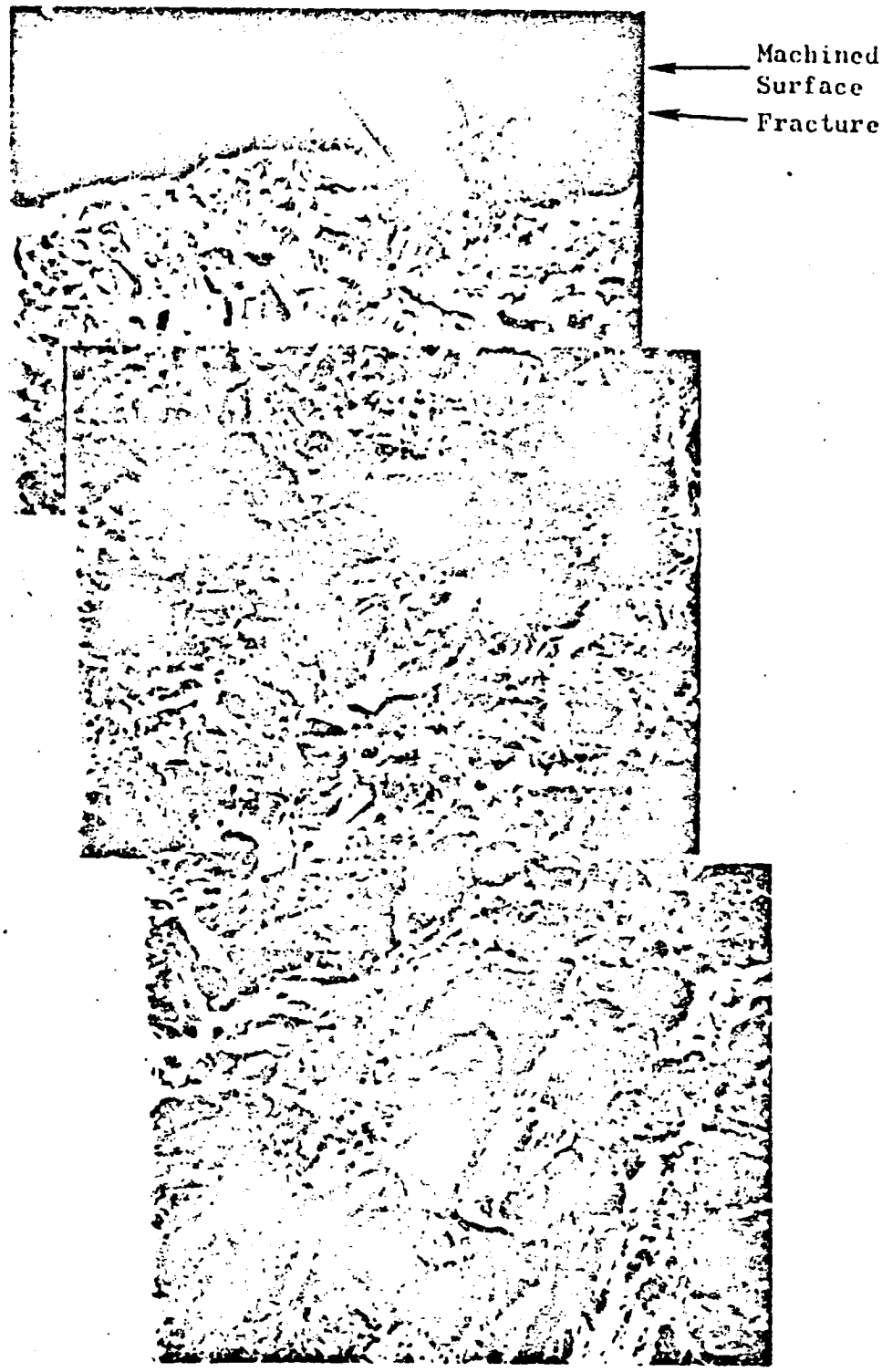

No. 1228 1030X

Scanning Electron Micrographs

Figure 68. Inconel 718 Unnotched Specimen Tested in 10,000-psi Hydrogen (location is at the fracture origin)

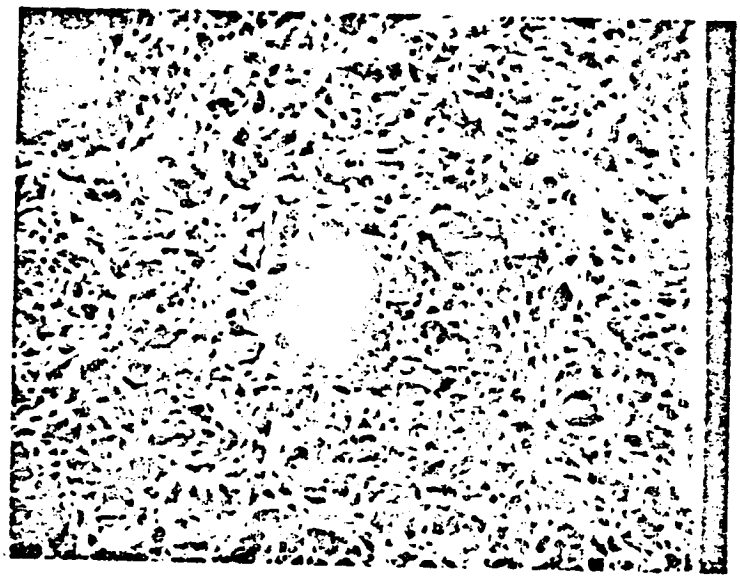

No. 1228 940X

Scanning Electron Micrograph

Figure 69. Inconel 718 Unnotched Specimen Tested in 10,000-psi Hydrogen (location is at the center of the specimen)

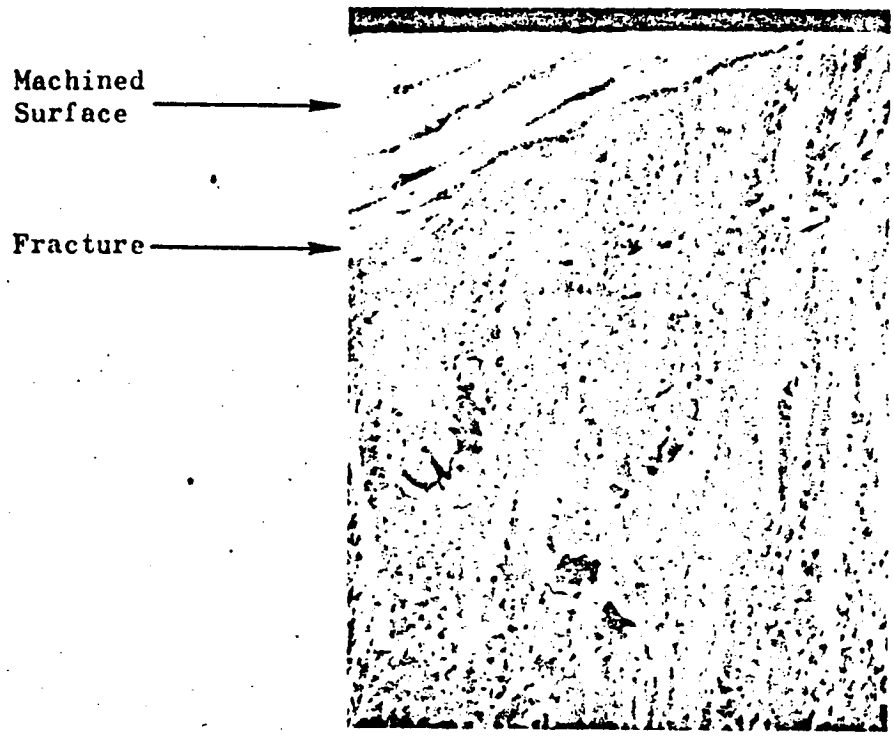

No. 1228 940X

Scanning Electron Micrograph

Figure 70. Inconel 718 Unnotched Specimen Tested in 10,000-psi Hydrogen (location is at the shear lip opposite the origin)

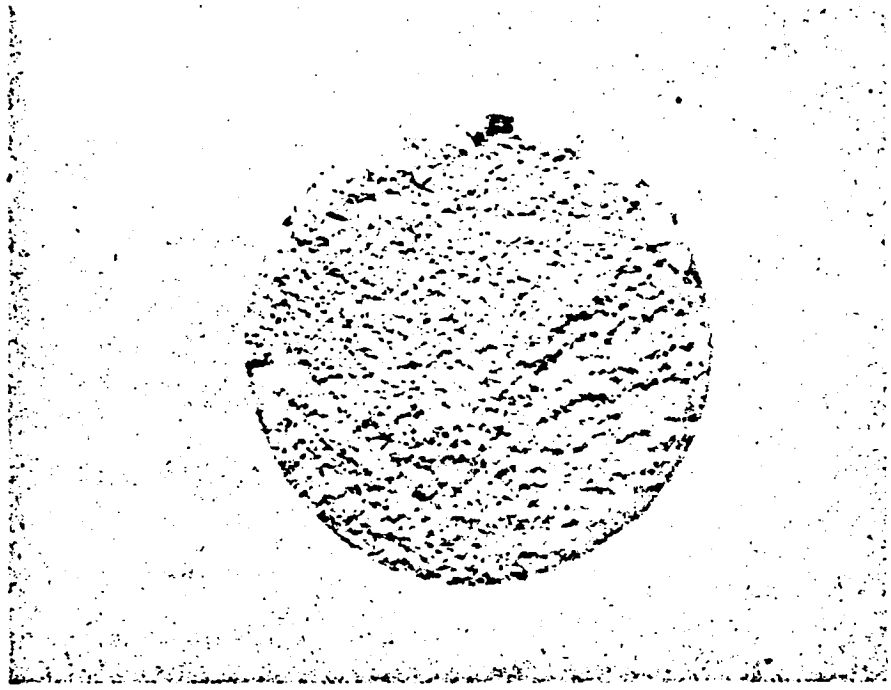

No. 1277 Photomacrograph 10X

Figure 71. Rene 41 Unnotched Specimen Tested in 10,000-psi Hydrogen (fracture origin is the region without a shear lip at the bottom of the photo)

Photomicrograph 500X

Figure 72. Typical Cross Section of Rene 41 Fractured Under Hydrogen (intergranular nature of fracture and normal microstructure may be observed; see Table 6 for heat treatment; etched with $HCl-H_2O_2$)

a. Unetched 2000X

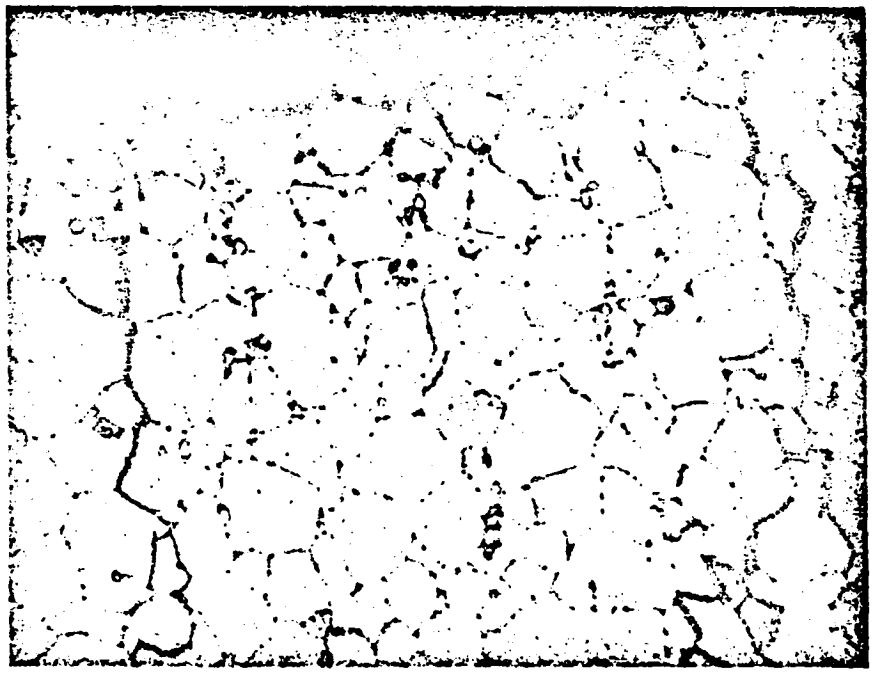

b. Etched ($HCl-H_2O_2$) 500X

Photomicrograph

Figure 73. Cross Section of Rene 41 Tested Under Hydrogen Showing Intergranular Fracture and Longitudinal Cracks (see Table 6 for heat treatment)

NOTCHED SPECIMENS

Optical and electron fractographic examinations were performed on representative notched specimens tested in this program. Results of this examination were informative for determining the fracture origin, fracture path, and types of fracture that occurred in the various environments.

Examination of Iron-Base Alloys

Photomacrographs of a series of fractures of notched low-alloy steel specimens ranging in order from least embrittled (Armco Iron) to extremely embrittled AISI type 440C stainless steel and H-11 tool steel are shown in Fig. 74 through 79. Fracture surfaces of the lower strength low-alloy steels (Armco Iron, ASTM A-302, and AISI 1042) have a brittle outer ring and a ductile inner portion.

Degree of embrittlement may be related to the outer ring depth because the relative depths increase from Armco Iron to ASTM A-302 to AISI 1042. The outer rings observed on the fracture surfaces of the specimens tested in hydrogen were not present on the specimens tested in air or in 10,000-psi helium. There is an extra inner ring on the fractured surface of the AISI 1042 specimens, as illustrated in Fig. 76.

Fracture of the higher strength steels appeared relatively brittle in both helium and hydrogen environments. Figure 77 shows the fractures of AISI type 430F stainless-steel specimens tested in 10,000-psi hydrogen and 10,000-psi helium. Longitudinal cracks are evident in both fractures. There is a broken thin shear lip around the periphery of the specimen tested in 10,000-psi helium, but the fracture in hydrogen was brittle across the specimen with no indication of any shear lip. Figure 78 shows the fractures of AISI 440C stainless-steel specimens tested in helium and in hydrogen environments. Fracture origin in helium was slightly below the specimen surface, while fracture origin in hydrogen

Photomacrograph 10X

a. Tested in 10,000-psi Helium

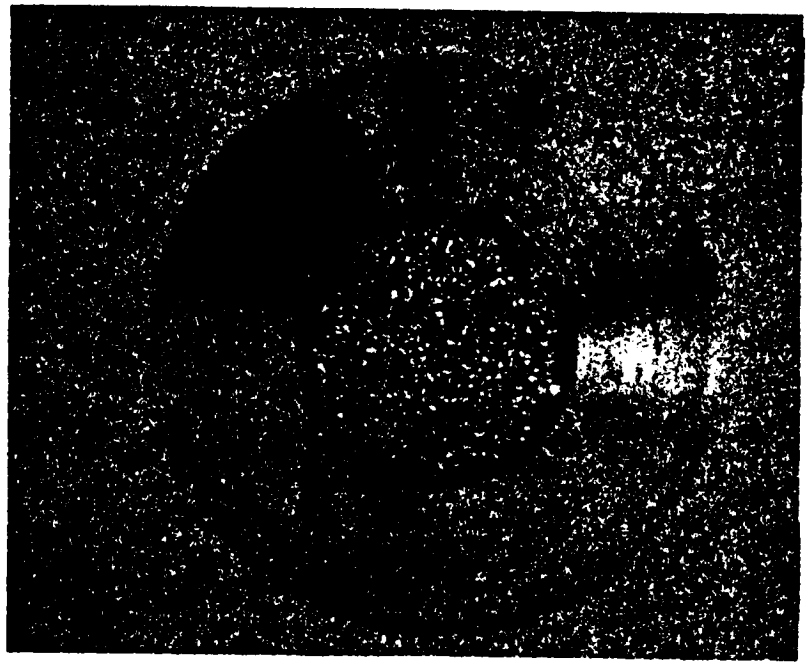

Photomacrograph 10X

b. Tested in 10,000-psi Hydrogen (note outer ring due to hydrogen environment)

Figure 74. Armco Iron Notched Specimens

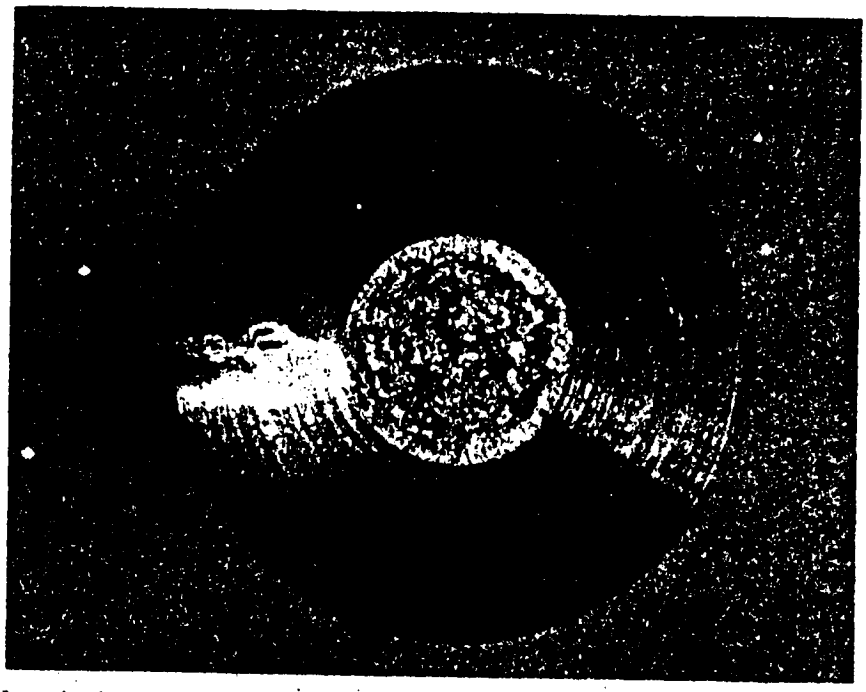

No. A158 Photomacrograph 10X

a. Tested in 10,000-psi Hydrogen (note brittle outer ring)

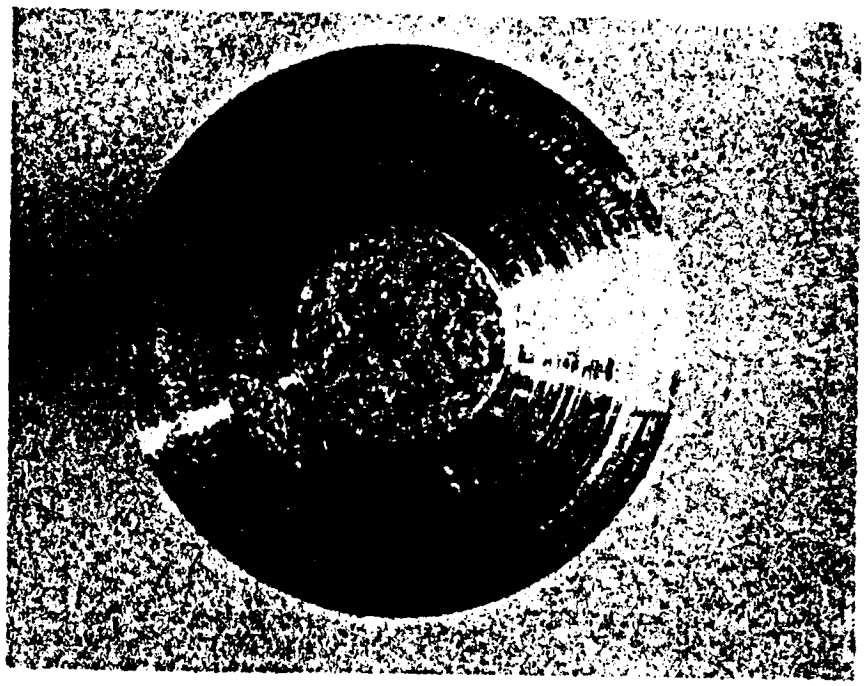

No. A153 Photomacrograph 10X

b. Tested in 10,000-psi Helium

Figure 75. ASTM A-302 Notched Specimens

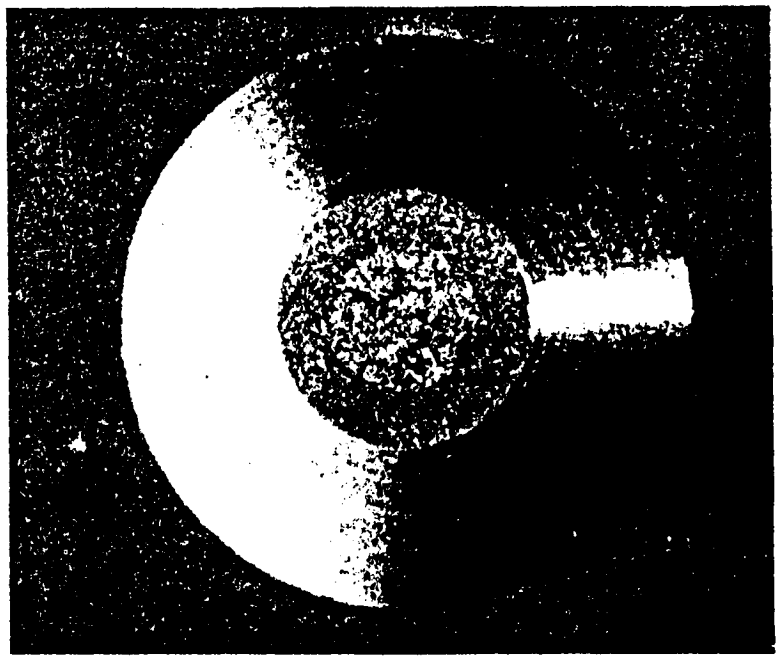

No. 51 Photomacrograph 10X

a. Tested in 10,000-psi Helium (note ductile outer ring and brittle center portion)

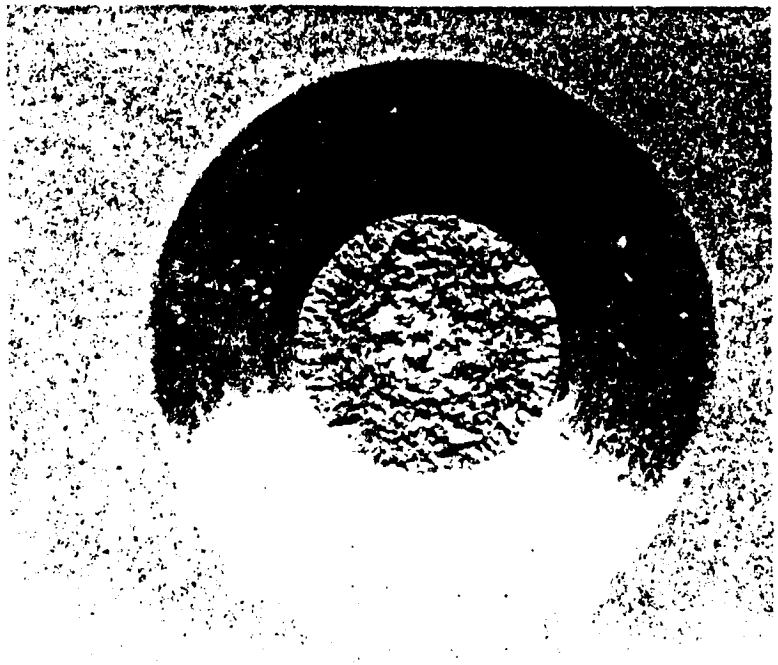

No. 56 Photomacrograph 10X

b. Tested in 10,000-psi Hydrogen (note bright brittle outer ring, dark inner ring, and bright center portion)

Figure 76. AISI 1042 Normalized Notched Specimens

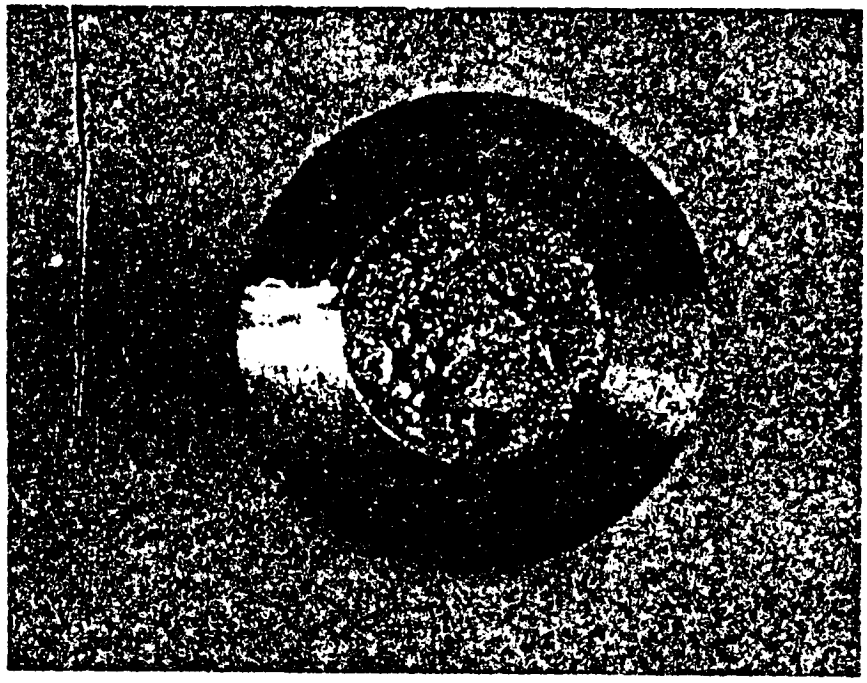

No. 551 Photomacrograph 10X

a. Tested in 10,000-psi Helium (note broken thin shear lip)

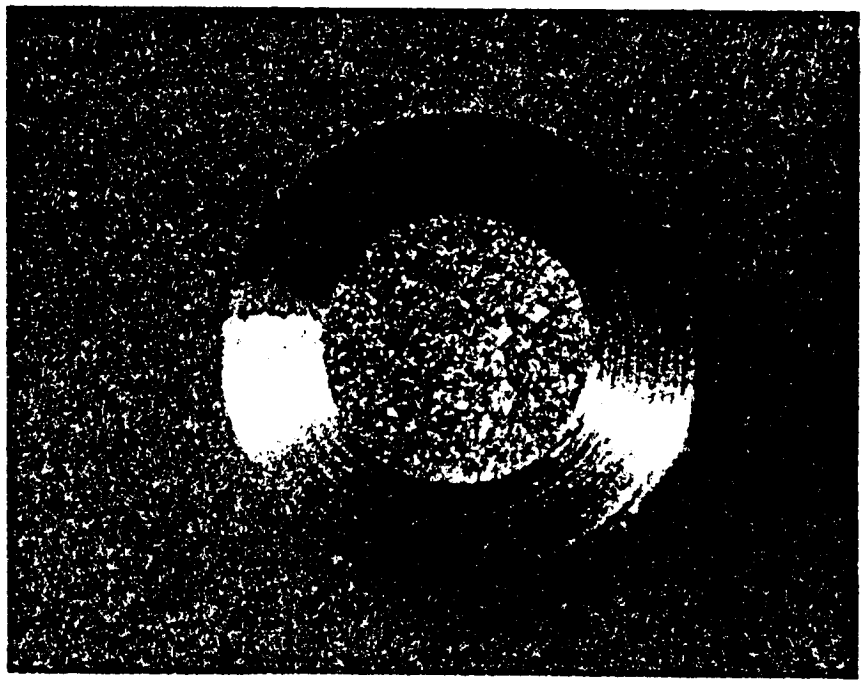

No. 556 Photomacrograph 10X

b. Tested in 10,000-psi Hydrogen (note brittle appearance across fracture)

Figure 77. AISI Type 430F Stainless-Steel Notched Specimens

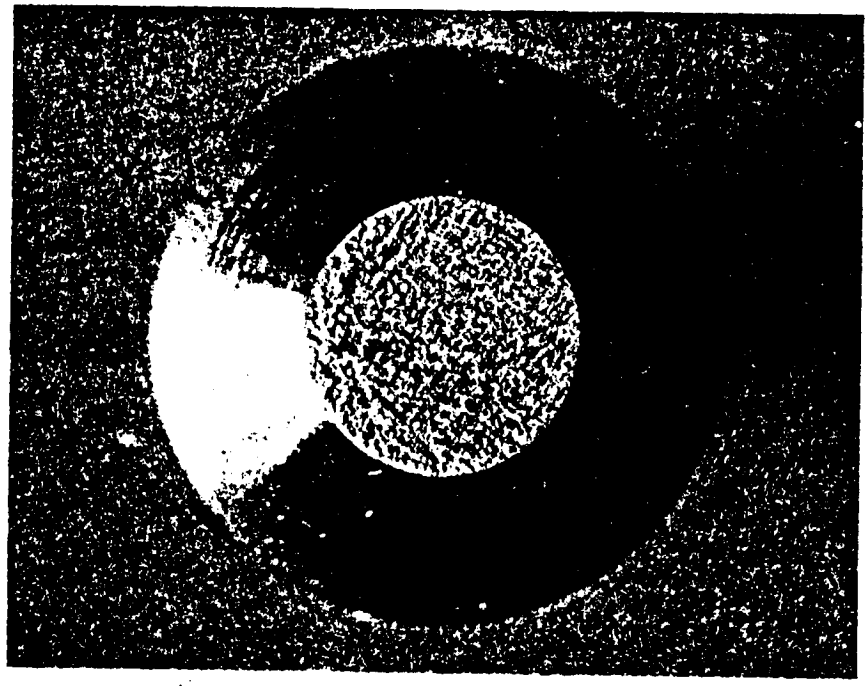

No. 652 Photomacrograph 10X

a. Tested in 10,000-psi Helium (note fracture initiation at left side inside the specimen)

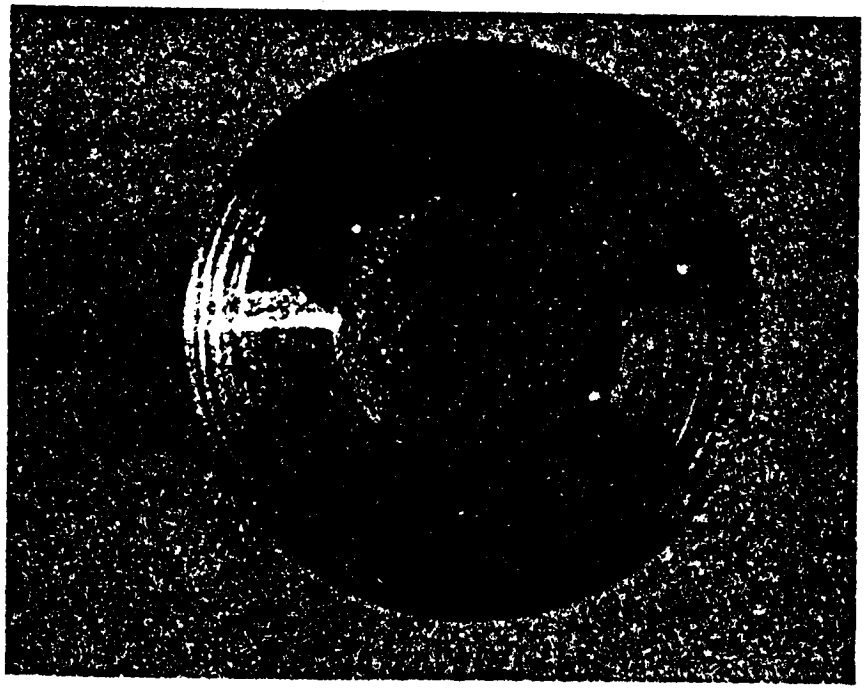

No. 656 Photomacrograph 10X

b. Tested in 10,000-psi Hydrogen (note fracture initiation is at left side of the fracture periphery)

Figure 78. AISI Type 440C Stainless-Steel Notched Specimens

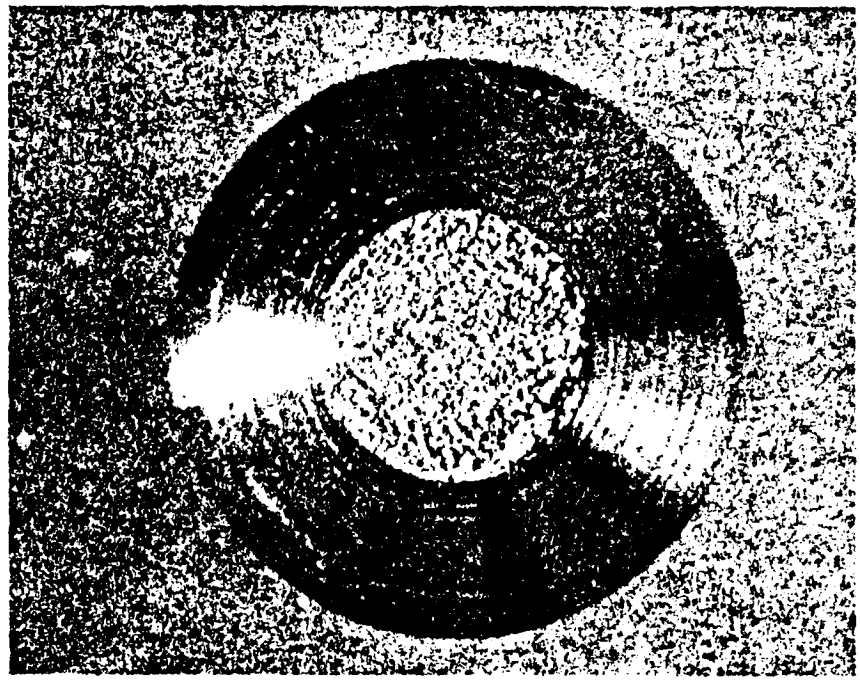

No. H157 Photomacrograph 10X

a. Tested in 10,000-psi Helium

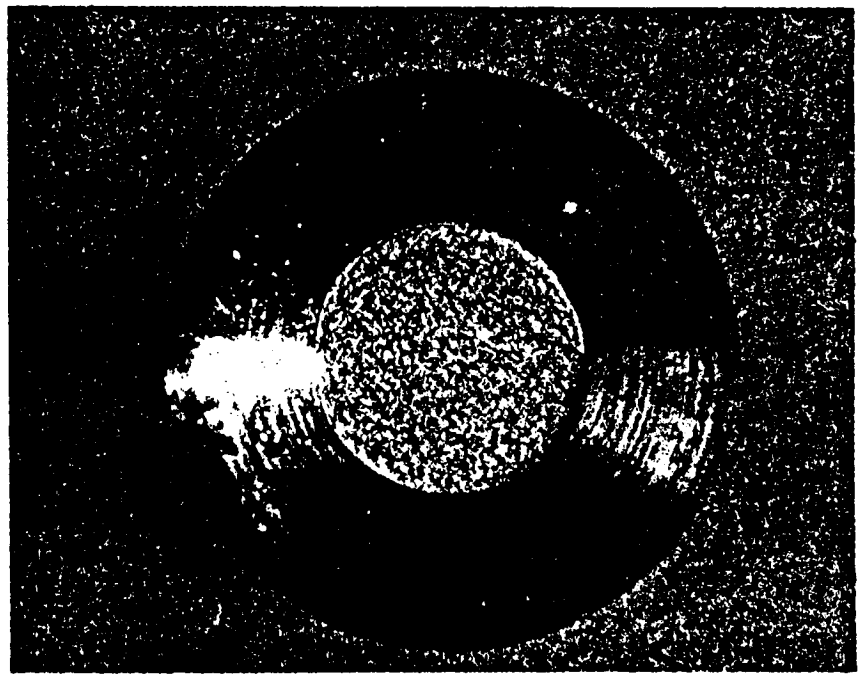

No. H152 Photomacrograph 10X

b. Tested in 10,000-psi Hydrogen (note fracture appears brittle over the entire fracture)

Figure 79. H-11 Tool-Steel Notched Specimens

is assumed to be on the left edge of the fracture, because the fracture is flatter at this spot. The H-11 tool steel fracture is illustrated in Fig. 79. In hydrogen the fracture was entirely flat, while in helium it had a slight texture, indicating greater ductility, although there was no measurable ductility in either environment. Ductility was determined by the reduction of area, which was not sensitive to ductility on a microscopic scale.

Electron fractographic examination conducted in the previous program on notched specimens of ASTM A-212, ASTM A-517, and ASTM A-302 low alloy steels showed: (1) fractures were more brittle in hydrogen than in air or helium environments; (2) fractures initiated at the specimen surface in hydrogen and below the surface in air and helium environments; and (3) the fracture surface of ASTM A-302 and ASTM A-517 specimens contained numerous secondary cracks. The second finding had to be regarded as somewhat tentative because of the few interfaces observed.

In the present program, the electron fractography was conducted so that a continuous record from the machine surface to the center of the specimen was obtained, in contrast to the usual method of taking isolated electron micrographs of limited portions of the surface. By this method, progression of the crack can be traced from its point of origin.

An electron fractographic composite of an AISI 1042 specimen tested in 10,000-psi helium is shown in Fig. 80. This composite shows that the outer portion of the fracture was ductile while the inner portion exhibits brittle, transgranular cleavage. Stereomicrographs indicate that the dark ridges in the brittle areas were caused by overlapping fracture regions and by folding over of carbon replica, and are not secondary cracks. Stereo examination of the brittle center region indicates that the dark interfaced regions were not surface cracks but overlapping fracture facets.

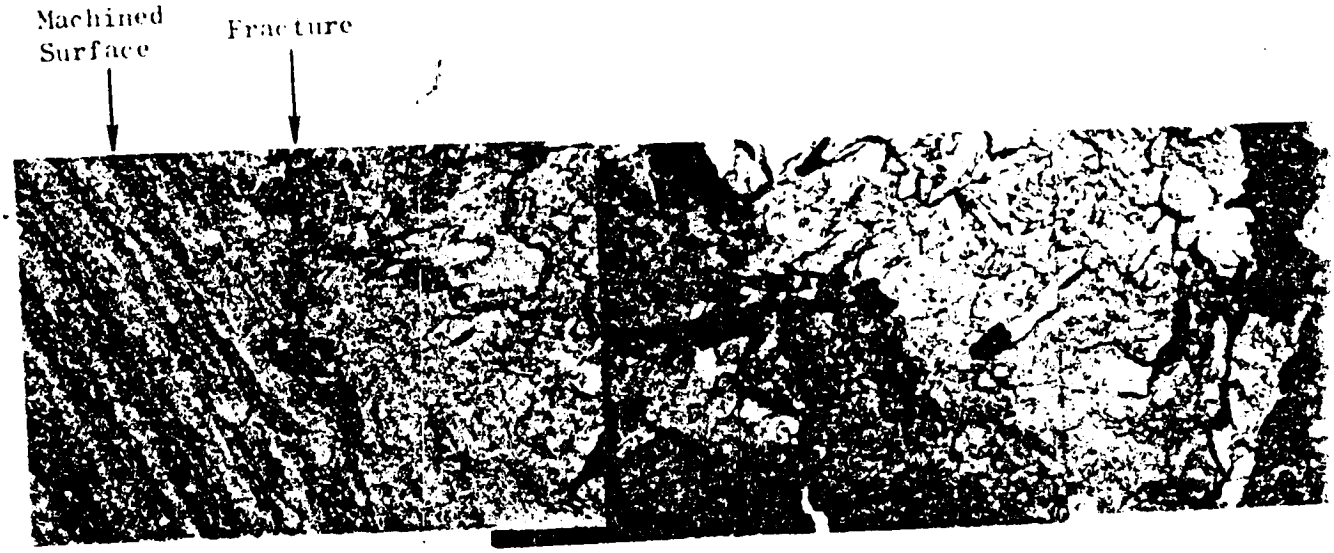

235/

Ductile Region

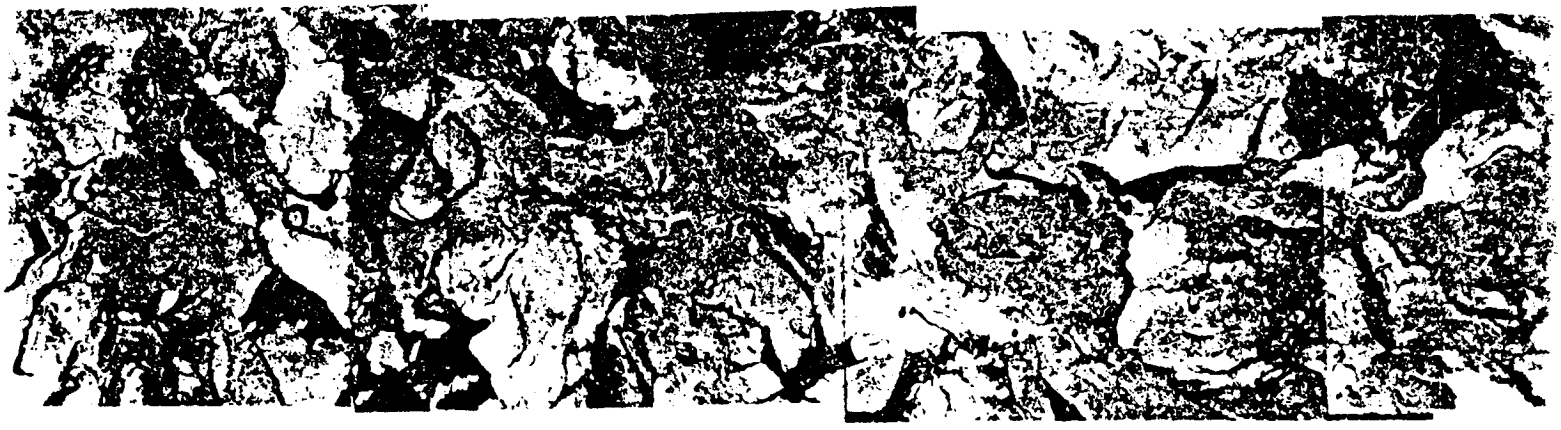

Brittle Region (Center of Specimen)

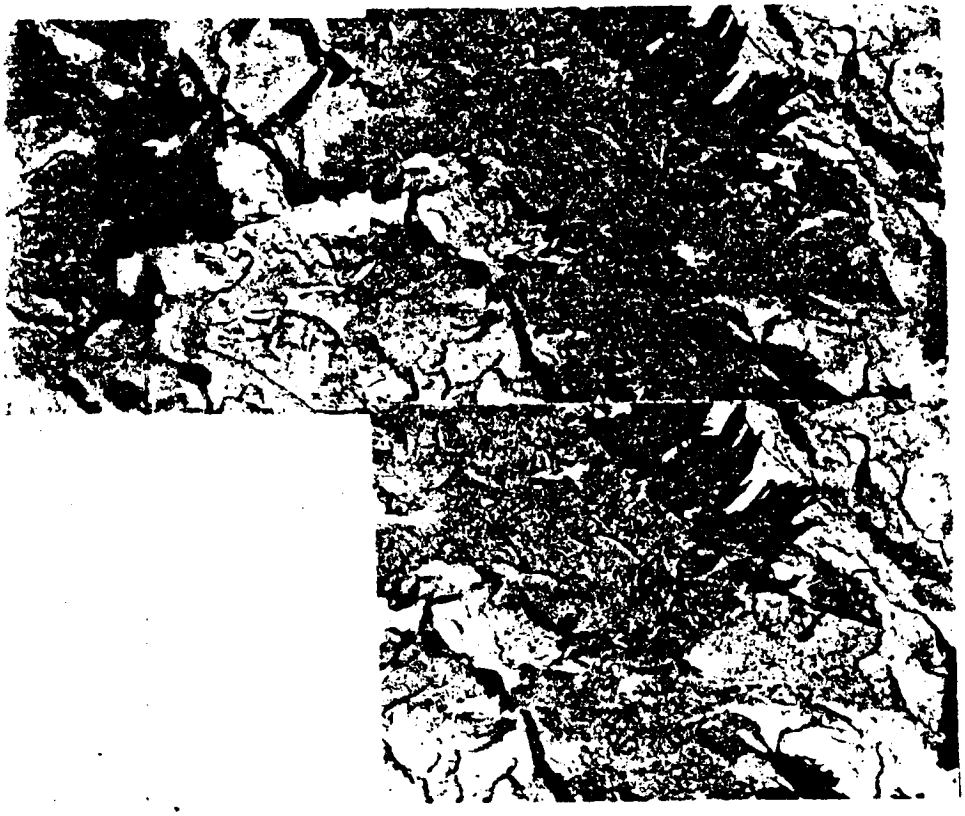

Stereo Pair

Figure

235/. B

Region A

Stereo Pair

No. 52 Electron Fractograph 1000X

Figure 80. AISI 1042 Normalized Specimen Tested in 10,000-psi Helium (view of machined surface, machined surface, fractured surface interface, and into fracture to the location of brittle region in center of specimen)

Figure 82 is a composite of an AISI 1042 specimen tested in 10,000-psi hydrogen. The outer region of this fracture is quasi-cleavage. The inside of this specimen tested in hydrogen fractured by cleavage; this portion appears the same as the inner portion of the specimen that was tested in 10,000-psi helium. Between these brittle regions is a ductile area. Thus, the three rings obtained from tests conducted in hydrogen correspond to the sequence brittle-ductile-brittle areas. Also present on the fracture surface are light bands that are believed to represent pearlite.

Electron fractography showed that the light regions on the inner portion of the fractures represent cleavage. This indicates that the plane strain conditions inside the metal lead to brittle fracture independently of whether the crack nucleated at the surface or inside the metal.

It was difficult to interpret the appearance of the fractures of the austentic stainless-steel specimens. The fracture of these specimens consisted of many shear-like peaks across the entire fracture, although the shear lips around the periphery were not observed. Figures 81 and 83 illustrate the fractures of AISI types 304L and 310 stainless-steel specimens. Visual examination of the fractures of these two steels indicated that the fracture peripheries were more brittle when the tests were conducted in hydrogen than when conducted in helium, although this is not apparent in the macrographs.

Examination of Nickel-Base Alloys

Careful light and electron-microscopic examinations were performed on notched specimens of Inconel 718 tested in air, helium (contaminated with hydrogen), and in 10,000-psi hydrogen environments. The fracture in air is illustrated in Fig. 84, where it may be seen that the fracture was ductile even at the surface. There was no cracking on the machined surface, and there was a smooth transition from the machined surface into the fracture. The dimpled texture in Fig. 84 is representative of the entire fracture.

Preceding page blank

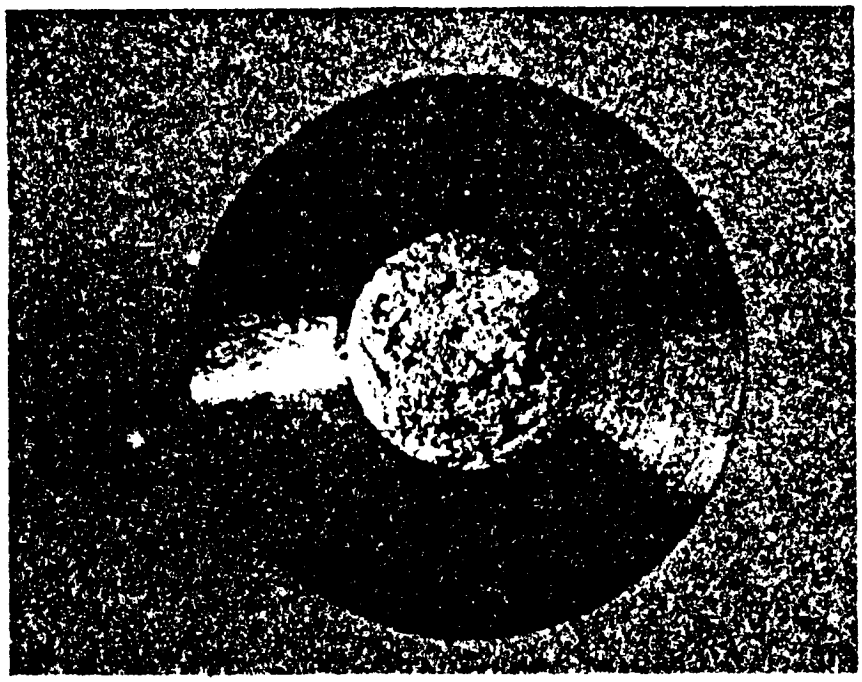

No. 401 Photomacrograph 10X

a. Tested in 10,000-psi Helium (20 percent reduction of area)

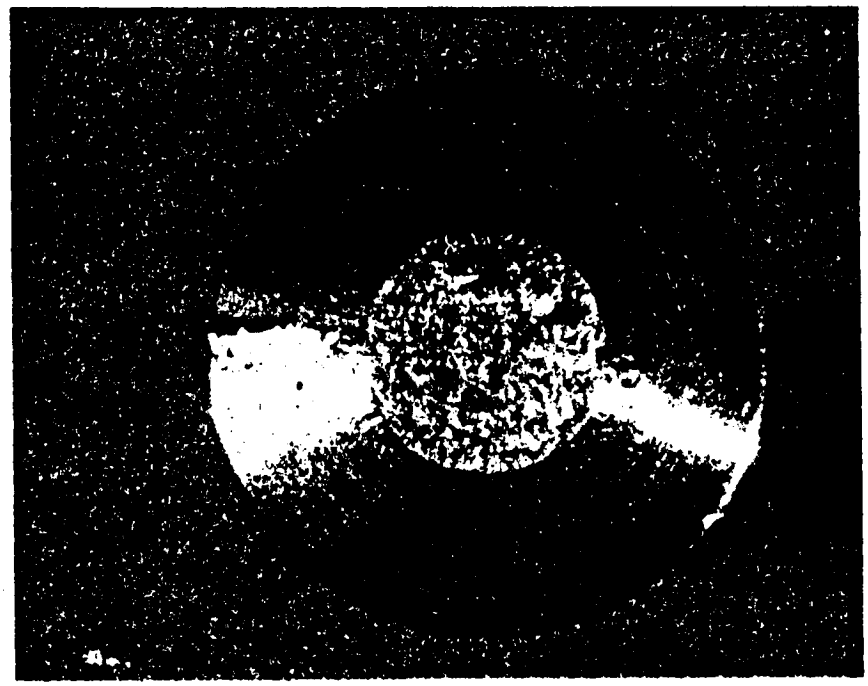

No. 407 Photomacrograph 10X

b. Tested in 10,000-psi Hydrogen (11 percent reduction of area)

Figure 81. AISI Type 304L Stainless-Steel Notched Specimens

Machined Surface

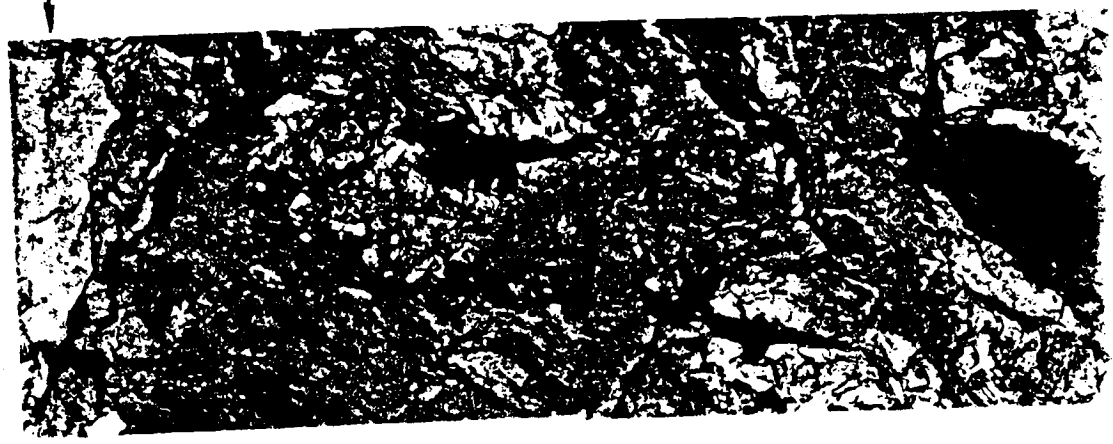

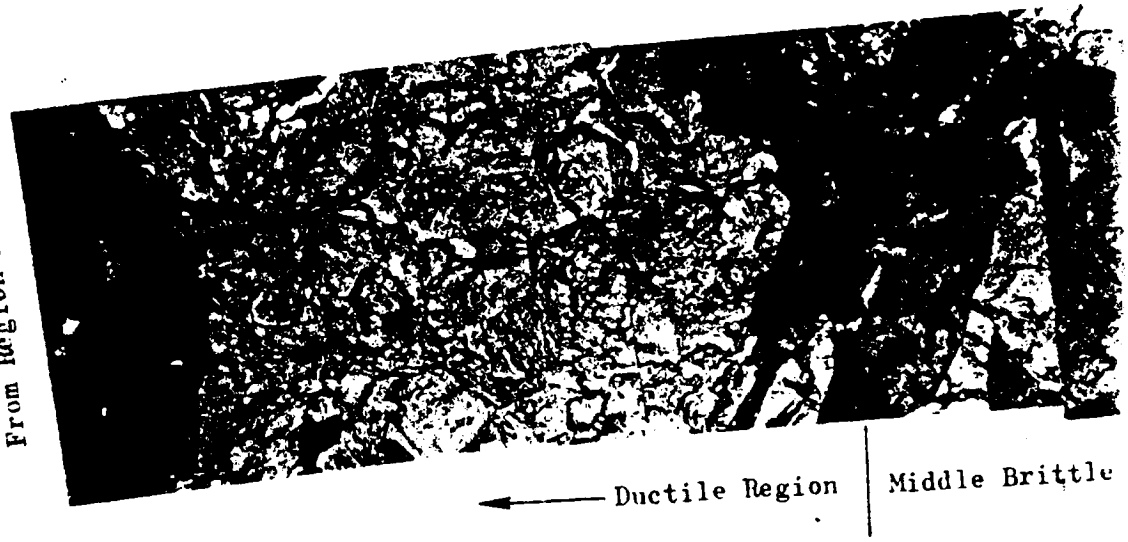

Pearlite Colony

Quasi-Cleavage Region

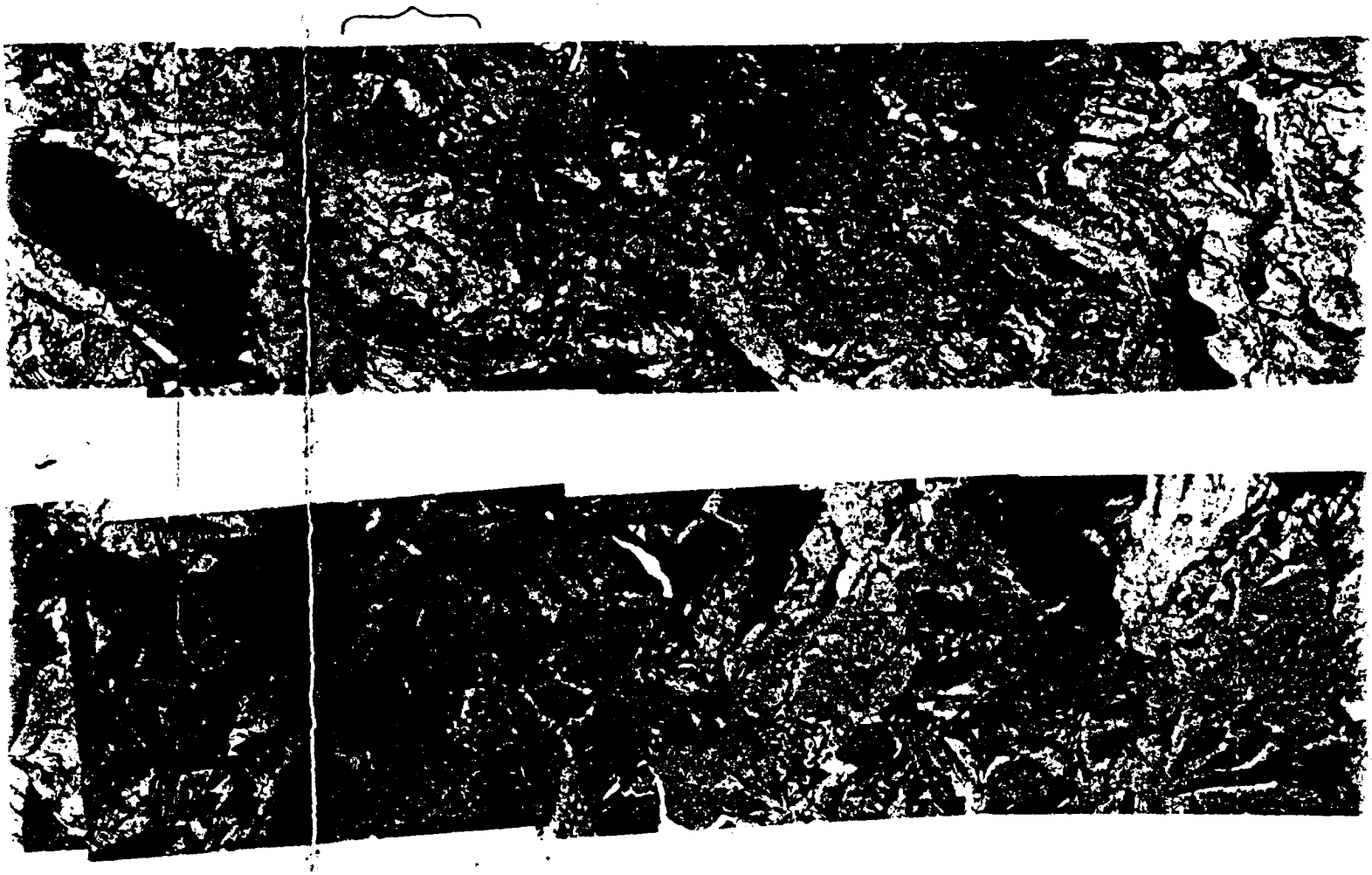

Brittle Region

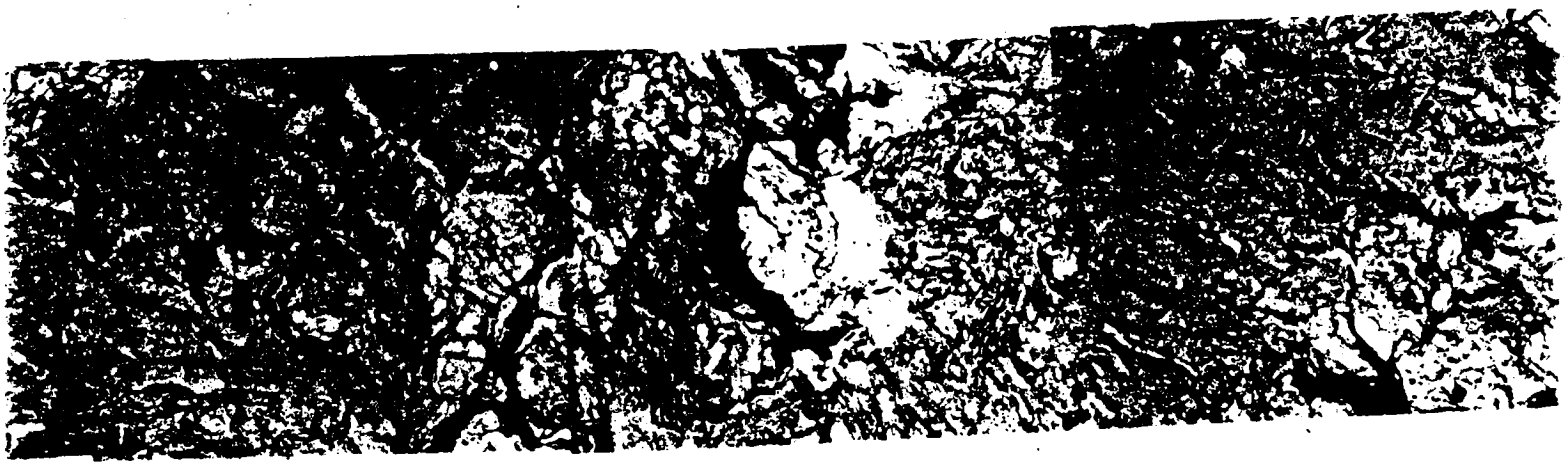

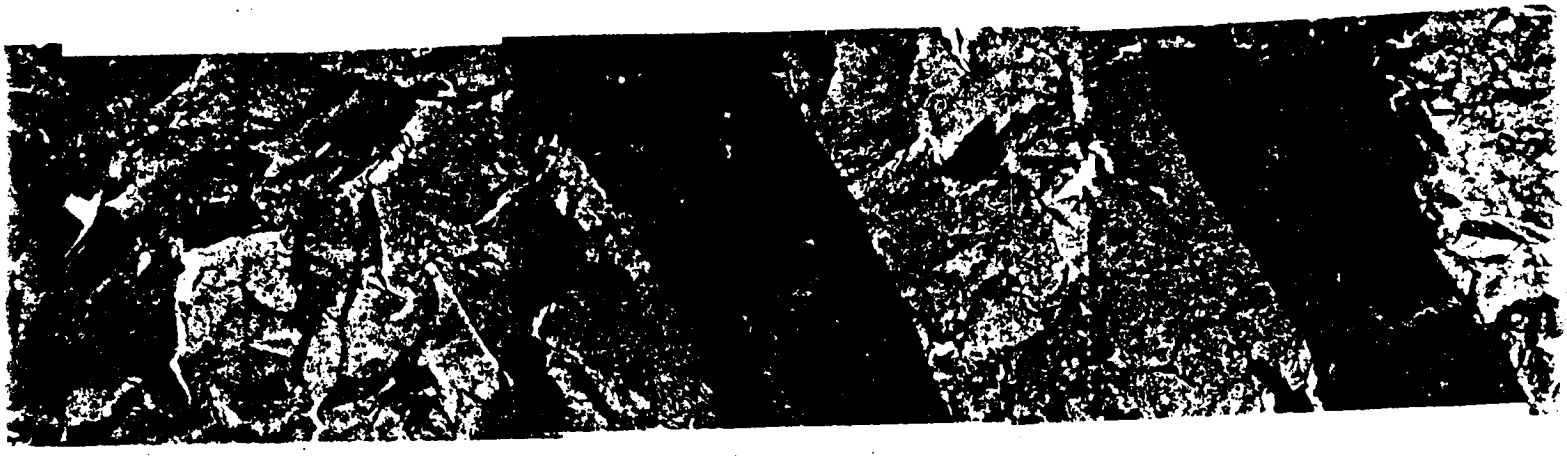

239-b

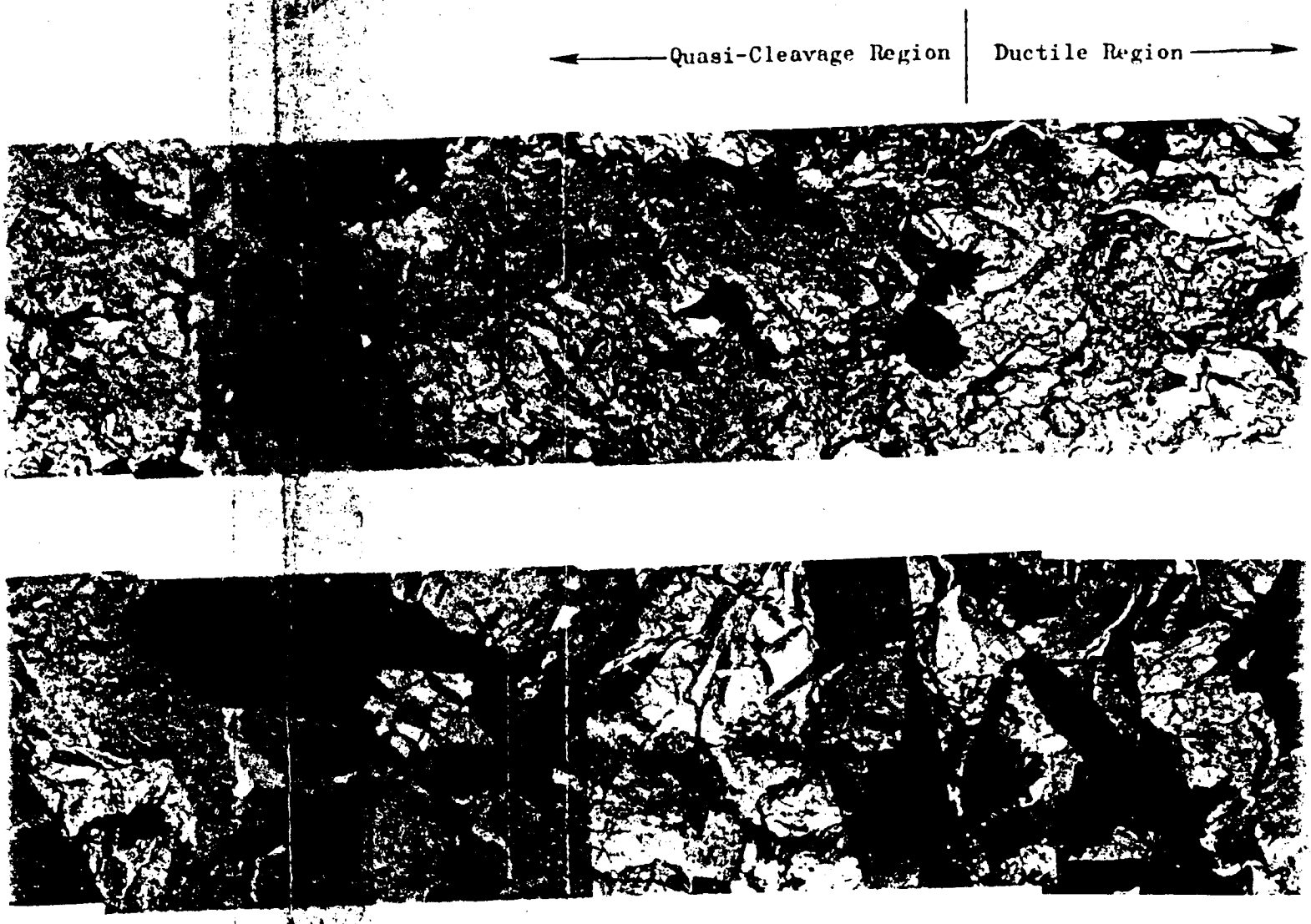

239-C

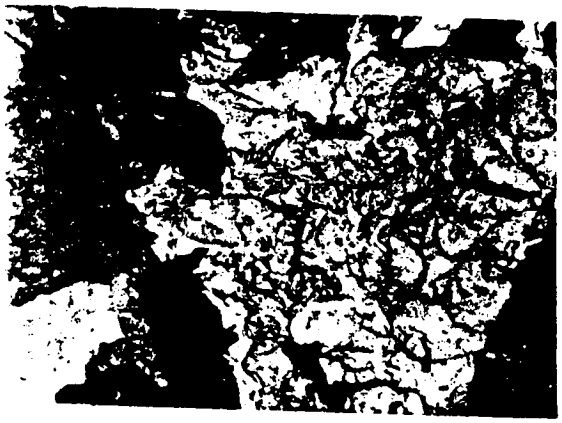

Region A

No. 56 Electron Fractograph 1300X

Figure 82. AISI 1042 Normalized Specimen Tested in 10,000-psi Hydrogen (view of machined surface/fractured surface interface into the fracture through the quasi-cleavage region on the surface followed by a ductile region and brittle middle region)

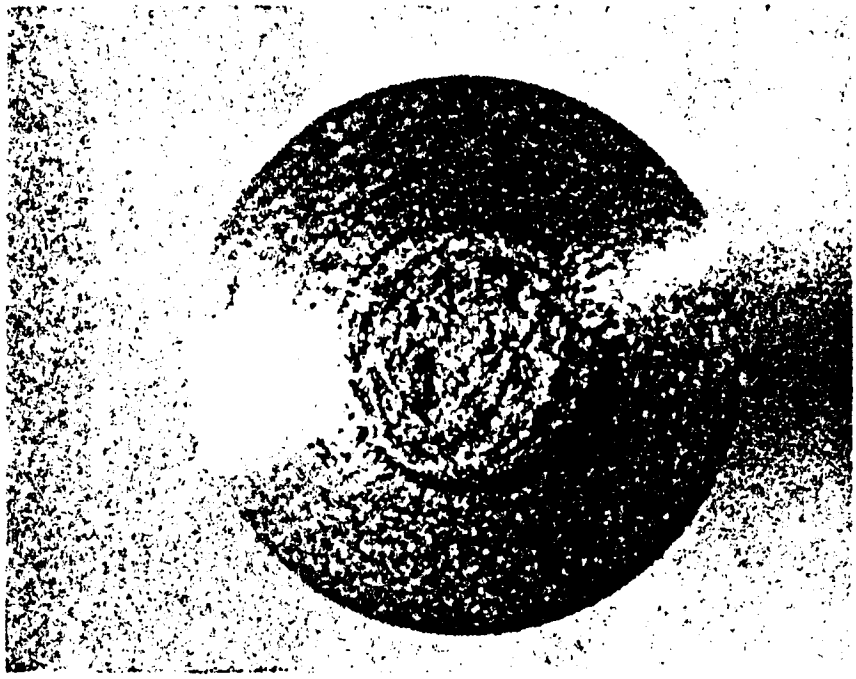

No. C150 Photomacrograph 10X

a. Tested in 10,000-psi Helium (19 percent reduction of area)

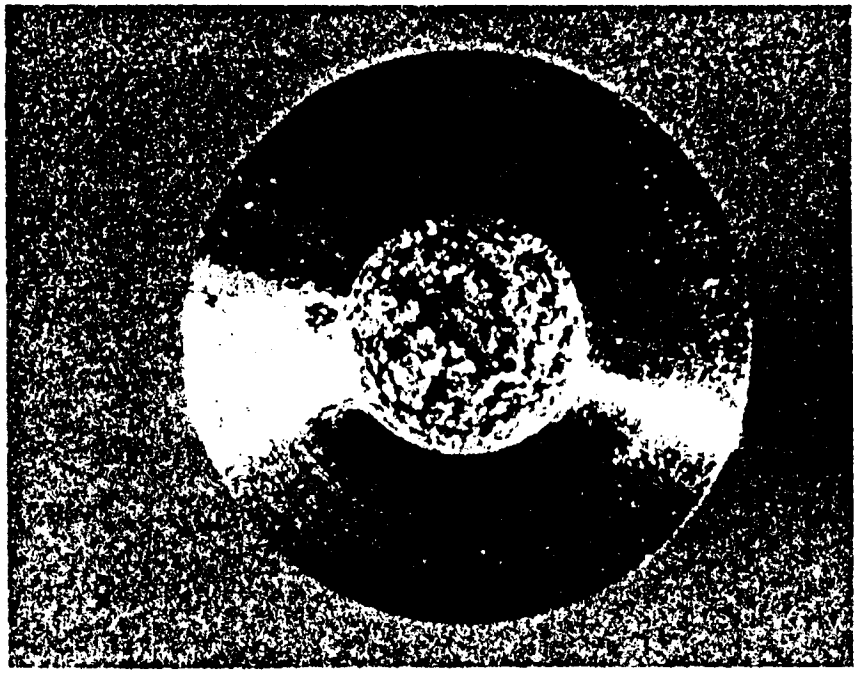

No. C168 Photomacrograph 10X

b. Tested in 10,000-psi Hydrogen (14 percent reduction of area)

Figure 83. AISI Type 310 Stainless-Steel Notched Specimens

Preceding page blank

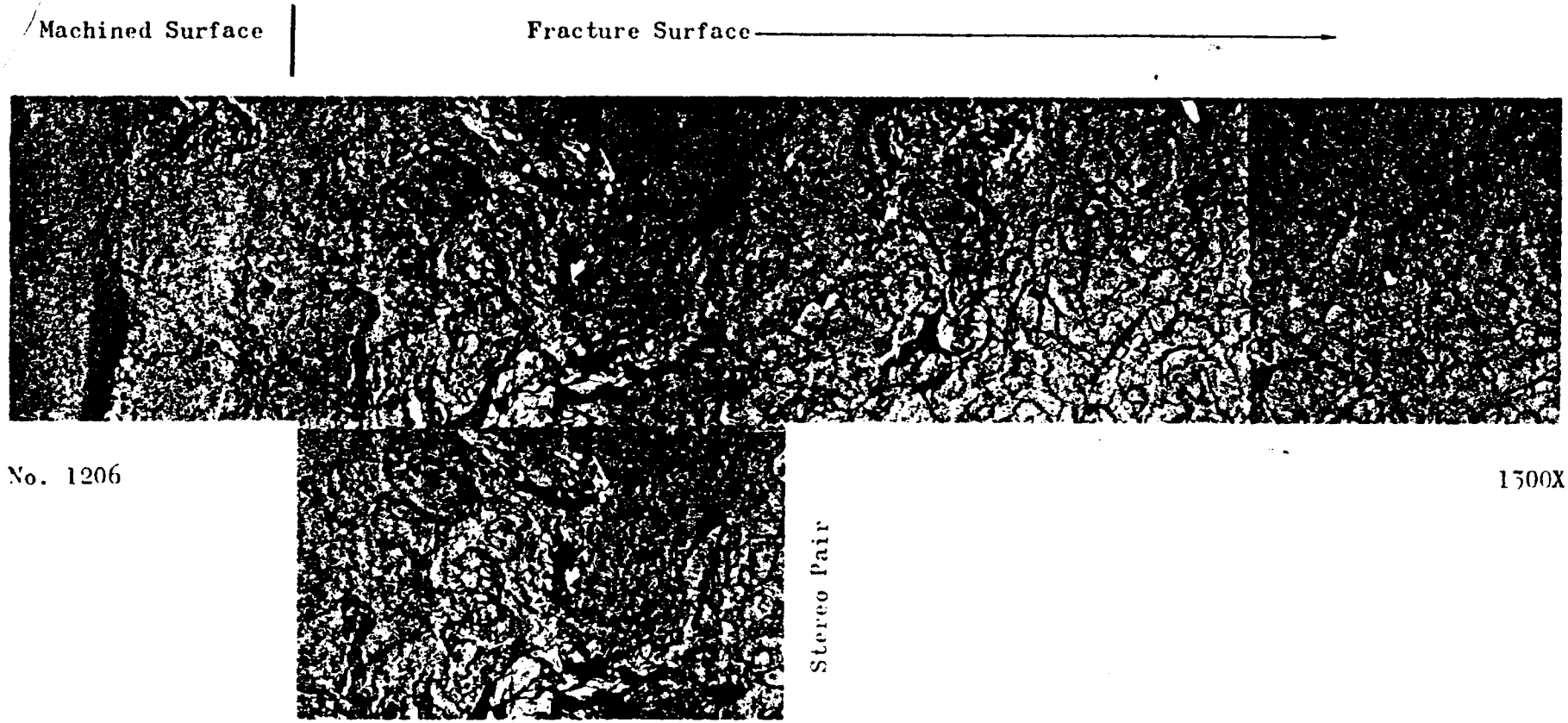

Electron Fractograph

Figure 84. View of Edge of Fracture Surface of Inconel 718 Notched Specimen Tested in Air at 1 Atmosphere (This structure is representative of the entire fracture)

A photomacrograph of the fracture of an Inconel 718 specimen tested in 10,000-psi hydrogen is shown in Fig. 85. The light reflection on the top indicates the fracture origin, while the dark line across the specimen is a crack parallel to the specimen axis. Figure 86 shows a composite of the fracture from the origin at the machined surface to the point at which the fracture becomes ductile. It is difficult to be certain at which point the fracture surface begins, becuase of the extensive cracking on the machined surface caused by the hydrogen environment. The fracture surface may begin at the point shown in Fig. 87, because the discontinuity at this location produced folding over of part of the carbon replica. The fracture appears somewhat intergranular and brittle at the inner edge and continues to be brittle for a considerable distance into the metal. The transition to ductile fracture near the specimen center was fairly sharp. There was no brittle-ductile-brittle transition from the surface to the specimen center, as occurred in 1042 specimens tested in 10,000-psi hydrogen.

Examination of the Inconel 718 fracture also was made by means of the scanning electron microscope, and Fig. 89 shows a scanning electron fractograph composite from approximately the same region as Fig. 86. The fracture appears intergranular and fairly brittle with cracks between the grains.

Figure 87 is a scanning electron micrograph of the crevice across the fracture in Fig. 85. This region is very ductile, indicating that this was not the fracture origin. The fracture surface from the side of the specimens opposite that in Fig. 86 and 89 is shown in Fig. 88. It can be seen that the fracture, including the edge, was considerably more ductile on this side. Thus, the region shown in Fig. 86 and 88 is believed to have been the fracture origin.

As discussed in Phase II, the Inconel 718 notched specimens were tested in a 10,000-psi helium environment contaminated with hydrogen. Examination was made of a specimen which had a 20 percent reduction of notch

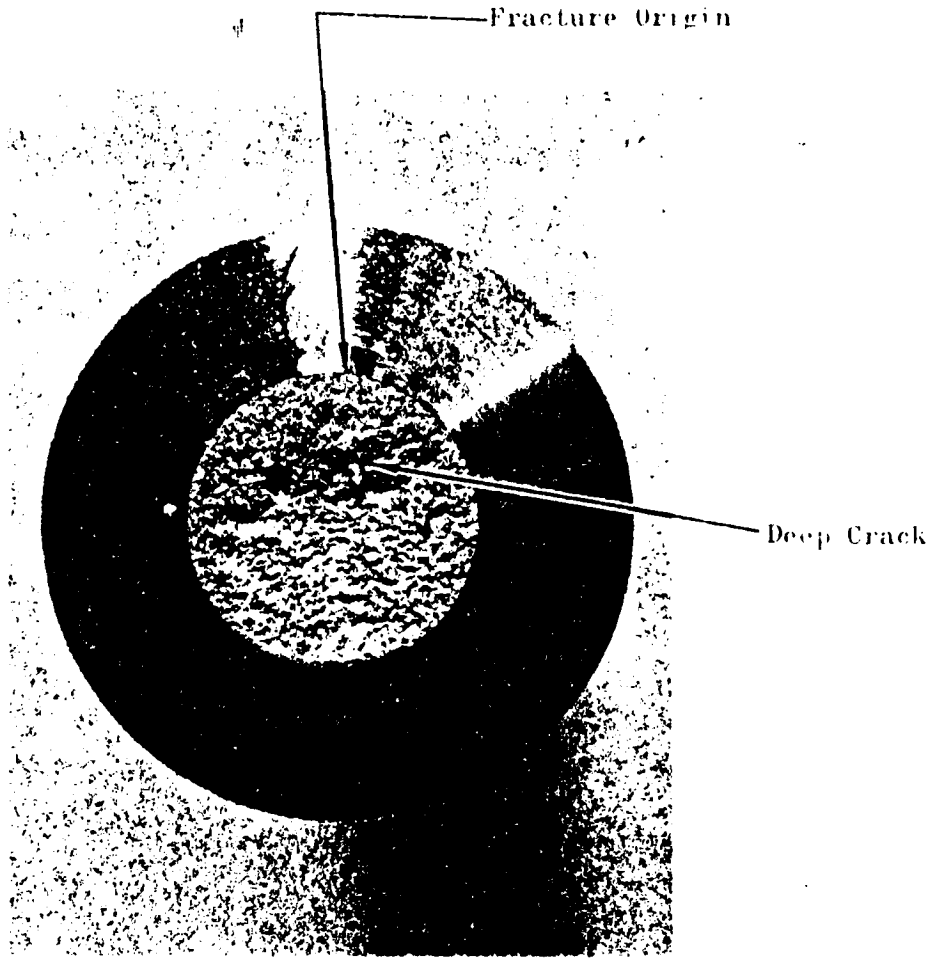

No. 1201 Photomacrograph 10X

Figure 85. Inconel 718 Notched Specimen Tested in 10,000-psi Hydrogen

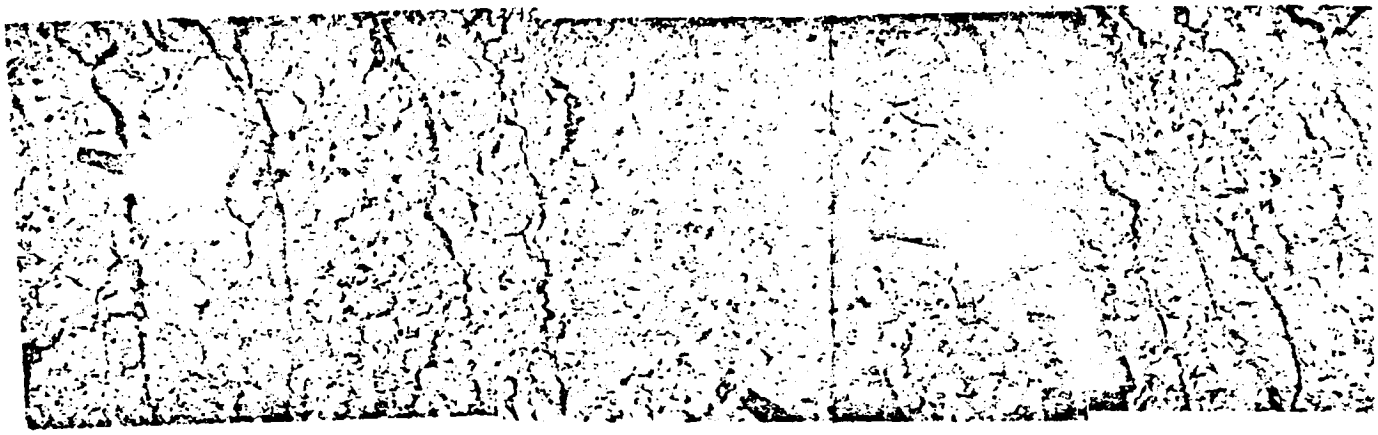

Continuation From A

Continuation From Region B

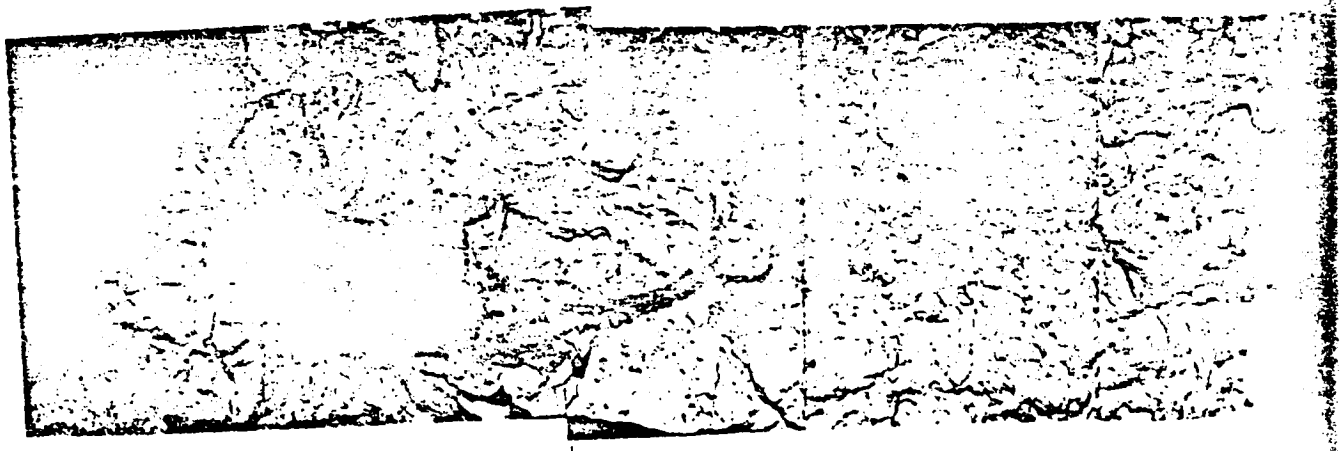

← Brittle Region | Ductile Region →

:ion Ductile Region →

245-A

← Machi

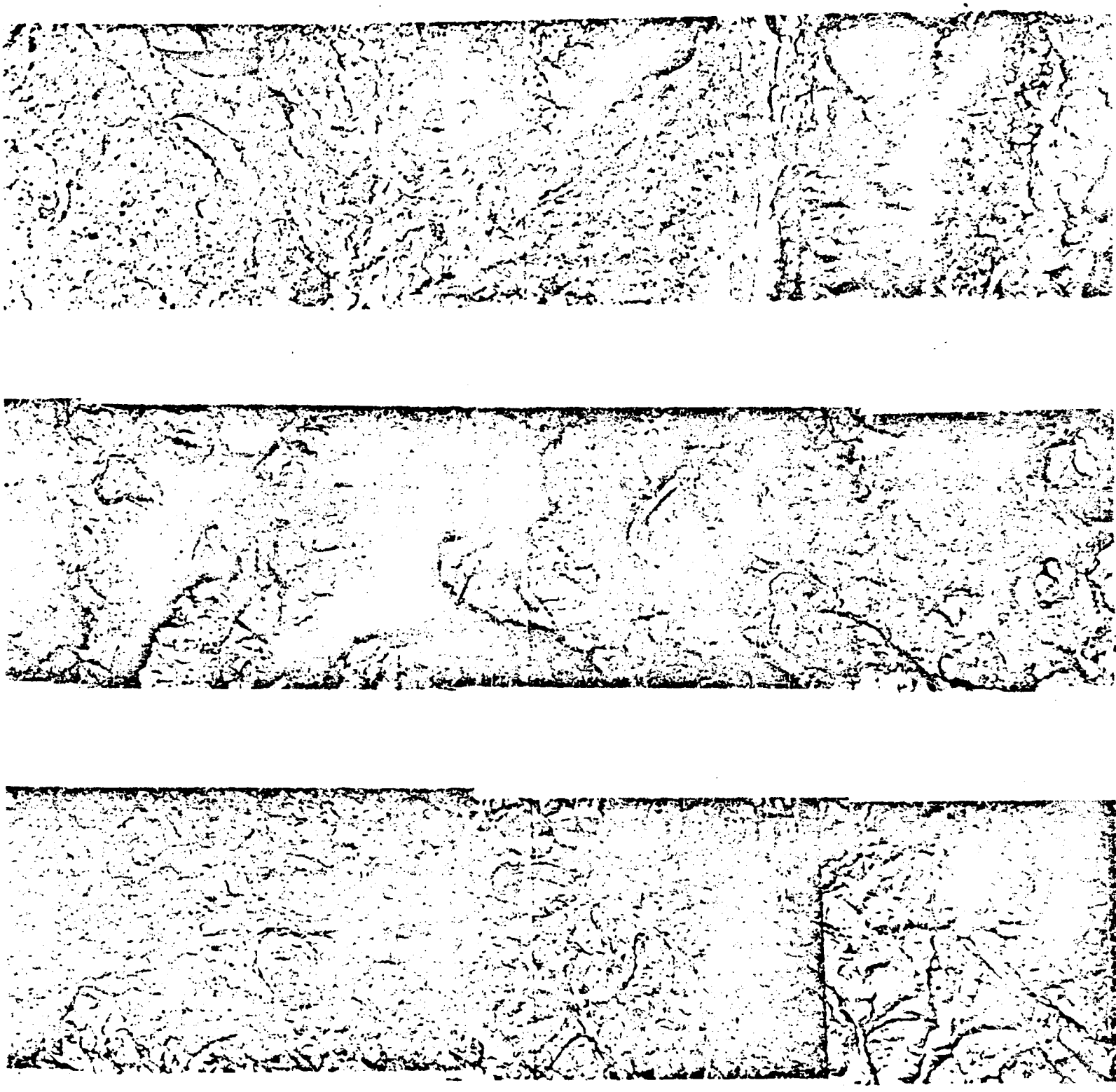

245/B

245/2

—— Machined Surface | Fractured Surface ⟶ Britt

Brittle Region

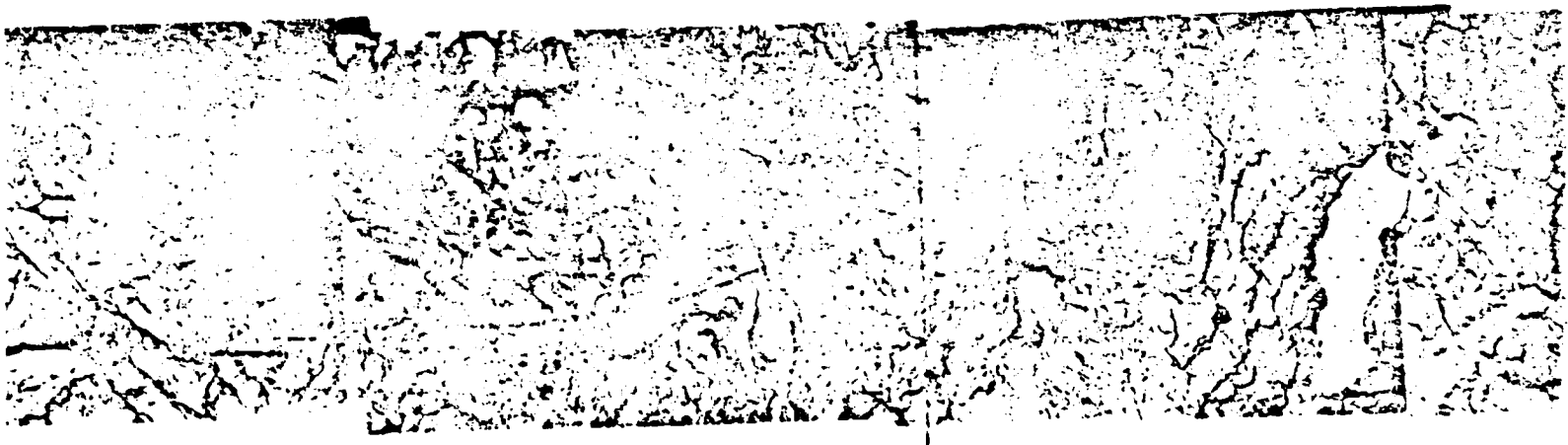

2 K5/c

I

Brittle Region

A

Region B

Fig

A

Region B

No. 1201 Electron Fractograph 1300X

Figure 86. Inconel 718 Notched Specimen Tested in 10,000-psi Hydrogen (view of the machined surface, machined surface, fractured surface interface, and into the fracture to the location of ductile region in center of specimen)

245- E

No. 1201 210X

Scanning Electron Fractograph

Figure 87. Inconel 718 Notched Specimen Tested in 10,000-psi Hydrogen (shows the crack in Fig. 85 at a higher magnification)

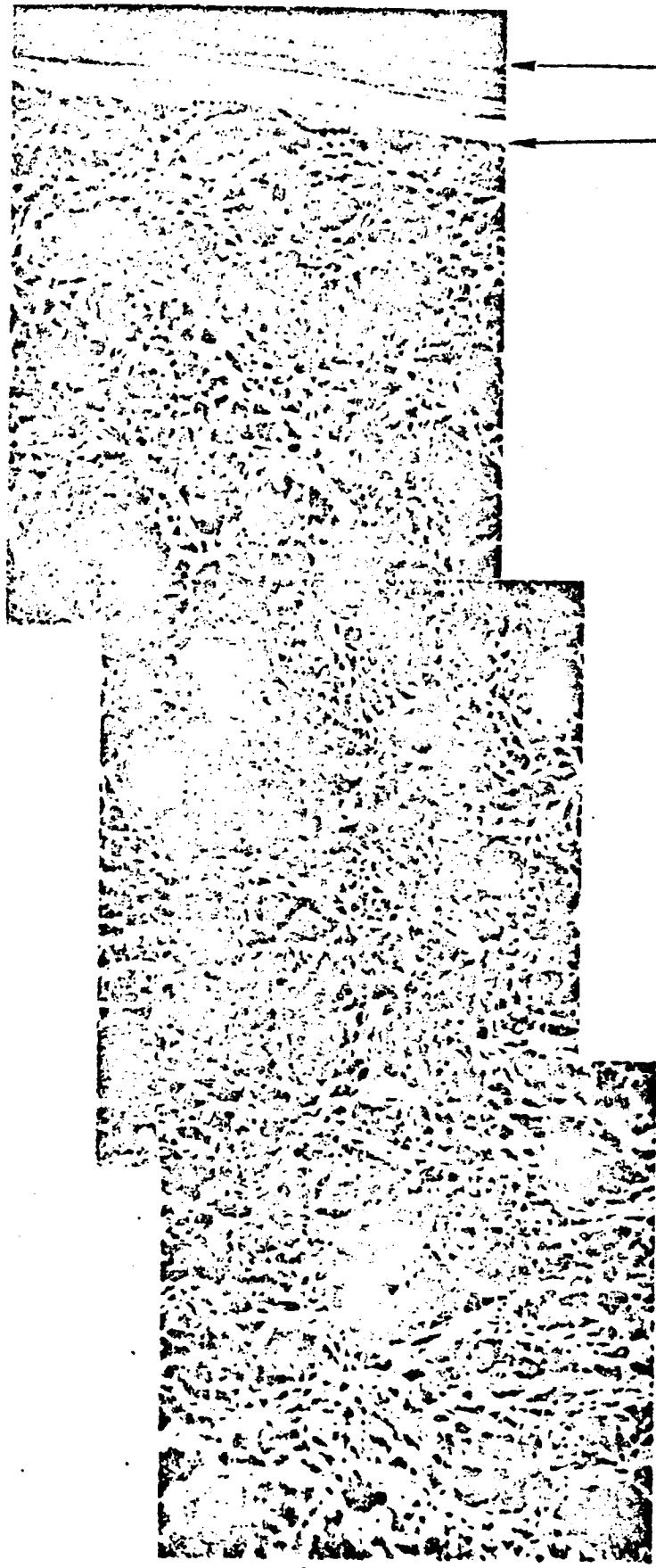

No. 1201 1020X

Scanning Electron Fractograph

Figure 88. Inconel 718 Notched Specimen Tested in 10,000-psi Hydrogen (opposite side of fracture shown in Fig. 86 and 89)

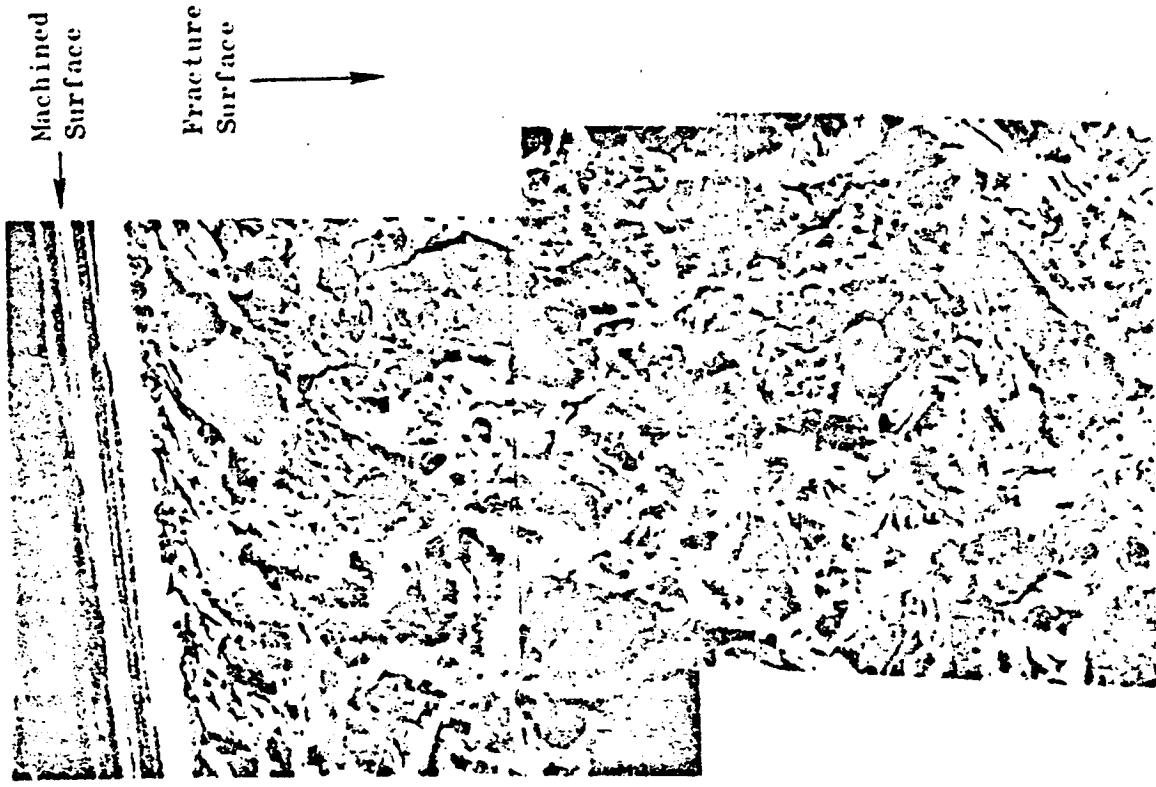

249

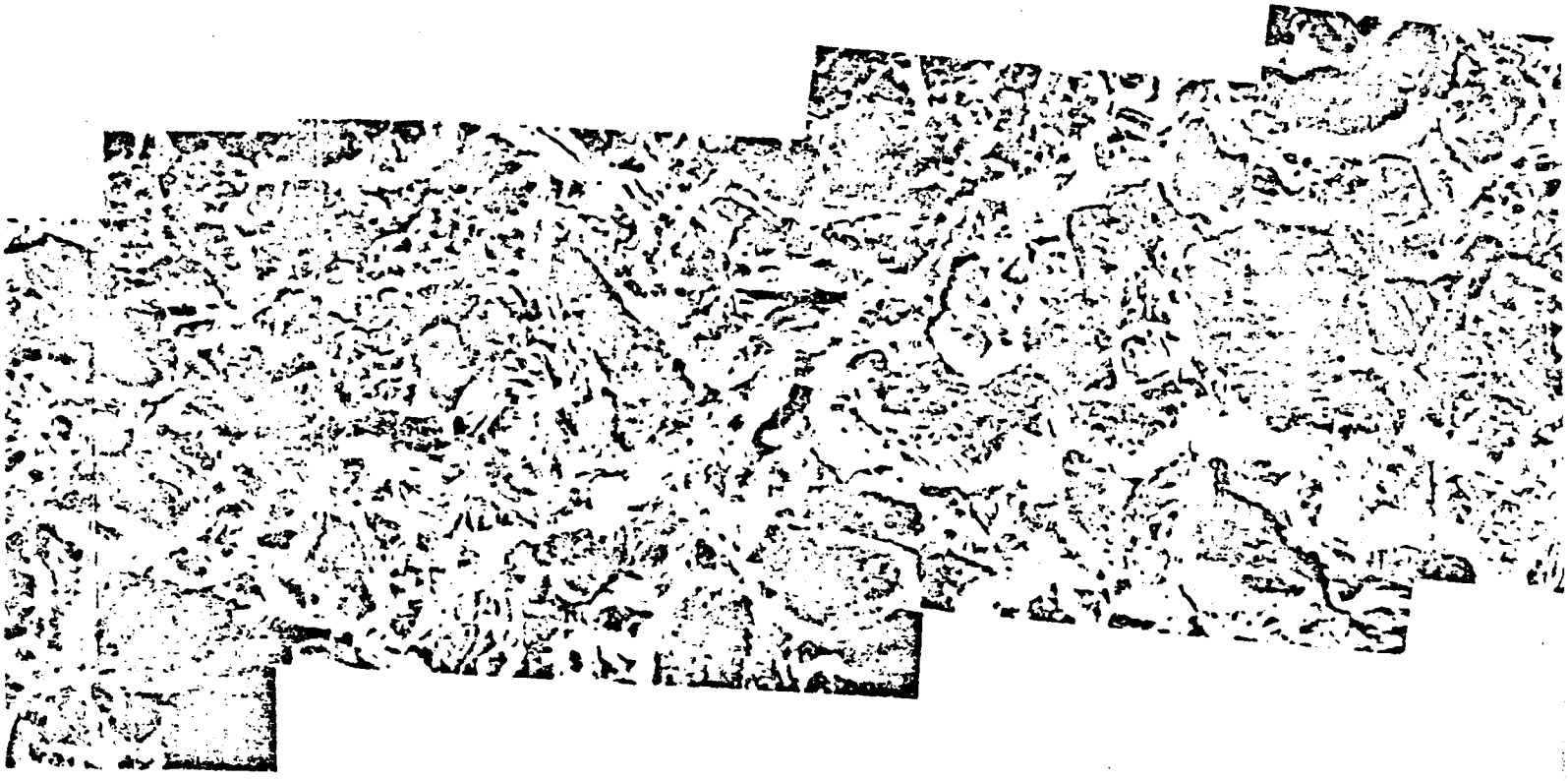

A

249,

B

249,

c

249

No. 1201 Scanning Electron Fractograph 1080X

Figure 89. Inconel 718 Notched Specimen Tested in 10,000-psi Hydrogen (the same specimen and approximately the same region as shown in Fig. 88; view of machined surface, machined surface, fractured surface interface and a short distance into the specimen)

strength due to the hydrogen contamination. Figure 90 is a low-magnification scanning electron micrograph of the fracture, with regions indicated that were examined at higher magnification. The fracture origin appeared as a dark ridge when viewed optically.

Figure 91 shows the fracture origin; it is seen that the fracture at this location was brittle and intergranular, with cracking at the edge. This fracture is thus similar to the fracture (Fig. 86 and 89) of an Inconel 718 specimen tested in 10,000-psi hydrogen.

Figure 92 is a scanning electron micrograph of the side opposite the fracture origin. It can be seen that this region is ductile, and therefore the area shown in Fig. 91 was indeed the point of crack initiation. The depression marked by "B" in Fig. 90 is shown at higher magnification in Fig. 93. This region is also very ductile, thus eliminating it as the point of crack initiation.

Examination of Titanium-Base Alloys

Fracture surfaces of the titanium specimens showed a considerable difference between those tested in air (or helium) and hydrogen environments. Visual examination showed a dark band on the fracture periphery of pure titanium and titanium alloy specimens that were embrittled by 10,000-psi hydrogen. There was no shear lip in the regions containing the dark band, although there was a thin, sometimes broken shear lip on the remainder of the specimen. The size of the band appeared to be directly proportional to the degree of embrittlement. That is, the specimens with the most strength reduction also had the largest dark band. Figure 94, a photomacrograph of the fracture of a notched Ti-6Al-4V STA specimen tested in 10,000-psi hydrogen, shows a dark band over 50 percent of the distance around this specimen. The specimen had 47 percent reduction of notch strength due to the hydrogen environment.

Preceding page blank

Fracture Origin

No. 1204 22X

Scanning Electron Fractograph

Figure 90. Inconel 718 Notched Specimen Tested in 10,000-psi Helium (Hydrogen Contaminated)

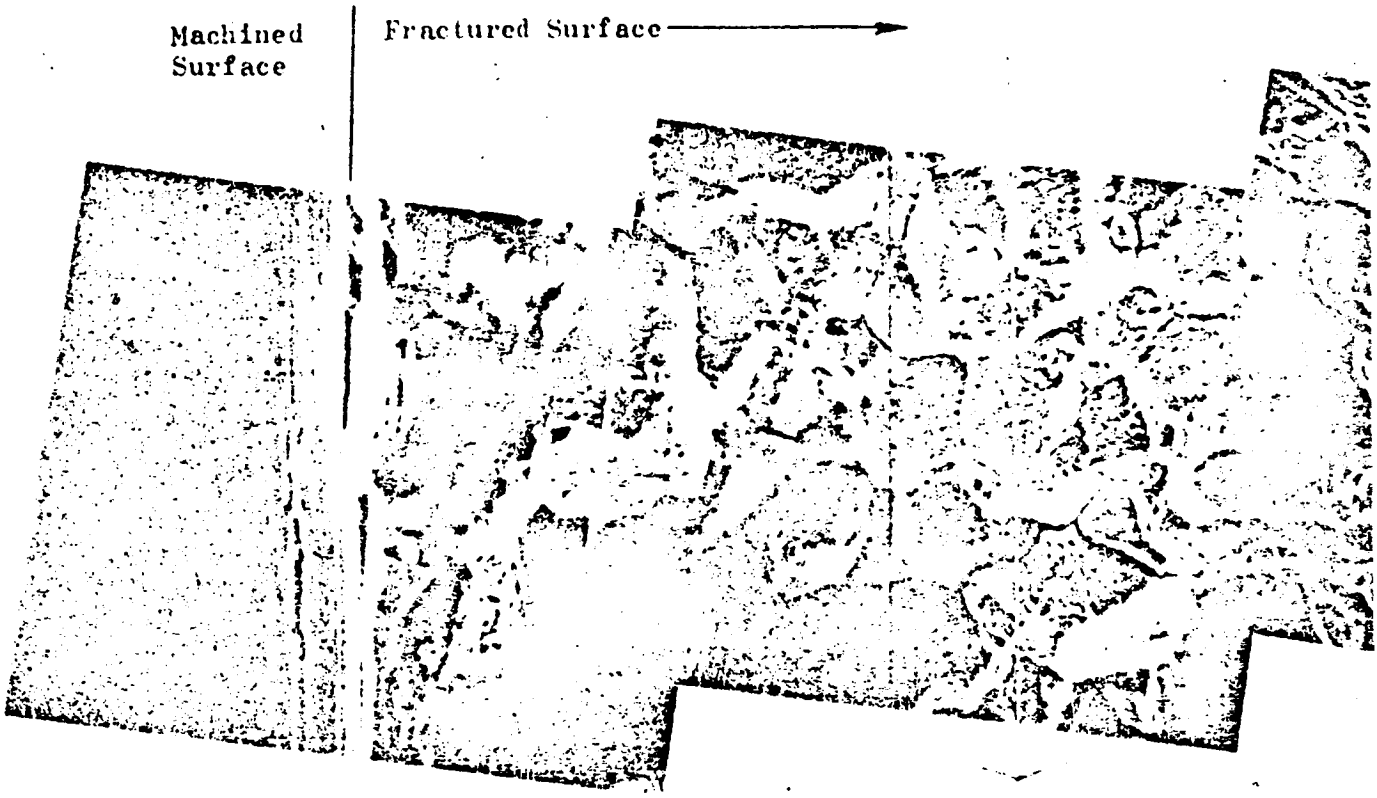

No. 1204

253 A

R-7780-1

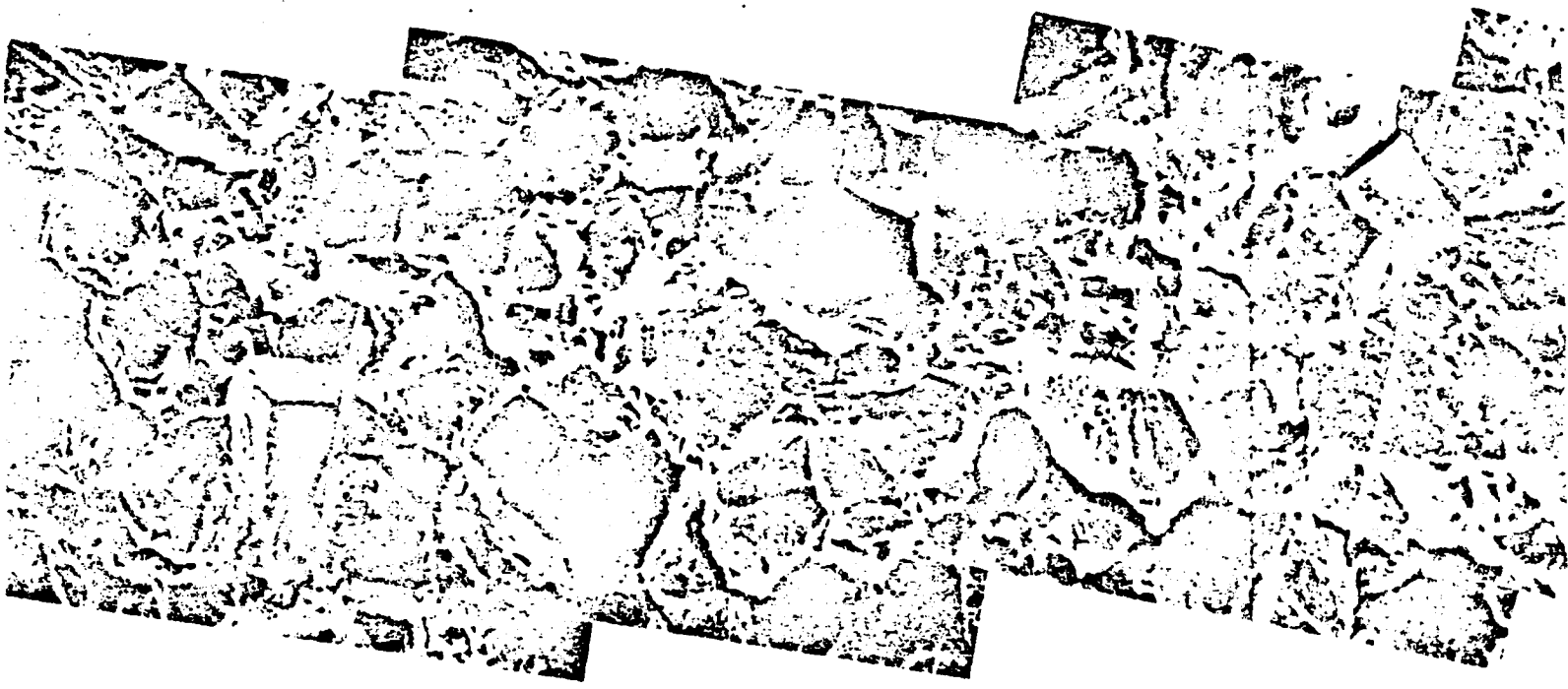

Scanning Electron Fractograph

253 B

1080X

Figure 91. Inconel 718 Notched Specimen Tested in 10,000-psi Helium (hydrogen contaminated); View of Machined Surface Fractured Surface Interface at Fracture Origin (shows brittle, intergranular fracture)

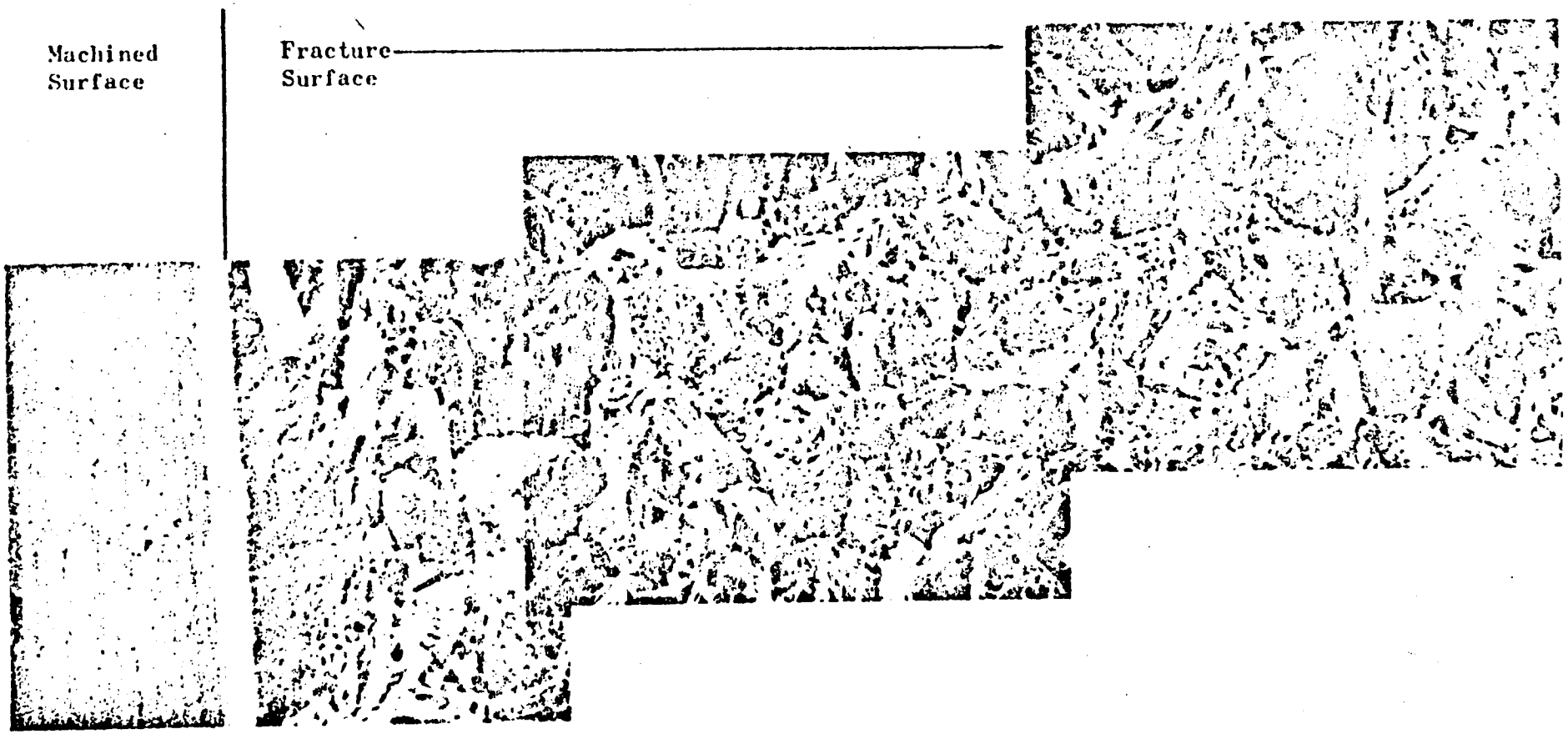

No. 1204 Scanning Electron Fractograph 1080X

Figure 92. Inconel 718 Notched Specimen Tested in 10,000-psi Helium (Hydrogen Contaminated); View of Edge of Fracture Surface at Side Opposite Fracture Origin; Position "A" in Figure

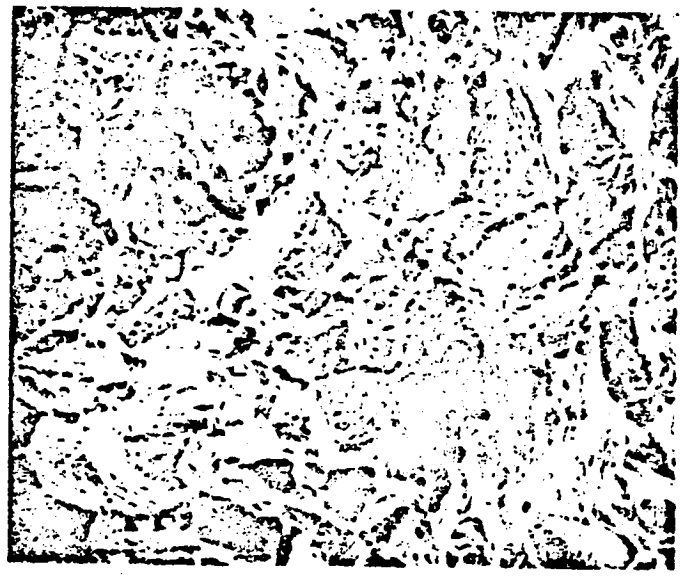

No. 1204 1080X

Scanning Electron Fractograph

Figure 93. Inconel 718 Notched Specimen Tested in 10,000-psi Helium (Hydrogen Contaminated); Region "B" of Figure 90

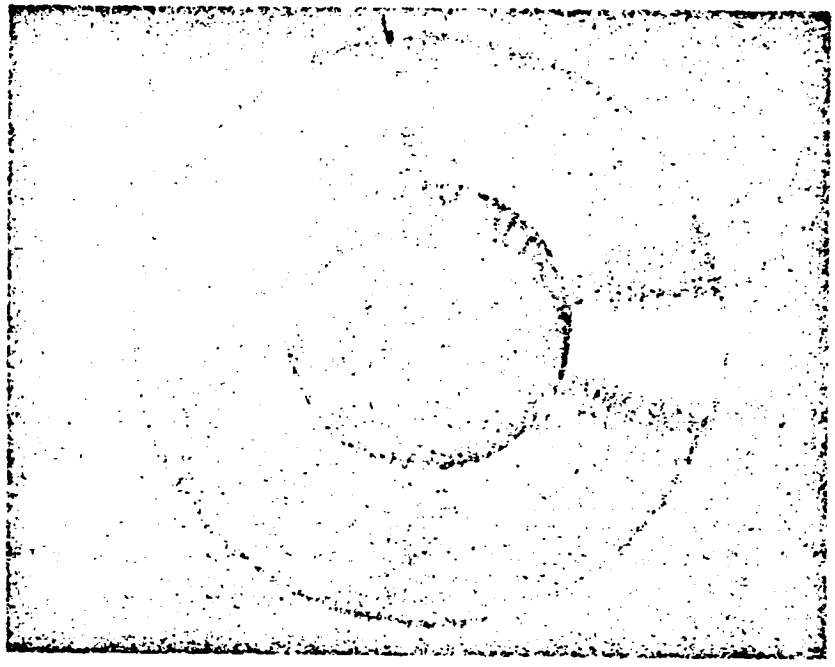

No. E207 Photomacrograph 10X

Figure 94. Ti-6Al-4V STA Notched Specimen Tested in 10,000-psi Hydrogen (47 percent reduction of notch strength)

Composite electron fractographs of commercially pure titanium specimens tested in air and in 10,000-psi hydrogen are shown in Fig. 95 and 96. The fracture in air is very ductile, consisting entirely of large dimples. The fracture in 10,000-psi hydrogen was very brittle at the edge and into the metal about 0.01 inch. This brittle region contained a large number of short secondary cracks, while the ductile region had the same appearance as the fracture of the titanium specimen tested in air.

The specimen illustrated in Fig. 96 was tested after the test vessel was evacuated and, consequently, there was a large reduction of notch ductility. A titanium specimen was also tested in 10,000-psi hydrogen without prior test vessel evacuation, and there was essentially no embrittlement. A composite electron fractograph of this specimen is shown in Fig. 97, and stereo views at two positions on the fracture periphery appear in Fig. 100. A thin dark ring was present around the entire fracture periphery of this specimen. This brittle region is considerably shorter than that of the more severely embrittled specimen shown in Fig. 96. The most interesting part of the fractograph is the nature of the machine marks on the machined surface adjacent to the machine surface-fracture surface interface. The curved nature of these marks indicate that some deformation has occurred. It is evident that fracture initiated at the surface, but only after a considerable amount of plastic deformation. This suggests that the role of vacuum evacuation may be to decrease the amount of plastic deformation required to initiate a crack at this location because the machine marks are not curved when vacuum purging precedes hydrogen environment testing (Fig. 96).

Composite electron fractographs from annealed Ti-6Al-4V specimens tested in 10,000-psi helium and 10,000-psi hydrogen are shown in Fig. 98 and 99. The fracture of the specimen that was tested in 10,000-psi helium was ductile even at the edge. The dark band along the edge was examined by means of stereoscopic micrographs and was found to represent a ledge rather than a broad crack. It appears that there was shear-like tearing near the edge that produced this ledge. The dimples had a finer texture in Ti-6Al-4V than in the commercially pure titanium specimen examined.

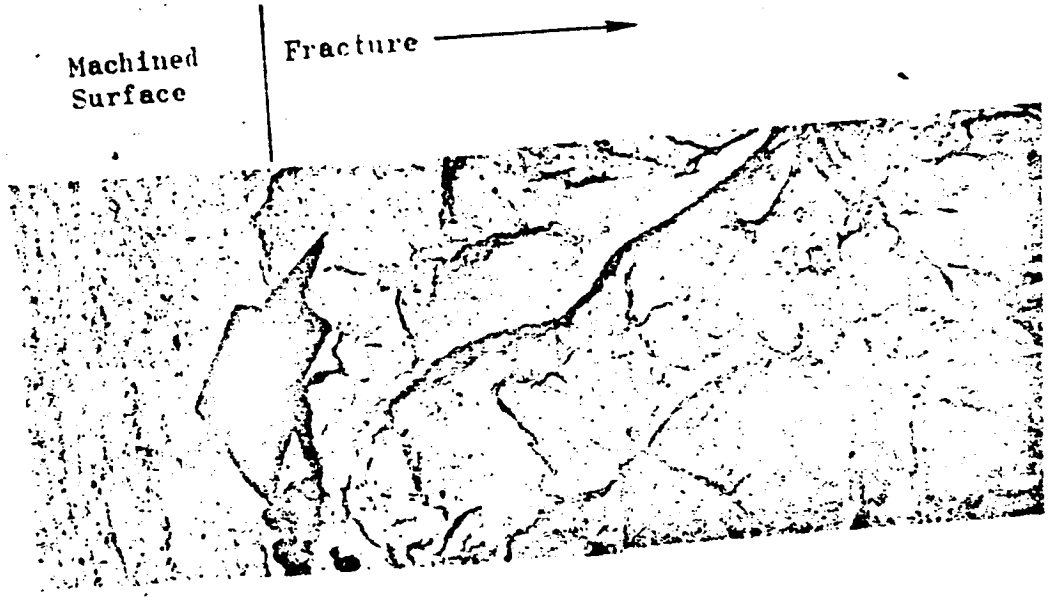

No. 955

A 259

R-7780-1

e

259-B

Electron Fractograph

259-d

Figure 95. Commercial Pure Titanium Notched Specimen Tested in Air (1 atm); View of Machined Surface Fractured Surface Interface and Into the Fracture. Fracture Consists of Large Ductile Dimples

No. 957

Preceding page blank

261-A

Brittle Hydrogen-Aff

261-B.

Brittle Hydrogen-Affected Region ⟶

Electron Fractograph

261-C

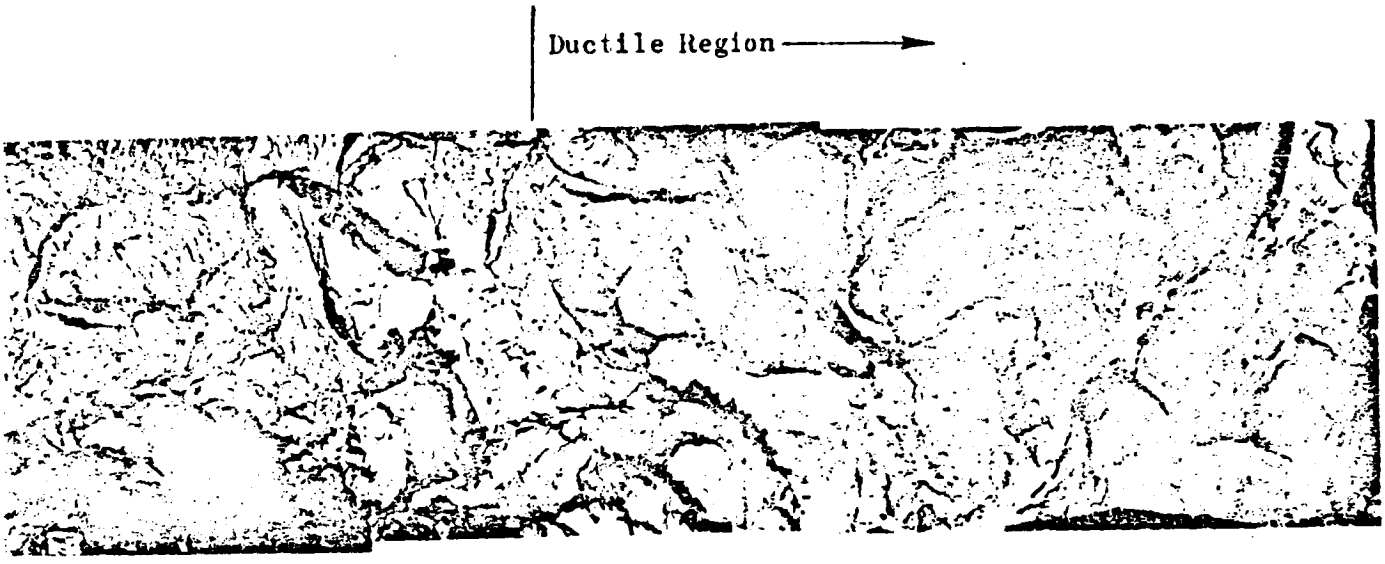

Figure 96. Commercially Pure Titanium Notched Specimen Tested in 10,000-psi Hydrogen (Test cell evacuated prior to testing); View of Machined Surface, Fractured Surface Interface and Into the Fracture to the Location of the Ductile Region.

Machined Surface

No. 954

263-A

Preceding page blank

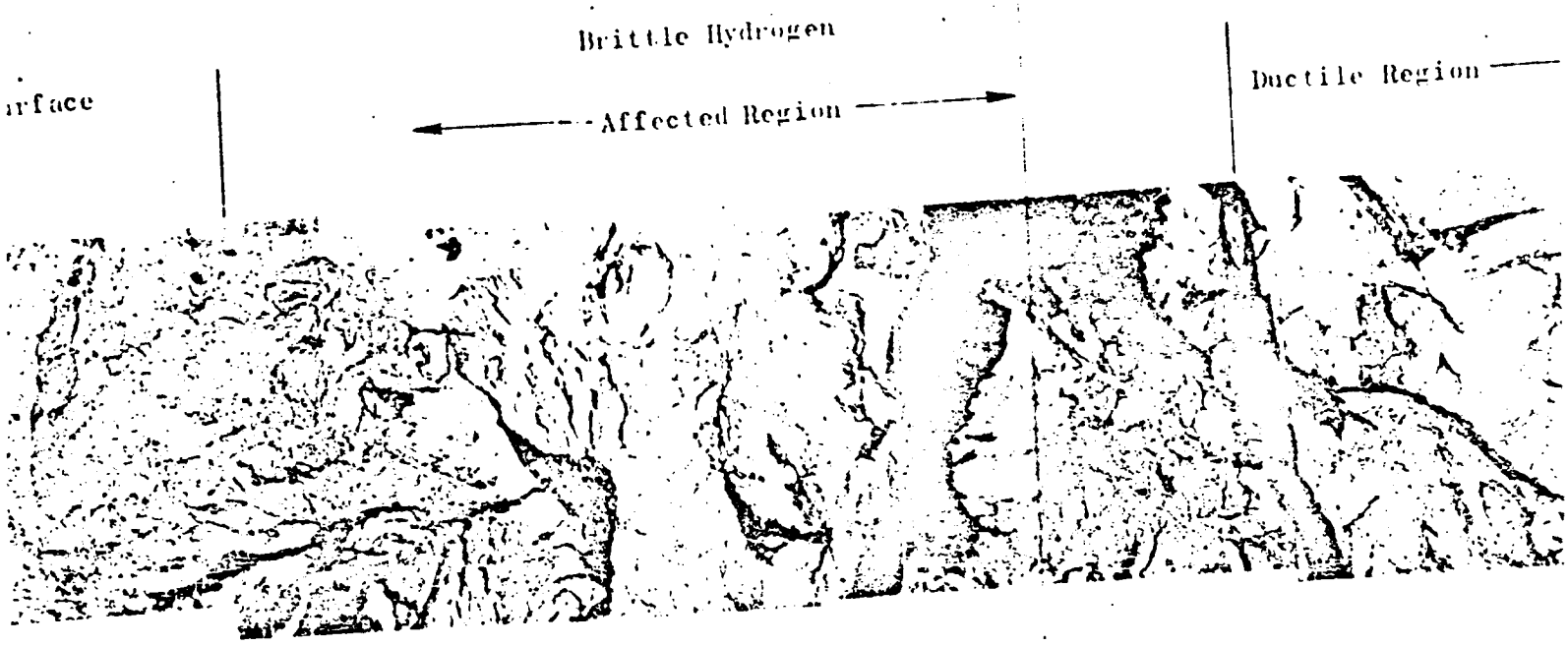

263-B

ctile Region →

Electron Fractograph

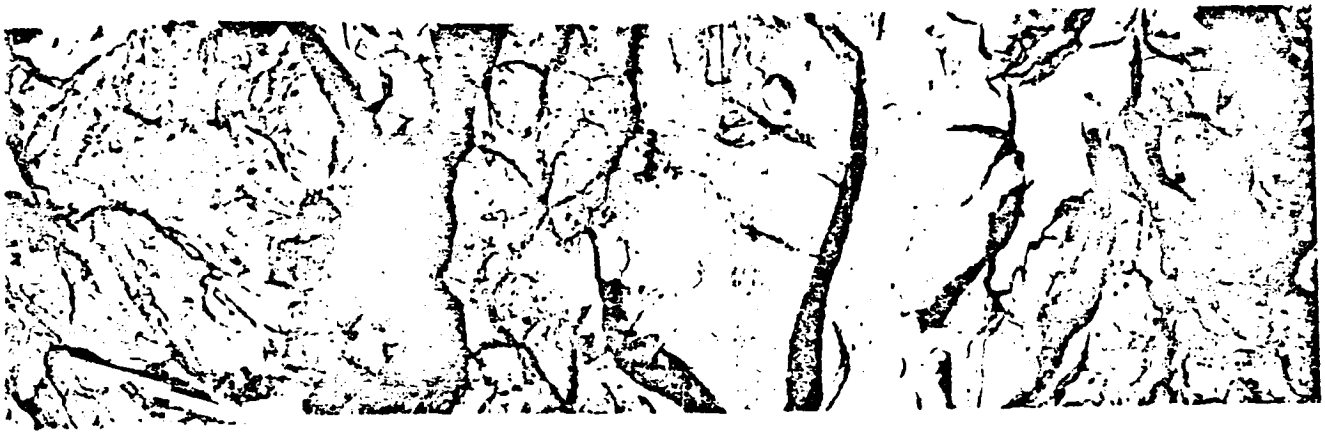

X

Figure 97. Commercially Pure Titanium Notched Specimen Tested in 10,000-psi Hydrogen (Test cell not evacuated prior to testing); View of Machined Surface, Fractured Surface, Interface and Into the Fracture to the Location of the Ductile Region

Machined Surface

Fractured Su

Stereo Pair

No. E 150

265-A

R-7780-1

Preceding page blank

Fractured Surface

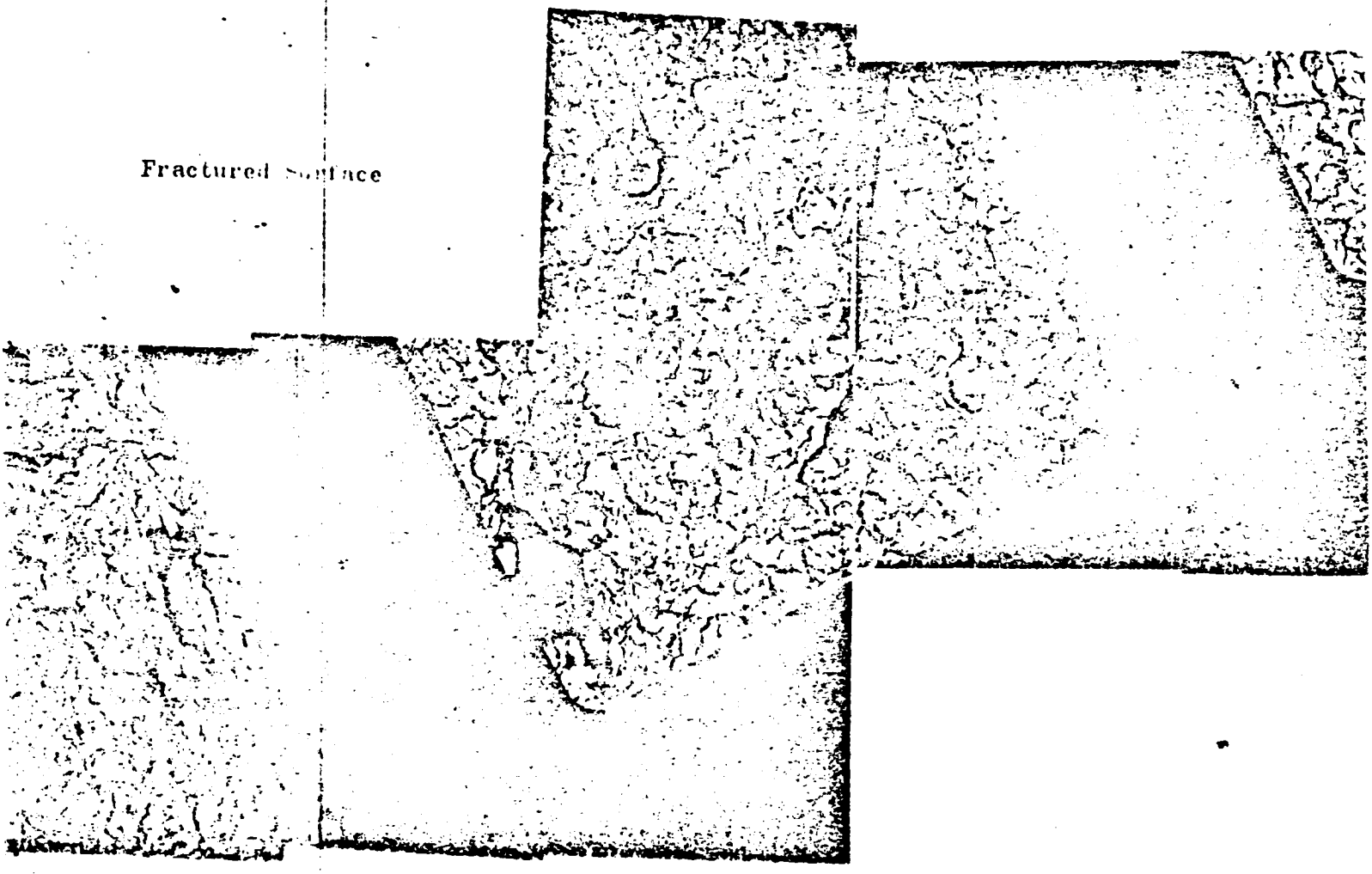

Electron Fractograph

A
5/266

265-B

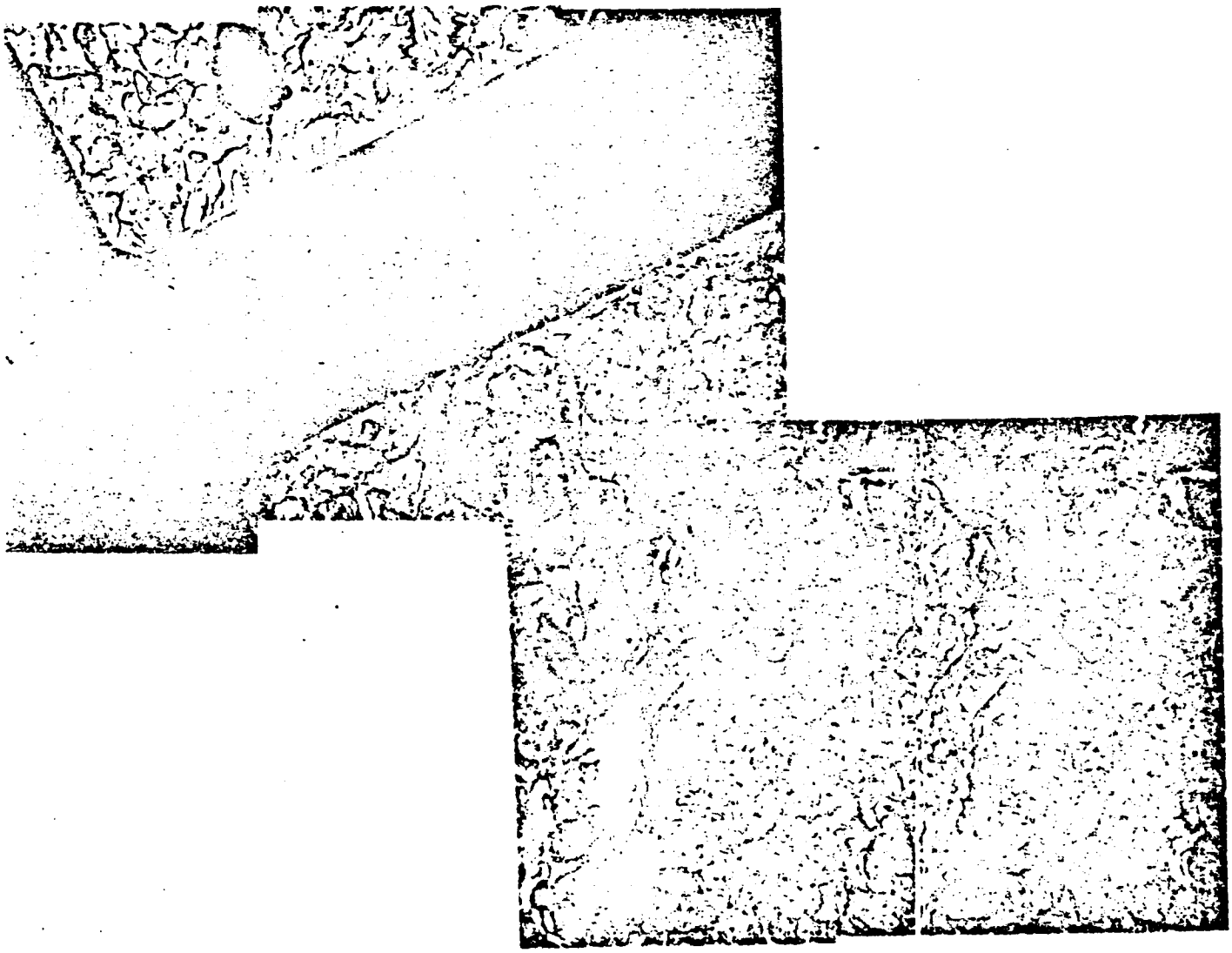

Figure 98. Ti-6Al-4V Annealed Specimen Tested in 10,000-psi Helium; View of Machined Surface, Machined Surface-Fractured Surface Interface, and the Fractured Surface

Machined Surface

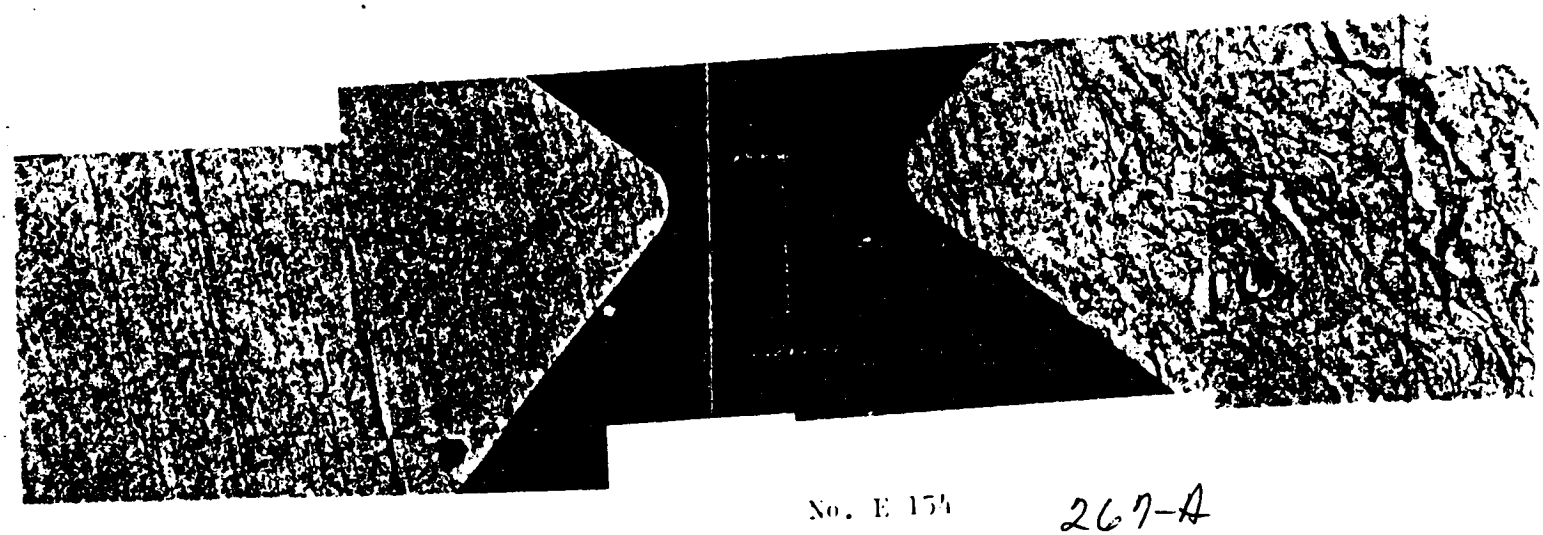

No. E 154 267-A

Preceding page blank

d Surface

Fractured Surface

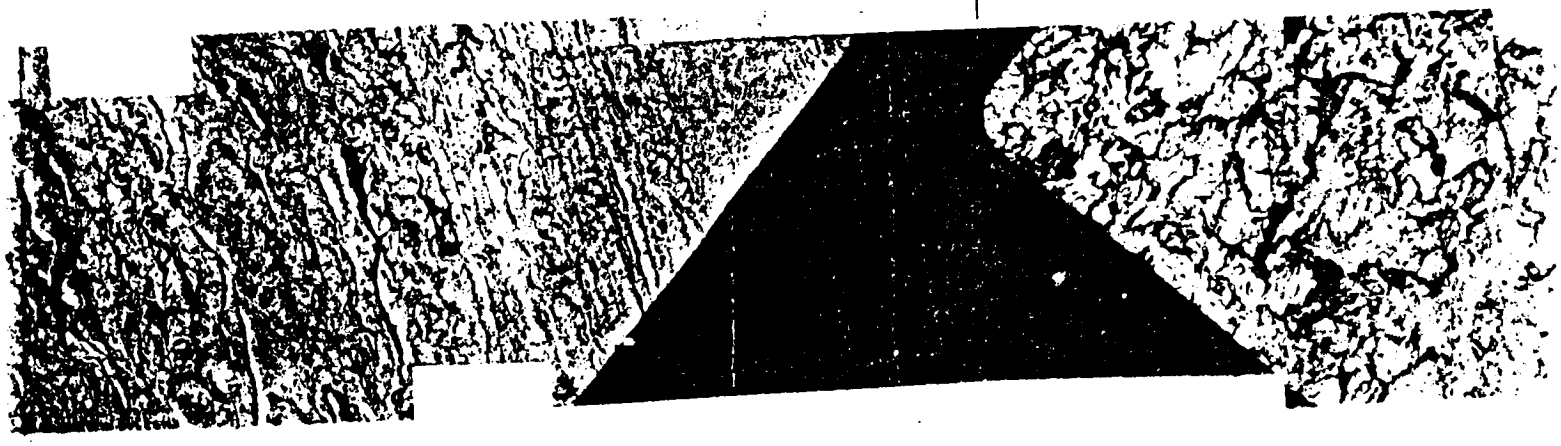

267-B

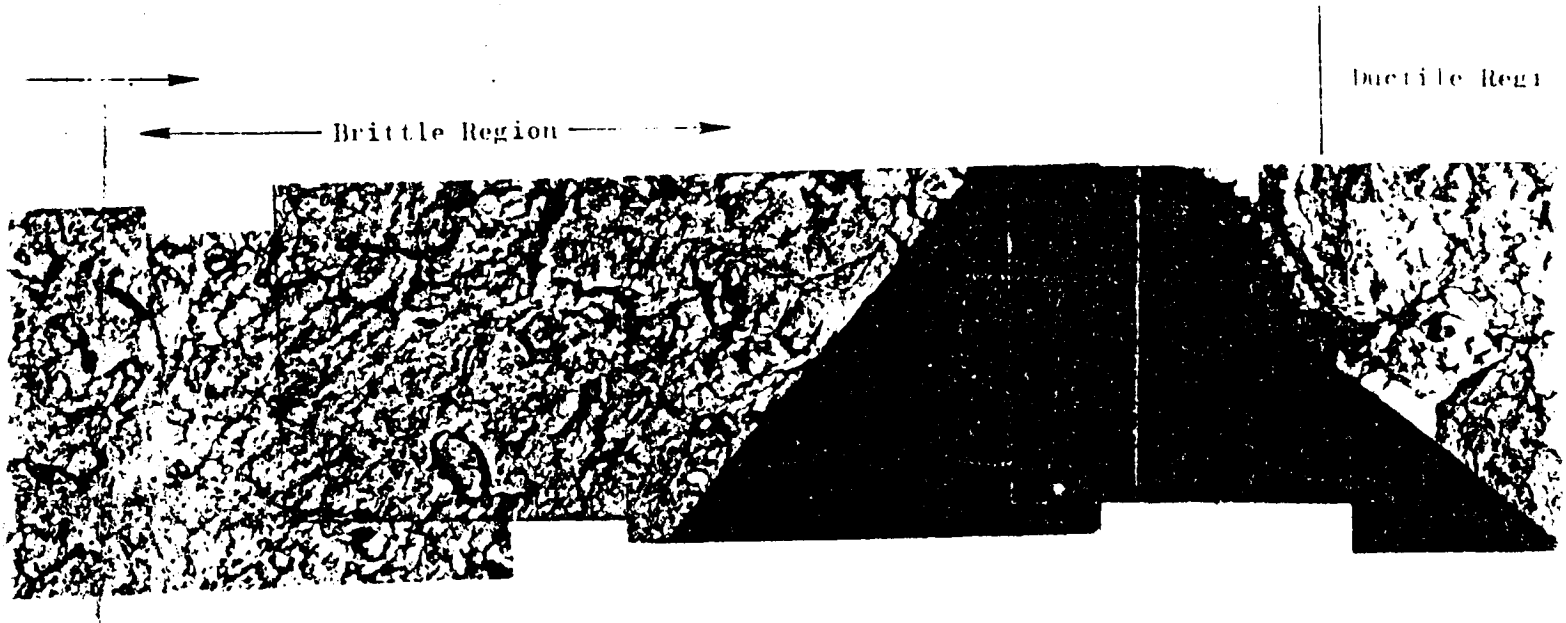

Electron Fractograph

267-C

uctile Region

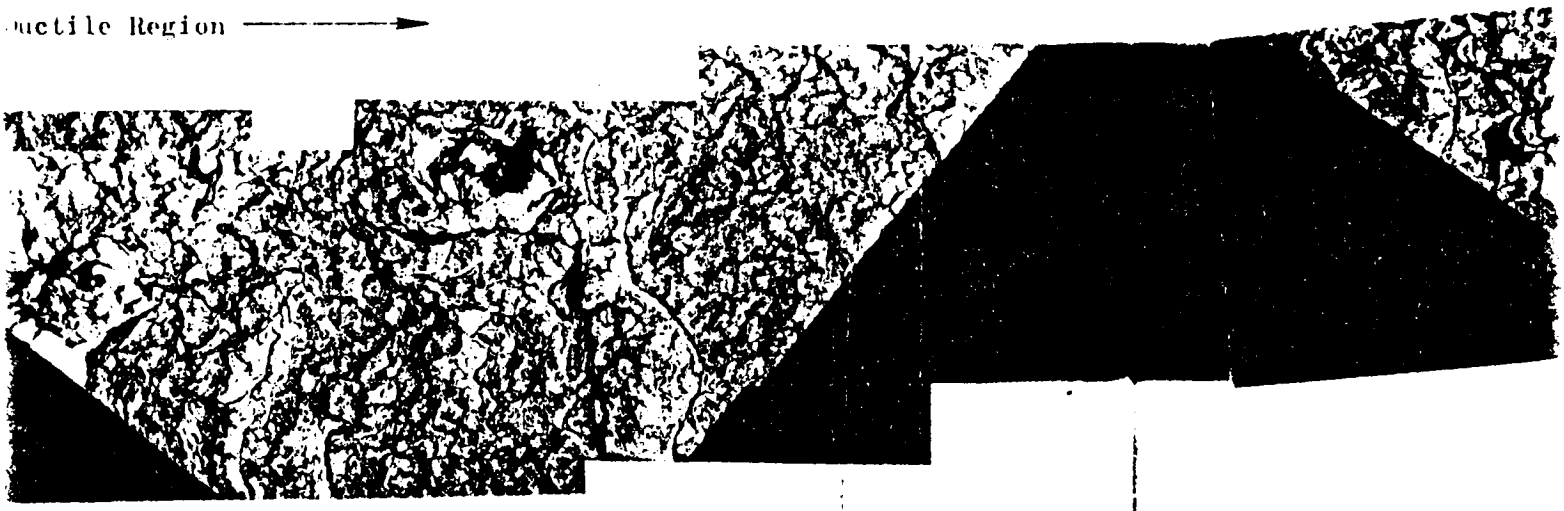

Figure 99. Ti-6Al-4V Annealed, No[illegible] [illegible]n Tested in 10,000 [illegible] Hydrogen; View of the [illegible]face, Machined Surfa[illegible] Fractured Surface Inte[illegible] [illegible]into the Fracture to [illegible] Location of Ductile Re[illegible] [illegible]er of Specimen

267-D

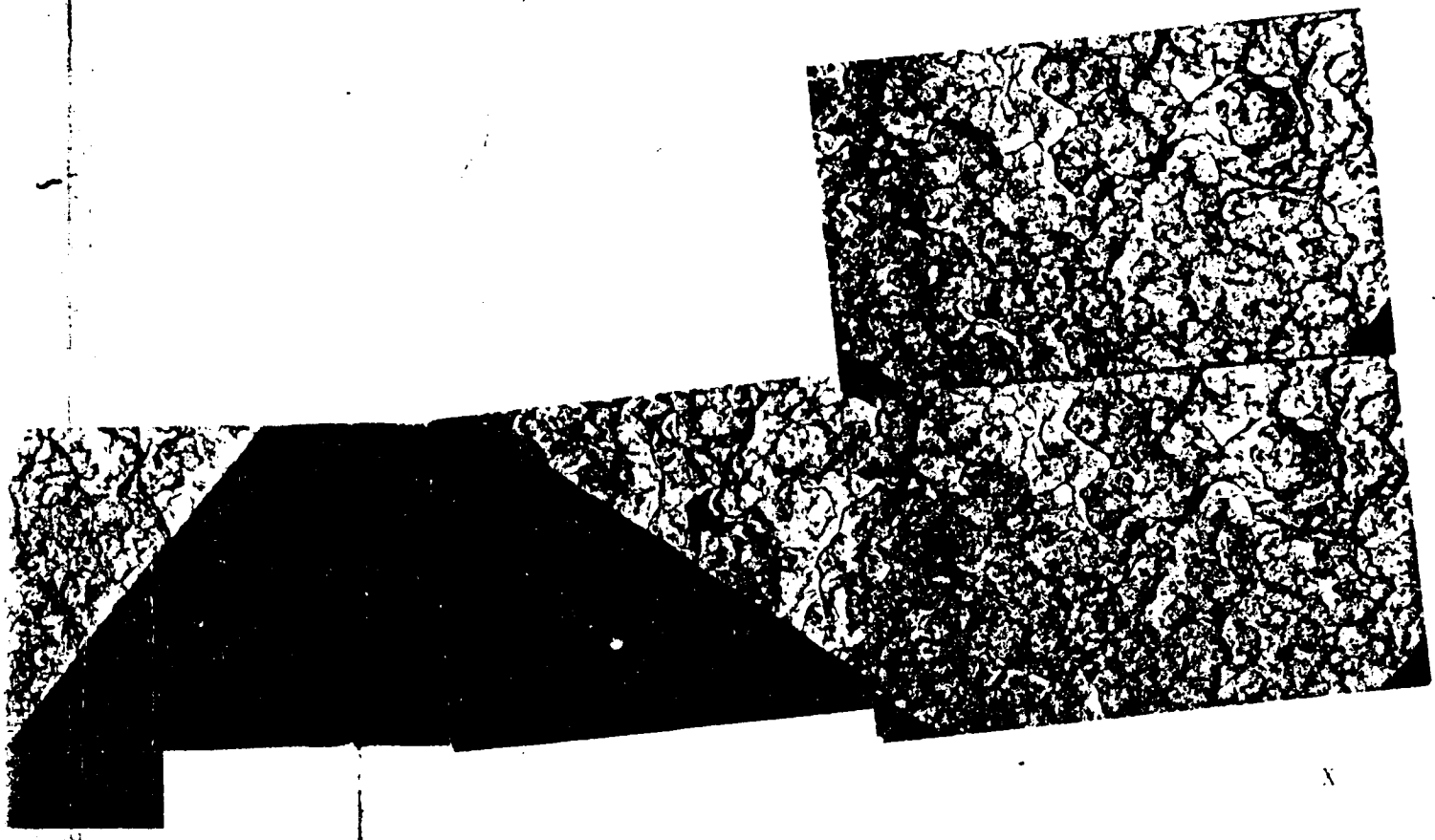

Stereo Pair

X

·Al-4V Annealed, Not[illegible] [illegible]en Tested in 10,000-psi
·ogen; View of the M[illegible] [illegible]rface, Machined Surface
·ctured Surface Inter[illegible] [illegible] Into the Fracture to the
·ation of Ductile Re[illegible] [illegible]er of Specimen

267-E

No. 954 Electron Fractograph 1000X

a. Edge Shown in Figure 97

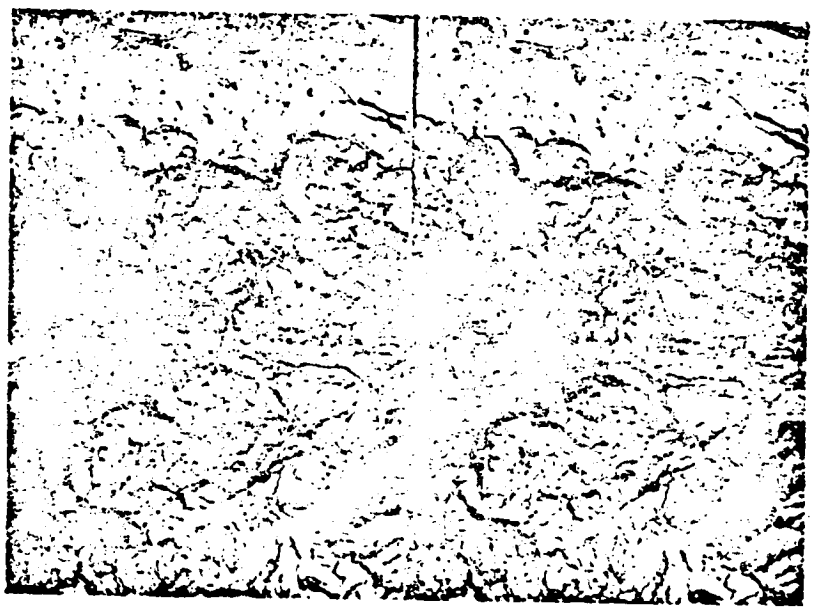

No. 954 Electron Fractograph 1000X

b. Edge at Another Point

Figure 100. Commercially Pure Titanium Notched Specimen Tested in 10,000-psi Hydrogen (Test cell not previously evacuated prior to testing); Stereo Views at the Edge of the Fracture Surface

Figure 99 shows that cracking of the machined surface immediately adjacent to the edge of the fracture surface occurred in 10,000-psi hydrogen. The fracture immediately adjacent to the edge was brittle and contained a large density of secondary cracking. The amount of secondary cracking of the fracture decreased, and the fracture appearance became more ductile with increasing distance from the edge.

Fractures of the commercially pure titanium and Ti-6Al-4V specimens tested in hydrogen were basically the same, although there was considerable more cracking on the machined surface of Ti-6Al-4V than on commercially pure titanium. Secondary cracking in the fracture appeared as fine parallel lines on commercially pure titanium but as random lines on Ti-6Al-4V.

For both materials the brittle areas were transgranular rather than intergranular. The latter is characteristic of the embrittlement of titanium alloys by absorbed hydrogen. There was also no indication of a second phase (hydride) associated with the fractures. Optical micrographs also showed no indication of a hydride phase or of intergranular attack (Fig. 101).

Shear Lip Formation on Notched Specimens

Posttest examination of the notched specimens of the iron-, nickel-, and titanium-base alloys indicated that shear lip formation was generally characteristic of fractures occurring in air and helium environments, but not of fractures occurring in hydrogen environments. In some instances (i.e., titanium alloys) a shear lip formed on the side opposite the region of fracture initiation on specimens tested in hydrogen. The hydrogen-affected region of the severely embrittled low-alloy steels extends around the entire fracture; no shear lip was observed on these specimens. These same specimens usually contained complete shear lips when tested in air or in helium environments. There were, however, many specimens that did not form shear lips in either 10,000-psi helium or 10,000-psi hydrogen environments. High-strength steels were in this

No. 979 Photomicrograph 500X

Figure 101. Commercially Pure Titanium Unnotched Specimen Tested in 10,000-psi Hydrogen

category. Notched austenitic stainless-steel specimens also did not have shear lips, as such, but instead contained numerous shear-type hilly regions throughout the fracture.

The previous program (Ref. 2) was conducted on low alloy steels, which are in the "severely" embrittled category, and it was observed that shear lip formation on notched specimens occurred in inert environment, but not in hydrogen environments. Results of the present program therefore showed that the existence of a shear lip was not as definitive an indication of hydrogen-environment embrittlement as it was for the three steels studied previously.

Examination of Fatigue-Tested Specimens

Electron fractographs were obtained from representative notched and precracked specimens fatigue cycled in 10,000-psi helium and 10,000-psi hydrogen. Figure 102 shows the fracture of an ASTM A-517 specimen that failed after 250 cycles in helium. Fatigue striations are quite evident on this fracture. Those adjacent to the machine surface may be from the high-cycle pre-cracking, while those somewhat removed from the initial group were caused by low-cycle fatigue. Examination of other fractures, however, required high magnification to resolve the fatigue striations in high-cycle fatigue precrack region, and it is therefore possible that essentially all of the observed striations in Fig. 102 are due to the low-cycle fatigue. Final failure of this specimen was very ductile as indicated by the dimples on the right side of Fig. 102.

Electron fractographs of an ASTM A-517 specimen that failed after 191 cycles in 10,000-psi hydrogen and on ASTM A-302 specimen that failed after 3281 cycles in 10,000-psi hydrogen are shown in Fig. 103 and 104. There are no indications of fatigue striations on any part of the fractures, including the fracture area adjacent to the machined surface which was high cycle fatigue precracked in air. The brittle region in

Machined Surface

No. B-168

273-A

Fatigue Region

Electron Fractograph

273-B

Ductile Failure

1500X

Figure 102. ASTM A-517 Notched and Precracked Specimen Tested in Low Cycle Fatigue in 10,000-psi Helium Environment; Failed After 250 Cycles

273-C

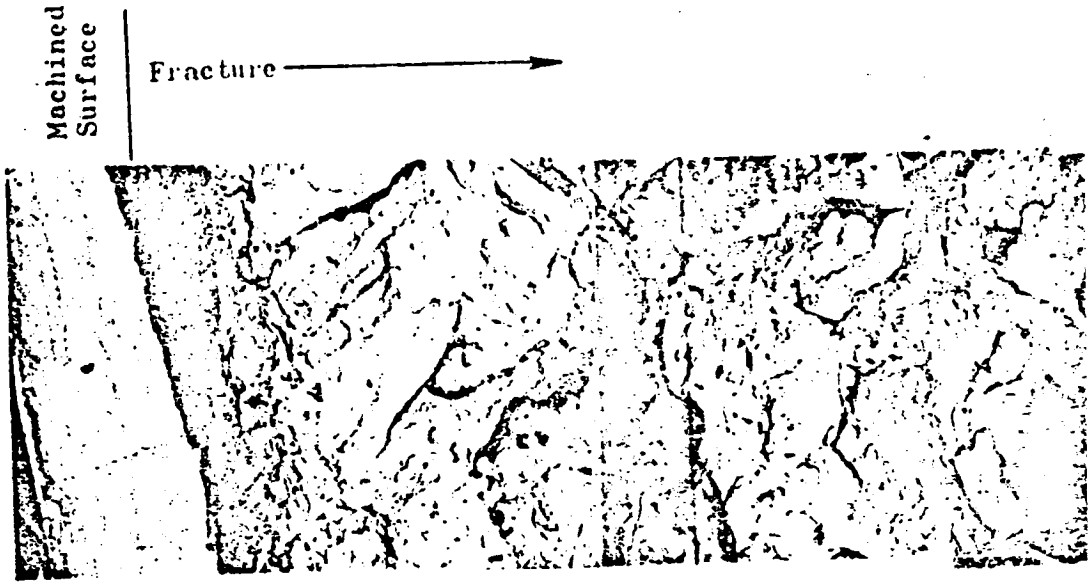

Continuation

Preceding page blank

275-A

Electron Fractograph

275-B

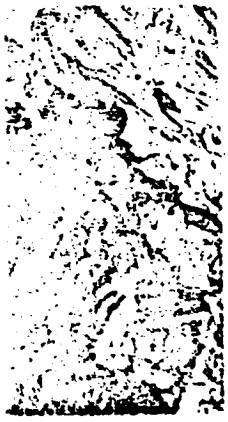

Figure 103. ASTM A-517 Notched and Precracked Specimen Tested in Low Cycle Fatigue in 10,000-psi Hydrogen Environment; Failed After 191 Cycles.

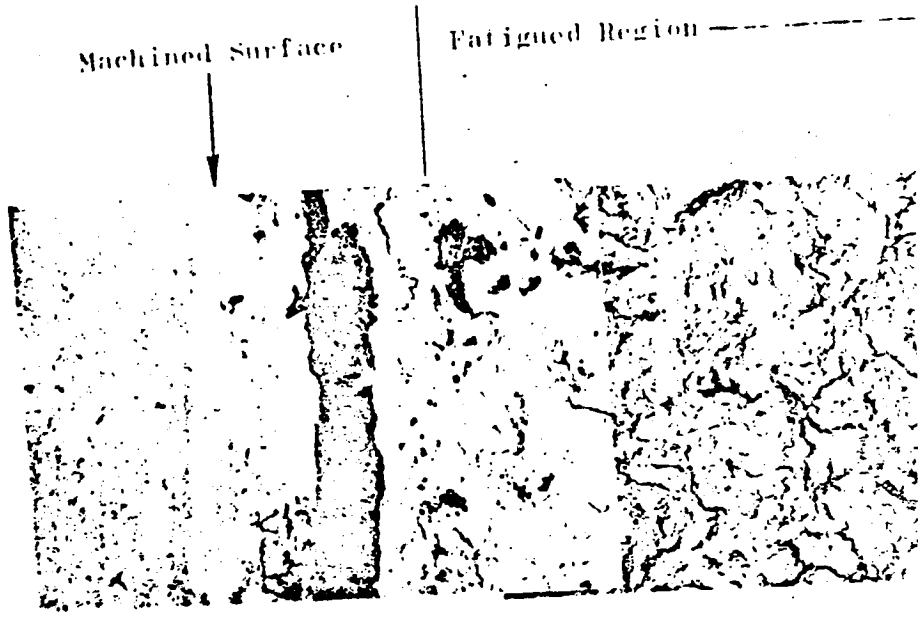

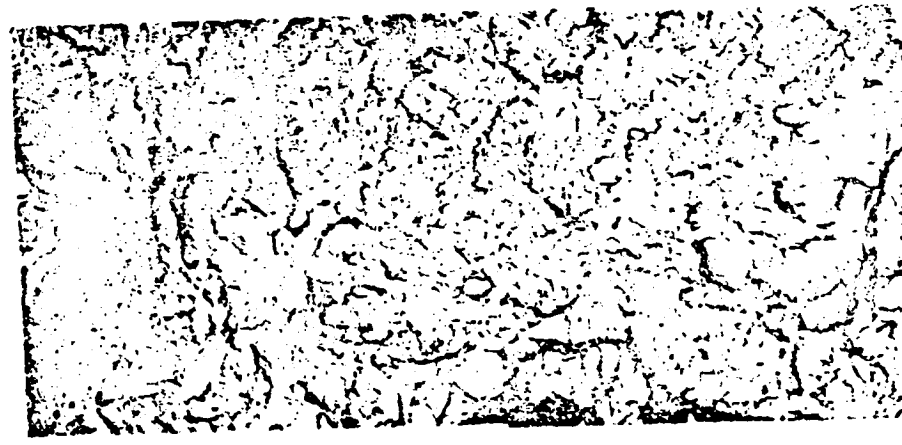

No. A-185

277-a

B-7780-1

Preceding page blank

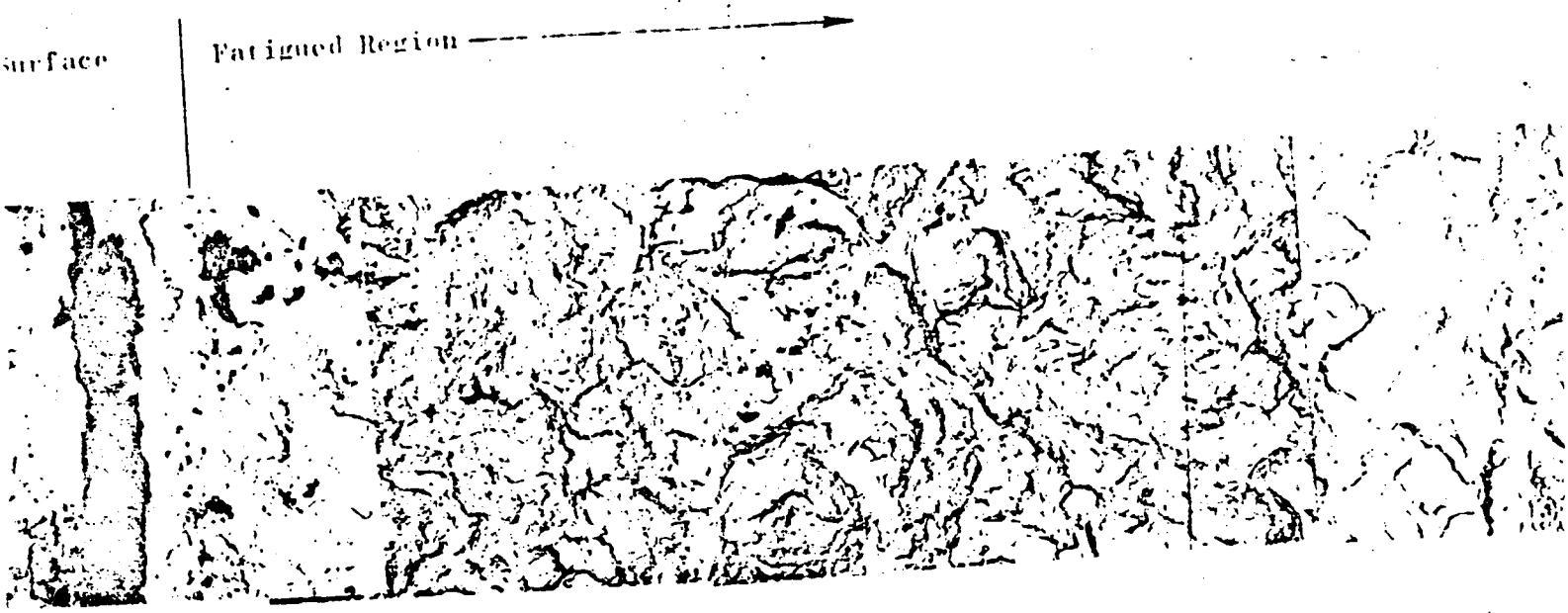

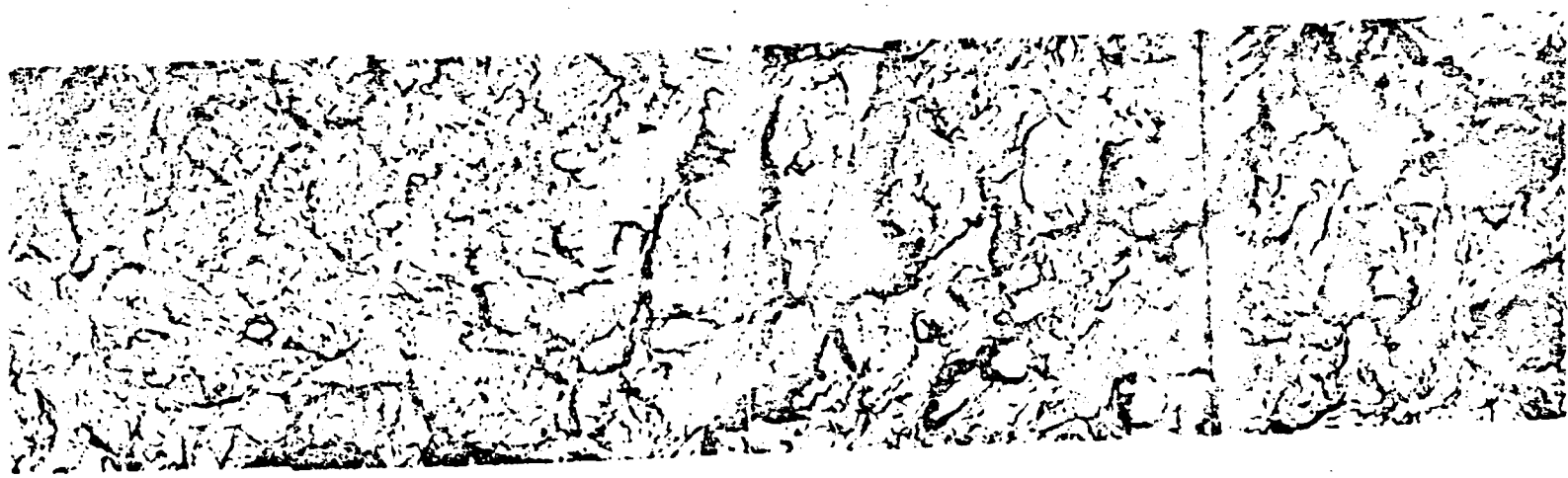

A-185

277-B

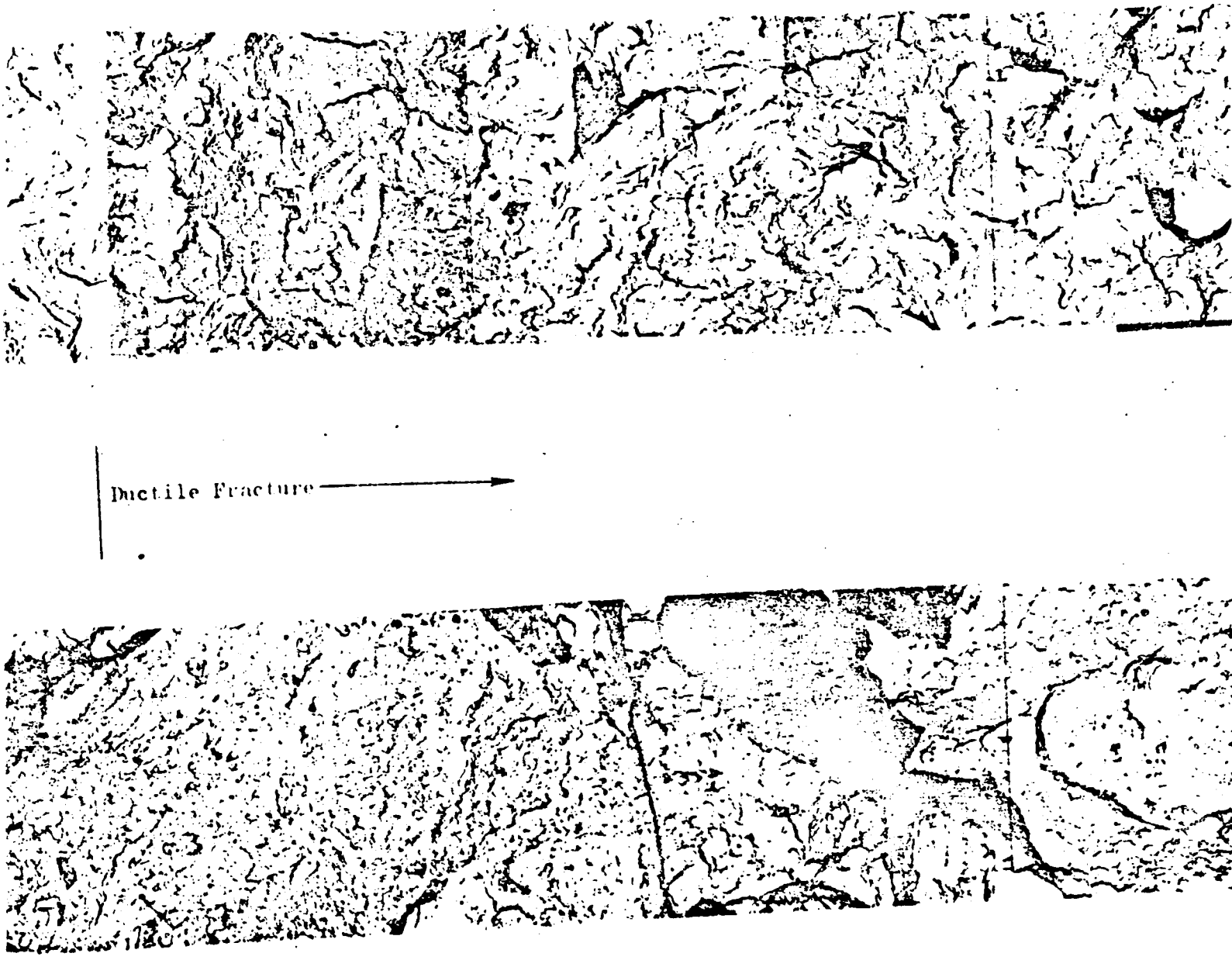

Electron Fractograph

277-C

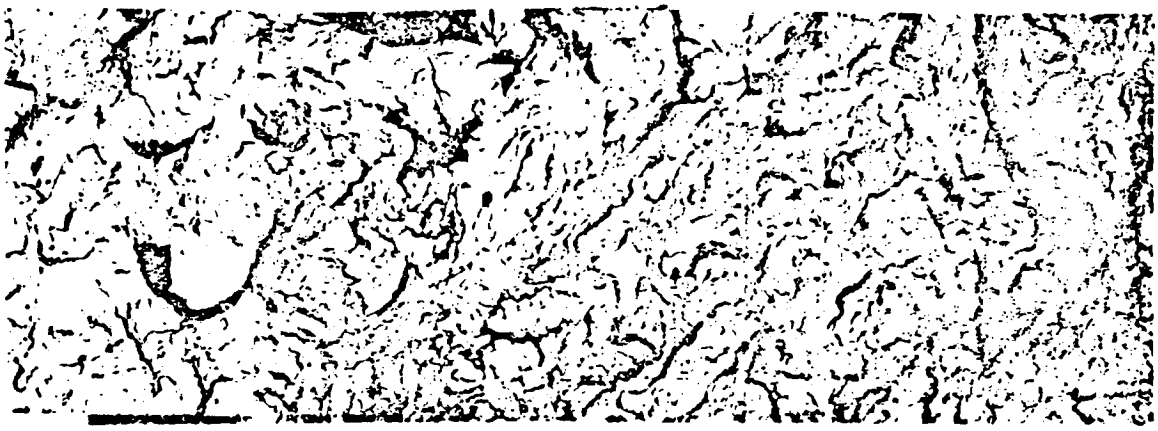

Figure 104. ASTM A-302 Notched and Precracked Specimen Tested in Low Cycle Fatigue in 10,000-psi Hydrogen Environment Failed After 3281 Cycles

Fig. 104 is quite similar to the brittle areas of the ASTM A-302 parent metal specimens tensile tested in 10,000-psi hydrogen and examined in the previous program (Ref. 2). The ASTM A-517 specimens tensile tested in 10,000-psi hydrogen have not been examined by electron fractography, but it is expected that the brittle nature of the fracture in Fig. 103 is representative of tensile fracture in 10,000-psi hydrogen.

For these two low alloy steels, there is so far no way of distinguishing between tensile failure in high-pressure hydrogen and low cycle fatigue failure in high-pressure hydrogen.

Recently, Pelloux and Wallner (Ref. 19) examined a 2043-T3 aluminum specimen, which was cycled alternately in air and in 5×10^{-6} torr vacuum. They observed that fatigue striations developed at even intervals in air ceased to appear when the test chamber was evacuated. Thus, the striations may be peculiar to fatigue in air environments. The presence of striations on specimens tested in 10,000-psi helium suggests that the helium environment contained sufficient impurities so that the fatigue crack growth behaved as in an air rather than a vacuum environment.

SUMMARY

Results of the posttest metallographic examination of surface cracking showed that the Phase II hydrogen-environment embrittlement categories could be used to classify surface-crack formation and propagation characteristics. The metals belonging to category 4, non-embrittled metals, did not form surface cracks after being tested in the hydrogen environments. The metals in category 4 are the stable AISI type 300 series stainless steels, aluminum alloys, and pure copper.

Metals in category 3 (slight embrittlement) are commercially pure titanium, Be-Cu Alloy 25, and AISI types 304L and 303 stainless steels. These metals were very little embrittled in the unnotched condition, but were slightly

Preceding page blank

embrittled in the notched condition. Numerous surface cracks were observed with the aid of low power (10X) magnification on commercially pure titanium and AISI type 304L stainless-steel specimens after testing in 10,000-psi hydrogen. These cracks were shallow and very blunt, and were not sufficiently deep to initiate fracture, as indicated by well-formed shear lips completely around the fractures. Fracture, therefore, initiated inside the metal in hydrogen as well as in air and helium environments.

The metals in category 2 (severe embrittlement) are the ductile, low- and moderate-strength steels, pure nickel, and the titanium alloys. These metals were considerably embrittled in both unnotched and notched conditions, and there were many surface cracks on the specimens severely embrittled by hydrogen. The cracks were easily observed without the aid of magnification, and some were fairly deep. Metallographic examination showed that the cracks blunted and terminated by branching. These surface cracks were fracture initiation sites, and it was obvious from inspection of the fracture that the crack origins were at the surface. Failure was evidently caused by reduction of the cross section by one or usually several surface cracks, and final rupture was probably quite ductile. There was no shear lip formation on the severely embrittled specimens, indicating that fracture initiated at the surface rather than inside the specimens.

Metals in category 1 (extreme embrittlement) are the high-strength steels and high-strength nickel-base alloys. These metals were extremely embrittled by hydrogen in notched and unnotched conditions. Specimens tested in hydrogen were likely to have only one crack, and this crack initiated catastrophic failure. Shear lip formation on some of the metals was complete except at the region of the surface crack. Thus, fracture initiated from a single crack and propagated inwards, while final failure at the side opposite the origin occurred by ductile shear independent of the environment. Optical metallography and scanning

electron fractography of Inconel 718 specimens showed that fracture was initiated by a single surface crack in a brittle intergranular manner, but propagation across most of the fracture was ductile. Metallographic examination of surface cracks in AISI 4140 and Fe-9Ni-4Co-0.25C specimens showed that the cracks were very sharp, and propagation was not appreciably hindered by branching, although minor branching was prevalent.

There were two characteristics of the surface cracks in all embrittlement categories; crack initiation was a function of degree of plastic deformation and the type of cracks was independent of hydrogen pressure. It was observed that surface cracks were generally restricted to the necked-down region and that the cracks were most numerous and deepest close to the fracture. Those metals tested in various hydrogen pressures (i.e., ASTM A-302, a category 2 metal; and Inconel 718, a category 1 metal) had the same type of surface cracking at all hydrogen pressures. The degree of plastic deformation required for crack formation, however, increased with increasing hydrogen pressure.

It can be deduced from examination of surface cracking of the unnotched specimens that the degree of embrittlement was not determined by the susceptibility to form surface cracks per se, but instead was determined by the material's ability to blunt these cracks in the hydrogen environment.

Notched specimens fractured in hydrogen had a brittle outer ring and a ductile inner region. The outer ring had a bright appearance and extended completely around the periphery of the severely embrittled low-alloy steel specimens. The outer ring, however, faded into the entire fracture in the case of the extremely embrittled higher-strength steels, the fractures of which were brittle across the entire specimen whether it was fractured in hydrogen or in inert environments. The outer ring on the nickel- and titanium-base alloys was dark and extended only partially around the fracture.

The outer rings represented the hydrogen-affected region, and no shear lips were ever observed in this area. Shear lips were, however, present on those portions of the fracture periphery of the titanium- and nickel-base alloys that did not have a dark outer ring. Shear lips were also present on the entire fracture periphery of the specimens tested in air or 10,000-psi helium. The high-strength steels and the AISI type 300 series stainless steels did not, however, form shear lips in any environment. Fractures of the AISI type 300 series stainless steels were quite ductile, but shear lips as such were not observed; instead, shear-like peaks occupied the entire fracture.

The outer rings are surface cracks that formed at the root of the notch. In most instances, the restricted region in the notch allowed only a single crack to form, which then propagated to failure. The observation of surface cracking in notched specimens is, therefore, much more difficult than in unnotched specimens. Characteristics associated with surface crack formation and propagation in unnotched specimens should, however, hold true for notched specimens as well.

Electron fractography showed that the outer region of the fractures of iron-, nickel-, and titanium-base alloys were ductile for specimens tested in air or helium environments.

The fractures of all specimens embrittled by hydrogen had similar features:

1. Surface cracking, which could be observed only by electron fractography, was present on the machined surface near the fracture of most specimens examined.
2. The region of fracture initiation at the machined surface/fracture surface interface was brittle in all cases.
3. Initial crack propagation was brittle. The brittle regions were transgranular in steels and titanium-base alloys, and intergranular in the nickel-base alloys and in welded low alloy steel

specimens containing a notch in the weld metal (Ref. 2). Secondary cracking was usually present in the brittle region. This secondary cracking probably corresponds to branching of f surface cracks observed in unnotched specimens.

4. The inner region and the edge across from the origin were ductile, and appeared to be the same as the fractures in helium or air.

These observations on hydrogen-environment embrittled specimens substantiate the findings reported in the previous program (Ref. 2), which could only be regarded as tentative at the time because of the limited scope of the investigation.

It was interesting that the fracture of an Inconel 718 specimen tested in hydrogen-contaminated helium was similar to the fracture of this material in 10,000-psi hydrogen even though the degree of embrittlement was much less in the former case. This would suggest that the qualitative aspects of embrittlement are the same, but the extent of embrittlement is a function of hydrogen pressure.

In testing of commercially pure titanium, it was found that the effect of test vessel evacuation was to decrease the amount of plastic deformation required to initiate brittle failure at the specimen surface. There was no indication of intergranular attack or of a hydride phase associated with the fracture of any commercially pure titanium or Ti-6Al-4V specimen examined. On the contrary, the fractures of these specimens appeared very much like the fractures of the low alloy steel specimens that were tested in hydrogen. Since hydride formation and intergranular fracture are characteristic of internal hydrogen embrittlement, it is assumed that the mechanism by which titanium is embrittled by gaseous hydrogen is different from the mechanism by which titanium is embrittled by internal hydrogen; the mechanism appears rather to be the same as that of the gaseous hydrogen embrittlement of iron- and nickel-base alloys.

Examination of the low alloy steel specimens tested by low cycle fatigue showed fatigue striations on a specimen tested in 10,000-psi helium, but no striations on specimens tested in 10,000-psi hydrogen. It was concluded that the oxygen partial-pressure in the helium environment was sufficient to delineate the fatigue striations. There is no known way to distinguish between tensile and fatigue failure in hydrogen.

CONCLUSIONS

Based on the preceding information the following conclusions were reached:

1. Fracture initiation in hydrogen occurred at the surface.
2. The degree of embrittlement was determined by the material's ability to blunt cracks in hydrogen rather than by surface crack initiation per se.
3. Fracture characteristics of iron-base (BCC), nickel-base (FCC), and titanium-base (HCP) alloy specimens tested in hydrogen were basically the same.

FUTURE WORK

From the very small number and limited scope of previous investigations into hydrogen-environment embrittlement, as discussed in the Introduction, and from the limited studies of a number of variables in this program, it is evident that only initial steps have been taken in developing the required understanding and information on the effects of high-pressure hydrogen environments on the mechanical properties of metals. Because so much remains to be accomplished, recommended future work will only be outlined here under the four broad objectives below:

1. Delineation and characterization of hydrogen-environment embrittlement: Most of the investigations conducted to date are in this category, i.e., these investigations show how hydrogen-environment embrittlement manifests itself and, comparatively, the extent of embrittlement of the different metals at least under the specific test conditions. Much work remains to be done even in this area. For example, screening tests should be performed on additional alloys and those alloys found in the present program to be highly susceptible to embrittlement by 10,000-psi hydrogen should be tested at lower hydrogen pressures. The effects on high-pressure hydrogen-environment embrittlement of variables such as temperature and strain rate should be investigated, and tests should be performed to determine if a high-pressure hydrogen environment has any effect on compressive properties.

2. Development of design data for alloys used in hydrogen environments: Tests of the type indicated in (1) have served well to indicate the nature of hydrogen-environment embrittlement, to give a qualitative comparison of alloys as to their propensity toward such embrittlement, and thus to prevent obvious mistakes in the use of alloys in hydrogen environments. However, structures are in existence, and must be constructed in the future,

in which metals and alloys whose properties are affected by hydrogen environments are used in contact with those environments. Thus, it is imperative to begin obtaining those data required to factor correctly and quantitatively into future designs the effects of the hydrogen environments. Such data can also be used to evaluate the magnitude of any hydrogen-environment embrittlement problems in existing structures and to indicate suitable compensatory steps. The recommended approach for obtaining the desired data includes, but is not limited to, the use of fracture toughness testing in hydrogen environments.

3. Clarification of the fundamental mechanism of hydrogen-environment embrittlement: Without knowing the mechanism of hydrogen-environment embrittlement it is dangerous to attempt to extrapolate from the results obtained in laboratory tests in hydrogen under a certain set of conditions to structures operating in hydrogen environments under different conditions. Conversely, an understanding of the mechanism would add to the relevancy of all data that has been and will be generated, and it would serve to direct all subsequent investigations so that the information most relevant to engineering structures would be obtained in the most efficient and economical manner.

4. Determination of methods of prevention or minimization of hydrogen environments embrittlement: Although it is doubtful that methods can be found to eliminate universally hydrogen-environment effects, and thus they will have to be considered in designs as indicated in (3), there may be certain individual cases in which the effects can be eliminated or at least reduced. An example of a prevention method now being implemented is the use of a stable austenitic stainless-steel liner in a vented structural-steel pressure vessel for storage of hydrogen at 10,000 psi. Where feasible, other possible techniques include addition of inhibitors (e.g., oxygen) to the hydrogen gas, coatings, and development of alloys more resistant to hydrogen-environment embrittlement.

Suggested individual tasks are listed below:

Task I: Screening Tests to Extend the Present Knowledge to Include the Effects of Varying Pressure, Temperature, and Strain Rate on the Hydrogen-Environment Embrittlement of Various Alloys

Task II: Effect of Hydrogen Environments on Fatigue Strengths of Various Alloys

Task III: Effect of Surface Abrasion on the Susceptibility to Hydrogen-Environment Embrittlement of Metals

Task IV: Fracture Mechanics Behavior in High-Pressure Hydrogen Using Specimens Precracked in Hydrogen

Task V: Characterization of Crack Propagation in Metals in High-Pressure Hydrogen

Task VI: Prevention of High-Pressure Hydrogen Embrittlement

REFERENCES

1. Raring, R. H., et al.: Report of NASA Working Group on Storage of Hydrogen at High Pressure, National Aeronautic and Space Administration, Washington, 13 September 1967.

2. R-6851, Walter, R. J., and W. T. Chandler: Effects of High-Pressure Hydrogen on Storage Vessel Materials, final report on Task VIII of NASA Contract NAS8-19, Rocketdyne, a division of North American Rockwell Corporation, Canoga Park, California, January 1967.

3. Walter, R. J., and W. T. Chandler: Effects of High-Pressure Hydrogen on Storage Vessel Materials, presented at 1968 Western Metal and Tool Conference, Los Angeles, California, March 1968. ASM Report No. W8-2.4, ASM Report System, Metals Park, Ohio 44073. To be published in ASM Engineering Quarterly.

4. Peterson, R. E.: Stress Concentration Design Factors, John Wiley & Sons, New York, 1953.

5. Forman, R. G.: Private communication.

6. Groeneveld, T. P., E. F. Fletcher, and A. R. Elsea: A Study of Hydrogen Embrittlement of Various Alloys, annual summary report, contract NAS 8-20029, to NASA Huntsville, Alabama, by Battelle Memorial Institute, Columbus, Ohio, 23 June 1966.

7. Davidson, T. E., and G. S. Ansell: "The Structure Sensitivity of the Effects of Pressure Upon the Ductility of FC-C Materials," Trans. ASM, Vol. 61, pages 242-254, 1968.

8. Wilson, D. V., and B. Russell: "The Contribution of Atmosphere Locking to the Strain-Aging of Low Alloy Steels." Acta Met., Vol. 8, pages 36-45, January 1960.

9. Wilson, D. V., and B. Russell: "The Contribution of Precipitation to Strain Aging in Low Carbon Steels," Acta Met., Vol. 8 pages 468-479, July 1960

Preceding page blank

10. Goel, V., R. Busch, and V. G. Zackay: "Dynamic Strain Aging of a High Strength Steel," Journal of Basic Engineering, pages 871-876, December 1967.

11. Stephenson, E. T., and Morris Cohen: "The Effect of Prestraining and Retempering on AISI Type 4340," Trans. ASM, Vol. 54, pages 72-83, 1961.

12. Harrington, R. H.: "Stress Aging: A New Treatment for Alloys--Part Three; Effect of Standard Tensile Properties of Four Ultra-High Strength Steels," Benet Laboratories Watervliet Arsenal WVT-6501, February 1965.

13. Harrington, R. H.: "Stress-Aging and Its Effects on the Standard, Tensile Properties of Some Stainless Steels," Trans. ASM. Vol. 58, No. 2, pages 119-141, June 1965.

14. Hofmann, W., and W. Rauls: "Ductility of Steel Under the Influence of External High Pressure Hydrogen," Welding Journal. Vol. 44, page 255s, 1965.

15. Steinman, J. B., H. C. Van Ness, and G. S. Ansell: "The Effect of High-Pressure Hydrogen Upon the Notch Tensile Strength and Fracture Mode of 4140 Steel," Welding Journal, pages 221s-224s, May 1965.

16. Williams, Dell P.: "Comments on Slow Crack Growth in Hydrogen and Water Environments," Scripta Met., Vol. 2, pages 285-292, 1968.

17. Johnson, H. H.: On Hydrogen Brittleness in High Strength Steel, paper to be published in Proceedings of the International Conference on Fundamental Aspects of Stress-Corrosion Cracking held at Ohio State University, Columbus, Ohio, from 11 to 15 September 1967.

18. Ham, R. K.: "The Metallurgy of Transition-Life Fatigue," Thermal and High-Strain Fatigue, The Metals and Metallurgy Trust of the Institute of Metals and the Institute of Metallurgists, 17 Belgrave Square, London, S.W.1, 1967.

19. Pelloux, R. M. N., and Mrs. H. Wallner: "How Fatigue Cracks Grow in Air and Vacuum," Metals Progress, page 82, December 1968.